CBPF - CENTRO BRASILEIRO DE PESQUISAS FÍSICAS
COTEO - COORDENAÇÃO DE FÍSICA TEÓRICA

P.H.D. THESIS

BCS-BEC Crossover Induced by Antisymmetric Hybridization

GUILHERME NUNES BREMM

Advisor
Tobias Micklitz

Rio de Janeiro - RJ
2021

“BCS-BEC CROSSOVER INDUCED BY ANTISYMMETRIC HIBRIDIZATION”

GUILHERME NUNES BREMM

Tese de Doutorado em Física apresentada no Centro Brasileiro de Pesquisas Físicas do Ministério da Ciência Tecnologia e Inovação. Fazendo parte da banca examinadora os seguintes professores:

Tobias Micklitz – Presidente/Orientador/CBPF

Raimundo Rocha dos Santos - UFRJ

Daniel Gustavo Barci– UERJ

José Abdala Helayel Neto - CBPF

Itzhak Roditi – CBPF

Rio de Janeiro, 29 de novembro de 2021.

Acknowledgments

There are many people that I am grateful for being part of this journey, specially to

- my advisor professor Dr. Tobias Micklitz, for the patience, the dedication and the several teachings. A great teacher I was fortunate to meet;
- my CBPF's teachers, for sharing their knowledge and contribute to my academic formation;
- the CBPF's staff, in particular, to Bete and Ricardo for their attention and efficiency;
- my colleagues, Lucas, José, Antônio, Zé, Luciana, Thalis and Eric, not only for their friendship but also for the several interesting discussions we had. One could not ask for better classmates!
- my tango friends, Alecs, Diana, Jorge, Vivi, Mari, Javi and Theresa simply for being such a wonderful people and always make me laugh;
- CAPES, for the financial support. I hope they agree the money was well spent;
- and last but not the least, my mother, for always believing in me (and also for the financial support!). I love you.

"Não há alternativa, é a única opção
Unir o otimismo da vontade e o pessimismo da razão
Contra toda expectativa, contra qualquer previsão
Há um ponto de partida, há um ponto de união
Sentir com inteligência, pensar com emoção!"

Abstract

We study the evolution from the weak coupling Bardeen-Cooper-Schrieffer (BCS) state to Bose-Einstein condensation (BEC) at strong coupling in a two-band superconductor with orbitals of opposite parity coexisting at a common Fermi surface in the metallic state. We analyze, independently, the intra and the interband interactions where, in the former, hybridization destroys superconductivity and in the latter it plays a role similar to spin-orbit interaction in fermionic spinor gases, enhancing the interband pairing and opening the possibility for driving the BCS-BEC crossover. In multi-band superconductors the mass difference of the interacting fermions is also a relevant parameter to be considered and we show that the interband crossover is favored in systems with one dispersive and one flat band. Starting with a mean-field analysis, at both zero and finite temperatures, we investigate the crossover induced by an odd-parity hybridization. The divergence in the interband critical temperature at the strong coupling limit is corrected with the inclusion of the thermal pair-fluctuations in a one-loop approximation. We then calculate the dependence of the condensation temperature on the microscopic parameters, namely hybridization, scattering length and mass anisotropy. Finally we show that a smooth interband BCS-BEC crossover can indeed be attained via hybridization.

Keywords: Superconductivity, multi-band superconductors, hybridization, BCS-BEC crossover.

Resumo

Estudamos a evolução do estado Bardeen-Cooper-Schrieffer (BCS) de acoplamento fraco à condensação de Bose-Einstein (BEC) no acoplamento forte em um supercondutor de duas bandas com orbitais de paridades opostas coexistindo em uma mesma superfície de Fermi no estado metálico. Analisamos, de forma independente, as interações intra e interbandas onde, no primeiro, a hibridização destrói a supercondutividade e no segundo ela desempenha um papel semelhante à interação spin-órbita em gases espinoriais fermiônicos, aumentando o pareamento interbanda e abrindo a possibilidade de conduzir o crossover BCS-BEC. Em supercondutores multibandas, a diferença de massa dos férmions interagentes também é um parâmetro relevante a ser considerado e mostramos que o crossover interbanda é favorecido em sistemas com uma banda dispersiva e outra plana. Partindo de uma análise de campo médio, tanto para temperatura zero quanto finita, investigamos o crossover induzido por uma hibridização de paridade ímpar. A divergência na temperatura crítica do setor interbanda no limite de acoplamento forte é corrigida com a inclusão das flutuações térmicas em uma aproximação a nível de um loop. Em seguida, calculamos a dependência da temperatura de condensação em relação aos parâmetros microscópicos, nomeadamente hibridização, comprimento de espalhamento e anisotropia de massa. Finalmente, mostramos que um crossover BCS-BEC no setor interbanda pode de fato ser obtido por meio da hibridização.

Palavras-chave: Supercondutividade, supercondutores multibandas, hibridização, BCS-BEC crossover.

Contents

List of Figures

Chapter 1

Introduction

The idea of a connection between Cooper pairs and diatomic molecules is not new, it perhaps can be traced back to the work of Scharfroth, Blatt and Butler [1] even before the advent of Bardeen-Cooper-Shrieffer's theory (BCS) for conventional superconductivity [2].

However it was only in 1980 that A. J. Leggett [3] showed theoretically that a dilute gas of weakly interacting fermions at $T = 0$K could attain, depending on the strength of the attractive interaction, the behavior of BCS pairs or the behavior of tight bound bosons, which could undergo Bose-Einstein condensation (BEC). Such a system also possesses a universal character since its properties are only dependent on a single parameter given by the ratio of the interparticle distance k_F^{-1}, where $k_F = (3\pi^2 n)^{1/3}$ is the Fermi momentum with n the gas density, and the length scale of pairing correlations expressed through the s-wave scattering length a_s. Thus tuning $(k_F a_s)^{-1}$, with the Feshbach resonance technique for example, it was possible to smoothly link the BCS limit (weak coupling regime) characterized by $(k_F a_s)^{-1} \ll -1$ to the BEC limit (strong coupling regime) where $(k_F a_s)^{-1} \gg 1$. The unitary point $(k_F a_s)^{-1} = 0$ signals the appearance of a two-body bound state and the region around it $|k_F a_s|^{-1} \approx 1$, where the system shifts its character, is the so called BCS-BEC crossover.

The finite temperature problem was then considered by Nozières and Schmitt-Rink [4] where the authors pointed out the limitation of the mean-field approach to deal with the intermediary and strong coupling regions: within this approximation the fermions pair binding is not properly taken into account, which leads to a divergent condensation temperature. A full disclosure of the problem was reached by Sá de Melo et. al. [5] with the inclusion of thermal fluctuations around the saddle-point solution, where they have been able to obtain the complete profile of the critical temperature as a function of the coupling.

Although well understood theoretically it was only recently that the crossover was indeed observed in ultracold gases [6–8]. This delay, partially due to the difficulty of tuning the coupling constant, propelled the seek for other ways to promote the BCS-BEC crossover. Thus the experimental development in the ultracold gases scenario motivated extensive theoretical studies of more realistic models, such as the ones taking into account the spin-orbit coupling (SOC) of fermionic gases at $T = 0$ [9] as well finite temperature [10–12]. A very interesting result of these studies is that depending on the kind of the spin-orbit interaction the system may present a pseudogap even in the weak-coupling regime and consequently the possibility of a BCS-BEC crossover induced by SOC.

In the condensed matter realm other fruitful proposals [13–15] indicated that metallic multi-band systems under the influence of hybridization could also present the BCS-BEC crossover signature. A close inspection of both models reveals the mathematical similarities between them which explains the coincidence of some qualitative results, however the multi-band models are not limited to describe fermions with the same effective masses. Furthermore a huge experimental advantage of the multi-band systems over the ultracold gases lies in the tuning of the hybridization since it can be achieved simply through doping or pressure.

Despite of the promising results achieved, the aforementioned works [13–15] deal solely at a mean-field level preventing a more detailed analysis of the two-band system in the strong-coupling regime. Therefore we intend to correct and expand their work as Sá de Melo did with Leggett's. Naturally with the inclusion of new variables the richness and complexity of the problem take new turns, pose new issues and here we shed some light over the effects of the hybridization and mass asymmetry besides the usual scattering length parameter. More specifically, we consider a two-band model, focusing our attention in the interband sector, calculate the mean-field solution and the one-loop correction to it. We show that there is no physical divergence in the condensation temperature and indeed a legit BCS-BEC crossover can be attained through hybridization.

This thesis is divided as follows, chapter 2 aims to review the basic concepts involved in the Bose condensation, the superconductivity phenomena and the BCS-BEC crossover as obtained by Leggett and the one achieved through SOC; in chapter 3 we introduce the two-band model and its mean-field treatment which provide numerical solutions that indicate the need of the inclusion of the gaussian fluctuations as done in chapter 4, where we are finally able to obtain the profile of the BCS-BEC crossover; chapter 5 summarizes and gives a glimpse over the future possibilities of work.

Chapter 2

Theoretical Framework

In this chapter we review the basic concepts and mathematical tools to understand the BCS-BEC crossover. Section 2.1 is dedicated to briefly describe a Bose-Einstein condensate and to derive its critical temperature. Sections 2.2 and 2.2.2 are dedicated to explore the interacting fermions in the weak and strong coupling regimes respectively, followed by section 2.3 in which we show Leggett's results for the crossover theory at $T = 0$ K. The expansion of Leggett's work is done in sections 2.4 and 2.5 where the thermal fluctuations are included in order to find the correct critical temperature in the strong coupling regime. In section 2.6 we present the influence of the spin-orbit coupling in the fermionic gas.

Throughout this thesis will use natural units $k_B = \hbar = 1$.

2.1 Bose-Einstein Condensation in an Ideal Gas

The advent of quantum mechanics propelled many new theoretical investigations. Among those is the one conjectured in the years of 1924-25 by Satyendra Bose [16] while corresponding with Albert Einstein [17] in which they predicted that a dilute gas of particles with integer spin (later on called bosons) at extremely low temperatures could undergo a new form of matter, the Bose-Einstein condensate (BEC). Close to the absolute zero all the bosonic particles occupy the lowest energy state, increase their wavelength, interfere with each other and then come together in a macroscopic condensate. It was experimentally achieved in 1995 by Eric Cornell et. al. [18] using a vapor of ^{87}Rb atoms cooled down to 170 nK. Their result can be summarized in Fig. 2.1 which presents the particle density versus the velocity distribution as the temperature decreases and shows the concentration of atoms around the ground state.

To derive the BEC properties let us consider a gas of N identical bosons with mass m_b within a three dimensional box of unit volume $V = 1\text{m}^3$ in contact with a particle reservoir characterized by the chemical potential μ. There are several ways to approach the problem but here we shall make use of the path integral formalism represented by the partition function $\mathcal{Z} = \int \mathfrak{D}[\phi] e^{-S[\phi]}$, where the ideal bosonic action, in the imaginary-time notation, is given by

$$S[\phi] = \int_V \mathrm{d}^3x \int_0^\beta \mathrm{d}\tau \bar{\phi}(\mathbf{x},\tau) \left(\partial_\tau - \frac{\nabla^2}{2m_b} - \mu \right) \phi(\mathbf{x},\tau), \tag{2.1}$$

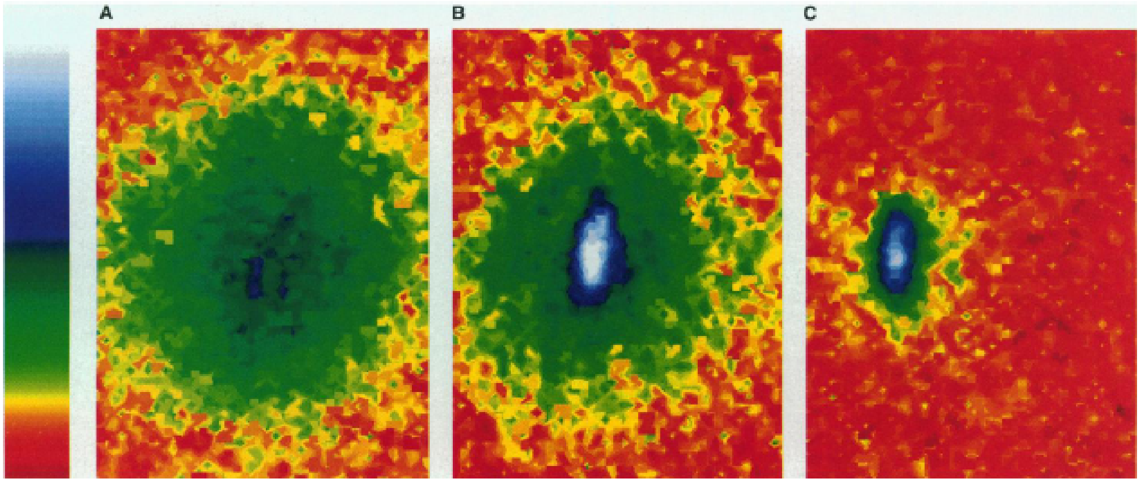

Figure 2.1: Bose-Einstein condensate obtained with a ^{87}Rb gas around 170 nK. The image shows the velocity distribution (fast moving particles indicated in red and slower ones in blue and white) of the cloud (A) just before the appearance of the condensate, (B) just after the appearance of the condensate, and (C) after a nearly complete BEC. The anisotropic distribution around the zero velocity peak is a characteristic of the condensate. Extracted from reference [18].

with ϕ a complex scalar field subjected to the periodic boundary condition $\phi(\mathbf{x}, 0) = \phi(\mathbf{x}, \beta)$ and $\beta = \frac{1}{T}$ the inverse temperature.

Switching to the frequency-momentum representation $\phi(\mathbf{x}, \tau) = \frac{1}{\sqrt{\beta}} \sum_{\mathbf{k},\omega_m} \phi(\mathbf{k}, m) e^{i\mathbf{k}\cdot\mathbf{x} - i\omega_m \tau}$, where the periodic boundary condition imposes the Matsubara frequencies to be even functions $\omega_m = 2m\pi/\beta$ with $m \in \mathbb{Z}$, the partition function reads

$$\mathcal{Z} = \prod_{\mathbf{k},\omega_m} \frac{1}{\beta} \frac{1}{-i\omega_m + \epsilon_{\mathbf{k}} - \mu}, \tag{2.2}$$

with energy dispersion $\epsilon_{\mathbf{k}} \equiv \mathbf{k}^2/(2m_b)$. To ensure a well behaved gaussian integral, the chemical potential obeys $\mu < \min_{\mathbf{k}} \{\epsilon_{\mathbf{k}}\}$.

The thermodynamic number of particles[1] can be calculated from the Helmholtz free energy $\Omega \equiv -\beta^{-1} \ln \mathcal{Z}$. Summing over the bosonic frequencies

$$n(\mu, T) = -\frac{\partial \Omega}{\partial \mu} = \frac{1}{\beta} \sum_{\mathbf{k},\omega_m} \frac{1}{-i\omega_m + \epsilon_{\mathbf{k}} - \mu} = \sum_{\mathbf{k}} n_B(\epsilon_{\mathbf{k}}), \tag{2.3}$$

where $n_B(\epsilon_{\mathbf{k}}) = 1/(e^{\beta(\epsilon_{\mathbf{k}} - \mu)} - 1)$ is the well-known Bose-Einstein distribution. As $T \to 0$ the particles seek the ground state and the phase transition occurs in the limit $\mu \to 0$ so that the $\mathbf{k} = 0$ mode in Eq. 2.3 becomes macroscopically occupied and must be set aside from the rest of the sum which then may be replaced by an integral

$$n(\mu \to 0) = n_0 + \int \frac{\mathrm{d}^3 k}{(2\pi)^3} \frac{1}{e^{\beta \epsilon_{\mathbf{k}}} - 1} = n_0 + \zeta(3/2) \left(\frac{m_b T}{2\pi} \right)^{3/2}, \tag{2.4}$$

[1] Or particle density since we are using $n = N/V$ with $V = 1\text{m}^3$.

where $\zeta(3/2) = 2.612$ is the Riemann ζ-function $\zeta(s) = \sum_{n=1}^{\infty} n^{-s}$ evaluated at $3/2$ and n_0 is the condensate's particles density. Yet the latter can be written in terms of the particle number as

$$n_0 = n\left[1 - \left(\frac{T}{T_c}\right)^{3/2}\right] \quad \text{for} \quad T < T_c, \tag{2.5}$$

with the condensation temperature T_c defined as

$$\boxed{T_c \equiv \frac{2\pi}{m_b}\left(\frac{n}{\zeta(3/2)}\right)^{2/3}.} \tag{2.6}$$

Typically, T_c is of the order of nK and, as expected, as $T \to 0$ all particles are in the ground state $n_0 \to n$.

This section's results will be particularly useful to link a Fermi to a Bose gas, and later on to deduce the condensation temperature in the two-band system.

2.2 Superconductivity

The race to achieve the absolute zero allowed the discovery of the *superconductivity* by the Dutch physicist Heike Kamerlingh Onnes in 1911 [19]. Using liquid helium he found out that below $T_c = 4.20$K the *electrical resistance* of mercury *vanishes* abruptly, as shown in Fig. 2.2. He also observed that the superconductor state was destroyed in the presence of a critical magnetic field H_c. Two years later W. Meissner and R. Ochsenfeld added that if an external magnetic field, below the critical value, is applied to a superconductor it is ejected from the material interior [20] (there is actually a penetration depth, an exponentially small distance penetrated by the magnetic field). This became known as the *Meissner effect* and it is manifested solely in conventional or type-I superconductors. Type-II superconductors were first observed in 1935 by J. Rjabinin and L. Shubnikow [21] and present two characteristic magnetic fields: above a certain value H_{c1} there are the formation of magnetic vortices but the superconductivity persists locally; as the strength of the magnetic field increases and reaches H_{c2} the superconductivity is destroyed. Almost all single element superconductors are type-I while metal alloys and oxide ceramics are type-II.

The first successful attempt to explain the Meissner effect and the penetration depth has been made in 1933 by the brothers Fritz and Heinz London [22] and subsequently improved by V. L. Ginzburg and L. Landau [23], and B. Pippard [24] with the introduction of the coherence length ξ_0, a parameter indicating the coherence scale of the superconductor. However it was only in 1957 with J. Bardeen, L. Cooper and J. R. Schrieffer's seminal work [2] that a full understanding of conventional superconductivity came to light. Grounded on Cooper's *hypothesis* [25] of the coupling of an electron pair with opposite momentum and spin in the vicinity of the Fermi surface, the Cooper pair, a microscopic theory has been built. The pairing mechanism, strong enough to overcome the Coulomb repulsion, was attributed to the lattice deformation from the first passing electron which creates an energetically favorable path for the second one forming a weakly bound pair with size of the order $\xi_0 \sim 10^2$nm. The BCS theory was able to successfully explain many properties of conventional superconductors such as the critical temperature, the appearance of an isotropic gap in the excitation energies and the specific heat discontinuity. Another BCS triumph was the prediction of the isotope effect in Hg [26] linking its isotopic mass, M, to the frequency of lattice vibration and to the critical temperature as $T_c \propto M^{-1/2}$ (also verified in other elements).

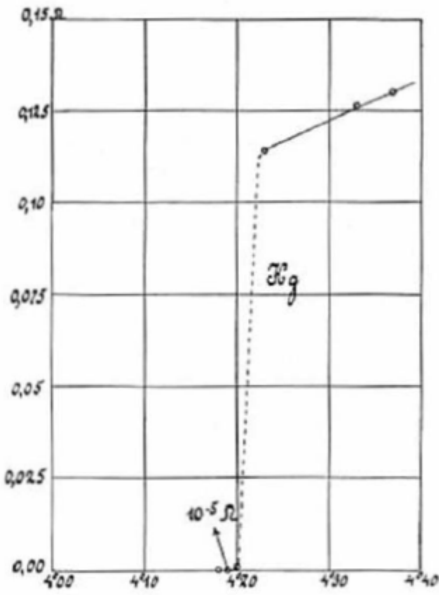

Figure 2.2: Onnes' original plot from 26 October 1911 showing the electrical resistance (Ω) of Hg versus the temperature (K). The abrupt decrease in the resistance at 4.20 K is the first record of superconductivity.

The faith in the BCS theory was such that superconductivity was thought to be impossible at temperatures above 30 K, but as the experimental works intensified a new kind of superconductor was announced by K. A. Müller and J. G. Bednorz [27] in 1986. The new compound of the cuprate family (CuO) showed a slightly higher critical temperature than the one allowed by the BCS paradigm and soon afterwards even higher T_c materials, up to 138 K, have been produced as indicated in Fig. 2.3. The absence of the isotope effect in high temperature superconductors (HTSC) indicated a pairing mechanism other than the electron-phonon attraction although up to date no conclusion has been reached upon the subject. It is possible however to spin-density waves to play this role [28].

Another remarkable difference from conventional superconductors is the much smaller coherence length, typically of the order $\xi_0 \sim 1$nm, suggesting that HTSC belong to the class of strongly correlated electron systems (SCES) [29], where the superconductor pair is so tight bound that can effectively behave as a boson and thus undergo BEC [30].

To further discuss the relation between superconductivity and BEC let us next consider two limit cases.

2.2.1 Fermions in the Weak Coupling Regime

In order to obtain some quantitative results of the BCS theory we shall consider a similar configuration as the one described in the previous section but with a dilute gas of interacting fermions of spin 1/2 and mass m. To make the notation clearer, from now on, let us adopt a four-dimensional convention $x \equiv (\mathbf{x}, \tau)$ and $\int \mathrm{d}x \equiv \int_V \mathrm{d}^3x \int_0^\beta \mathrm{d}\tau$, thus the action reads $S[\psi] = \int \mathrm{d}x(\bar{\psi}_\sigma \partial_\tau \psi_\sigma + \mathcal{H}_{\mathrm{BCS}})$ with the BCS Hamiltonian density given by

$$\mathcal{H}_{\mathrm{BCS}}(x) = \bar{\psi}_\sigma(x) \left(-\frac{\nabla^2}{2m} - \mu \right) \psi_\sigma(x) - g\bar{\psi}_\uparrow(x)\bar{\psi}_\downarrow(x)\psi_\downarrow(x)\psi_\uparrow(x), \tag{2.7}$$

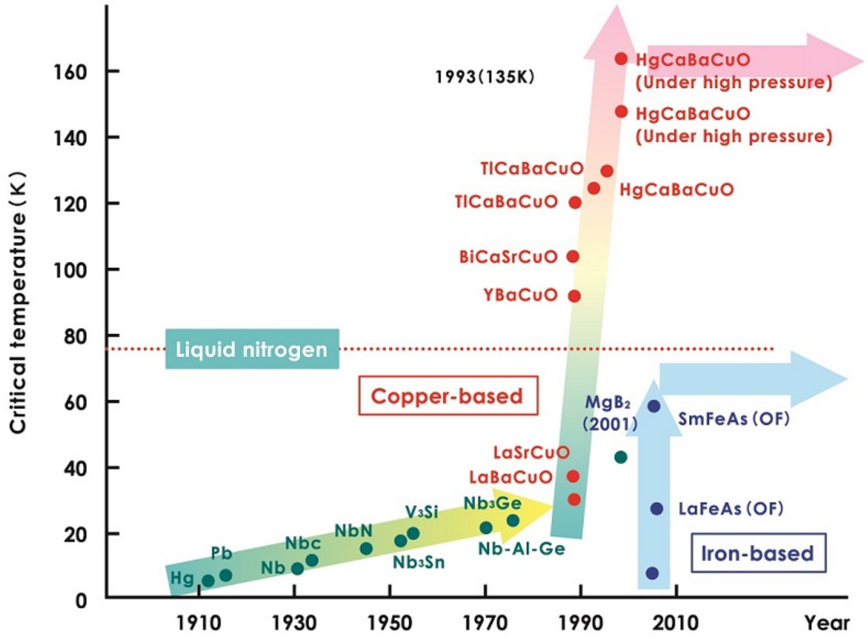

Figure 2.3: Chronology of the superconductor materials. Extracted from `https://www.u-tokyo.ac.jp/focus/en/features/f_00070.html`.

where the positive constant g indicates an attractive interaction and ψ_σ are Grassmann fields with spin projection σ subjected to the anti-periodic boundary condition $\psi_\sigma(\mathbf{x},0) = -\psi_\sigma(\mathbf{x},\beta)$. Summation over σ is implicit. The interaction term can be seen as the product of particle and anti-particle pair amplitudes in the s-band and it destroys the gaussian character of the partition function preventing it to be evaluated exactly. The standard procedure is to use a Hubbard–Stratonovich transformation in the Cooper channel, or in other words, we insert into the partition function $\mathcal{Z} = \int \mathfrak{D}[\psi] e^{-S[\psi]}$ the following gaussian identity

$$\exp\left(g \int \mathrm{d}x \bar{\psi}_\uparrow \bar{\psi}_\downarrow \psi_\downarrow \psi_\uparrow\right) \equiv \int \mathfrak{D}[\Delta] \exp\left[\int \mathrm{d}x \left(-\frac{|\Delta|^2}{g} + \bar{\Delta}\psi_\downarrow\psi_\uparrow + \Delta\bar{\psi}_\uparrow\bar{\psi}_\downarrow\right)\right], \tag{2.8}$$

where $\Delta(x)$ is a complex auxiliary field which couples $\bar{\psi}_\uparrow\bar{\psi}_\downarrow$ and soon will be identified as the pairing energy gap. Using the Nambu spinor representation $\bar{\Psi}(x) \equiv [\bar{\psi}_\uparrow(x) \quad \psi_\downarrow(x)]$ we arrive at

$$\mathcal{Z} = \int \mathfrak{D}[\Psi]\mathfrak{D}[\Delta] \exp\left[\int \mathrm{d}x \left(-\frac{|\Delta(x)|^2}{g} + \bar{\Psi}(x)\mathbf{G}^{-1}(x)\Psi(x)\right)\right], \tag{2.9}$$

where the inverse Nambu-Gorkov Green's function is defined as

$$\mathbf{G}^{-1}(x) = \begin{pmatrix} -\partial_\tau + \frac{\nabla^2}{2m} + \mu & \Delta(x) \\ \bar{\Delta}(x) & -\partial_\tau - \frac{\nabla^2}{2m} - \mu \end{pmatrix} \tag{2.10}$$

comprising particle and hole inverse Green's functions and superconducting parameter.

Since the partition function's dependence in the spinors is now quadratic they can be readily integrated out

$$\mathcal{Z} = \int \mathfrak{D}[\Delta] \exp\left[-\int \mathrm{d}x \frac{|\Delta(x)|^2}{g} + \ln \mathrm{Det}\,\mathbf{G}^{-1}(x)\right], \tag{2.11}$$

and so our effective action can be written as[2]

$$\boxed{S[\Delta] = \int \mathrm{d}x \frac{|\Delta(x)|^2}{g} - \mathrm{Tr}\ln \mathbf{G}^{-1}(x),} \tag{2.12}$$

where Tr includes the sum over the two-dimensional Nambu space and the x integration.

The assumption that the saddle-point solution is real, static and spatially uniform[3] $\Delta(x) = \bar{\Delta}(x) \equiv \Delta_0$[4] (and thus possessing a s-wave symmetry) leads us to

$$\left.\frac{\delta S}{\delta \Delta}\right|_{\Delta(x)=\Delta_0} = \left.\left[\frac{\bar{\Delta}(x)}{g} - \mathrm{Tr}(\mathbf{G}\delta_\Delta \mathbf{G}^{-1})\right]\right|_{\Delta(x)=\Delta_0} = 0. \tag{2.13}$$

At this stage it is convenient to perform the Fourier transform $\psi_\sigma(x) = \frac{1}{\sqrt{\beta}} \sum_k \psi_\sigma(k) e^{ik\cdot x}$, where $k \equiv (\mathbf{k}, \omega_n)$ incorporates the momentum $\mathbf{k}$ and the odd Matsubara frequencies $\omega_n = (2n+1)\pi/\beta$ with $n \in \mathbb{Z}$. So it is straightforward to obtain the inverse of Eq. 2.10

$$\mathbf{G}_k = \frac{1}{\omega_n^2 + \xi_\mathbf{k}^2 + \Delta_0^2} \begin{pmatrix} -i\omega_n - \xi_\mathbf{k} & \Delta_0 \\ \Delta_0 & -i\omega_n + \xi_\mathbf{k} \end{pmatrix} \tag{2.14}$$

with $\xi_\mathbf{k} \equiv \epsilon_k - \mu$. Thus Eq. 2.13 becomes

$$\frac{1}{g} = \frac{1}{\beta} \sum_{\mathbf{k},\omega_n} \frac{1}{\omega_n^2 + \omega_\mathbf{k}^2}, \tag{2.15}$$

where we have introduced the quasiparticle excitation $\omega_\mathbf{k} \equiv \sqrt{\xi_\mathbf{k}^2 + \Delta_0^2}$ with a minimum

$$\min\{\omega_\mathbf{k}\} = \begin{cases} \sqrt{\Delta_0^2 + \mu^2} & \text{if } \mu \leq 0 \\ \Delta_0 & \text{if } \mu > 0 \end{cases} \tag{2.16}$$

that results in an energy gap between the $\pm\omega_\mathbf{k}$ bands of size $2\Delta_0$. In fact it is the presence of this gap that explains the discontinuity at low temperatures in the specific heat of superconductors.

Summing Eq. 2.15 over the odd frequencies [31] and using the identity $1 - 2n_F(x) = \tanh(x/2T)$, where $n_F(\xi_\mathbf{k}) = 1/(e^{\beta\xi_\mathbf{k}}+1)$ is the Fermi-Dirac distribution, we reproduce the famous BCS gap equation

$$\frac{1}{g} = \sum_\mathbf{k} \frac{1 - 2n_F(\omega_\mathbf{k})}{2\omega_\mathbf{k}} = \int_0^\infty \mathrm{d}\epsilon \nu(\epsilon) \frac{\tanh[\omega(\epsilon)/2T]}{2\omega(\epsilon)}, \tag{2.17}$$

with $\nu(\epsilon) = \frac{m^{3/2}\sqrt{\epsilon}}{\sqrt{2}\pi^2}$ the three dimensional density of states. We shall also nominate the density of states at the Fermi level (ϵ_F) by $\nu_0 \equiv \nu(\epsilon_F)$.

An inspection in Eq. 2.17 reveals a problem in the ultraviolet limit: a divergence proportional to $\sqrt{\epsilon}$. To understand this issue we recall that the two-body interaction in a fermion gas is

[2] We used that $\ln \mathrm{Det}\, \mathbf{A} = \mathrm{Tr} \ln \mathbf{A}$ for any non-singular square matrix $\mathbf{A}$.

[3] The procedure of ignoring the quantum fluctuations of some operators and replace them by their averages is known as the mean-field approximation.

[4] To calculate the dynamical equations it is simpler to consider Δ and $\bar{\Delta}$ as independent fields and only then apply the s-wave ansatz. In this case we have two variational equations providing exactly the same information so we do not need to repeat it. This will be particularly useful in the two-band system where the calculations are not so straightforward.

attractive only beyond a minimum distance a_0 (the effective size of the bound state) which is assumed to be much smaller than the average interparticle spacing k_F^{-1}, i. e., the condition for a dilute gas regime. Therefore the momentum sum should be submitted to a natural cut-off of the order $\sim a_0^{-1}$. On the other hand, in conventional superconductors, where the pairing mechanism is the electron-phonon attraction, the cut-off parameter is played by the lattice characteristic frequency, namely the Debye frequency $\omega_D \ll \epsilon_F$, and only a fraction of electrons in the vicinity of the Fermi surface $[\epsilon_F - \omega_D, \epsilon_F + \omega_D]$ takes part in the superconducting phase.

However the cut-off approach is less reliable if dealing with poorly understood microscopic physics like SCES. Thus it is convenient to replace the microscopic parameter with a more phenomenological one. It has originally been done in 1947 by N. Bogoliubov [32] with a regularization procedure relating the s-wave scattering length a_s of fermions to the bare coupling parameter g as

$$\frac{m}{4\pi a_s} = -\frac{1}{g(\Lambda)} + \sum_{|\mathbf{k}|<\Lambda} \frac{1}{2\epsilon_{\mathbf{k}}} = -\frac{1}{g(\Lambda)} + \frac{m\Lambda}{2\pi^2}, \tag{2.18}$$

where Λ is a momentum cut-off (usually much higher than the Fermi wavelength k_F so it is assumed $\Lambda \to \infty$) and, as expected, the sum term in Eq. 2.18 cancels out the UV divergence in Eq. 2.17.

Furthermore in the BCS regime, characterized by $g \to 0$, the cut-off term is negligible thus the scattering length scales as $a_s = -mg/(4\pi) \to 0^-$; conversely in the BEC regime $g \to \infty$ so $a_s = \pi/(2\Lambda) \to 0^+$ as $\Lambda \to \infty$. It is also possible to show [33] that for a negative scattering length there is the presence of a two-body bound state with energy $-E_B = -1/(ma_s^2)$. In the cold gas literature the ratio of the interparticle distance to the scattering length is a dimensionless parameter often used to classify the system. So the weak coupling regime is associated to $(k_F a_s)^{-1} \ll -1$, while the strong coupling one is described by $(k_F a_s)^{-1} \gg +1$. It is interesting to note that the point $(k_F a_s)^{-1} = 0$ not only corresponds to the bound state formation, but also (at zero temperature) implicates in a universal behavior of the system since all physical quantities are functions solely of the Fermi energy or the Fermi wavelength, thus resembling a unitary gas [34].

Returning to the analysis of the BCS limit we may now obtain the gap parameter as a function of the scattering length at $T = 0$. Since the chemical potential is approximately the Fermi energy $\mu \simeq \epsilon_F$ and $\tanh(\omega/T) \to 1$ the gap equation turns out to be

$$\frac{m}{2\pi a_s} = \int_0^\infty \mathrm{d}\epsilon \nu(\epsilon) \left[\frac{1}{\epsilon} - \frac{1}{\sqrt{(\epsilon - \epsilon_F)^2 + \Delta_0^2}} \right], \tag{2.19}$$

the integral can be analytically solved and results in

$$\Delta_0 = \frac{8\epsilon_F}{e^2} \exp\left(-\frac{\pi}{2k_F |a_s|} \right), \quad \text{for} \quad (k_F a_s)^{-1} \ll -1, \tag{2.20}$$

The critical temperature T_c is determined by the condition $\Delta_0 = 0$ (dissolution of the Cooper pair) so Eq. 2.17 yields

$$\frac{m}{2\pi a_s} = \int_0^\infty \mathrm{d}\epsilon \nu(\epsilon) \left[\frac{1}{\epsilon} - \frac{\tanh[(\epsilon - \epsilon_F)/2T_c]}{\epsilon - \epsilon_F} \right] \tag{2.21}$$

and one obtains[5]

$$T_c = \frac{8\epsilon_F}{\pi e^{2-\gamma}} \exp\left(-\frac{\pi}{2k_F|a_s|}\right), \quad \text{for} \quad (k_F a_s)^{-1} \ll -1, \tag{2.22}$$

where $\gamma = 0.577$ is the Euler-Mascheroni constant and we see that both gap and critical temperature decrease exponentially with $|a_s^{-1}|$. Here the Fermi energy plays an analogous role as the Debye frequency in the original BCS treatment, where $\Delta_0 = 2\omega_D \exp(-1/g\nu_0)$ and $T_c = (2e^\gamma/\pi)\omega_D \exp(-1/g\nu_0)$. Note that the ratio $\Delta_0/T_c \simeq 1.764$ remains the same no matter if one uses the frequency cut-off or the scattering length regularization. The isotope effect is also reproduced since $T_c \propto \omega_D \propto M^{-1/2}$.

2.2.2 Fermions in the Strong Coupling Regime

As already discussed, the BEC limit is characterized by a positive scattering length and a chemical potential below excitations minimum. Here however the variation of the chemical potential must be taken into account. Also, in the limit $(k_F a_s)^{-1} \gg 1$, the critical temperature (we shall call it T_0 for a reason that will soon become clear) is expected to be much smaller than the absolute value of the chemical potential $T_0 \ll |\mu|$ so that Eq. 2.17 reads

$$\frac{m}{2\pi a_s} = \int_0^\infty \mathrm{d}\epsilon \nu(\epsilon) \left(\frac{1}{\epsilon} - \frac{1}{\epsilon - \mu}\right), \tag{2.23}$$

and, differently from the weak coupling case, it determines how the chemical potential scales with the scattering length[6]

$$\mu(T_0) = -\frac{\epsilon_F}{(k_F a_s)^2} = -\frac{E_B}{2}, \quad \text{for} \quad (k_F a_s)^{-1} \gg 1 \tag{2.24}$$

where, as previously mentioned, E_B is the bound state energy.

In the strong coupling regime, T_0 is derived from the occupation number equation, extracted from $n = T\partial_\mu \ln \mathcal{Z}$, and resulting in

$$\begin{aligned} n(\mu, T) &= \sum_{\mathbf{k}} (1) + T\partial_\mu (\ln \mathrm{Det}\, \mathbf{G}_k^{-1}) \\ &= \sum_{\mathbf{k}} \left[1 + T\partial_\mu \sum_{\omega_n} \ln(\omega_n^2 + \omega_{\mathbf{k}}^2)\right] \\ &= \sum_{\mathbf{k}} \left[1 - \frac{\xi_{\mathbf{k}}}{\omega_{\mathbf{k}}} \tanh\left(\frac{\omega_{\mathbf{k}}}{2T}\right)\right], \end{aligned} \tag{2.25}$$

where the first contribution in Eq. 2.25 comes from the constant term in the effective action that appears when using the Nambu representation.

At $T = T_0$ the gap parameter vanishes and we are left with the usual expression

$$n(\mu, T_0) = 2\sum_{\mathbf{k}} n_F(\xi_{\mathbf{k}}) = 2\int_0^\infty \frac{\mathrm{d}\epsilon \nu(\epsilon)}{\exp[(\epsilon - \mu)/T_0] + 1}, \tag{2.26}$$

[5] Knowing that $\int_0^\infty \mathrm{d}x \sqrt{x} \left[\frac{\tanh((x-1)/2T)}{x-1} - \frac{1}{x}\right] = 2\ln\left(\frac{8e^{\gamma-2}}{\pi T}\right)$.

[6] Using $\int_0^\infty \mathrm{d}x \sqrt{x} \left(\frac{1}{x} - \frac{1}{x+a}\right) = \pi\sqrt{a}$ for $a > 0$.

with the factor 2 associated with the spin degeneracy.

The chemical potential is such that the particle number is kept constant at any given temperature. In particular $T = 0$K allowing us to normalize Eq. 2.26 by $n = \sum_\sigma \int_0^{\epsilon_F} \mathrm{d}\epsilon \nu(\epsilon) = \frac{4}{3}\nu_0 \epsilon_F$. Using the result provided by Eq. 2.24, we can estimate T_0 in the strong coupling regime as[7]

$$T_0 \simeq \frac{1}{3} \frac{E_B}{\ln(E_B/\epsilon_F)}, \quad \text{for} \quad (k_F a_s)^{-1} \gg 1. \tag{2.27}$$

Eq. 2.27 shows an unsettling result. While we expected a saturated behavior to the condensation temperature as in Eq. 2.6 we see that T_0 actually diverges as $(k_F a_s)^{-1} \to \infty$. In part this expectation is due to the misconceived analogy of the pair formation in the BCS limit in which the critical temperature is directly linked to the dissociation of the Cooper pairs. However in the BEC limit dissociation and condensation temperatures are not the same ($T_0 \neq T_c$), indeed T_0 appears to be associated with large pseudogaps in HTSC [35]. Since the mean-field approximation is adequate to describe slow varying fields we can now understand why it fails to reproduce the BEC physics: in the high temperature scenario thermal fluctuations can no longer be neglected.

Lastly, at $T = 0$ we still have $\mu \simeq -E_B/2$ so Eq. 2.25 reads

$$\frac{4}{3}\nu_0 \epsilon_F = \int_0^\infty \mathrm{d}\epsilon \nu(\epsilon) \left[1 - \frac{\epsilon + E_B/2}{\sqrt{(\epsilon + E_B/2)^2 + \Delta_0^2}} \right] \tag{2.28}$$

and provides a solution for the gap parameter[8]

$$\Delta_0 \simeq \frac{2\sqrt{2}}{\sqrt{\pi}} \frac{\epsilon_F}{\sqrt{k_F a_s}}, \quad \text{for} \quad (k_F a_s)^{-1} \gg 1, \tag{2.29}$$

which also diverges in the strong coupling regime. These and the previous section's results can also be found through other calculation methods as pointed out in Ref. [36].

2.3 The BCS-BEC Crossover

Up to now we have been able to obtain the analytical behavior of the physical quantities at both ends of the scattering length and even though a continuous evolution between them was long considered [1] it had not been demonstrated until 1980 by A. J. Leggett [3]. He noted the common structure shared by the ground state wave functions of the BCS and BEC regimes what lead him to consider an evolution without a phase transition. In his original work at $T = 0$ he obtained the same mean-field equations as we did in the previous section, namely

$$\int_0^\infty \mathrm{d}\tilde{\epsilon} \sqrt{\tilde{\epsilon}} \left[\frac{1}{\tilde{\epsilon}} - \frac{1}{\sqrt{(\tilde{\epsilon} - \tilde{\mu})^2 + \tilde{\Delta}_0^2}} \right] = \frac{\pi}{k_F a_s} \tag{2.30}$$

$$\int_0^\infty \mathrm{d}\tilde{\epsilon} \sqrt{\tilde{\epsilon}} \left[1 - \frac{\tilde{\epsilon} - \tilde{\mu}}{\sqrt{(\tilde{\epsilon} - \tilde{\mu})^2 + \tilde{\Delta}_0^2}} \right] = \frac{4}{3}, \tag{2.31}$$

[7] Knowing that $\int_0^\infty \frac{\mathrm{d}x \sqrt{x}}{\exp(x+a)+1} = -\frac{\sqrt{\pi}}{2} \mathrm{Li}_{3/2}(-e^{-a})$, where $\mathrm{Li}_s(z) = \sum_{k=1}^\infty \frac{z^k}{k^s}$ is the polylogarithm function.

[8] Using $\int_0^\infty \mathrm{d}x \sqrt{x} \left(1 - \frac{x+a}{\sqrt{(x+a)^2 + b^2}} \right) = \frac{2}{3}(a^2+b^2)^{1/4} \left[(\sqrt{a^2+b^2} + a) K(x) - 2aE(x) \right] \overset{a \gg b}{=} \frac{\pi}{6} \frac{b^2}{\sqrt{a}}$, where $K(x)$ and $E(x)$ are elliptic integrals of first and second kind respectively, with parameter $x = 1/2 - a/(2\sqrt{a^2+b^2})$.

where the tilde symbol indicates dimensionless quantities scaled by the Fermi energy. Although a complete analytical solution is not possible (or at least it has not yet been found) it is a numerically achievable task. Self-consistent solutions of Eqs. 2.30 and 2.31 are shown in Fig. 2.4 where the chemical potential, starting from the Fermi level, decreases and becomes negative as the coupling strength increases. On the other hand, the energy gap goes to zero in the weak coupling regime and grows abruptly in the BEC limit, as expected from the previous analytical results.

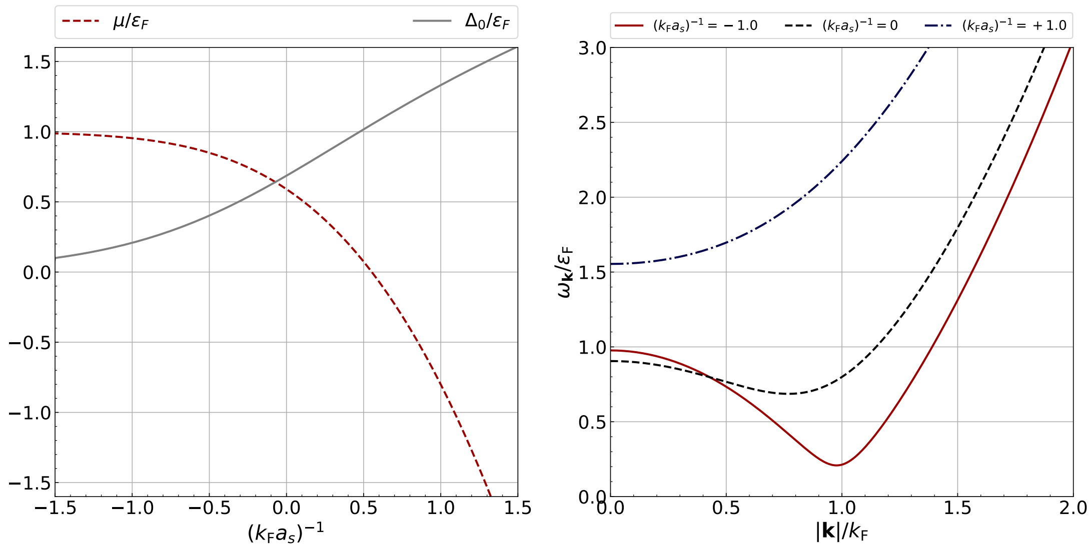

Figure 2.4: In the left panel we have the BCS-BEC crossover; the red line represents the decrease of the chemical potential and the blue one shows the increase of the gap parameter as function of the scattering length at $T = 0\text{K}$. The right panel shows the excitation energy for $(k_F a_s)^{-1} = \{-1, 0, +1\}$; as the excitation reaches zero, the gap closes and superconductivity is lost.

Close to the transition point, we can extend the analysis to finite temperatures where the mean-field equations hold

$$\int_0^\infty \mathrm{d}\tilde{\epsilon}\sqrt{\tilde{\epsilon}}\left[\frac{1}{\tilde{\epsilon}} - \frac{\tanh[(\tilde{\epsilon}-\tilde{\mu})/(2\tilde{T}_0)]}{\tilde{\epsilon}-\tilde{\mu}}\right] = \frac{\pi}{k_F a_s} \tag{2.32}$$

$$\int_0^\infty \mathrm{d}\tilde{\epsilon}\sqrt{\tilde{\epsilon}}\left[1 - \tanh\left(\frac{\tilde{\epsilon}-\tilde{\mu}}{2\tilde{T}_0}\right)\right] = \frac{4}{3}, \tag{2.33}$$

and solving them numerically provides us with Fig. 2.5.

The existence of a mathematical solution in the crossover region gives a solid indication of a smooth transition between the BCS and BEC limits, however its physical correspondence in the strong coupling regime, as already discussed, is not so trustworthy; this issue is addressed next.

2.4 Thermal Fluctuations

From Eq. 2.27 and the divergence of T_0 in Fig. 2.5 we see that the mean-field hypothesis is unable to reproduce the proper BEC condensation temperature expressed by Eq. 2.6. To physically understand it we observe that in the BCS regime the Cooper pair is diluted in space

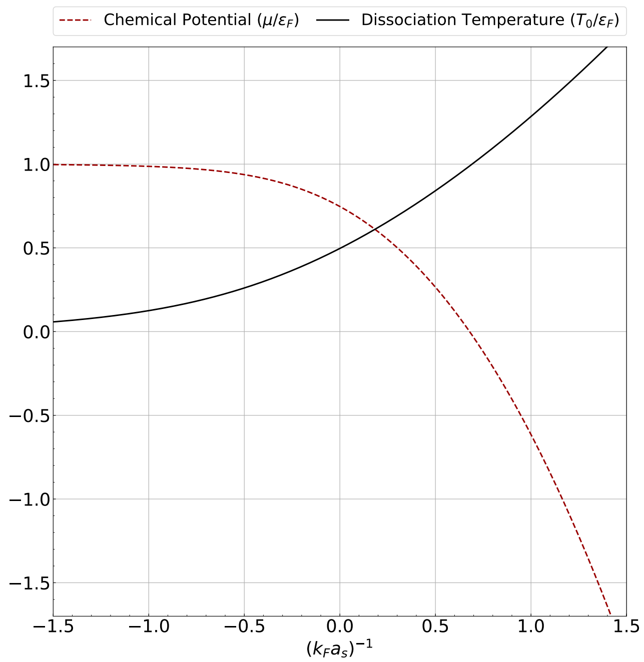

Figure 2.5: BCS-BEC crossover at finite temperature; the red line represents the decrease of the chemical potential and the blue one shows the increase of the dissociation temperature as function of the scattering length around the crossover region.

and characterized by a low critical temperature which justifies its description by a mean-field treatment. However as we approach the strong-coupling regime the bosonic pair becomes more localized and the temperature scale increases derailing its representation by a constant field.

Mathematically we shall consider the thermal fluctuations as a one-loop correction around the saddle-point solution, $\Delta = \Delta_0 + \Delta_q$, with $\Delta_q \ll \epsilon_{\mathrm{F}}$ and, since we are interested in the vicinity of the transition point, we assume $\Delta_0 \simeq 0$. Our strategy is to correct the effective action, show its equivalence to a non-interacting bosonic one and then extract the proper condensation temperature.

We start recalling the effective action, Eq. 2.12, in the momenta space

$$S[\Delta] = \frac{1}{g}\sum_q |\Delta_q|^2 - \operatorname{Tr}\ln \mathbf{G}_\Delta^{-1}, \tag{2.34}$$

where the inverse Nambu-Gorkov Green's function can be split into its free and interacting components

$$\mathbf{G}_\Delta^{-1}(k,q) = \underbrace{\begin{pmatrix} i\omega_n - \xi_{\mathbf{k}} & 0 \\ 0 & i\omega_n + \xi_{\mathbf{k}} \end{pmatrix}}_{\mathbf{G}_0^{-1}(k)} + \underbrace{\begin{pmatrix} 0 & \Delta_q \\ \bar{\Delta}_{-q} & 0 \end{pmatrix}}_{\mathbf{\Delta}(q)}; \tag{2.35}$$

and expanding the logarithm function for $\mathbf{\Delta} \ll \mathbf{G}_0^{-1}$ we may rewrite

$$S[\Delta] = -\operatorname{Tr}\ln \mathbf{G}_0{}^{-1} + \frac{1}{g}\sum_q |\Delta_q|^2 + \sum_{n=1}^{\infty} \frac{1}{2n}\operatorname{Tr}(\mathbf{G}_0\mathbf{\Delta})^{2n}, \tag{2.36}$$

where the odd terms vanish due to the off-diagonal shape of $\mathbf{\Delta}$ and the operator $\mathbf{G}_0$ is a particular case of Eq. 2.14 for $\Delta_0 = 0$

$$\mathbf{G}_0(k) = \begin{pmatrix} G_k & 0 \\ 0 & -G_{-k} \end{pmatrix}, \tag{2.37}$$

with $G_k \equiv (i\omega_n - \xi_\mathbf{k})^{-1}$ the Green's function of a single free fermion.

Thus the zeroth order term $S^{(0)} = -\operatorname{Tr}\ln \mathbf{G}_0{}^{-1}$ is just the free-energy of the non-interacting fermionic system discussed in the mean-field analysis; while the second order correction is given by

$$S^{(2)} = \frac{1}{g}\sum_q |\Delta_q|^2 + \frac{1}{2}\operatorname{Tr}(\mathbf{G}_0\mathbf{\Delta})^2; \tag{2.38}$$

the fourth order term corresponds to a repulsive two-body interaction between bosons and does not alter substantially the condensation temperature so we may restrict ourselves to one-loop correction.

Furthermore the gaussian action can expressed as $S^{(2)} = \sum_q \Gamma_q^{-1}|\Delta_q|^2$, where we have introduced the well-known vertex function

$$\Gamma_q^{-1} \equiv \frac{1}{g} - \frac{1}{\beta}\sum_{\mathbf{k},\omega_n} G_k G_{-k+q}. \tag{2.39}$$

Recalling that ω_n and ω_m are, respectively, fermionic and bosonic frequencies we can write $i\omega_{n+m} = i\omega_n + i\omega_m$ so the summation over the odd frequencies results in (see App. B for more details)

$$\frac{1}{\beta}\sum_{\omega_n} G_k G_{-k+q} = -\frac{1 - n_F(\xi_\mathbf{k}) - n_F(\xi_{\mathbf{k}-\mathbf{q}})}{i\omega_m - \xi_\mathbf{k} - \xi_{\mathbf{k}-\mathbf{q}}}, \tag{2.40}$$

and finally with the translation $\mathbf{k} \to \mathbf{k} + \mathbf{q}/2$

$$\xi_\mathbf{k} + \xi_{\mathbf{k}-\mathbf{q}} \to \xi_{\mathbf{k}+\mathbf{q}/2} + \xi_{\mathbf{k}-\mathbf{q}/2} = 2\xi_\mathbf{k} + \frac{\mathbf{q}^2}{4m} \tag{2.41}$$

it is easy to see that the linear contribution in $\mathbf{q}$ vanishes yielding

$$\boxed{\Gamma_q^{-1} = \frac{1}{g} + \sum_\mathbf{k} \frac{1 - n_F(\xi_{\mathbf{k}+\mathbf{q}/2}) - n_F(\xi_{\mathbf{k}-\mathbf{q}/2})}{i\omega_m - 2\xi_\mathbf{k} - \mathbf{q}^2/4m}.} \tag{2.42}$$

Eq. 2.42 is the most general form Γ_q^{-1} can assume, so now let us consider the limits of interest.

2.4.1 BEC Limit

In the strong coupling regime we have a negative chemical potential and $|\mu| \gg T_c$, thus $n_F(\xi_\mathbf{k}) \to 0$ and the vertex function can be solved exactly

$$\begin{aligned} \Gamma_q^{-1} &= -\frac{m}{4\pi a_s} + \sum_\mathbf{k}\left(\frac{1}{2\epsilon_\mathbf{k}} - \frac{1}{2\xi_\mathbf{k} - i\omega_m + \mathbf{q}^2/4m}\right) \\ &= -\frac{m}{4\pi a_s} + \frac{\pi}{2}\frac{\nu_0}{\sqrt{\epsilon_F}}\sqrt{-\mu - \frac{i\omega_m}{2} + \frac{\mathbf{q}^2}{8m}}. \end{aligned} \tag{2.43}$$

Considering a gradient expansion for small momenta $q \ll k_F$ we may write

$$\sqrt{-\mu - \frac{i\omega_m}{2} + \frac{\mathbf{q}^2}{8m}} \simeq \sqrt{-\mu} + \frac{-i\omega_m + \mathbf{q}^2/4m}{4\sqrt{-\mu}} \tag{2.44}$$

and with a reparametrization of the fields to incorporate the overall multiplicative factor, using $k_F = 2\pi^2\nu_0/m$ together with Eq. 2.24, we finally arrive at

$$S_{\text{BEC}}[\Delta] = \sum_q \bar{\Delta}_q \left(-i\omega_m + \frac{\mathbf{q}^2}{4m} - \mu_{\text{eff}} \right) \Delta_q, \tag{2.45}$$

which in fact represents the propagation of non-interacting bosons with mass $2m$ subjected to the effective chemical potential $\mu_{\text{eff}} = 4(\mu + \sqrt{-\mu E_B/2})$. Close to the transition point $\mu_{\text{eff}} \simeq 2\mu + E_B$ and the effective number of particles n_{eff} is related to the original n fermions by

$$n_{\text{eff}} = \frac{\partial \mu}{\partial \mu_{\text{eff}}} n \simeq \frac{n}{2} \tag{2.46}$$

indicating, as expected, the bound pairs formed by all fermions. Thus the system's transition temperature is the same as the one calculated in Sec. 2.1 with half the density and twice the mass.

2.4.2 BCS Limit

Even though the weak coupling regime remains essentially unaltered by the gaussian fluctuations, it is instructive to establish the BCS action in order to compare it with the BEC one. Differently from what has been done so far, here we will use the standard energy-cut off ω_D from the BCS over the regularization given by Eq. 2.18 for no other reason than calculation convenience.

In this regime the Fermi function cannot be neglected but the expansion for $\mathbf{q}$ is still valid and thus the vertex function yields

$$\begin{aligned} \Gamma_q^{-1} &= \frac{1}{g} + \int \mathrm{d}\epsilon \nu(\epsilon) \frac{1 - 2n_F(\xi) - (\mathbf{q}^2/2m)\epsilon \partial_\epsilon^2 n_F(\xi)}{i\omega_m - 2\xi - \mathbf{q}^2/4m} \\ &= \frac{1}{g} + \int \mathrm{d}\epsilon \nu(\epsilon) \frac{1 - 2n_F(\xi)}{i\omega_m - 2\xi} + \frac{\mathbf{q}^2}{2m} \int \mathrm{d}\epsilon \frac{\nu(\epsilon)}{2\xi} \left[\frac{1 - 2n_F(\xi)}{2\xi} + \epsilon \partial_\epsilon^2 n_F(\xi) \right] \end{aligned} \tag{2.47}$$

where the first $\mathbf{q}^2$ integral vanishes due to its antisymmetric character

$$\int \mathrm{d}\epsilon \nu(\epsilon) \frac{1 - 2n_F(\xi)}{(2\xi)^2} \simeq \nu_0 \int_{\epsilon_F - \omega_D}^{\epsilon_F + \omega_D} \mathrm{d}\epsilon \frac{\tanh(\xi/2T_c)}{(2\xi)^2} = 0 \tag{2.48}$$

and the other integral is known to result in

$$\int \mathrm{d}\epsilon \nu(\epsilon) \frac{\epsilon \partial_\epsilon^2 n_F(\xi)}{2\xi} \simeq \frac{7\zeta(3)}{4\pi^2} \frac{\nu_0 \epsilon_F}{T_c^2} \tag{2.49}$$

with $\zeta(3) \simeq 1.202$.

The ω_m expansion is not as straightforward since the main contribution from this integral comes from small values of $\xi_{\mathbf{k}}$. We have

$$\int \mathrm{d}\epsilon\nu(\epsilon)\frac{1-2n_F(\xi)}{i\omega_m-2\xi} \simeq \nu_0\int_{\epsilon_F-\omega_D}^{\epsilon_F+\omega_D}\mathrm{d}\epsilon\frac{\tanh(\xi/2T_c)}{i\omega_m-2\xi}$$

$$= \nu_0\int_{-\frac{\omega_D}{2T_c}}^{+\frac{\omega_D}{2T_c}}\mathrm{d}x\left(\frac{\tanh x}{i\omega_m/2T_c-2x}+\frac{\tanh x}{2x}-\frac{\tanh x}{2x}\right) \tag{2.50}$$

where in the second line we have added and subtracted Γ_0^{-1} responsible for the integral convergence

$$\int_0^{\frac{\omega_D}{2T_c}}\mathrm{d}x\frac{\tanh x}{x} \simeq \ln\left(\frac{\omega_D}{2T_c}\right). \tag{2.51}$$

The antisymmetric part of Eq. 2.50 will only be relevant in the region $2x \simeq i\omega_m/2T_c \simeq 0$ allowing us to take $\tanh x \simeq x$

$$\int \mathrm{d}\epsilon\nu(\epsilon)\frac{1-2n_F(\xi)}{i\omega_m-2\xi} = -\nu_0\ln\left(\frac{\omega_D}{2T_c}\right)+\nu_0\int_{-\infty}^{+\infty}\mathrm{d}x\frac{\tanh x}{2x}\frac{(i\omega_m/2T_c)^2}{(i\omega_m/2T_c)^2-(2x)^2}$$

$$\simeq -\nu_0\ln\left(\frac{\omega_D}{2T_c}\right)+\nu_0\left(\frac{\omega_m}{2T_c}\right)^2\int_0^{\infty}\frac{\mathrm{d}x}{(\omega_m/2T_c)^2+(2x)^2}$$

$$\simeq -\nu_0\ln\left(\frac{\omega_D}{2T_c}\right)+\pi\nu_0\frac{|\omega_m|}{8T_c}, \tag{2.52}$$

where we have taken $\omega_D \gg T_c$; thus

$$\Gamma_q^{-1} = \frac{1}{g}-\nu_0\ln\left(\frac{\omega_D}{2T_c}\right)+\pi\nu_0\frac{|\omega_m|}{8T_c}+\frac{7\zeta(3)}{4\pi^2}\frac{\nu_0\epsilon_F}{T_c^2}\frac{\mathbf{q}^2}{2m} \tag{2.53}$$

and the action takes the form

$$S_{\mathrm{BCS}}[\Delta] \approx \sum_q\bar{\Delta}_q\left(\frac{T_c}{\epsilon_F}|\omega_m|+\frac{\mathbf{q}^2}{4m}+const.\right)\Delta_q, \tag{2.54}$$

which differs from the BEC case by the presence of the absolute value of ω_m (the imaginary factor is absent) indicating a damped mode in the BCS limit.

2.5 BCS-BEC Crossover Corrected for Finite Temperature

Once we have showed that the inclusion of the gaussian fluctuations correctly reproduces a Bose gas in the strong coupling regime, one might wonder how it affects the whole BCS-BEC crossover. This inquiry started in 1985 with Nozières and Schmitt-Rink [4] and reached a conclusion only eight years later with Sá de Melo et. al. [5]. Since a constant pairing field does not contemplate the formation of the bosonic pair properly we may expect the main alteration in our coupled equations to be in the occupation number. Thus we use the vertex function to write down the correction to Eq. 2.25 as

$$\delta n = \frac{1}{\beta}\frac{\partial}{\partial\mu}\sum_q\ln\Gamma_q^{-1}, \tag{2.55}$$

separating the real and imaginary parts of the vertex function $\Gamma_q^{-1} = \mathrm{Re}\Gamma_q^{-1} - i\mathrm{Im}\Gamma_q^{-1}$, where

$$\mathrm{Re}\Gamma_q^{-1} = \frac{1}{g} - \sum_{\mathbf{k}} \left(2\xi_{\mathbf{k}} + \frac{\mathbf{q}^2}{4m}\right) \frac{1 - n_F(\xi_{\mathbf{k}+\mathbf{q}/2}) - n_F(\xi_{\mathbf{k}-\mathbf{q}/2})}{\omega_m^2 + (2\xi_{\mathbf{k}} + \mathbf{q}^2/4m)^2}, \tag{2.56}$$

$$\mathrm{Im}\Gamma_q^{-1} = \omega_m \sum_{\mathbf{k}} \frac{1 - n_F(\xi_{\mathbf{k}+\mathbf{q}/2}) - n_F(\xi_{\mathbf{k}-\mathbf{q}/2})}{\omega_m^2 + (2\xi_{\mathbf{k}} + \mathbf{q}^2/4m)^2} \tag{2.57}$$

we may write $\Gamma^{-1}(\mathbf{q}, \omega \pm i0) = |\Gamma_q^{-1}| \exp[\pm i\phi(\mathbf{q}, \omega)]$ with $\phi(\mathbf{q}, \omega) = \arctan\left(\frac{\mathrm{Im}\Gamma_q^{-1}}{\mathrm{Re}\Gamma_q^{-1}}\right)$.

We can evaluate the sum over the bosonic frequencies by noting that the integral over the contour C will assume non zeros values only at the vicinity of the logarithm branch cut

$$\begin{aligned}
\frac{1}{\beta} \sum_{\omega_m} \ln \Gamma_q^{-1} &= \frac{1}{2\pi i} \int_C \mathrm{d}\omega n_B(\omega) \ln \Gamma_q^{-1} \\
&= \frac{1}{2\pi i} \int_{-\infty}^{+\infty} \mathrm{d}\omega n_B(\omega) \left\{ \ln[|\Gamma_q^{-1}| \exp(+i\phi)] - \ln[|\Gamma_q^{-1}| \exp(-i\phi)] \right\} \\
&= \frac{1}{\pi} \int_{-\infty}^{+\infty} \mathrm{d}\omega n_B(\omega) \phi(\mathbf{q}, \omega),
\end{aligned} \tag{2.58}$$

where $n_B(\omega)$ is the Bose distribution. Thus the corrected number equation becomes[9]

$$n(\mu, T) = \sum_{\mathbf{k}} \left[1 - \tanh\left(\frac{\xi_{\mathbf{k}}}{2T}\right)\right] + \sum_{\mathbf{q}} \int_{-\infty}^{+\infty} \frac{\mathrm{d}\omega}{\pi} n_B(\omega) \partial_\mu \phi(\mathbf{q}, \omega), \tag{2.59}$$

with the second term describing the effect of pair correlations and, in the strong coupling regime, the formation of bound states.

The gap equation 2.17 does not require further modification since it is responsible for the determination of the chemical potential that is accurately described within the mean-field analysis. So bringing together the coupled equations we obtain the numerical solution showed in Fig. 2.6, where the condensation temperature has a peak around the unitarity point and then saturates at $T_c \simeq 0.218\epsilon_F$ in the strong-coupling regime. Despite the slightly higher result at the unitary point than the one predicted by quantum Monte Carlo simulations [37, 38] the fluctuation approach is in good agreement with the overall behavior of the BCS-BEC transition.

[9]Explicitly $\partial_\mu \phi(\mathbf{q}, \omega) = (\mathrm{Re}\Gamma_q^{-1} \partial_\mu \mathrm{Im}\Gamma_q^{-1} - \mathrm{Im}\Gamma_q^{-1} \partial_\mu \mathrm{Re}\Gamma_q^{-1}) / |\Gamma_q^{-1}|^2$ where the derivatives are

$$\begin{aligned}
\partial_\mu \mathrm{Re}\Gamma_q^{-1} = 2 \sum_{\mathbf{k}} &\left[\omega_m^2 - \left(2\xi_{\mathbf{k}} + \frac{\mathbf{q}^2}{4m}\right)^2\right] \frac{1 - n_F(\xi_{\mathbf{k}+\mathbf{q}/2}) - n_F(\xi_{\mathbf{k}-\mathbf{q}/2})}{[\omega_m^2 + (2\xi_{\mathbf{k}} + \mathbf{q}^2/4m)^2]^2} \\
&+ \sum_{\mathbf{k}} \left(2\xi_{\mathbf{k}} + \frac{\mathbf{q}^2}{4m}\right) \frac{\partial_\mu [n_F(\xi_{\mathbf{k}+\mathbf{q}/2}) + n_F(\xi_{\mathbf{k}-\mathbf{q}/2})]}{\omega_m^2 + (2\xi_{\mathbf{k}} + \mathbf{q}^2/4m)^2}
\end{aligned}$$

and

$$\partial_\mu \mathrm{Im}\Gamma_q^{-1} = 4\omega_m \sum_{\mathbf{k}} \left(2\xi_{\mathbf{k}} + \frac{\mathbf{q}^2}{4m}\right) \frac{1 - n_F(\xi_{\mathbf{k}+\mathbf{q}/2}) - n_F(\xi_{\mathbf{k}-\mathbf{q}/2})}{[\omega_m^2 + (2\xi_{\mathbf{k}} + \mathbf{q}^2/4m)^2]^2} - \omega_m \sum_{\mathbf{k}} \frac{\partial_\mu [n_F(\xi_{\mathbf{k}+\mathbf{q}/2}) + n_F(\xi_{\mathbf{k}-\mathbf{q}/2})]}{\omega_m^2 + (2\xi_{\mathbf{k}} + \mathbf{q}^2/4m)^2},$$

with $\partial_\mu n_F(\xi_{\mathbf{k}\pm\mathbf{q}/2}) = \beta n_F(\xi_{\mathbf{k}\pm\mathbf{q}/2})[1 - n_F(\xi_{\mathbf{k}\pm\mathbf{q}/2})]$.

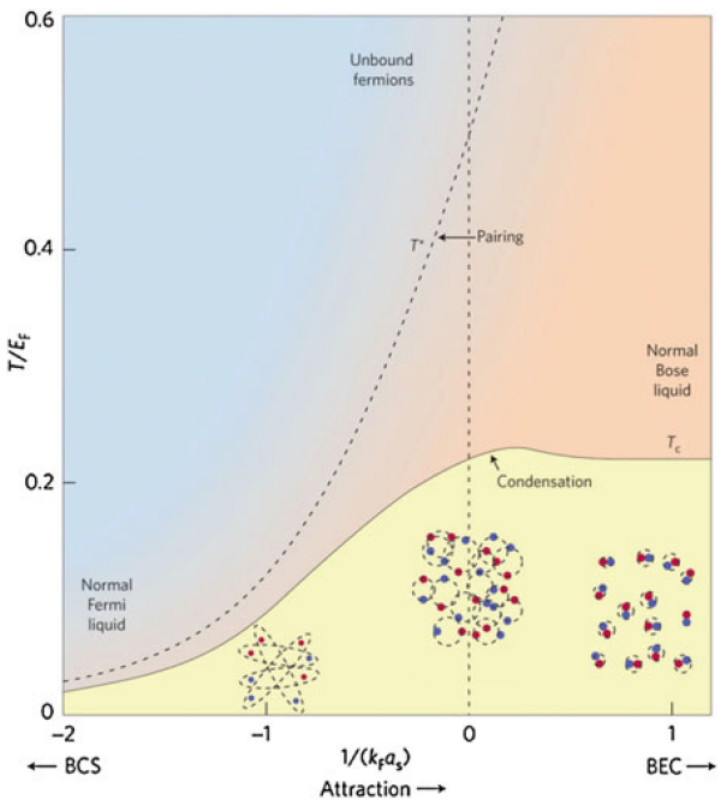

Figure 2.6: Critical temperature profile as function of the ratio $(k_F a_s)^{-1}$. The BCS limit corresponds to $(k_F a_s)^{-1} \to -\infty$ while the BEC limit is obtained as $(k_F a_s)^{-1} \to +\infty$. The divergence represented by the dashed line in the strong coupling regime corresponds to the dissociation temperature; a more physical result is obtained in the full line with the inclusion of the thermal fluctuations. Figure extracted from Ref. [39].

2.6 BCS-BEC Crossover in Fermi Gases with Spin-orbit Coupling

About two decades of theoretical investigation have passed before the experimental realization of the crossover in ultracold gases [6–8] and in recent studies [9, 12, 40] more complex models including spin-orbit coupling (SOC) interactions have been extensively considered, although even with the current technological improvements the tuning of SO interaction remains a challenging task. Besides the influence of SOC over the physical quantities these studies also indicate that SOC plays a similar role as the scattering length driving a BCS-BEC crossover.

Among those works the one who better suits ours is of L. He et. al. [11] where the authors consider a 3D model imbued with a synthetic uniform SU(2) gauge field

$$\mathcal{H}_{\text{SOC}}(x) = -i \sum_{i=1}^{3} \bar{\psi}_\sigma(x) \lambda_i \sigma_i \partial_i \psi_\sigma(x), \tag{2.60}$$

with λ_i $(i = x, y, z)$ representing the anisotropic SOC strengths and σ_i the Pauli matrices.

Here we shall not reproduce their calculations but limit ourselves to present their main results. A characteristic of this model is the split of the excitation spectra as $E_{\mathbf{k}}^{\pm} = \sqrt{\xi_{\mathbf{k}}^{\pm 2} + \Delta_0^2}$, with Δ_0 the usual mean-field gap and the fermion dispersion relation $\xi_{\mathbf{k}}^{\pm} = \xi_{\mathbf{k}} \pm \sqrt{\sum_{i=1}^{3} \lambda_i^2 k_i^2}$.

To simplify the analysis they consider three particular cases of interaction (1) $\lambda_x = \lambda_y = 0$ and $\lambda_z = \lambda$, called extreme prolate (EP), (2) $\lambda_x = \lambda_y = \lambda$ and $\lambda_z = 0$, called extreme oblate (EO), and (3) $\lambda_x = \lambda_y = \lambda_z$, called spherical (S). The EO SOC is physically equivalent to the Rashba SOC (which also has a direct correspondence with the hybridized two-band model we develop in the following chapter) and the EP SOC to an equal mixture of Rashba and Dresselhaus SOCs.

In Fig. 2.7 we observe the change in the temperatures profile with and without the inclusion of the thermal fluctuations, T_c and T^* respectively, for each of the particular cases mentioned. The left side plots shows the standard variation with the scattering length while the right side ones shows the temperatures evolution with the SOC strength for fixed values of the scattering length. We see that the EP case is not altered in any way by SOC since this interaction is equivalent to a constant shift in the chemical potential. The remaining cases are similar on both scenarios, the dissociation temperature increases with λ and the condensation temperature remains unaltered in the limit $(k_F a_s)^{-1} \to \infty$. As they vary λ the saturation temperature obtained is lower than in the scattering length case. As expected, in all scenarios the dissociation temperature is above the condensation one allowing the study of the pseudogaps via SOC.

Finally we observe that, in the BEC limit for the EO case, the presence of SOC induces an anisotropy in the effective bosonic mass

$$m_b^{\perp} \approx 2m \left[1 - \frac{m\lambda^2}{2E_B} - \frac{E_B - m\lambda^2}{2E_B} \ln\left(\frac{E_B - m\lambda^2}{2E_B}\right)\right]^{-1}, \tag{2.61}$$

$$m_b^{\parallel} \approx 2m, \tag{2.62}$$

where m is the fermion mass and E_B the binding energy determined by

$$\sqrt{\frac{E_B}{m\lambda^2}} - \frac{1}{2}\ln\left(\frac{\sqrt{E_B} + \sqrt{m\lambda^2}}{\sqrt{E_B} - \sqrt{m\lambda^2}}\right) = \frac{m}{\lambda a_s}. \tag{2.63}$$

In particular for a strong SOC interaction, $\lambda \gg 1$, they obtained $m_b^{\perp} \simeq 2.40m$. These results are specially interesting since analogous effects will also be present in our model.

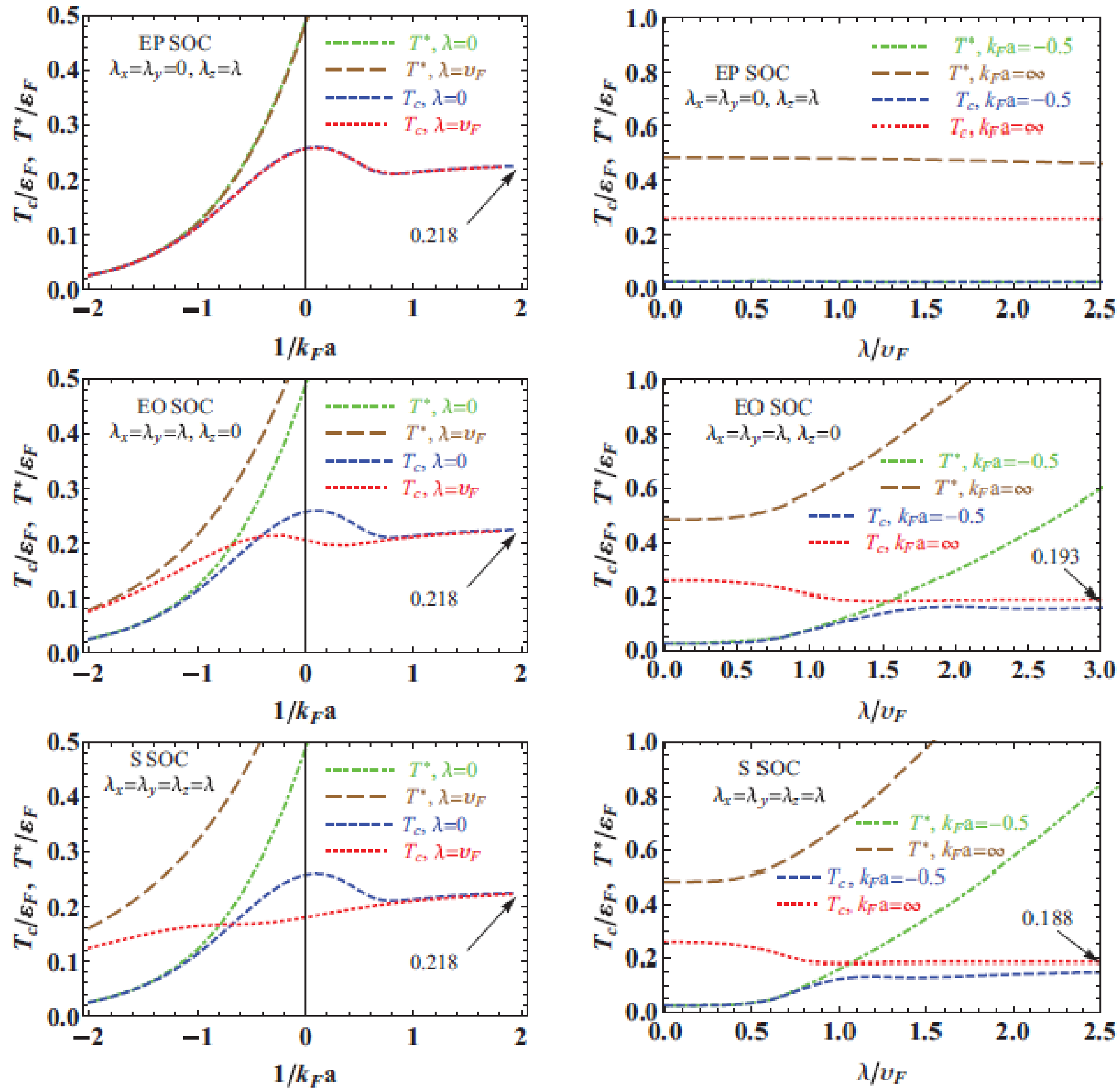

Figure 2.7: The BCS-BEC crossover in the spin-orbit coupling scenario. Comparison between the temperature profiles as function of the scattering length (left) and SOC strength (right). For the cases EO and S there is a BCS-BEC crossover induced by SOC. Extracted from Ref. [11].

Chapter 3

Two-band Superconductor with Odd-parity Hybridization: A Mean-field Analysis

In this chapter our actual contribution begins, we motivate the introduction of a hybridized two-band superconductor model, subsequently we obtain its mean-field equations and then carefully explore the numerical solutions under the influence of every physical parameter of the theory.

3.1 Superconductivity in Multi-band Systems

As previously mentioned the standard BCS model is not adequate to describe complex structures as the ones present in HTSC like cuprates compounds [41] or iron-based superconductors [42] and in heavy fermions (HF) materials that, in spite of their low critical temperature, present clear evidence of superconductivity associated to a magnetic quantum critical point [43]. The main distinction between such systems and type-I superconductors lies in the band structure; single elements superconductors show localized bands and thus can be accurately explained via *intra-band* interactions, i. e., the usual phonon driven attraction between fermions belonging to a common band. However type-II superconductors possess an intricate gap signature since several bands overlap; this feature makes them a much more complex and exciting research subject. Although multi-band superconductors have been studied for several years now the experimental breakthroughs of the last couple decades motivated many new works [44–48]. Also it has been becoming more evident the relevance of *interband* interactions in type-II superconductors [49–52].

Theoretically, the first extended model was proposed in 1959 by H. Suhl, B. Matthias and L. Walker [53] where the authors considered a two-band superconductor with s-s and d-d interactions together with an interband attraction between the itinerant s and d electrons. The latter is described by the Hamiltonian $\hat{\mathcal{H}}_{\rm SMW} \propto -\sum_{\mathbf{k}\mathbf{k}'} \hat{s}^\dagger_{\mathbf{k}\uparrow}\hat{s}^\dagger_{-\mathbf{k}\downarrow}\hat{d}_{-\mathbf{k}'\downarrow}\hat{d}_{\mathbf{k}'\uparrow}$, with $\hat{s}$ ($\hat{s}^\dagger$) and $\hat{d}$ ($\hat{d}^\dagger$) the annihilation (creation) operators of the s and d electrons, respectively. They predicted the existence of two superconducting gaps which was experimentally verified by J. Nagamatsu et. al. in magnesium diboride (MgB_2) [54, 55] more than 40 years later.

Another possibility of interband scattering well suited for cuprates [56], cold atom systems [57] and even quantum chromodynamics [58] was studied in 1987 by O. V. Dolgov et. al. [59, 60] to describe heavy fermion systems with coupling between (d- and f-) electrons with very distinct effective masses following the Hamiltonian $\hat{\mathcal{H}}_{\text{inter}} \propto -\sum_{\mathbf{k}\mathbf{k}'\sigma} \hat{d}^{\dagger}_{\mathbf{k}\sigma}\hat{f}^{\dagger}_{-\mathbf{k}-\sigma}\hat{f}_{-\mathbf{k}'-\sigma}\hat{d}_{\mathbf{k}'\sigma}$ [1]. In solids this interaction describes a material that is simultaneously superconducting and metallic. In ultracold gases it results in a spectrum with both gapped and gapless quasiparticle excitations defining a system containing both a superfluid or a normal Fermi liquid [57]. However, this system has been shown to be unstable and therefore not physical [62, 63].

The physical process due to the interband interaction in SMW's model can be understood as the annihilation of a Cooper pair in one band, formed by electrons of the same kind, and the creation of a pair with different momentum in the other band; while in Dolgov's case the pair is hybrid and it only alters its momentum. Naturally the most sophisticated model would include both Hamiltonians, however we will be interested in HF materials which the physics are mainly captured by Dolgov's model.

It is worth to mention the repulsive Coulomb interaction between electrons, particularly important in the flat band of HF. Exploring in this direction was J. Kondo who considered the same but repulsive interband scattering as SMW, $-\mathcal{H}_{\text{SMW}}$, predicting an enhancement of superconductivity and reduction of the isotope effect over the single-band case [64]. Furthermore the repulsive potential is the core of the so called Kondo insulators [65]. In this thesis however we shall not consider it.

Finally there is the possibility of hybridization, which we address in the following.

3.1.1 Hybridization

In systems composed of different species of quasi-particles the transmutation among them is often referred as *hybridization*. Its microscopic origin varies from case to case. In transition metals [66], actinide compounds and heavy fermions [67], it is due to the wavefunctions superposition between neighboring orbitals of the lattice. In the problem of color superconductivity, it is the weak interaction that allows the transformation between down- and up-quarks [68, 69]. For a system of cold fermionic atoms in an optical lattice with two atomic states, the hybridized term is due to Raman transitions with an effective Rabi frequency which is directly proportional to the hybridization strength [70]. Furthermore, in condensed matter experiments hybridization can be tuned through doping or pressure [71] giving rise to an efficient way to explore the phase diagram of multi-band superconductors.

Additionally a direct parallel can be traced between the single-band superconductor with SOC and the two-band case with hybridization [11]. However, in contrast with the ultracold gas scenario, the fermions in metallic systems usually possess different effective masses. The ratio of these masses will play a key role in the theory which we shall explore. We will also see that, as in the SOC case, hybridization will provide an alternative way for the implementation of the BCS-BEC crossover [13].

In metallic systems, a constraint in hybridization can be found [2] by assuming that the lattice in which the electrons are immersed in, characterized by the potential $v(\mathbf{x})$, has inversion symmetry, i. e., $v(-\mathbf{x}) = v(\mathbf{x})$. Such symmetry is reflected in the electron-electron interaction through the

[1] This interband model was first presented in a more general study in 1968 by W. S. Chow [61] while analyzing two-band superconductors in the presence of nonmagnetic impurities.

[2] Although we illustrate the symmetry procedure in a condensed matter context the results are not limited to it.

hybridization (V) matrix elements

$$V_{ll'}(\mathbf{x}) = \int_{-\infty}^{+\infty} \mathrm{d}^3y\, \bar{\psi}_l(\mathbf{y}) v(\mathbf{y}) \psi_{l'}(\mathbf{y}+\mathbf{x}), \tag{3.1}$$

with $\psi_l(\mathbf{y})$ representing the electron in the orbital l. Expressing the wave-functions in spherical coordinates and after some manipulations one can show that hybridization inherits a symmetry dependent only on the difference of the quantum numbers $l' - l$[3]

$$V_{ll'}(\mathbf{x}) = (-1)^{l'-l} V_{ll'}(-\mathbf{x}). \tag{3.2}$$

Thus an even (odd) difference gives rise to an even (odd) parity hybridization. The former case was show to diminish [73] while the latter increases superconductivity [74, 75].

Since many relevant cases in condensed matter physics involves the interaction of neighboring orbitals, such as the *s-p* and *d-p* mixing present in copper oxides, and *d-f* relevant in rare-earth systems we shall consider an odd-parity hybridization which in momentum space is translated as $V_{-\mathbf{k}} = -V_{\mathbf{k}}$. Another important remark is that due to time reversal symmetry $V_{\mathbf{k}}$ has to be a purely imaginary quantity.

More specifically, having in mind HF materials which exhibits nearly a two-dimensional behavior [76], we consider the hybridization potential describing a system with tetragonal symmetry in which the main interaction between orbitals resides within the layers. Thus, with a small momentum expansion, the hybridization reads

$$V_{\mathbf{k}} = i\alpha v_F(k_x + k_y + \gamma k_z) \equiv i v_F \mathbf{v}\cdot\mathbf{k}, \tag{3.3}$$

with v_F the Fermi velocity and $\mathbf{v} = \alpha(1,1,\gamma)$ where the dimensionless parameters α and γ control, respectively, the overall strength of the hybridization and the attraction between the planes of the lattice, $|\gamma| \ll 1$. Notice that in the strong-coupling limit there are no Fermi surfaces and the Fermi velocity is then measured from the number density, $v_F \propto n^{1/3}$. Finally, we also observe that since hybridization turns a quasi-particle into another only the total particle number is conserved.

3.2 The Model

Our two-band system can be viewed as a three-dimensional dilute gas containing two species of spin 1/2 fermions represented by the Grassmann fields ψ_σ^A and ψ_σ^B. We assume that these fermions are subjected not only to the usual weak attraction responsible for the superconductivity in the A band, the *intraband* interaction, but also an attractive potential between bands, the *interband* interaction. For simplification we ignore the B band fermions interaction among themselves. It is important to point out that the microscopic origin of these interactions are not under scrutiny here so that very different systems may still be suitably described by this effective theory. Furthermore, since we are interested in materials possessing orbital overlapping, such as HF superconductors, we shall include the possibility of hybridization between bands in the specific form discussed on Sec. 3.1.1.

The emphasis will be in the interband sector in accordance with Dolgov's model with the inclusion of hybridization [13]. So within the Functional Integral Formalism we can describe our

[3]A detailed calculation can be found in Sec. 3.1 of the Ref. [72].

model through the imaginary time action $S = S_0 + S_{\text{Inter}} + S_{\text{Intra}} + S_{\text{Hyb}}$ composed by the free term

$$S_0 = \int \mathrm{d}x\, \bar{\psi}^l_\sigma(x) \left(\partial_\tau - \frac{\partial^2_{\mathbf{x}}}{2m_l} - \mu \right) \psi^l_\sigma(x), \tag{3.4}$$

where the sum over the band indexes $l = \{A, B\}$ and the spin projection $\sigma = \{\uparrow, \downarrow\}$ is implicit, m_l denotes the effective masses of the fermions subjected to a common chemical potential μ; the interband interaction

$$S_{\text{Inter}} = -\frac{g_1}{2} \int \mathrm{d}x\, \bar{\psi}^A_\sigma(x) \bar{\psi}^B_{-\sigma}(x) \psi^B_{-\sigma}(x) \psi^A_\sigma(x), \tag{3.5}$$

which is regulated by the positive coupling constant g_1; the intraband interaction

$$S_{\text{Intra}} = -g_2 \int \mathrm{d}x\, \bar{\psi}^A_\uparrow(x) \bar{\psi}^A_\downarrow(x) \psi^A_\downarrow(x) \psi^A_\uparrow(x), \tag{3.6}$$

mediated by the coupling constant g_2, and the hybridization term

$$S_{\text{Hyb}} = \int \mathrm{d}x \mathrm{d}x'\, \bar{\psi}^l_\sigma(x) V_{ll'}(\mathbf{x} - \mathbf{x}') \psi^{l'}_\sigma(x'). \tag{3.7}$$

The inter and intraband quartic terms prevent us from solving the partition function $\mathcal{Z} = \int \mathfrak{D}[\psi] e^{-S[\psi]}$ exactly. And, although the action is fairly more complex than in the single-band case, the mathematical approach is strictly the same as the one developed in the previous chapter. Thus, firstly, we shall identify the adequate degrees of freedom of the effective theory in order to use a mean-field treatment.

In our model since the Cooper pairs still play the relevant role we can perform a coupling in the Cooper channel which, upon a Fourier transform, may be written as

$$\rho_{q\sigma} \equiv \sum_k \psi^B_{-k-\sigma} \psi^A_{k+q\sigma} \tag{3.8}$$

for the interband and

$$\eta_q \equiv \sum_k \psi^A_{-k\downarrow} \psi^A_{k+q\uparrow} \tag{3.9}$$

for the intraband. We now introduce two bosonic fields, $\Delta(x)$ and $\Omega(x)$, one for each sector, in order to use the follow Gaussian integral identity

$$\exp(-S_{\text{Inter}}) = \int \mathfrak{D}[\Delta] e^{-\sum_q \left(\frac{2}{g_1} |\Delta_q|^2 - \sum_\sigma \Delta_q \bar{\rho}_{q\sigma} - \sum_\sigma \bar{\Delta}_q \rho_{q\sigma} \right)}, \tag{3.10}$$

and

$$\exp(-S_{\text{Intra}}) = \int \mathfrak{D}[\Omega] e^{-\sum_q \left(\frac{1}{g_2} |\Omega_q|^2 - \Omega_q \bar{\eta}_q - \bar{\Omega}_q \eta_q \right)}, \tag{3.11}$$

so that the (still exact) partition function becomes

$$\mathcal{Z} = \int \mathfrak{D}[\psi] \mathfrak{D}[\Delta] \mathfrak{D}[\Omega] e^{-S[\psi, \Delta, \Omega]}, \tag{3.12}$$

where the action is

$$\begin{aligned} S[\psi,\Delta,\Omega] =& \sum_{k,\sigma} \bar{\psi}^A_{k\sigma}(\xi^A_{\mathbf{k}} - i\omega_n)\psi^A_{k\sigma} + \sum_{k,\sigma} \bar{\psi}^B_{k\sigma}(\xi^B_{\mathbf{k}} - i\omega_n)\psi^B_{k\sigma} \\ &+ \sum_q \left(\frac{2}{g_1}|\Delta_q|^2 + \frac{1}{g_2}|\Omega_q|^2\right) + \sum_{k,\sigma}(V_{\mathbf{k}}\bar{\psi}^A_{k\sigma}\psi^B_{k\sigma} + \text{H.c.}) \\ &- \sum_{k,q,\sigma}\left(\Delta_q\bar{\psi}^A_{k+q\sigma}\bar{\psi}^B_{-k-\sigma} + \text{H.c.}\right) - \sum_{k,q}\left(\Omega_q\bar{\psi}^A_{k+q\uparrow}\bar{\psi}^A_{-k\downarrow} + \text{H.c.}\right), \end{aligned} \tag{3.13}$$

with $\xi^l_{\mathbf{k}} \equiv \mathbf{k}^2/(2m_l) - \mu \equiv \epsilon^l_{\mathbf{k}} - \mu$ and the odd Matsubara frequencies ω_n.

Using a four dimensional Nambu spinor representation

$$\bar{\Psi}_k \equiv (\bar{\psi}^A_{k\uparrow} \;\; \bar{\psi}^B_{k\uparrow} \;\; \psi^A_{-k\downarrow} \;\; \psi^B_{-k\downarrow}) \tag{3.14}$$

we may rewrite

$$S[\psi,\Delta,\Omega] = \sum_q \left(\frac{2}{g_1}|\Delta_q|^2 + \frac{1}{g_2}|\Omega_q|^2 - \sum_k \bar{\Psi}_{k+q}\mathbf{G}^{-1}\Psi_{k-q}\right) + \beta\sum_{\mathbf{k}}(\xi^A_{\mathbf{k}} + \xi^B_{\mathbf{k}}) \tag{3.15}$$

where we have defined the inverse Nambu-Gorkov Green's function

$$\mathbf{G}^{-1}(k,q) \equiv \mathbf{G}_0^{-1}(k)\delta(q) + \mathbf{\Delta}_q + \mathbf{\Omega}_q, \tag{3.16}$$

with the free propagator

$$\mathbf{G}_0^{-1}(k) = \begin{bmatrix} i\omega_n - \xi^A_{\mathbf{k}} & -\bar{V}_{\mathbf{k}} & 0 & 0 \\ -V_{\mathbf{k}} & i\omega_n - \xi^B_{\mathbf{k}} & 0 & 0 \\ 0 & 0 & i\omega_n + \xi^A_{\mathbf{k}} & -V_{\mathbf{k}} \\ 0 & 0 & -\bar{V}_{\mathbf{k}} & i\omega_n + \xi^B_{\mathbf{k}} \end{bmatrix} \tag{3.17}$$

and the interaction terms

$$\mathbf{\Delta}_q = \begin{bmatrix} 0 & 0 & 0 & -\Delta_q \\ 0 & 0 & \Delta_q & 0 \\ 0 & \bar{\Delta}_{-q} & 0 & 0 \\ -\bar{\Delta}_{-q} & 0 & 0 & 0 \end{bmatrix}, \tag{3.18}$$

$$\mathbf{\Omega}_q = \begin{bmatrix} 0 & 0 & \Omega_q & 0 \\ 0 & 0 & 0 & 0 \\ \bar{\Omega}_{-q} & 0 & 0 & 0 \\ 0 & 0 & 0 & 0 \end{bmatrix}. \tag{3.19}$$

These manipulations allow to write the effective action as a quadratic function of Ψ so we can readily integrate out the fermionic fields yielding

$$S[\Delta,\Omega] = \sum_q \left(\frac{2}{g_1}|\Delta_q|^2 + \frac{1}{g_2}|\Omega_q|^2 - \sum_k \ln\det\mathbf{G}^{-1}\right) + \beta\sum_{\mathbf{k}}(\xi^A_{\mathbf{k}} + \xi^B_{\mathbf{k}}), \tag{3.20}$$

with the determinant of $\mathbf{G}^{-1}$ given by

$$\det \mathbf{G}^{-1} = \omega_n^4 + 2A_{\mathbf{k}}\,\omega_n^2 + B_{\mathbf{k}} \tag{3.21}$$

which, from the condition $\det \mathbf{G}^{-1}(\omega_n = \pm\omega_{\mathbf{k}}^{\pm}) = 0$, provides the (real) excitation spectra

$$\omega_{\mathbf{k}}^{\pm} = \sqrt{A_{\mathbf{k}} \pm \sqrt{A_{\mathbf{k}}^2 - B_{\mathbf{k}}}}, \tag{3.22}$$

where we have introduced

$$\begin{aligned} A_{\mathbf{k}} &\equiv \frac{\xi_{\mathbf{k}}^{A2} + \xi_{\mathbf{k}}^{B2} + |\Omega_q|^2}{2} + |V_{\mathbf{k}}|^2 + |\Delta_q|^2, \\ B_{\mathbf{k}} &\equiv (\xi_{\mathbf{k}}^{A}\xi_{\mathbf{k}}^{B} - |V_{\mathbf{k}}|^2 + |\Delta_q|^2)^2 + \xi_{\mathbf{k}}^{B2}|\Omega_q|^2 + 4|V_{\mathbf{k}}|^2|\Delta_q|^2. \end{aligned} \tag{3.23}$$

Finally using the identity $\ln\det \mathbf{G}^{-1} = \mathrm{tr}\ln \mathbf{G}^{-1}$[4] the action becomes

$$\boxed{S[\Delta,\Omega] = \sum_q \left(\frac{2}{g_1}|\Delta_q|^2 + \frac{1}{g_2}|\Omega_q|^2 - \sum_k \mathrm{tr}\ln \mathbf{G}^{-1}\right) + \beta\sum_{\mathbf{k}}(\xi_{\mathbf{k}}^{A} + \xi_{\mathbf{k}}^{B}),} \tag{3.24}$$

which, not surprisingly, shares the same structure as the single-band action, differing solely in the $\mathbf{G}^{-1}$ matrix content. Up to here our mathematical expressions are exact and to proceed further we will need to turn to the mean-field approximation.

3.3 Mean-field Equations

In the previous section we have been able to replace the fermionic degrees of freedom for bosonic fields, the order parameters of the superconducting transition, that comprises the relevant physical phenomena. Here we shall assume that these order parameters vary so slowly in time and space that can we replace them by their mean-value. Therefore we will explore both, but independently, interband and intraband mean-field equations obtained through variational principle.

3.3.1 Interband Gap Equation

At mean-field level the gap parameter is taken to be static and homogenous, $\Delta_q = \Delta_0$, thus the gap equation obtained from $\delta_\Delta S = 0$ becomes

$$\frac{2\bar{\Delta}}{g_1} - \sum_k \mathrm{tr}\left(\mathbf{G}\delta_\Delta \mathbf{G}^{-1}\right) = 0 \tag{3.25}$$

and since the only non-zero components are $(\delta_\Delta \mathbf{G}^{-1})_{23} = 1$ and $(\delta_\Delta \mathbf{G}^{-1})_{14} = -1$ it implies that $\mathrm{tr}(\mathbf{G}\delta_\Delta \mathbf{G}^{-1}) = \mathbf{G}_{32} - \mathbf{G}_{41}$. The algebraic manipulations to obtain the relevant $\mathbf{G}$ components are calculated in App.A where we assumed a s-wave order parameter, $\Delta_0 = \bar{\Delta}_0$. The saddle-point equation takes the form (App.A.1)

$$\frac{1}{g_1} = \frac{1}{\beta}\sum_{\mathbf{k},\omega_n} \frac{\omega_n^2 + \xi_{\mathbf{k}}^{A}\xi_{\mathbf{k}}^{B} + |V_{\mathbf{k}}|^2 + \Delta_0^2}{\omega_n^4 + 2A_{\mathbf{k}}\,\omega_n^2 + B_{\mathbf{k}}}, \tag{3.26}$$

[4]The lowercase letter “tr” and “det” indicates the operation solely in the Nambu space.

with $A_{\mathbf{k}}$ and $B_{\mathbf{k}}$ evaluated at $\Delta_q = \Delta_0$ and $\Omega_q = 0$. Upon performing the Matsubara sum, as indicated in App. A.3, we get

$$\begin{aligned}\frac{1}{g_1} &= \frac{1}{2}\sum_{\mathbf{k}} \frac{\omega_{\mathbf{k}}^{+}\tanh\left(\beta\omega_{\mathbf{k}}^{+}/2\right) - \omega_{\mathbf{k}}^{-}\tanh\left(\beta\omega_{\mathbf{k}}^{-}/2\right)}{\omega_{\mathbf{k}}^{+2} - \omega_{\mathbf{k}}^{-2}} \\ &+ \frac{1}{2}\sum_{\mathbf{k}} \frac{\xi_{\mathbf{k}}^{A}\xi_{\mathbf{k}}^{B} + |V_{\mathbf{k}}|^2 + \Delta_0^2}{\omega_{\mathbf{k}}^{+2} - \omega_{\mathbf{k}}^{-2}} \left[\frac{\tanh\left(\beta\omega_{\mathbf{k}}^{-}/2\right)}{\omega_{\mathbf{k}}^{-}} - \frac{\tanh\left(\beta\omega_{\mathbf{k}}^{+}/2\right)}{\omega_{\mathbf{k}}^{+}}\right]\end{aligned} \tag{3.27}$$

where the interband excitation spectra become

$$\omega_{\mathbf{k}}^{\pm}(\Omega_q = 0) = \sqrt{(\xi_{\mathbf{k}}^{A2} + \xi_{\mathbf{k}}^{B2})/2 + |V_{\mathbf{k}}|^2 + \Delta_0^2 \pm E_{\mathbf{k}}(\Omega_q = 0)}, \tag{3.28}$$

with $E_{\mathbf{k}}(\Omega_q = 0) = \sqrt{[\Delta_0^2 + (\xi_{\mathbf{k}}^{A} + \xi_{\mathbf{k}}^{B})^2/4](\xi_{\mathbf{k}}^{A} - \xi_{\mathbf{k}}^{B})^2 + (\xi_{\mathbf{k}}^{A} + \xi_{\mathbf{k}}^{B})^2|V_{\mathbf{k}}|^2}$.

At mean-field level we are interested at zero temperature implying $\tanh(\beta\omega_{\mathbf{k}}^{\pm}) = 1$ and

$$\frac{1}{g_1} = \sum_{\mathbf{k}} \underbrace{\frac{1}{2}\frac{1}{\omega_{\mathbf{k}}^{+} + \omega_{\mathbf{k}}^{-}}\left(1 + \frac{\xi_{\mathbf{k}}^{A}\xi_{\mathbf{k}}^{B} + |V_{\mathbf{k}}|^2 + \Delta_0^2}{\omega_{\mathbf{k}}^{+}\omega_{\mathbf{k}}^{-}}\right)}_{f_1(\mathbf{k})}, \tag{3.29}$$

as expected, the same divergence issue appears here. The regularization procedure follows similar lines as the ones we have already presented in the previous chapter with inclusion of the scattering length and subtraction of the ultraviolet term. It is important however to observe that since we are dealing with a pair formed from different fermions we must consider the reduced mass

$$m = \frac{2m_A m_B}{m_A + m_B} \tag{3.30}$$

in the divergence correction. Later on we will identify $2m$ as the mass of the fermionic pair in the BEC limit if $m_A = m_B$. In practice, we can make the substitution[5] [78]

$$\frac{1}{g_1} = -\frac{m}{4\pi a_s} + \sum_{\mathbf{k}} f_1(\mathbf{k} \to \infty), \tag{3.31}$$

with

$$f_1(\mathbf{k} \to \infty) = \frac{m}{\mathbf{k}^2} \equiv \frac{1}{2\epsilon_{\mathbf{k}}}, \tag{3.32}$$

the asymptotic behavior of the interband gap equation for large values of $\mathbf{k}$.

Thus we finally write the regularized mean-field interband equation as

$$\boxed{\frac{m}{2\pi a_s} = \sum_{\mathbf{k}} \left[\frac{1}{\epsilon_{\mathbf{k}}} - \frac{1}{\omega_{\mathbf{k}}^{+} + \omega_{\mathbf{k}}^{-}}\left(1 + \frac{\xi_{\mathbf{k}}^{A}\xi_{\mathbf{k}}^{B} + |V_{\mathbf{k}}|^2 + \Delta_0^2}{\omega_{\mathbf{k}}^{+}\omega_{\mathbf{k}}^{-}}\right)\right],} \tag{3.33}$$

with the interaction varying $a_s^{-1} \to -\infty$ in the weak coupling regime to $a_s^{-1} \to +\infty$ in the strong coupling regime.

[5]This procedure is further explored in Ref. [77]

3.3.2 Intraband Gap Equation

At the intraband sector we set $\Delta_q = 0$ so the saddle-point solution for Ω_0 reads

$$\frac{\bar{\Omega}}{g_2} - \sum_k \mathrm{tr}\left(\mathbf{G}\delta_\Omega \mathbf{G}^{-1}\right) = 0, \tag{3.34}$$

with the only non-zero component $(\delta_\Omega \mathbf{G}^{-1})_{13} = 1$, thus $\mathrm{tr}(\mathbf{G}\delta_\Omega\mathbf{G}^{-1}) = \mathbf{G}_{31}$.

The calculation of $\mathbf{G}_{31}$ is presented in App. A.2 and leads to

$$\frac{1}{g_2} = \frac{1}{\beta}\sum_{k,\omega_n} \frac{\omega_n^2 + \xi_{\mathbf{k}}^{B2}}{\omega_n^4 + 2A_{\mathbf{k}}\omega_n^2 + B_{\mathbf{k}}}, \tag{3.35}$$

with $A_{\mathbf{k}}$ and $B_{\mathbf{k}}$ evaluated at $\Delta_q = 0$ and $\Omega_q = \Omega_0$.

The Matsubara sum shares the same structure as the one in the interband case yielding

$$\begin{aligned}\frac{1}{g_2} &= \frac{1}{2}\sum_{\mathbf{k}} \frac{\omega_{\mathbf{k}}^+ \tanh\left(\beta\omega_{\mathbf{k}}^+/2\right) - \omega_{\mathbf{k}}^- \tanh\left(\beta\omega_{\mathbf{k}}^-/2\right)}{\omega_{\mathbf{k}}^{+2} - \omega_{\mathbf{k}}^{-2}} \\ &+ \frac{1}{2}\sum_{\mathbf{k}} \frac{\xi_{\mathbf{k}}^{B2}}{\omega_{\mathbf{k}}^{+2} - \omega_{\mathbf{k}}^{-2}} \left[\frac{\tanh\left(\beta\omega_{\mathbf{k}}^-/2\right)}{\omega_{\mathbf{k}}^-} - \frac{\tanh\left(\beta\omega_{\mathbf{k}}^+/2\right)}{\omega_{\mathbf{k}}^+}\right],\end{aligned} \tag{3.36}$$

where the intraband excitation spectra are given by

$$\omega_{\mathbf{k}}^{\pm}(\Delta_q = 0) = \sqrt{(\xi_{\mathbf{k}}^{A2} + \xi_{\mathbf{k}}^{B2})/2 + |V_{\mathbf{k}}|^2 + \Omega_0^2/2 \pm E_{\mathbf{k}}(\Delta_q = 0)} \tag{3.37}$$

with $E_{\mathbf{k}}(\Delta_q = 0) = \sqrt{[\Omega_0^2 + (\xi_{\mathbf{k}}^A + \xi_{\mathbf{k}}^B)^2]|V_{\mathbf{k}}|^2 + \left(\xi_{\mathbf{k}}^{B2} - \xi_{\mathbf{k}}^{A2} - \Omega_0^2\right)^2/4}$.

At $T = 0$K Eq. 3.36 simplifies to

$$\frac{1}{g_2} = \sum_{\mathbf{k}} \underbrace{\frac{1}{2}\frac{1}{\omega_{\mathbf{k}}^+ + \omega_{\mathbf{k}}^-}\left(1 + \frac{\xi_{\mathbf{k}}^{B2}}{\omega_{\mathbf{k}}^+\omega_{\mathbf{k}}^-}\right)}_{f_2(\mathbf{k})}. \tag{3.38}$$

Here the regularization procedure follows the same lines as before, the only difference is the replacement of the reduced mass solely by m_A, i. e.,

$$\frac{1}{g_2} = -\frac{m_A}{4\pi a_s} + \sum_{\mathbf{k}} f_2(\mathbf{k} \to \infty), \tag{3.39}$$

where

$$f_2(\mathbf{k} \to \infty) = \frac{m_A}{\mathbf{k}^2} = \frac{1}{2\epsilon_{\mathbf{k}}^A} \tag{3.40}$$

and also keeping in mind that a_s now represents the scattering length of the A fermions among themselves.

Thus the regularized intraband mean-field equation reads

$$\boxed{\frac{m_A}{2\pi a_s} = \sum_{\mathbf{k}} \left[\frac{1}{\epsilon_{\mathbf{k}}^A} - \frac{1}{\omega_{\mathbf{k}}^+ + \omega_{\mathbf{k}}^-}\left(1 + \frac{\xi_{\mathbf{k}}^{B2}}{\omega_{\mathbf{k}}^+\omega_{\mathbf{k}}^-}\right)\right].} \tag{3.41}$$

3.4 Occupation Number

As it will be clear next section, besides the gap parameter or the critical temperature, the chemical potential must also be obtained via consistent equations. Therefore, an additional constraint is required for the calculation of the physical quantities we are interested in. That constraint is given by the occupation number extracted from the thermodynamical relation $n = \beta^{-1}\partial_\mu \ln \mathcal{Z}$, recalling $\mathcal{Z} = \int \mathfrak{D}[\Delta]\mathfrak{D}[\Omega]e^{-S[\Delta,\Omega]}$ with the effective action given in Eq. 3.20.

Taking the derivative in respect to the chemical potential reads

$$\begin{aligned} n(T) &= -\frac{1}{\beta}\frac{1}{\mathcal{Z}}\int \mathfrak{D}[\Delta]\mathfrak{D}[\Omega]e^{-S[\Delta,\Omega]}\frac{\partial S[\Delta,\Omega]}{\partial_\mu} \\ &= -\frac{1}{\beta}\frac{\partial S[\Delta,\Omega]}{\partial_\mu} \\ &= \sum_{\mathbf{k}}\left[2 + \frac{1}{\beta}\frac{\partial}{\partial\mu}\sum_{\omega_n}\ln\det\mathbf{G}^{-1}(k)\right] \\ &= \sum_{\mathbf{k}}\left[2 + \frac{1}{\beta}\sum_{\omega_n}\frac{2\partial_\mu A_{\mathbf{k}}\omega_n^2 + \partial_\mu B_{\mathbf{k}}}{\omega_n^4 + 2A_{\mathbf{k}}\omega_n^2 + B_{\mathbf{k}}}\right] \end{aligned} \tag{3.42}$$

since $\partial_\mu S[\Delta,\Omega]$ is field independent. Explicitly from the definitions 3.23

$$\begin{aligned} \partial_\mu A_{\mathbf{k}} &= -(\xi_{\mathbf{k}}^A + \xi_{\mathbf{k}}^B) \\ \partial_\mu B_{\mathbf{k}} &= -(\xi_{\mathbf{k}}^A\xi_{\mathbf{k}}^B - |V_{\mathbf{k}}|^2 + \Delta_0^2)(\xi_{\mathbf{k}}^A + \xi_{\mathbf{k}}^B) - 2\xi_{\mathbf{k}}^A\Omega_0^2, \end{aligned} \tag{3.43}$$

and summing over the Matsubara frequencies (we can use the result from the gap equation sum in App. A.3) we obtain

$$\begin{aligned} n(T) = \sum_{\mathbf{k}}\Bigg\{2 &- \frac{\xi_{\mathbf{k}}^A + \xi_{\mathbf{k}}^B}{\omega_{\mathbf{k}}^{+2} - \omega_{\mathbf{k}}^{-2}}\left[\omega_{\mathbf{k}}^+\tanh\left(\frac{\beta\omega_{\mathbf{k}}^+}{2}\right) - \omega_{\mathbf{k}}^-\tanh\left(\frac{\beta\omega_{\mathbf{k}}^-}{2}\right)\right] \\ &- \frac{(\xi_{\mathbf{k}}^A + \xi_{\mathbf{k}}^B)(\xi_{\mathbf{k}}^A\xi_{\mathbf{k}}^B - |V_{\mathbf{k}}|^2 + \Delta_0^2) + \xi_{\mathbf{k}}^B\Omega_0^2}{\omega_{\mathbf{k}}^{+2} - \omega_{\mathbf{k}}^{-2}}\left[\frac{\tanh(\beta\omega_{\mathbf{k}}^-/2)}{\omega_{\mathbf{k}}^-} - \frac{\tanh(\beta\omega_{\mathbf{k}}^+/2)}{\omega_{\mathbf{k}}^+}\right]\Bigg\} \end{aligned} \tag{3.44}$$

which at $T = 0$K reads

$$n(0) = \sum_{\mathbf{k}}\left[2 - \frac{\xi_{\mathbf{k}}^A + \xi_{\mathbf{k}}^B}{\omega_{\mathbf{k}}^+ + \omega_{\mathbf{k}}^-} - \frac{(\xi_{\mathbf{k}}^A + \xi_{\mathbf{k}}^B)(\xi_{\mathbf{k}}^A\xi_{\mathbf{k}}^B - |V_{\mathbf{k}}|^2 + \Delta_0^2) + \xi_{\mathbf{k}}^B\Omega_0^2}{\omega_{\mathbf{k}}^+\omega_{\mathbf{k}}^-(\omega_{\mathbf{k}}^+ + \omega_{\mathbf{k}}^-)}\right] \tag{3.45}$$

with

$$n(0) = \sum_\sigma\left[\int_{k_F^A}\frac{\mathrm{d}^3k}{(2\pi)^3} + \int_{k_F^B}\frac{\mathrm{d}^3k}{(2\pi)^3}\right] = \frac{8\pi}{3}\frac{k_F^{A3} + k_F^{B3}}{(2\pi)^3}, \tag{3.46}$$

determined from the requirement of the complete occupation at $T = 0\,$K of the Fermi sphere with radius $k_F^l = \sqrt{2\epsilon_F m_l}$.

The occupation number plays different roles: it determines the behavior of the chemical potential in the weak coupling regime and the behavior of the complementary variable in the strong coupling one. Although the total number of particles is kept constant the quantity of the fermions of each band is distinct (the more energetic ones will be less predominant so that the Fermi level of both bands coincide).

3.5 Numerical Solutions

The previous expressions are as far as we can go with analytic mathematics. In this section we present the numerical solutions to the mean-field equations. To make this analysis feasible we shall consider two scenarios: the pure intraband ($\Delta_q = 0$) and the pure interband ($\Omega_q = 0$) cases. Despite being a simplification required mainly to make our codes run it still comprises a very rich physics, specially the interband sector to which we shall dedicate most of our attention.

Basically we have two variables to be calculated from two coupled integral equations. We shall deal first with the zero temperature limit in which case we will need to determine the gap parameter and the chemical potential and then we shall study the behavior of our model close to the transition point analyzing the critical temperature and chemical potential.

All the following results have been obtained through Python coding.

3.5.1 Definitions and Conventions

One original feature of our work is the exploration of the difference in the masses of the A and B fermions. So it will prove to be very useful to define a dimensionless parameter δ to measure the mass asymmetry

$$\delta \equiv \frac{m_A - m_B}{m_A + m_B}, \tag{3.47}$$

which ranges from $[0, 1)$. The lower limit implying in the case of equal masses and the upper one for the case that m_A greatly exceeds m_B. In the interband scenario $m_B > m_A$ is completely equivalent to $m_A > m_B$ as it will become clear from the equations ahead in which the symmetry $\delta \to -\delta$ is present. We will be particularly interested in the limit $\delta \approx 1$ since it describes systems possessing a narrow and a wide band, such as HF. In the intraband case we do not have the δ-symmetry but the numerical results for negative δ are qualitatively the same as the positive ones.

Mainly for the sake of coding it will be necessary to convert all integrals into dimensionless quantities thus we will normalize the energy scales by the Fermi energy

$$\epsilon_F = \frac{k_F^{A2}}{2m_A} = \frac{k_F^{B2}}{2m_B} \equiv \frac{k_F^2}{2m} \tag{3.48}$$

and the wavevectors by the the Fermi wavevector

$$k_F = \sqrt{1-\delta}k_F^A = \sqrt{1+\delta}k_F^B. \tag{3.49}$$

So recalling the definitions above and Eq. 3.30 the fermion masses can be expressed as a function of the reduced mass and the mass asymmetry parameter as

$$m_A = \frac{m}{1-\delta}, \tag{3.50}$$

$$m_B = \frac{m}{1+\delta}, \tag{3.51}$$

so that the (normalized) energies become

$$\frac{\epsilon_{\mathbf{k}}^{A}}{\epsilon_F} = (1-\delta)\frac{\epsilon_{\mathbf{k}}}{\epsilon_F} = (1-\delta)\frac{\mathbf{k}^2}{k_F^2} \tag{3.52}$$

$$\frac{\epsilon_{\mathbf{k}}^{B}}{\epsilon_F} = (1+\delta)\frac{\epsilon_{\mathbf{k}}}{\epsilon_F} = (1+\delta)\frac{\mathbf{k}^2}{k_F^2}. \tag{3.53}$$

With these conventions we can look at the interband problem as a system composed by two fermions with same mass m but distinct energies $\epsilon_{\mathbf{k}} \pm \delta\epsilon_{\mathbf{k}}$. Yet we shall use the characteristic average distance k_F^{-1} of these "new" fermions as the standard distance scale even in the intraband case so we can easily compare it with the interband one.

The common structures appearing in the mean-field analysis are then written as

$$\frac{\xi_{\mathbf{k}}^{A} + \xi_{\mathbf{k}}^{B}}{2} = \epsilon_{\mathbf{k}} - \mu \equiv \xi_{\mathbf{k}}, \tag{3.54}$$

$$\frac{\xi_{\mathbf{k}}^{B} - \xi_{\mathbf{k}}^{A}}{2} = \delta\epsilon_{\mathbf{k}}, \tag{3.55}$$

$$\frac{(\xi_{\mathbf{k}}^{A})^2 + (\xi_{\mathbf{k}}^{B})^2}{2} = \xi_{\mathbf{k}}^2 + (\delta\epsilon_{\mathbf{k}})^2, \tag{3.56}$$

$$\xi_{\mathbf{k}}^{A}\xi_{\mathbf{k}}^{B} = \xi_{\mathbf{k}}^2 - (\delta\epsilon_{\mathbf{k}})^2 \tag{3.57}$$

that together with

$$\Lambda_{\mathbf{k}} \equiv \sqrt{(\delta\epsilon_{\mathbf{k}})^2 + |V_{\mathbf{k}}|^2}, \tag{3.58}$$

will allow our equations to be written in a simpler form. Definition 3.58 will be particularly useful when studying the spectra at finite temperatures since, in the absence of an energy gap, $\Lambda_{\mathbf{k}}$ becomes the difference between the quasi-particles excitations which is finite even without hybridization due to the mass difference. More specifically we can trace a direct parallel of the term $\delta\epsilon_{\mathbf{k}}$ with a Zeeman field and $|V_{\mathbf{k}}|^2$ to Rashba SOC interaction in ultracold atoms [79].

The occupation number at $T = 0\,\mathrm{K}$, Eq. 3.46, as a function of δ and k_F is then

$$n(0) = 2F_\delta \left(\frac{k_F}{2\pi}\right)^3, \tag{3.59}$$

with

$$F_\delta \equiv \frac{4\pi}{3}\left[\frac{1}{(1+\delta)^{3/2}} + \frac{1}{(1-\delta)^{3/2}}\right]. \tag{3.60}$$

We notice that the divergence of F_δ for $\delta \to 1$ reflects the diverging density of states in the flat band limit $1/m_A \to 0$.

Lastly taking the continuum limit the momentum sum becomes

$$\sum_{\mathbf{k}} = \left(\frac{k_F}{2\pi}\right)^3 \int \mathrm{d}^3(k/k_F), \tag{3.61}$$

recalling that we are assuming a unit volume.

3.5.2 A Consideration on Hybridization

Before starting the numerical calculations let us observe that the follow change of coordinates

$$\tilde{k}_x \equiv \frac{\sqrt{2}k_z - \frac{\gamma}{\sqrt{2}}(k_x + k_y)}{\sqrt{2+\gamma^2}} \tag{3.62}$$

$$\tilde{k}_y \equiv \frac{k_x - k_y}{\sqrt{2}} \tag{3.63}$$

$$\tilde{k}_z \equiv \frac{k_x + k_y + \gamma k_z}{\sqrt{2+\gamma^2}} \tag{3.64}$$

will allow us to solve analytically one of the triple integrals. One can check that $k_x^2 + k_y^2 + k_z^2 = \tilde{k}_x^2 + \tilde{k}_y^2 + \tilde{k}_z^2$ and the Jacobian reads

$$J \equiv \begin{vmatrix} \frac{\tilde{k}_x}{k_x} & \frac{\tilde{k}_x}{k_y} & \frac{\tilde{k}_x}{k_z} \\ \frac{\tilde{k}_y}{k_x} & \frac{\tilde{k}_y}{k_y} & \frac{\tilde{k}_y}{k_z} \\ \frac{\tilde{k}_z}{k_x} & \frac{\tilde{k}_z}{k_y} & \frac{\tilde{k}_z}{k_z} \end{vmatrix} = \begin{vmatrix} -\frac{\gamma}{\sqrt{2}\sqrt{2+\gamma^2}} & -\frac{\gamma}{\sqrt{2}\sqrt{2+\gamma^2}} & \frac{\sqrt{2}}{\sqrt{2+\gamma^2}} \\ \frac{1}{\sqrt{2}} & -\frac{1}{\sqrt{2}} & 0 \\ \frac{1}{\sqrt{2+\gamma^2}} & \frac{1}{\sqrt{2+\gamma^2}} & \frac{\gamma}{\sqrt{2+\gamma^2}} \end{vmatrix}$$

$$= \frac{\gamma^2}{2(2+\gamma^2)} + \frac{1}{2+\gamma^2} + \frac{1}{2+\gamma^2} + \frac{\gamma^2}{2(2+\gamma^2)} = 1, \tag{3.65}$$

thus we are effectively aligning the hybridization with the $\tilde{k}_z$ direction allowing us to write

$$\boxed{V_{\tilde{\mathbf{k}}} = i\alpha\sqrt{2+\gamma^2}\tilde{k}_z.} \tag{3.66}$$

Furthermore, we can see that a small anisotropic parameter, $|\gamma| \ll 1$, do not considerable alter the hybridization strength, so we shall assume $\gamma = 0$. We also omit the tilde symbol and use a cylindrical coordinate system ($k = \sqrt{k_x^2 + k_y^2}, k_z, \theta$), where the θ integration is now straightforward.

3.6 Intraband Scenario

Expliciting the mass asymmetry dependence in the intraband case Eq. 3.37 becomes

$$\omega_{\mathbf{k}}^{\pm}(\Delta_q = 0) = \sqrt{\xi_{\mathbf{k}}^2 + (\delta\epsilon_{\mathbf{k}})^2 + |V_{\mathbf{k}}|^2 + \Omega_0^2/2 \pm 2\sqrt{(\xi_{\mathbf{k}}^2 + \Omega_0^2/4)|V_{\mathbf{k}}|^2 + \left(\delta\epsilon_{\mathbf{k}}\xi_{\mathbf{k}} - \Omega_0^2/4\right)^2}}. \tag{3.67}$$

To translate graphically the meaning of Eq. 3.67 we show in Fig. 3.1 the intraband spectra as function of k_z, with $k_x = k_y = 0$, $(k_F a_s)^{-1} = -0.5$ and $\delta = 0.9$, for a given hybridization strength and the corresponding mean-field solutions (obtained in the next section) of the chemical potential and order parameter. Comparing both states we observe that $\omega_{\mathbf{k}}^{+}$ is the dominant mode, which becomes more evident as k_z increases. Furthermore we recall that $-\omega_{\mathbf{k}}^{\pm}$ also represents quasi-particles excitations thus the zero mode presented in $\omega_{\mathbf{k}}^{-}(\alpha = 0)$ indicates the existence of a gapless state with a finite order parameter. (Here we are assuming the transitions $-\omega_{\mathbf{k}}^{\pm} \to \omega_{\mathbf{k}}^{\pm}$ and $\omega_{\mathbf{k}}^{\pm} \to \omega_{\mathbf{k}}^{\mp}$ and observe that $\omega_{\mathbf{k}}^{-} - (-\omega_{\mathbf{k}}^{-}) = 0$ only for $\alpha = 0$.)

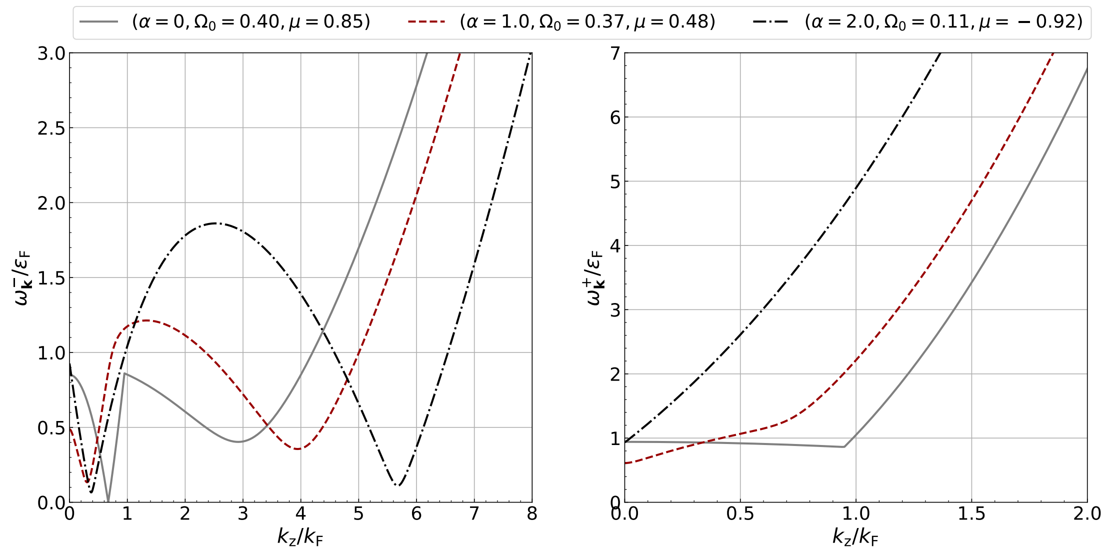

Figure 3.1: Intraband quasi-particles excitation energies, $\omega_{\mathbf{k}}^{\pm}$, for $(k_F a_s)^{-1} = -0.5$, $\delta = 0.9$ and $k_x = k_y = 0$. The chemical potential and the intraband order parameter are expressed in units of Fermi energy.

In the absence of hybridization, $\alpha = 0$, Eq. 3.67 can be simplified to

$$\omega_{\mathbf{k}}^-(\Delta_q = \alpha = 0) = \begin{cases} |\xi_{\mathbf{k}} + \delta\epsilon_{\mathbf{k}}| & \text{if} \quad \xi_{\mathbf{k}} \leq \Omega_0^2/(4\delta\epsilon_{\mathbf{k}}) \\ \sqrt{(\xi_{\mathbf{k}} - \delta\epsilon_{\mathbf{k}})^2 + \Omega_0^2} & \text{if} \quad \xi_{\mathbf{k}} \geq \Omega_0^2/(4\delta\epsilon_{\mathbf{k}}), \end{cases} \tag{3.68}$$

$$\omega_{\mathbf{k}}^+(\Delta_q = \alpha = 0) = \begin{cases} \sqrt{(\xi_{\mathbf{k}} - \delta\epsilon_{\mathbf{k}})^2 + \Omega_0^2} & \text{if} \quad \xi_{\mathbf{k}} \leq \Omega_0^2/(4\delta\epsilon_{\mathbf{k}}) \\ |\xi_{\mathbf{k}} + \delta\epsilon_{\mathbf{k}}| & \text{if} \quad \xi_{\mathbf{k}} \geq \Omega_0^2/(4\delta\epsilon_{\mathbf{k}}), \end{cases} \tag{3.69}$$

which sheds some light about the possibility of zeroes in the excitation energies for $\delta = 0.90$ and $\mu = 0.85\epsilon_F$ since it occurs only for $\omega_{\mathbf{k}}^-$ at $k_z = 0.67k_F$. However, as we turn the hybridization on both $\pm$ particles develop (small) finite minima.

Let us next explore both zero and finite temperatures solutions.

3.6.1 Intraband Solution at $T = 0\,\mathrm{K}$

Using the previous definitions we can bring Eq. 3.41 to the form

$$\frac{\pi}{k_F a_s} = \int \frac{\mathrm{d}^3k}{2\pi}\left[\frac{1}{\epsilon_{\mathbf{k}}} - \frac{1-\delta}{\omega_{\mathbf{k}}^+ + \omega_{\mathbf{k}}^-}\left(1 + \frac{(\xi_{\mathbf{k}} + \delta\epsilon_{\mathbf{k}})^2}{\sqrt{(\xi_{\mathbf{k}}^2 - \Lambda_{\mathbf{k}}^2)^2 + (\xi_{\mathbf{k}} + \delta\epsilon_{\mathbf{k}})^2\Omega_0^2}}\right)\right] \tag{3.70}$$

and the occupation number, Eq. 3.45, to

$$F_\delta = \int \mathrm{d}^3k\left[1 - \frac{1}{\omega_{\mathbf{k}}^+ + \omega_{\mathbf{k}}^-}\left(\xi_{\mathbf{k}} + \frac{1}{2}\frac{2\xi_{\mathbf{k}}(\xi_{\mathbf{k}}^2 - \Lambda_{\mathbf{k}}^2) + (\xi_{\mathbf{k}} + \delta\epsilon_{\mathbf{k}})\Omega_0^2}{\sqrt{(\xi_{\mathbf{k}}^2 - \Lambda_{\mathbf{k}}^2)^2 + (\xi_{\mathbf{k}} + \delta\epsilon_{\mathbf{k}})^2\Omega_0^2}}\right)\right], \tag{3.71}$$

where both equations are expressed in Fermi units. We recall that, here and in the following, we consider $\int \mathrm{d}^3k = 4\pi\int_0^\infty k\mathrm{d}k\int_0^\infty \mathrm{d}k_z$. To solve the coupled equations for Ω_0 and μ we need to fix two of the remaining parameters, namely the ratio of the average interparticle distance to the scattering length, $(k_F a_s)^{-1}$, the hybridization strength, α, and the mass asymmetry, δ.

We begin varying the scattering length, fixing $\alpha = \{0.1, 2.0\}$ and assume similar, $\delta = 0.1$, up to very different masses, $\delta = 0.9$. This way we get the results displayed in Fig. 3.2 where, overall, they resemble the single-band BCS-BEC crossover from Fig. 2.4. The order parameter continuously increases with $(k_F a_s)^{-1}$ but presents a small reduction with hybridization, especially in the BCS limit; its dependence with δ, at a fixed α, is not so evident (we will address it shortly). We also observe that, for plots with same δ, a higher α tends to considerably decrease the chemical potential. Roughly comparing, the BCS regime results in a shift by $\mu \approx (1-\alpha)\epsilon_F$ of the Fermi surface.

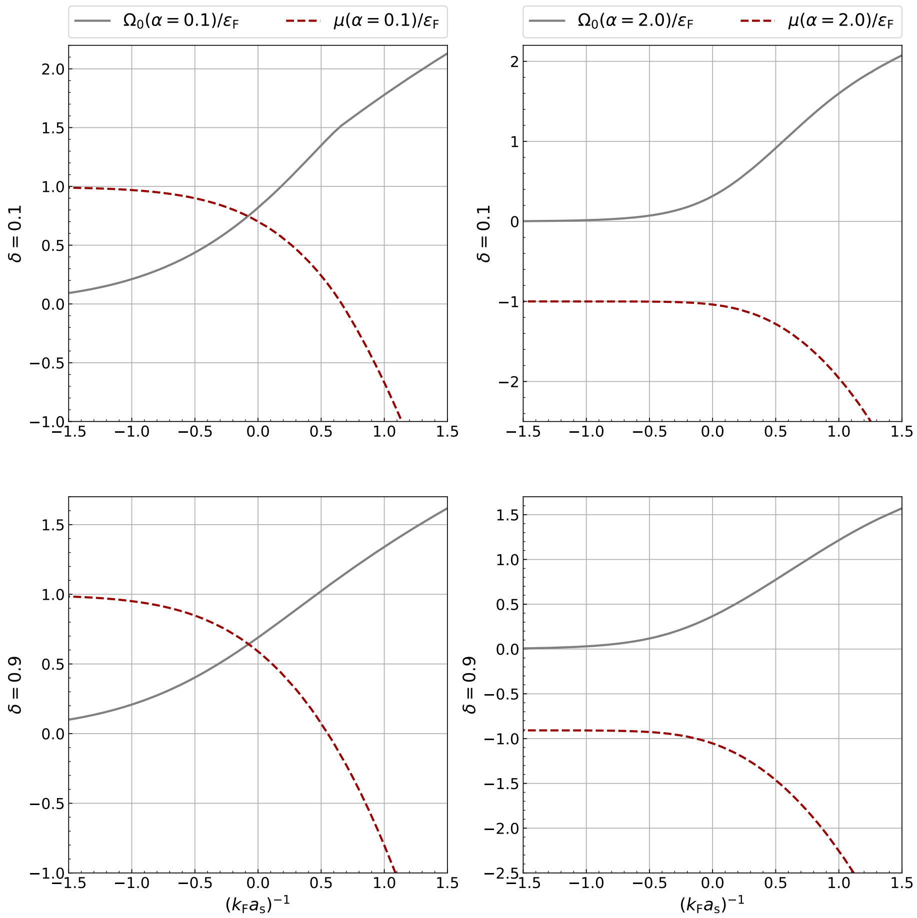

Figure 3.2: Evolution of the gap parameter and the chemical potential in the intraband scenario as function of the scattering length. In these plots we have used $\delta = 0.1$ (upper panels) and $\delta = 0.9$ (lower panels) for distinct values of hybridization $\alpha = 0.1$ (left) and $\alpha = 2.0$ (right).

Next, to further explore the influence of the hybridization in the intraband case, and more specifically to determine whether or not it presents an α-driven crossover, we set a small negative value of the scattering length, $(k_F a_s)^{-1} = -0.5$, characteristic of the BCS regime, and $\delta = \{0.1, 0.9\}$, while continuously varying α. Thus we present the numerical solutions as α-functions in Fig. 3.3. In all four scenarios we observe a decrease of the gap parameter which starts at a finite value, $\Omega_0 \approx 0.4$, and then drops to zero as the hybridization increases. Also the chemical potential falls continuously with α. The mass asymmetry does not seem to be a relevant parameter in the intraband case. Therefore we can conclude that *hybridization destroys the intraband superconducting effects.* We can understand this result by observing that hybridization "switches" the A and B fermions and, since the Cooper pair is formed solely in the A-band, converting at least one A fermion destroys superconductivity. Moreover, the other way around conversion (B into A fermions) does not compensate the previous one because the Cooper pair requires a very specific aligning between the fermions' momenta.

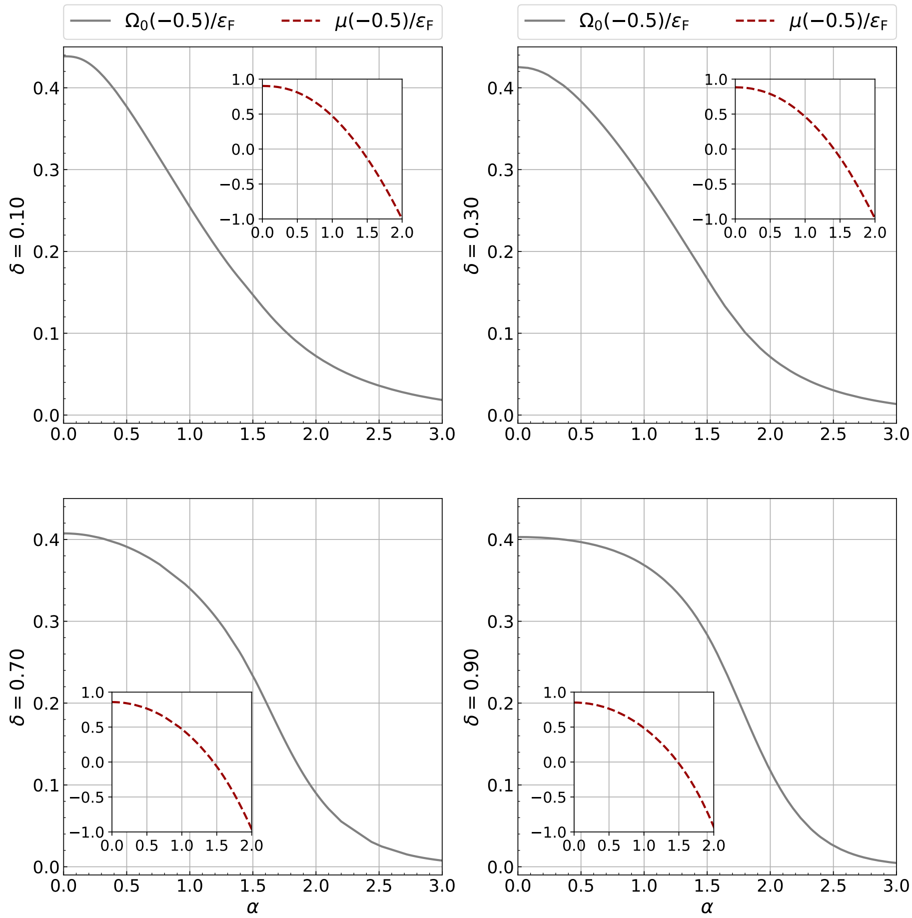

Figure 3.3: Evolution of the gap parameter and the chemical potential in the intraband scenario via hybridization. In these plots we have used $\delta = \{0.1, 0.3, 0.7, 0.9\}$ and $(k_F a_s)^{-1} = -0.5$ characteristic of the BCS regime.

Lastly, still with $(k_F a_s)^{-1} = -0.5$, we vary the mass asymmetry to obtain Fig. 3.4 for two values of hybridization $\alpha = 0.1$ and $\alpha = 2.0$. In the first case, $\alpha = 0.1$, both chemical potential and order parameter decreases with δ, the variation in Ω_0 however is of the order of 10% reforcing that for small hybridization values the mass asymmetry is not a relevant parameter. On the other hand, for $\alpha = 2.0$ there is an increase in the order parameter and the chemical potential with δ. Furthermore Ω_0 becomes twice as large as its minimum value. So despite not having an analytical expression relating both variables these results may indicate an association between α and δ. We will further investigate the δ influence at finite temperature in the next section.

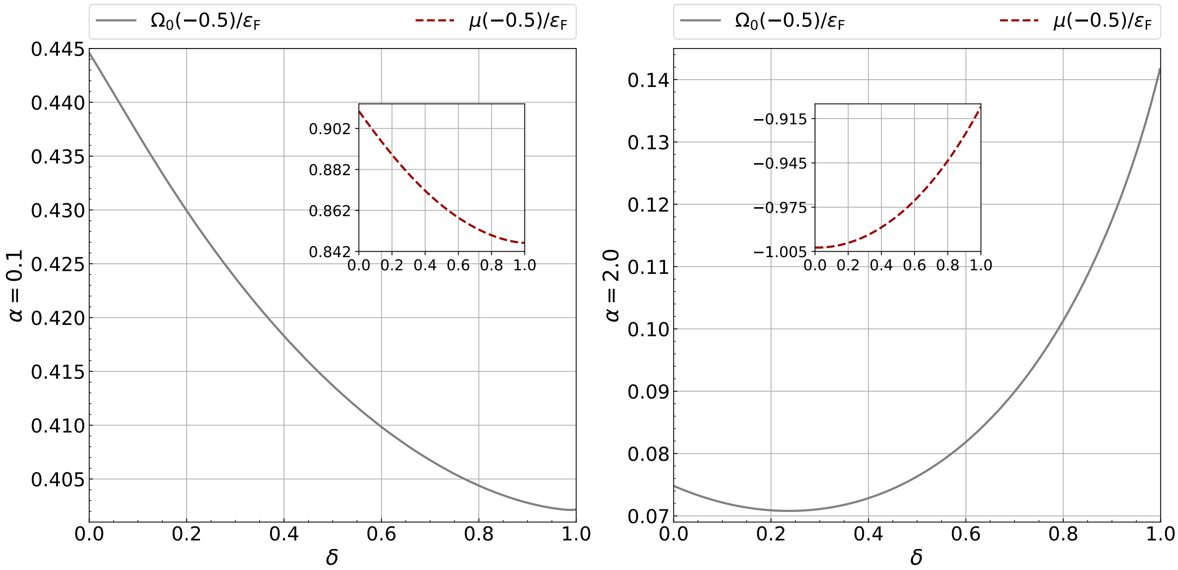

Figure 3.4: Evolution of the gap parameter and the chemical potential in the intraband scenario via mass asymmetry. In these plots we have used $(k_F a_s)^{-1} = -0.5$, characteristic of the BCS regime, together with $\alpha = 0.1$ (left) and $\alpha = 2.0$ (right).

3.6.2 Hybridized Bands' Minimum: E_0

Proceeding with the analysis close to the transition point characterized by a vanishing order parameter, $\Omega_0 = 0$, the excitation energies can be shown to yield

$$\omega_{\mathbf{k}}^{\pm}(\Omega_0 = \Delta_0 = 0) = |\xi_{\mathbf{k}} \pm \Lambda_{\mathbf{k}}| \equiv |\xi_{\mathbf{k}}^{\pm}|, \tag{3.72}$$

where we can see that the hybridization causes a change in the energy spectra of

$$(1 \pm \delta)\epsilon_{\mathbf{k}} \to \epsilon_{\mathbf{k}} \pm \sqrt{(\delta\epsilon_{\mathbf{k}})^2 + |V_{\mathbf{k}}|^2} \equiv \epsilon_{\mathbf{k}}^{\pm}. \tag{3.73}$$

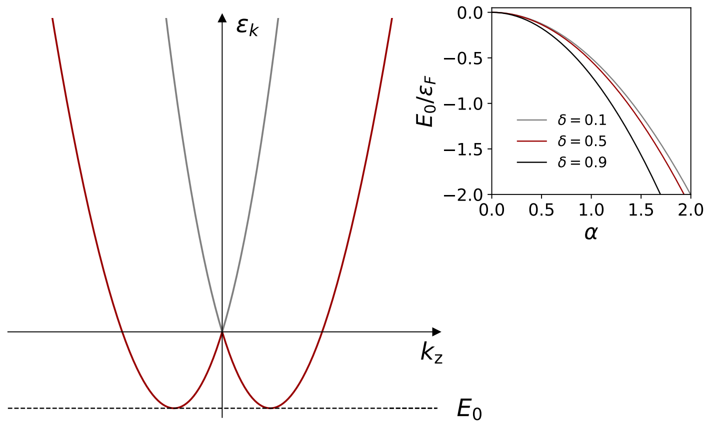

Figure 3.5: Schematic plot of the dispersion relations $\epsilon_{\mathbf{k}}^{-}$ (red line) and $\epsilon_{\mathbf{k}}^{+}$ (grey line) for $k_x = k_y = 0$ in absence of pairing correlations $\Delta_0 = \Omega_0 = 0$. The dashed line indicates the band minimum, E_0, defined in the main text. Inset: $E_0(\delta, \alpha)$ as function of α for three values of δ.

Thus the hybridized dispersions have the profile presented in Fig. 3.5. It is straightforward to see that the minimum of $\epsilon_{\mathbf{k}}^{+}$ is zero while the minimum of $\epsilon_{\mathbf{k}}^{-}$ is now finite. To calculate the band bottom, E_0, we consider

$$\left.\frac{\mathrm{d}\epsilon_{\mathbf{k}}^{-}}{\mathrm{d}k_z}\right|_{k_x=k_y=0,\ k_z=k_{\min}} = 0, \tag{3.74}$$

explicitly

$$\begin{aligned}
&\left.\frac{\mathrm{d}}{\mathrm{d}k_z}\left(k_z^2 - \sqrt{\delta^2 k_z^4 + 2\alpha^2 k_z^2}\right)\right|_{k_z=k_{\min}} = 2k_{\min} - \frac{1}{2}\frac{4\delta^2 k_{\min}^3 + 4\alpha^2 k_{\min}}{\sqrt{\delta^2 k_{\min}^4 + 2\alpha^2 k_{\min}^2}} = 0 \\
&\Rightarrow \sqrt{\delta^2 k_{\min}^4 + 2\alpha^2 k_{\min}^2} - \delta^2 k_{\min}^2 - \alpha^2 = 0 \\
&\Rightarrow \delta^2(1-\delta^2)k_{\min}^4 + 2\alpha^2(1-\delta^2)k_{\min}^2 - \alpha^4 = 0 \\
&\Rightarrow k_{\min}^2 = -\frac{\alpha^2}{\delta^2} \pm \frac{\sqrt{4\alpha^4(1+\delta^4-2\delta^2) + 4\delta^2(1-\delta^2)\alpha^4}}{2\delta^2(1-\delta^2)} \\
&\Rightarrow k_{\min}^2 = -\frac{\alpha^2}{\delta^2} \pm \frac{\alpha^2\sqrt{1-\delta^2}}{\delta^2(1-\delta^2)} \\
&\Rightarrow k_{\min}^2 = \frac{\alpha^2}{\delta^2}\left(\frac{1}{\sqrt{1-\delta^2}} - 1\right),
\end{aligned} \tag{3.75}$$

since $k_{\min}^2$ must be a positive quantity. Evaluating $\epsilon_{\mathbf{k}}^{-}$ at $k_{\min}$ we get (in units of the Fermi energy)

$$\begin{aligned}
E_0(\delta,\alpha) &\equiv \epsilon_{\mathbf{k}}^{-}(k_x = k_y = 0, k_{\min}) \\
&= \frac{\alpha^2}{\delta^2}\left(\frac{1}{\sqrt{1-\delta^2}} - 1\right) - \sqrt{\frac{\alpha^4}{\delta^2}\left(\frac{1}{\sqrt{1-\delta^2}} - 1\right)^2 + 2\frac{\alpha^4}{\delta^2}\left(\frac{1}{\sqrt{1-\delta^2}} - 1\right)} \\
&= \frac{\alpha^2}{\delta^2}\left(\frac{1}{\sqrt{1-\delta^2}} - 1\right) - \frac{\alpha^2}{\delta}\frac{\delta}{\sqrt{1-\delta^2}} \\
&= \frac{\alpha^2}{\delta^2}\frac{1-\sqrt{1-\delta^2}-\delta^2}{\sqrt{1-\delta^2}} \\
&= -\frac{\alpha^2}{\delta^2}(1-\sqrt{1-\delta^2}),
\end{aligned} \tag{3.76}$$

which is direct proportional to α^2 and decreases with δ as shown in the inset of Fig. 3.5. It is particularly useful to have an analytical expression for E_0 to determine whether or not the system is in the strong-coupling regime, since the BEC phase requires the chemical potential to fall below the band bottom. In other words, in a mean-field level, we can define the BCS-BEC crossover to take place at

$$\boxed{\mu \simeq E_0.} \tag{3.77}$$

3.6.3 Intraband Solution at the Critical Temperature

At the critical temperature, $T = T_c$, we can write the intraband gap equation 3.36 as[6]

$$\frac{\pi}{k_F a_s} = \int \frac{\mathrm{d}^3 k}{2\pi} \left[\frac{1}{\epsilon_{\mathbf{k}}} - (1-\delta) \frac{\xi_{\mathbf{k}}^{+} \tanh\left(\xi_{\mathbf{k}}^{+}/2T_c\right) - \xi_{\mathbf{k}}^{-} \tanh\left(\xi_{\mathbf{k}}^{-}/2T_c\right)}{4\xi_{\mathbf{k}}\Lambda_{\mathbf{k}}} \right.$$
$$\left. - (1-\delta)\frac{(\xi_{\mathbf{k}} + \delta\epsilon_{\mathbf{k}})^2}{4\xi_{\mathbf{k}}\Lambda_{\mathbf{k}}} \left(\frac{\tanh\left(\xi_{\mathbf{k}}^{-}/2T_c\right)}{\xi_{\mathbf{k}}^{-}} - \frac{\tanh\left(\xi_{\mathbf{k}}^{+}/2T_c\right)}{\xi_{\mathbf{k}}^{+}} \right) \right] \tag{3.78}$$

and, after some algebraic manipulations, the occupation number, Eq. 3.44, becomes

$$F_\delta = \int \mathrm{d}^3 k \left[1 - \frac{1}{2}\tanh\left(\frac{\xi_{\mathbf{k}}^{+}}{2T_c}\right) - \frac{1}{2}\tanh\left(\frac{\xi_{\mathbf{k}}^{-}}{2T_c}\right) \right], \tag{3.79}$$

that it is just the sum of two quasiparticles with energy dispersion $\xi_{\mathbf{k}}^{\pm}$, as one might have anticipated. Notice that Eq. 3.79 will also be applied to the interband case at finite temperature since both order parameters are zero.

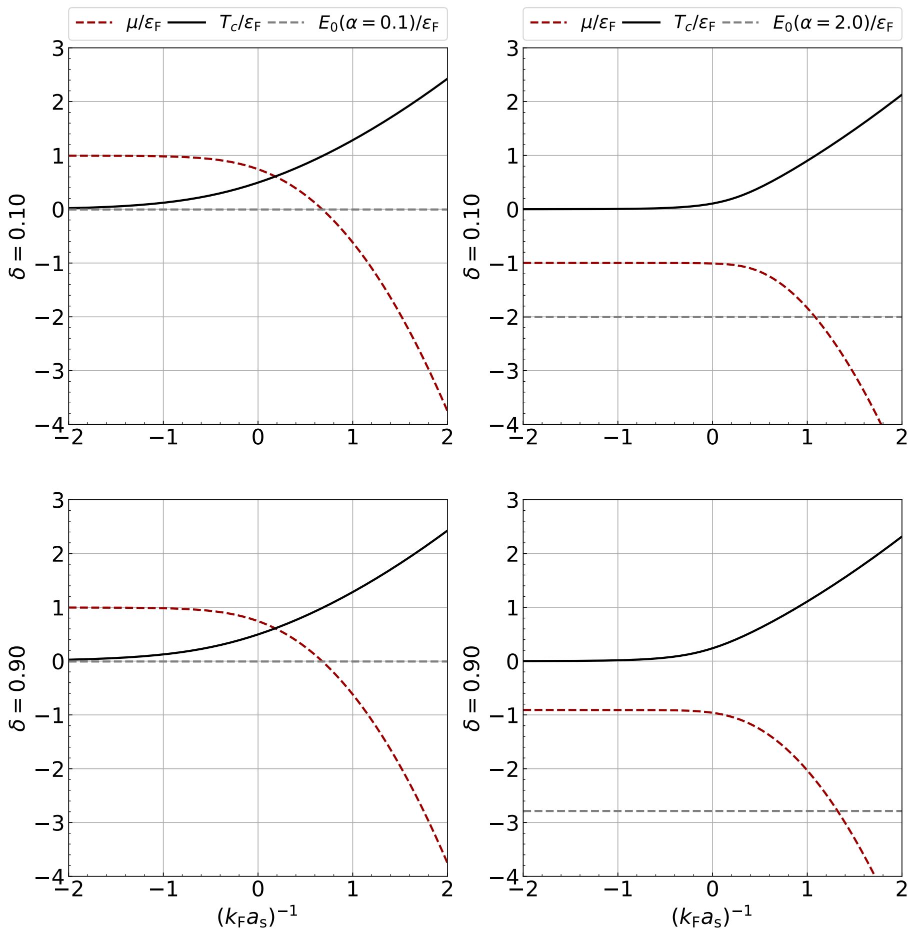

Figure 3.6: Evolution of the chemical potential and the critical temperature in the intraband scenario as functions of the scattering length. In these plots we have used $\delta = \{0.1, 0.9\}$ and $\alpha = \{0.1, 2.0\}$.

[6] We may safely dismiss the moduli of the excitation energies.

The numerical analysis in the finite temperature is less hardware demanding which allows us to explore the coupled equations a little bit deeper. First we plot in Fig. 3.6 the usual scattering length varying solutions for $\alpha = \{0.1, 2.0\}$ and $\delta = \{0.1, 0.9\}$. The intersection between E_0 (grey line) and the chemical potential characterizes the BCS to BEC transition. Here the results show the similar pattern as in the zero temperature case given in Fig. 3.2. We have the same behavior as in the single-band case, particularly for $\alpha = \delta = 0.1$, where these parameters can be understood as perturbations around the single-band case (compare with Fig. 2.5): the continuously decrease of the chemical potential starting at the Fermi level in the weak-coupling regime and becomes (more) negative as we approach the strong coupling regime; the critical temperature increases boundlessly. As the hybridization or mass asymmetry increases the BCS-BEC crossover requires higher values of $(k_F a_s)^{-1}$ to take place.

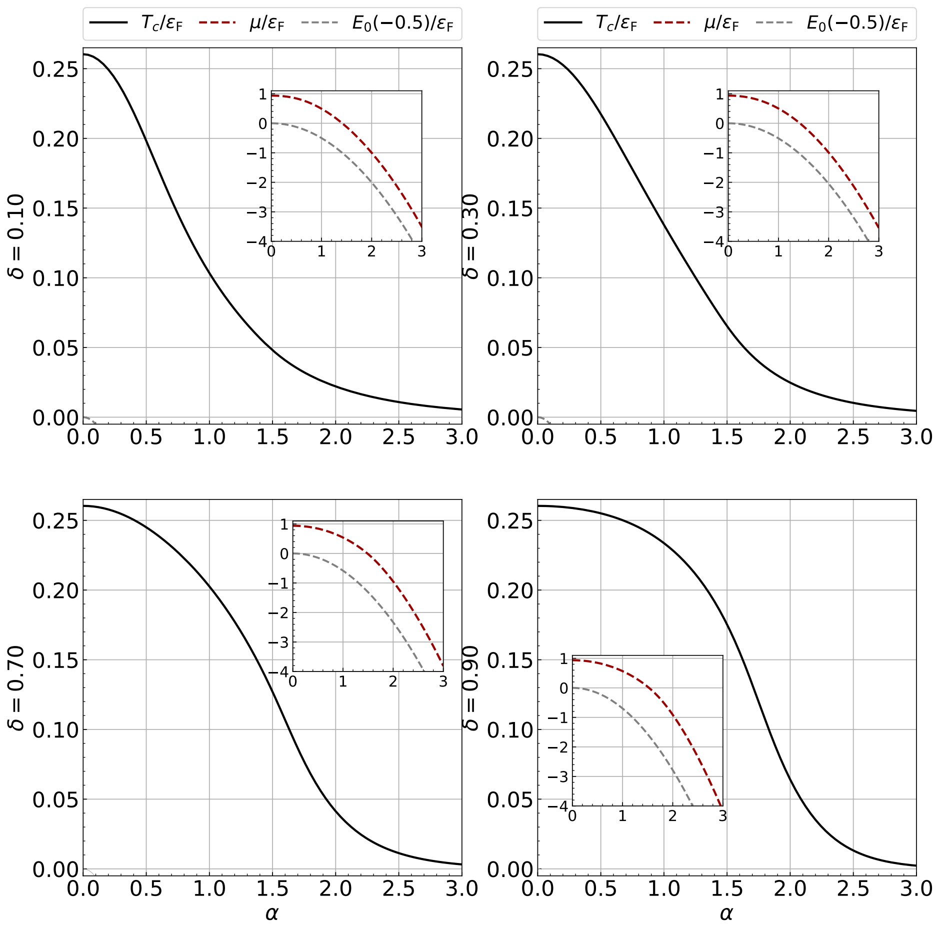

Figure 3.7: Evolution of the chemical potential and the critical temperature in the intraband scenario as functions of the hybridization strength. In these plots we have used $\gamma = 0$, $\delta = \{0.1, 0.3, 0.7, 0.9\}$ and $(k_F a_s)^{-1} = -0.5$ characteristic of the BCS regime. The chemical potential is always above E_0.

Secondly in Fig. 3.7 we present the chemical potential and critical temperature as functions of the hybridization for four different values of mass asymmetry while keeping $(k_F a_s)^{-1} = -0.5$. The chemical potential decreases with the hybridization and presents a weak dependence on δ.

The critical temperature mimics the behavior of the gap parameter showed in the $T = 0$ analysis vanishing as α increases. Thus the *intraband critical temperature decreases with the hybridization and slightly increases with the mass asymmetry.* We also note that band minimum is always below the chemical potential for $(k_F a_s)^{-1} = -0.5$ and therefore an $\alpha-$driven BCS-BEC crossover does not occur in the intraband scenario for any of the configurations considered.

Lastly, using $\gamma = 0$ and $(k_F a_s)^{-1} = \{-0.5, 0, 0.5\}$, we vary the mass asymmetry parameter to obtain the solutions shown in Fig. 3.8 for three values of the hybridization $\alpha = \{0.1, 1.0, 2.0\}$. The critical temperature increases with δ for all hybridization strengths, but, like in the $T = 0$ case, this increase seems to be directly associated with α. Conversely, the evolution of the chemical potential depends on $(k_F a_s)^{-1}$; it increases with δ if $(k_F a_s)^{-1} = \{-0.5, 0\}$ and decreases if $(k_F a_s)^{-1} = 0.5$. However for any value of the mass asymmetry the chemical potential remains above E_0.

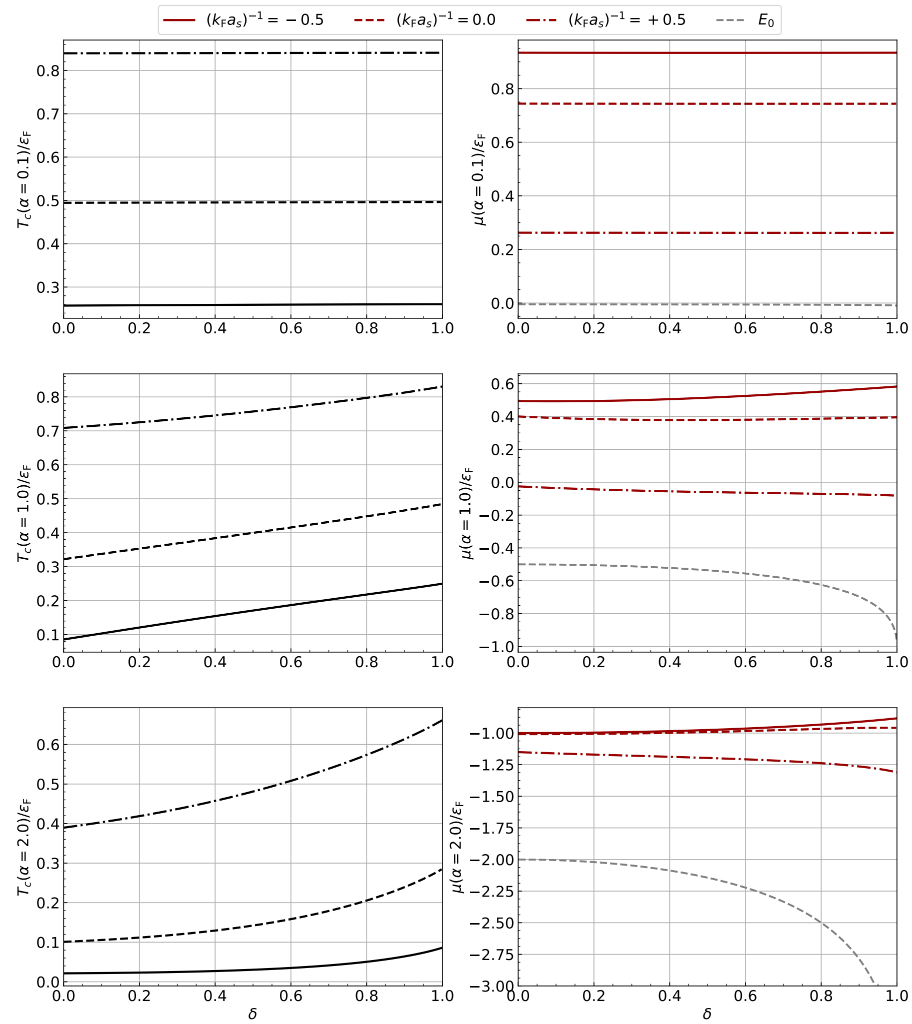

Figure 3.8: Evolution of the chemical potential and the critical temperature in the intraband scenario as functions of the mass asymmetry δ. In these plots we have used $\gamma = 0$, $\alpha = \{0.1, 1.0, 2.0\}$ (up to bottom) and $(k_F a_s)^{-1} = \{-0.5, 0, 0.5\}$.

3.7 Interband Scenario

Next we shall investigate the $\Omega_q = 0$ case which is argued to be the main contribution to superconductivity in cuprates where the $d-p$ interaction has a predominant role [56] and in heavy fermions involving f-electrons and conduction d-electrons [59,60].

The excitation energies are given by

$$\omega_{\mathbf{k}}^{\pm}(\Omega_q = 0) = \sqrt{\xi_{\mathbf{k}}^2 + (\delta\epsilon_{\mathbf{k}})^2 + |V_{\mathbf{k}}|^2 + \Delta_0^2 \pm 2\sqrt{\xi_{\mathbf{k}}^2|V_{\mathbf{k}}|^2 + (\delta\epsilon_{\mathbf{k}})^2(\xi_{\mathbf{k}}^2 + \Delta_0^2)}}. \tag{3.80}$$

Using the mean-field solutions for $(k_F a_s)^{-1} = -0.5$ and $\delta = 0.9$ we obtain Fig. 3.9. As in the intraband case, $\omega_{\mathbf{k}}^{+}$ is the dominant excitation, but two zero modes are present in $\omega_{\mathbf{k}}^{-}$ for small hybridization. As α increases the superconducting state is recovered. Another interesting observation is that the zero modes are absent in the excitations associated to small mass asymmetry values.

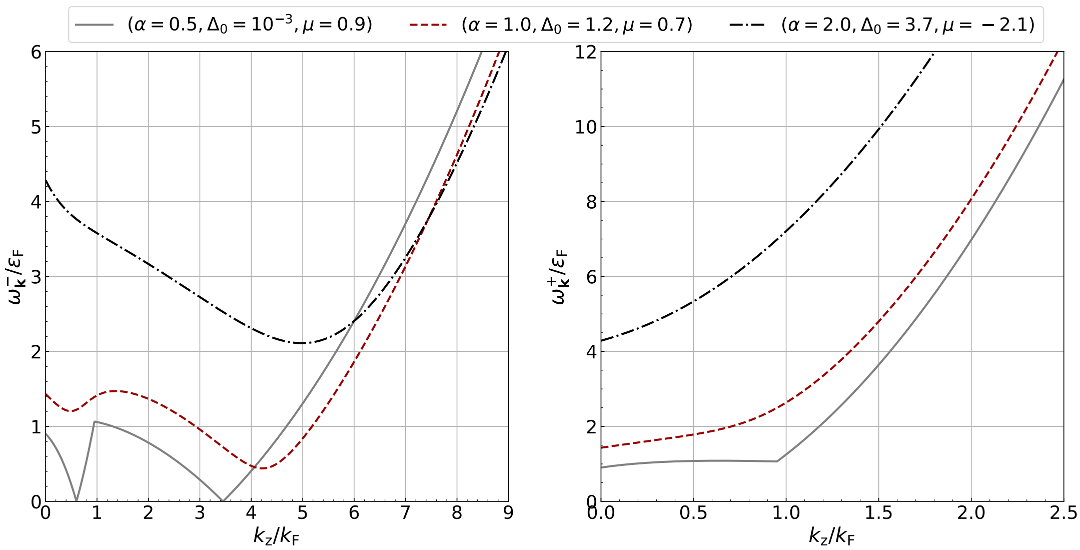

Figure 3.9: Interband quasi-particles excitation energies, $\omega_{\mathbf{k}}^{\pm}$, for $(k_F a_s)^{-1} = -0.5$, $\delta = 0.9$ and $k_x = k_y = 0$. The chemical potential and the intraband order parameter are expressed in units of Fermi energy.

If we turn the hybridization off, the excitation spectra become

$$\omega_{\mathbf{k}}^{\pm}(\Omega_0 = \alpha = 0) = \sqrt{\xi_{\mathbf{k}}^2 + \Delta_0^2} \pm \delta\epsilon_{\mathbf{k}} \tag{3.81}$$

where we observe that the energies differ only by a mass asymmetry term, $\delta\epsilon_{\mathbf{k}}$, and the zero modes happen twice for $\omega_{\mathbf{k}}^{-}$ at the points $(k_x = k_y = 0)$

$$k_z^2 = \frac{\mu}{1-\delta^2}\left[1 \pm \sqrt{1 - (1-\delta^2)/(1-\Delta_0^2/\mu^2)}\right]. \tag{3.82}$$

We note however that a numerical solution for $\delta = 0.9$ and $\alpha = 0$ has not been found, but as $\alpha \to 0$ the solution approaches $\Delta_0 \to 0$ and $\mu \to \epsilon_F$ implying in zeroes located at $k_z = 0.72k_F$ and $k_z = 3.2k_F$ as (closely) showed in Fig. 3.9.

3.7.1 Interband Solution at $T = 0\,\mathbf{K}$

In normalized units the interband gap equation 3.33 turns out to be

$$\frac{\pi}{k_F a_s} = \int \frac{\mathrm{d}^3 k}{2\pi}\left[\frac{1}{\epsilon_{\mathbf{k}}} - \frac{1}{\omega_{\mathbf{k}}^{+} + \omega_{\mathbf{k}}^{-}}\left(1 + \frac{\xi_{\mathbf{k}}^2 - (\delta\epsilon_{\mathbf{k}})^2 + |V_{\mathbf{k}}|^2 + \Delta_0^2}{\sqrt{(\xi_{\mathbf{k}}^2 - \Lambda_{\mathbf{k}}^2 + \Delta_0^2)^2 + 4|V_{\mathbf{k}}|^2\Delta_0^2}}\right)\right] \tag{3.83}$$

and together with the occupation number

$$F_\delta = \int \mathrm{d}^3 k\left[1 - \frac{\xi_{\mathbf{k}}}{\omega_{\mathbf{k}}^{+} + \omega_{\mathbf{k}}^{-}}\left(1 + \frac{\xi_{\mathbf{k}}^2 - \Lambda_{\mathbf{k}}^2 + \Delta_0^2}{\sqrt{(\xi_{\mathbf{k}}^2 - \Lambda_{\mathbf{k}}^2 + \Delta_0^2)^2 + 4|V_{\mathbf{k}}|^2\Delta_0^2}}\right)\right] \tag{3.84}$$

provide the solution for the chemical potential and the interband order parameter.

We begin analyzing the solutions as functions of the scattering length for $\delta = \{0.1, 0.5, 0.9\}$ and $\alpha = \{0.5, 2.0\}$. The results are displayed in Fig. 3.10 in which (again) we see a close resemblance with the single-band profile, the main difference is the linear divergence (in contrast with the exponential one in the single-band case) in the order parameter. As hybridization increases so does the order parameter while the chemical potential decreases. Additionally for small hybridization, $\alpha = 0.5$, we observe that as δ increases a pronounced discontinuity takes place.

It can be understood realizing that, in the BCS regime, the Cooper pair requires its fermions to be close to the Fermi surface and if their masses are too distinct this requirement cannot be met[7]. This difference is then compensated if we turn on the hybridization since the degeneracy of the excitation energies favors the pair formation and restores superconductivity. Conversely, if the system approaches the strong coupling regime, where the fermions are forming tight bound molecules, a large δ increases the interband order parameter.

This feature has also a parallel in degenerated Fermi gases with SOC, where we identify the hybridization with the spin-orbit interaction and the mass anisotropy with a Zeeman field [79]. So requiring the excitation gap to close, $\min_{\mathbf{k}}\{\omega_{\mathbf{k}}^{-}\} = \min_{\mathbf{k}}|\sqrt{\xi_{\mathbf{k}}^2 + \Delta_0^2} - \delta\epsilon_{\mathbf{k}}| = 0$ for $\alpha = 0$ and $|\mathbf{k}| = k_F$, we can estimate the discontinuity to occur around $\delta \approx \Delta_0/\epsilon_F$ in very good agreement with the results of Fig. 3.10.

[7] This is no longer true if we allow the chemical potential of each band to be different from each other [80].

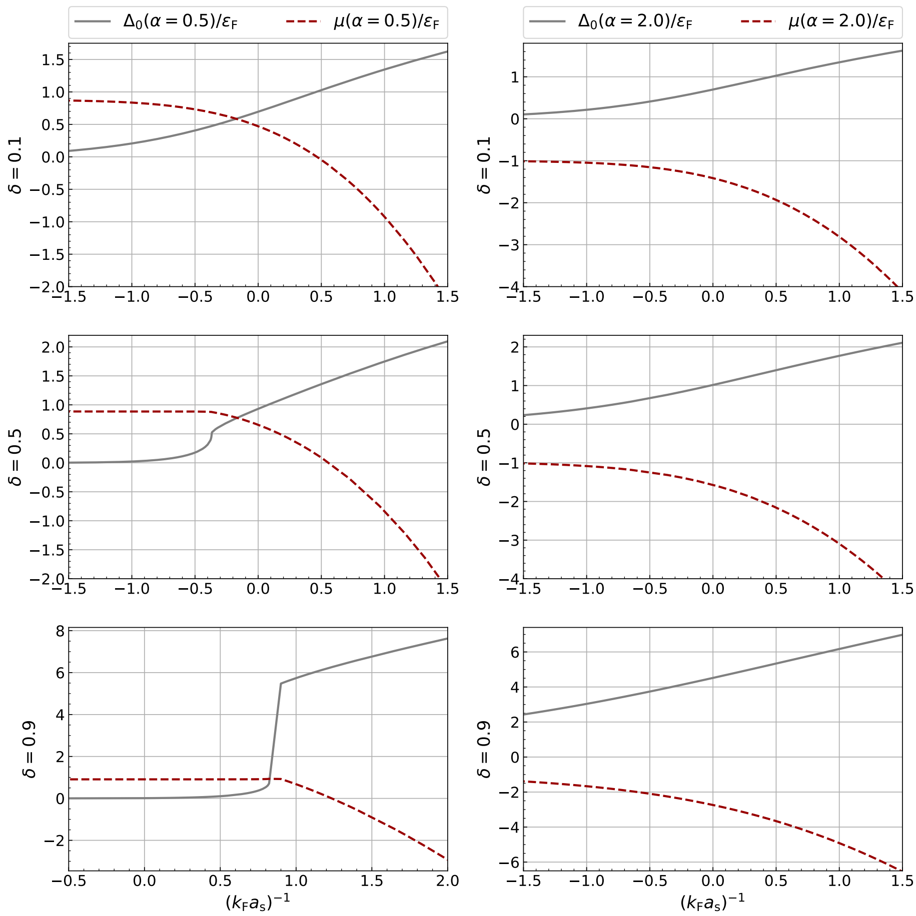

Figure 3.10: Evolution of the interband gap and the chemical potential as a function of the scattering length with the fixed parameters $\delta = \{0.1, 0.5, 0.9\}$ and $\alpha = \{0.5, 2.0\}$.

The previous results hint us about the possibility of a crossover into strong coupling regime induced by α. So next we keep the scattering length fixed at $(k_F a_s)^{-1} = -0.5$ while we vary the hybridization strength for the following mass asymmetry parameters $\delta = \{0.1, 0.3, 0.7, 0.9\}$; by doing so we obtain the curves displayed in Fig. 3.11.

The first two cases, $\delta = \{0.1, 0.3\}$, are very similar to each other: the chemical potential starts close to the Fermi level and decreases with α; the order parameter starts with a finite value, reaches a minimum and then grows with the hybridization. However its change is almost negligible so that, in the interval considered, one can safely assume the interband order parameter to be α-independent.

On the other hand, for $\delta = \{0.7, 0.9\}$ the investigated quantities exhibit a different behavior: the chemical potential still decreases with α but presents a subtle discontinuity; the order parameter starts from zero and grows up to a linear divergence that is accentuated increasing δ.

These results are in agreement with the ones obtained by F. Deus et. al. [13]. We can see the presence of the BCS-BEC crossover induced purely by an antisymmetric hybridization which is a new and exciting feature of the interband model.

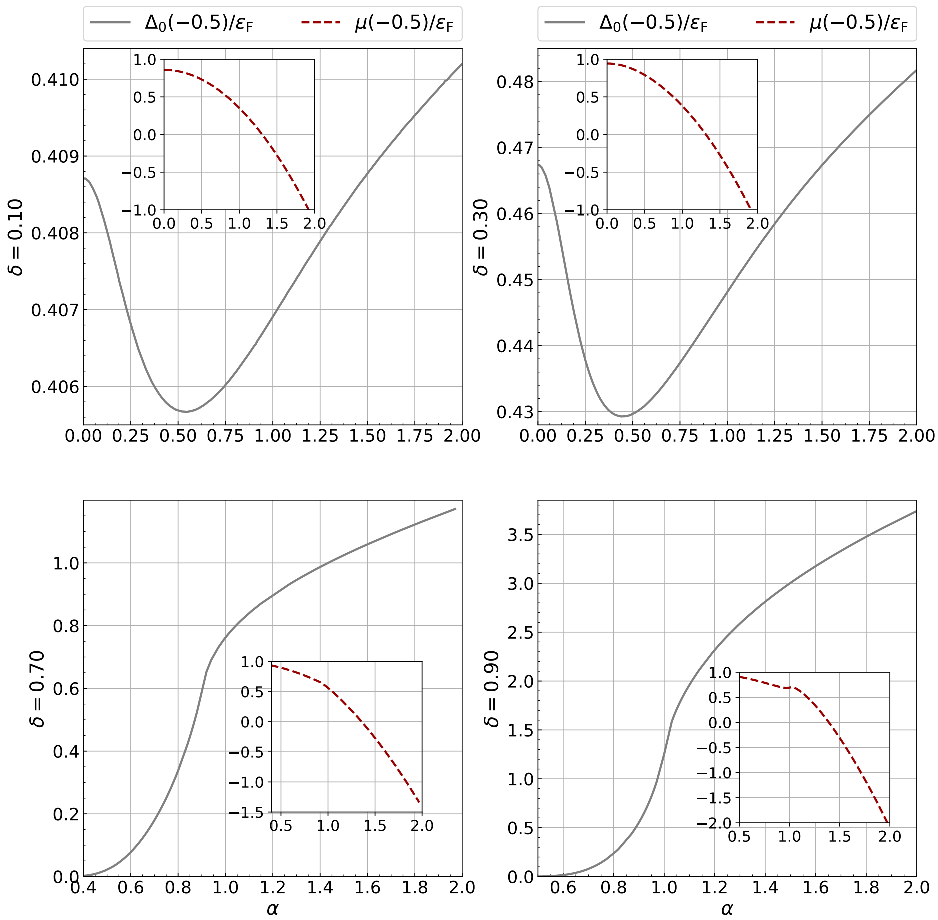

Figure 3.11: Evolution of the interband gap and the chemical potential via hybridization strength. In these plots we have used $\delta = \{0.1, 0.3, 0.7, 0.9\}$ (up to down) and $(k_F a_s)^{-1} = -0.5$ characteristic of the BCS regime.

The steep profiles presented in Figs. 3.10 and 3.11 for high values of mass asymmetry suggest a non-monotonous δ dependence. Thus let us continuously vary the mass difference parameter. We keep using $(k_F a_s)^{-1} = -0.5$ and $\alpha = \{0.5, 2.0\}$ in Fig. 3.12. For $\alpha = 0.5$ the main characteristic of the curves are their abrupt change, it shows that up to $\delta \approx 0.4$ both chemical potential and gap parameter present a crescent behavior. Beyond this point the chemical potential stabilizes at $\mu \approx 0.91\epsilon_F$. The interband order parameter falls vertiginously to zero as $\delta \to 1$. Increasing the hybridization to $\alpha = 2.0$ we observe a very different pattern. The chemical potential is always negative and decreases with the mass asymmetry. The gap parameter increases and then exponentially diverges as $\delta \to 1$ in agreement with the results of Figs. 3.10 and 3.11.

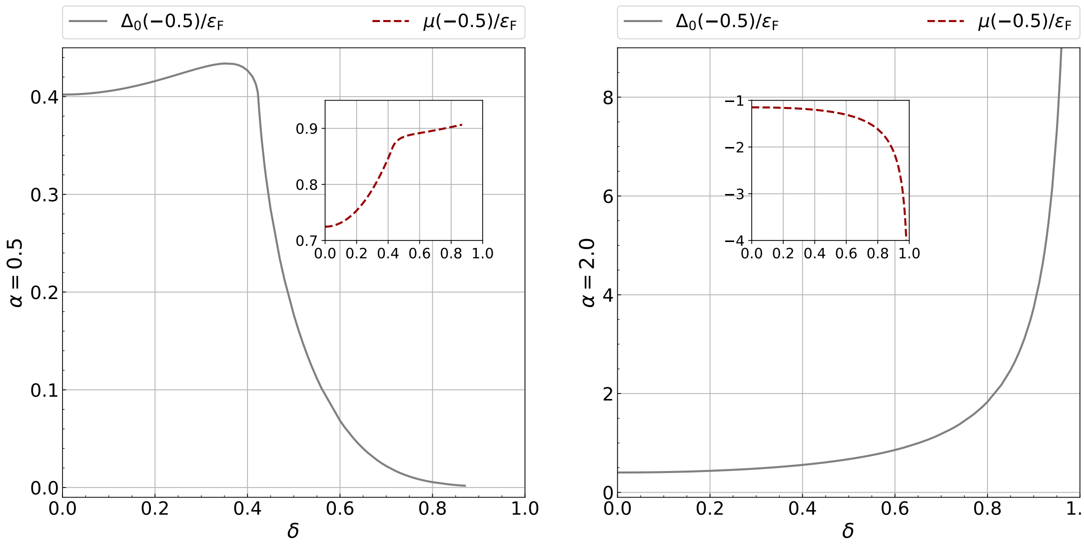

Figure 3.12: Evolution of the interband gap and the chemical potential via mass asymmetry parameter. In these plots we have used hybridization strengths $\alpha = \{0.5, 2.0\}$ and scattering length $(k_F a_s)^{-1} = -0.5$ within the weak coupling regime.

The opposite behavior of the order parameter for low and high hybridization values, $\alpha = 0.5$ and $\alpha = 2.0$, respectively, may provide a way to determine whether the system is in the weak or strong coupling regime. If the masses are too different and the system starts at the BCS phase (negative scattering length) a small hybridization cannot sustain the superconductivity, but as we increase α the transition to the BEC phase occurs and the pair bound becomes stronger as $\delta \to 1$.

3.7.2 Interband Solution at the Critical Temperature

Next we extend our discussion to the vicinity of the transition point where $\Delta_0 = 0$. Once again the excitation energies are given by $\xi^{\pm}_{\mathbf{k}} = \xi_{\mathbf{k}} \pm \Lambda_{\mathbf{k}}$ and we will still be using Eq. 3.79 for the occupation number. Furthermore we shall be able to check under what circumstances the criterion $\mu \simeq E_0$ is satisfied allowing us to determine the BCS-BEC transition more accurately than in the $T = 0$ case. So Eq. 3.27, in Fermi normalized units, after some arrangements reads

$$\frac{\pi}{k_F a_s} = \int \frac{\mathrm{d}^3 k}{2\pi} \left[\frac{1}{\epsilon_{\mathbf{k}}} - \frac{1}{2} \tanh\left(\frac{\xi^{+}_{\mathbf{k}}}{2T_c}\right) \left(\frac{1+\Theta_{\mathbf{k}}}{\xi_{\mathbf{k}}} - \frac{\Theta_{\mathbf{k}}}{\Lambda_{\mathbf{k}}}\right) - \frac{1}{2} \tanh\left(\frac{\xi^{-}_{\mathbf{k}}}{2T_c}\right) \left(\frac{1+\Theta_{\mathbf{k}}}{\xi_{\mathbf{k}}} + \frac{\Theta_{\mathbf{k}}}{\Lambda_{\mathbf{k}}}\right) \right], \tag{3.85}$$

where we have introduced $\Theta_{\mathbf{k}} \equiv \frac{|V_{\mathbf{k}}|^2}{\xi^2_{\mathbf{k}} - \Lambda^2_{\mathbf{k}}}$. Roughly speaking we replace the superconductivity order parameter by the critical temperature but, since they are closely related, we can expect T_c to show similar features as the ones presented by Δ_0 in the previous section.

Solving the coupled equations for the critical temperature and chemical potential as we continuously vary the scattering length with mass asymmetries $\delta = \{0.1, 0.5, 0.9\}$ we obtain the results presented in Fig. 3.13, where we show the solution for three values of the hybridization strength, $\alpha = \{0.5, 1.0, 2.0\}$ and the band minimum, E_0.

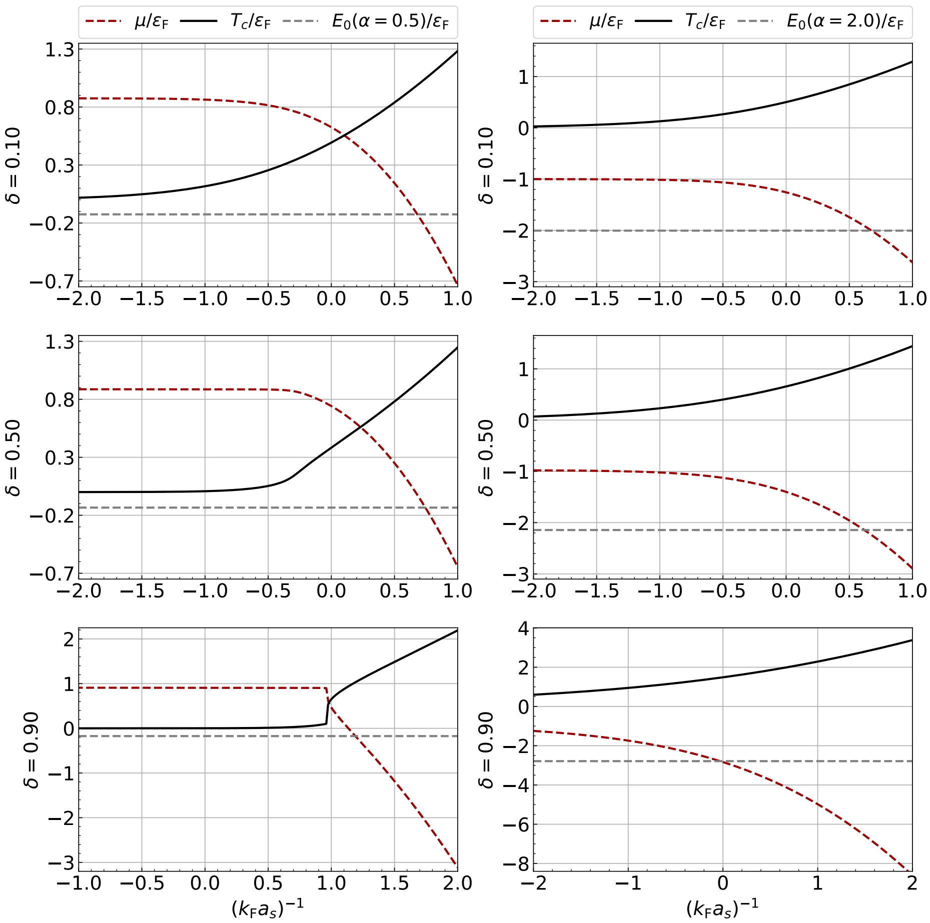

Figure 3.13: Evolution of the critical temperature and the chemical potential in the interband scenario through variation of the scattering length for $\alpha = 0.5$ (left panels) and $\alpha = 2.0$ (right panels) with $\delta = \{0.1, 0.5, 0.9\}$ (up to bottom).

First of all we observe the increase of the critical temperature, even its divergence, and the decrease of the chemical potential with $(k_F a_s)^{-1}$ so that, qualitatively, the structure from the single-band case is maintained. More specifically, for the left panels of Fig. 3.13 corresponding to $\alpha = 0.5$, there is an increasing discontinuity in the solutions as $\delta \to 1$, analogously to the $T = 0$ case. Furthermore the BEC transition, indicated by the intersection $\mu \simeq E_0$, occurs for smaller values of $(k_F a_s)^{-1}$ as the mass asymmetry increases. As the hybridization increases, in the right panels for $\alpha = 2.0$, the chemical potential is further down-shifted and the BCS-BEC crossover takes place sooner than in the $\alpha = 0.5$ counterparts. Here however all solutions are smooth.

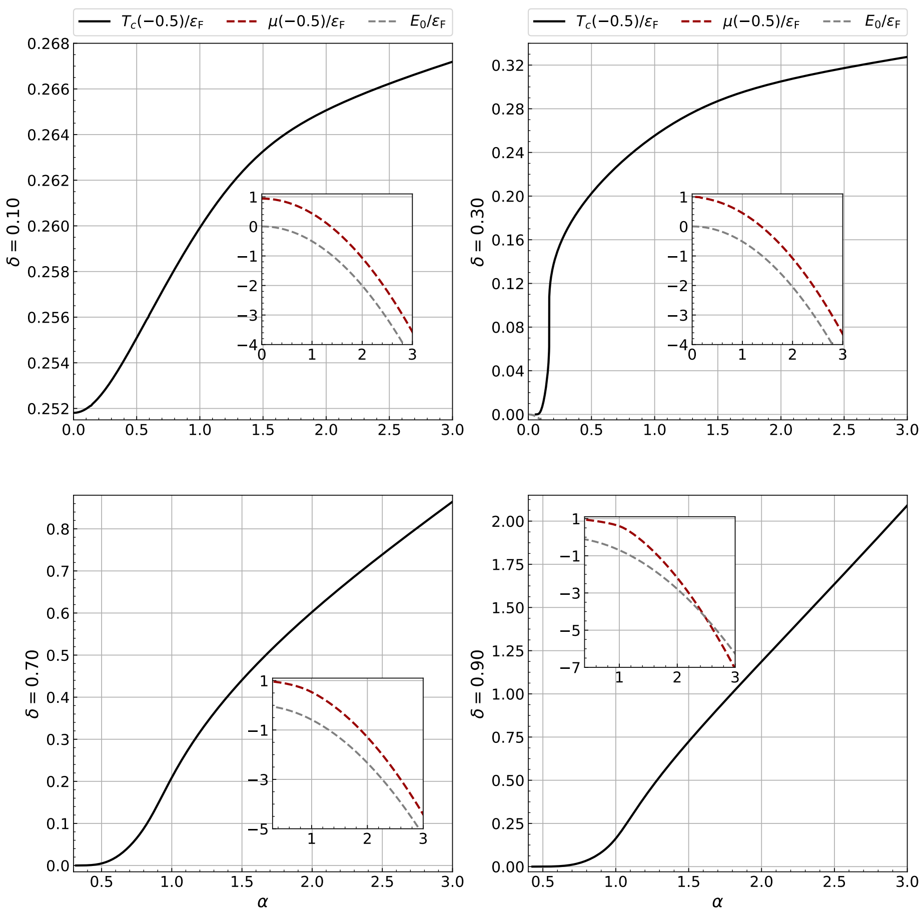

Figure 3.14: Evolution of the critical temperature and the chemical potential in the interband scenario with hybridization. In these plots we have used $(k_F a_s)^{-1} = -0.5$, characteristic of the BCS regime, and $\delta = \{0.1, 0.3, 0.7, 0.9\}$.

We proceed by presenting Fig. 3.14 where we vary the hybridization strength while keeping $(k_F a_s)^{-1} = -0.5$ for $\delta = \{0.1, 0.3, 0.7, 0.9\}$. All the chemical potential curves have a similar behavior starting from the Fermi surface and decreasing with α; for $\delta = 0.90$ there is a subtle discontinuity. Differently from the intraband case, here the BCS-BEC crossover does take place, but only in the very distinct masses scenario $\delta = 0.90$. It is important to notice that the realization of the crossover may still be possible for higher values of α, although such limit is not physically reasonable on most systems. Another point to bear in mind is that, by including of the thermal fluctuations, the chemical potential solutions decrease faster than the mean-field ones so that the crossover takes place a little bit earlier (see Fig. 4.4).

For fermions with similar masses, the critical temperature curve characterized by $\delta = 0.10$ presents a finite value in the absence of hybridization; on the other hand the temperatures labeled by $\delta \geq 0.3$ go to zero as α decreases. As in the scattering length variation case, all critical temperatures diverge for large α, more linearly-like for higher values of δ. Thus we have a strong indicative of an equivalence between the odd-parity hybridization and the scattering length in the promotion of the BCS-BEC crossover.

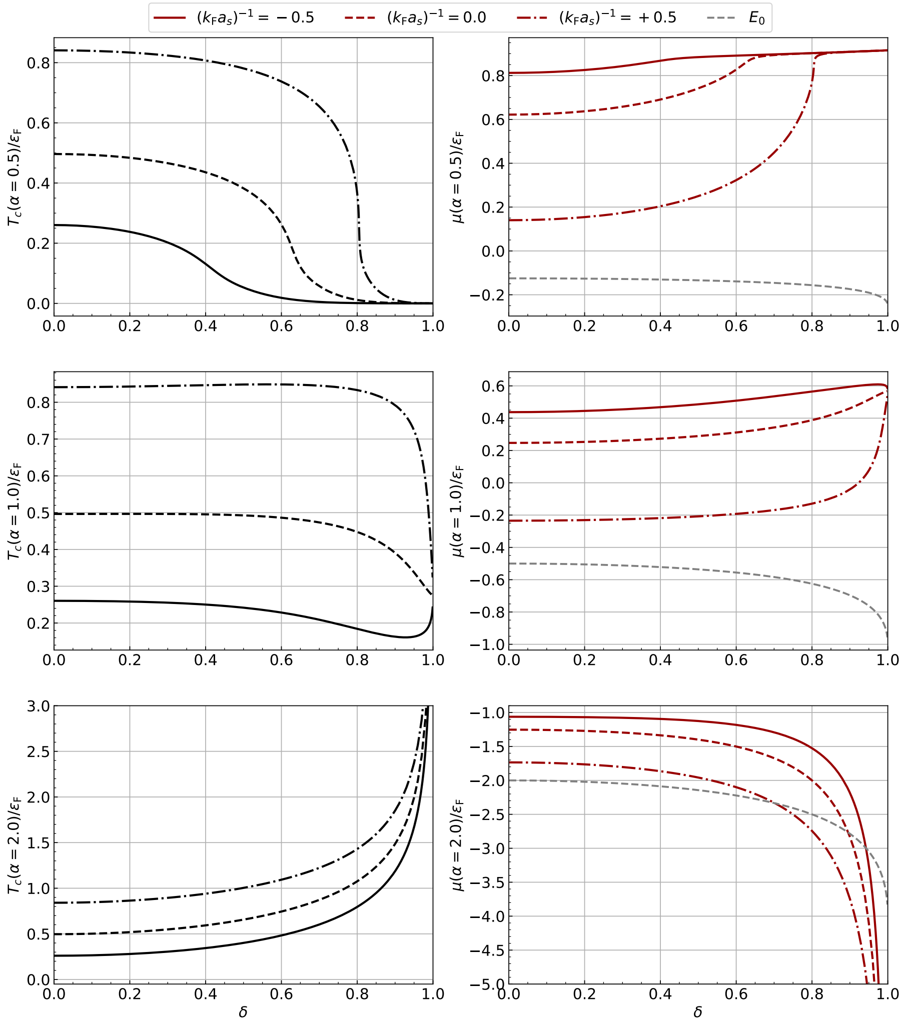

Figure 3.15: Evolution of the critical temperature and the chemical potential in the interband scenario through variation of δ for (from up to bottom) $\alpha = \{0.5, 1.0, 2.0\}$ and $(k_F a_s)^{-1} = \{-0.5, 0.0, 0.5\}$.

Once more the influence of δ instigates further analysis. So Fig. 3.15 shows the solution via mass asymmetry variation for $(k_F a_s)^{-1} = \{-0.5, 0, 0.5\}$ and three values of hybridization strength $\alpha = \{0.5, 1.0, 2.0\}$. Initially we note that temperature curves increase and the chemical potential ones decrease for higher scattering length values, in accordance with the previous results. For $\alpha = 0.5$ the system is always in the BCS phase, no matter the value of δ, and in this regime an increase of the mass difference of the fermions destroys superconductivity and collapses the chemical potential to a common Fermi surface $\mu \approx 0.91\epsilon_F$. As we increase the hybridization to $\alpha = 1.0$ all temperature values increase and are always finite; the chemical potential curves decrease and become distinct from one another, but are still above E_0. However for $\alpha = 2.0$ the critical temperatures diverge with δ and so does the chemical potential, decreasing and becoming infinitely negative as $\delta \to 1$. We also observe that BCS-BEC crossover may take place for $\alpha = 2.0$ if the mass asymmetry is $\delta > 0.6$. Again the numerical results are in agreement with the interpretation that in the BCS limit a high mass asymmetry prevents the Cooper pair formation, but as hybridization increases and leads the system to the strong-coupling regime the molecular binding benefits from very distinct masses. Thus it becomes evident that the role of the mass asymmetry parameter should not be overlooked while studying multi-band superconductors, and although HF systems usually involve high values of δ, its tuning may be important.

3.8 Considerations

In this chapter we have developed a systematic calculation of the mean-field equations of a two-band superconducting system under the influence of an odd-parity hybridization. A detailed mapping of the parameters of our theory in two specific cases, intra and interband was presented.

Although superconductivity in the intraband scenario was showed to be destroyed by hybridization, in the interband sector, the confirmation of a BCS-BEC crossover induced by hybridization was achieved in an analogous fashion as it occurs in ultracold gases with spin-orbit coupling. Additionally in our model we could explore the role played by the difference of the quasi-particles masses where, in the interband case, it is a key parameter to determine whether the system is in the weak or strong coupling regime.

Naturally, as it was expected from a mean-field treatment, the divergence of the condensation temperature is present in the intraband scenario, as function of $(k_F a_s)^{-1}$, and in the interband one, as function of $(k_F a_s)^{-1}$ or α. So, like we have done in the single-band case, we shall next include the thermal fluctuations to obtain the proper critical temperature in the strong coupling regime. However, from now on, we shall concentrate our analysis in the interband sector since, as already argued, we are mainly interested in an α-driven BCS-BEC crossover. Nevertheless, if the reader is interested in the details regarding the intraband in the strong coupling regime, the calculations presented in App. D show the equivalence between the intraband fermions and non-interacting bosons.

Chapter 4

Interband Thermal Fluctuations

In this chapter we will introduce the thermal fluctuations in the interband sector. The physical reasoning is exactly the same as in the single-band case, however, the actual calculation of the interband pair susceptibility is a much more troublesome task. Once we obtain the vertex function we then analyze the strong coupling limit in order to determine whether or not a physical condensation temperature is achievable via an odd-parity hybridization. We also explore the influence of the mass asymmetry and hybridization in the binding energy. Lastly we propose an interpolation between both BCS and BEC regimes.

4.1 Interband Vertex Function

As we reach the strong-coupling regime the quasi-particles become more localized and thus they are not properly described by a constant field. The extrapolation of the mean-field results leads to a misinterpretation of T_c which actually describes the dissociation temperature of the pairs rather than the condensation temperature. Next we will show that correcting the interband order parameter on a one-loop level heals this issue.

Our approach remains the same: a perturbation around the mean-field solution $\Delta = \Delta_q \ll \epsilon_F$ and the expansion of the

$$\mathrm{Tr}\ln \mathbf{G}^{-1} = \mathrm{Tr}\ln \mathbf{G}_0^{-1} - \sum_{n=1}^{\infty} \frac{1}{2n}\mathrm{Tr}(\mathbf{G}_0\boldsymbol{\Delta})^{2n} \tag{4.1}$$

in the effective action. To start let us recall that Eq. 3.15 is base independent, i. e., we can apply a rotation into the 4D Nambu spinor, Eq. 3.14, to diagonalize $\mathbf{G}_0$. Specifically we use a Bogoliubov-de Gennes transformation $\mathbf{U}_\mathbf{k} = \mathbb{1}_2 \otimes \exp(i\sigma_1\phi_\mathbf{k})$, with σ_1 the first Pauli matrix, $i\sin(2\phi_\mathbf{k}) = V_\mathbf{k}/\Lambda_\mathbf{k}$ and $\cos(2\phi_\mathbf{k}) = (\delta\epsilon_\mathbf{k})/\Lambda_\mathbf{k}$, as illustrated in Fig. 4.1.

Thus, considering the leading order in the expansion the action becomes

$$S^{(2)}[\Delta] = \sum_q \left[\frac{2|\Delta_q|^2}{g_1} + \frac{1}{2}\mathrm{Tr}(\tilde{\mathbf{G}}_0\tilde{\boldsymbol{\Delta}})^2\right], \tag{4.2}$$

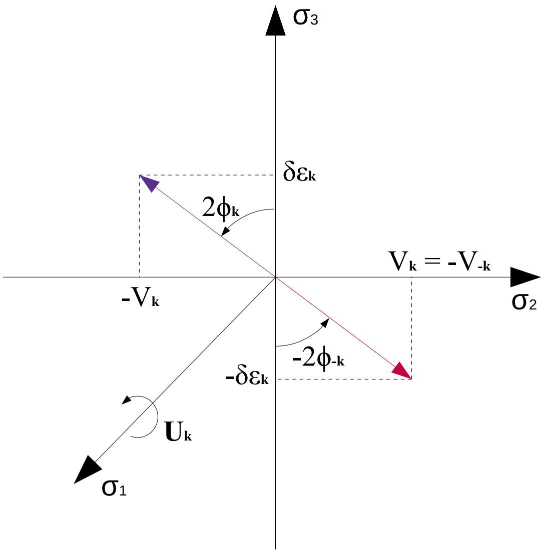

Figure 4.1: Effect of the unitary transformation $\mathbf{U}_{\mathbf{k}}$. The angle $2\phi_{\mathbf{k}}$ (instead of just $\phi_{\mathbf{k}}$) is a characteristic of the spinors rotation. Such rotation allows the diagonalization of $\mathbf{G}_0$ and simplifies the calculations involving it.

with the diagonal propagator (see App. B.1 for the details)

$$\tilde{\mathbf{G}}_0 = \mathbf{U}_{\mathbf{k}}^{\dagger}\mathbf{G}_0\mathbf{U}_{\mathbf{k}} = \begin{bmatrix} G_k^- & 0 & 0 & 0 \\ 0 & G_k^+ & 0 & 0 \\ 0 & 0 & -G_{-k}^- & 0 \\ 0 & 0 & 0 & -G_{-k}^+ \end{bmatrix}, \tag{4.3}$$

where

$$G_k^{\pm} \equiv \frac{1}{i\omega_n - \xi_{\mathbf{k}}^{\pm}} \tag{4.4}$$

is the Green's function of a single fermion with energy $\xi_{\mathbf{k}}^{\pm} = \xi_{\mathbf{k}} \pm \Lambda_{\mathbf{k}}$ (not surprisingly). Applying the same transformation to the fluctuations matrix results in (App. B.2)

$$\begin{aligned} \tilde{\mathbf{\Delta}}(k,q) &= \mathbf{U}_{\mathbf{k+q/2}}^{\dagger}\mathbf{\Delta}_q\mathbf{U}_{\mathbf{k-q/2}} \\ &= \cos(\phi_{\mathbf{k+q/2}} + \phi_{\mathbf{k-q/2}})\tilde{\mathbf{\Delta}}_{\text{Inter}}(q) + i\sin(\phi_{\mathbf{k+q/2}} + \phi_{\mathbf{k-q/2}})\tilde{\mathbf{\Delta}}_{\text{Intra}}(q), \end{aligned} \tag{4.5}$$

where

$$\tilde{\mathbf{\Delta}}_{\text{Inter}}(q) = \begin{bmatrix} 0 & 0 & 0 & -\Delta_q \\ 0 & 0 & \Delta_q & 0 \\ 0 & \bar{\Delta}_{-q} & 0 & 0 \\ -\bar{\Delta}_{-q} & 0 & 0 & 0 \end{bmatrix} \tag{4.6}$$

and

$$\tilde{\mathbf{\Delta}}_{\text{Intra}}(q) = \begin{bmatrix} 0 & 0 & -\Delta_q & 0 \\ 0 & 0 & 0 & \Delta_q \\ \bar{\Delta}_{-q} & 0 & 0 & 0 \\ 0 & -\bar{\Delta}_{-q} & 0 & 0 \end{bmatrix}. \tag{4.7}$$

Within the term $\tilde{\boldsymbol{\Delta}}_{\text{Intra}}$ we can see the existence of an intraband character even though we considered initially a pure interband model. To make it clearer let us observe that in the rotated basis $\tilde{\Psi}_k = \mathbf{U}_{\mathbf{k}}^{-1}\Psi_k$ we may write $\tilde{\Psi}_k^\dagger = (\beta_{k\uparrow}^\dagger\ \alpha_{k\uparrow}^\dagger\ \beta_{-k\downarrow}\ \alpha_{-k\downarrow})$, with the quasi-particles $\alpha_{k\sigma}$ and $\beta_{k\sigma}$ composed of the original A and B fermions as $\alpha_{k\sigma} = a_{k\sigma}\cos(\phi_{\mathbf{k}}) + ib_{k\sigma}\sin(\phi_{\mathbf{k}})$ and $\beta_{k\sigma} = b_{k\sigma}\cos(\phi_{\mathbf{k}}) + ia_{k\sigma}\sin(\phi_{\mathbf{k}})$. Thus implying the diagonalized Hamiltonian

$$\begin{aligned}\mathcal{H} = &\sum_{k,\sigma}\xi_{\mathbf{k}}^+\alpha_{k\sigma}^\dagger\alpha_{k\sigma} + \sum_{k,\sigma}\xi_{\mathbf{k}}^-\beta_{k\sigma}^\dagger\beta_{k\sigma}\\ &+\sum_{k,q,\sigma}\cos(\phi_{\mathbf{k+q}}+\phi_{\mathbf{k-q}})[\Delta_{2q}\alpha_{k+q\sigma}^\dagger\beta_{-k+q-\sigma}^\dagger + \text{H.c.}]\\ &+\sum_{k,q} i\sin(\phi_{\mathbf{k+q}}+\phi_{\mathbf{k-q}})[\Delta_{2q}\beta_{k+q\uparrow}^\dagger\beta_{-k+q\downarrow}^\dagger - \Delta_{2q}\alpha_{k+q\uparrow}^\dagger\alpha_{-k+q\downarrow}^\dagger + \text{H.c.}],\end{aligned}\tag{4.8}$$

which, if we consider the mean-field solution, becomes

$$\begin{aligned}\mathcal{H}_{\text{MF}} = &\sum_{k,\sigma}[(\xi_{\mathbf{k}} - \Lambda_{\mathbf{k}} - i\omega_n)\alpha_{k\sigma}^\dagger\alpha_{k\sigma} + (\xi_{\mathbf{k}} + \Lambda_{\mathbf{k}} - i\omega_n)\beta_{k\sigma}^\dagger\beta_{k\sigma}]\\ &+\sum_{k,\sigma}\frac{\delta\epsilon_{\mathbf{k}}}{\Lambda_{\mathbf{k}}}[\Delta_0\alpha_{k\sigma}^\dagger\beta_{-k-\sigma}^\dagger + \text{H.c.}] + \sum_k\frac{V_{\mathbf{k}}}{\Lambda_{\mathbf{k}}}[\Delta_0\beta_{k\uparrow}^\dagger\beta_{-k\downarrow}^\dagger - \Delta_0\alpha_{k\uparrow}^\dagger\alpha_{-k\downarrow}^\dagger + \text{H.c.}].\end{aligned}\tag{4.9}$$

Analyzing Eq. 4.9 we see that a pure interband model with odd-parity hybridization is equivalent to another one with an even s-wave symmetry in the interband order parameter proportional to the original fermions mass difference, $\Delta_{-\mathbf{k}} = \Delta_{\mathbf{k}} \propto \delta\epsilon_{\mathbf{k}}$, plus two purely imaginary intraband terms, both induced by hybridization and therefore with a p-wave character. It is interesting to note that the mass asymmetry also regulates the contribution of the intra and interband terms. Indeed, if we take $\delta = 0$ then

$$\begin{aligned}\mathcal{H}_{\text{MF}}(\delta=0) = &\sum_{k,\sigma}[(\xi_{\mathbf{k}} - |V_{\mathbf{k}}| - i\omega_n)\alpha_{k\sigma}^\dagger\alpha_{k\sigma} + (\xi_{\mathbf{k}} + |V_{\mathbf{k}}| - i\omega_n)\beta_{k\sigma}^\dagger\beta_{k\sigma}]\\ &-\sum_k\frac{V_{\mathbf{k}}}{|V_{\mathbf{k}}|}(\Delta_0\alpha_{k\uparrow}^\dagger\alpha_{-k\downarrow}^\dagger - \Delta_0\beta_{k\uparrow}^\dagger\beta_{-k\downarrow}^\dagger + \text{H.c.}),\end{aligned}\tag{4.10}$$

we see that Eq. 4.10 is equivalent to a two-particle Hamiltonian solely with intraband interactions. Conversely, if $V_{\mathbf{k}}$ is negligible compared to $\delta\epsilon_{\mathbf{k}}$ Eq. 4.10 becomes simply an interband Hamiltonian.

Focusing in the gaussian correction of Eq. 4.2 one can show that it yields (see App. B.3)

$$\begin{aligned}\frac{1}{2}\text{Tr}(\tilde{\mathbf{G}}_0\tilde{\boldsymbol{\Delta}})^2 = &-\frac{1}{\beta}\sum_{\mathbf{k},\omega_n}\cos^2(\phi_{\mathbf{k-q}}+\phi_{\mathbf{k+q}})(G_{k-q}^+G_{-k-q}^- + G_{k-q}^-G_{-k-q}^+)|\Delta_{2q}|^2\\ &-\frac{1}{\beta}\sum_{\mathbf{k},\omega_n}\sin^2(\phi_{\mathbf{k-q}}+\phi_{\mathbf{k+q}})(G_{k-q}^+G_{-k-q}^+ + G_{k-q}^-G_{-k-q}^-)|\Delta_{2q}|^2\end{aligned}\tag{4.11}$$

and summing over the fermionic frequencies as indicated in App. B.4 leads to

$$\frac{1}{\beta}\sum_{\omega_n}G_{k-q}^\pm G_{-k-q}^\pm = \frac{1-\eta_F(\xi_{\mathbf{k+q}}^\pm)-\eta_F(\xi_{\mathbf{k-q}}^\pm)}{2i\omega_m + \xi_{\mathbf{k+q}}^\pm + \xi_{\mathbf{k-q}}^\pm},\tag{4.12}$$

with η_F the Fermi distribution. So our second order effective action can be written as

$$S^{(2)}[\Delta] = \sum_q \Gamma_q^{-1} |\Delta_q|^2, \tag{4.13}$$

where

$$\begin{aligned}
\Gamma_q^{-1} = \frac{2}{g_1} &- \sum_{\mathbf{k}} \cos^2\left(\phi_{\mathbf{k}-\mathbf{q}/2} + \phi_{\mathbf{k}+\mathbf{q}/2}\right) \frac{1 - n_F(\xi^+_{\mathbf{k}-\mathbf{q}/2}) - n_F(\xi^-_{\mathbf{k}+\mathbf{q}/2})}{i\omega_m + \xi^+_{\mathbf{k}-\mathbf{q}/2} + \xi^-_{\mathbf{k}+\mathbf{q}/2}} \\
&- \sum_{\mathbf{k}} \cos^2\left(\phi_{\mathbf{k}-\mathbf{q}/2} + \phi_{\mathbf{k}+\mathbf{q}/2}\right) \frac{1 - n_F(\xi^-_{\mathbf{k}-\mathbf{q}/2}) - n_F(\xi^+_{\mathbf{k}+\mathbf{q}/2})}{i\omega_m + \xi^-_{\mathbf{k}-\mathbf{q}/2} + \xi^+_{\mathbf{k}+\mathbf{q}/2}} \\
&- \sum_{\mathbf{k}} \sin^2\left(\phi_{\mathbf{k}-\mathbf{q}/2} + \phi_{\mathbf{k}+\mathbf{q}/2}\right) \frac{1 - n_F(\xi^+_{\mathbf{k}-\mathbf{q}/2}) - n_F(\xi^+_{\mathbf{k}+\mathbf{q}/2})}{i\omega_m + \xi^+_{\mathbf{k}-\mathbf{q}/2} + \xi^+_{\mathbf{k}+\mathbf{q}/2}} \\
&- \sum_{\mathbf{k}} \sin^2\left(\phi_{\mathbf{k}-\mathbf{q}/2} + \phi_{\mathbf{k}+\mathbf{q}/2}\right) \frac{1 - n_F(\xi^-_{\mathbf{k}-\mathbf{q}/2}) - n_F(\xi^-_{\mathbf{k}+\mathbf{q}/2})}{i\omega_m + \xi^-_{\mathbf{k}-\mathbf{q}/2} + \xi^-_{\mathbf{k}+\mathbf{q}/2}}
\end{aligned} \tag{4.14}$$

is the interband vertex or pair susceptibility function. As pointed out, the mass difference is responsible for the mixing of the $\pm$ quasi-particles while the hybridization acts in the "new" intraband sector. Having derived the vertex function we can, at least in principle, obtain the corrected BCS-BEC crossover. Unfortunately it turns out to be a very arduous task, mainly, but not only, in the numerical calculation. However, we still can extract many interesting results focusing our attention in the strong coupling regime.

4.2 Interband Effective Action in the Strong Coupling Regime

We are mainly interested in the study of the strong coupling regime, since we have seen that in a hybridization driven BCS-BEC crossover, there is still a non-physical condensation temperature. Here we intend to correct this temperature and, later on, suggest a complete interpolation of both BCS and BEC limits. So, let us start recalling that close to the transition point the characteristic excitations are given by $\epsilon^\pm_{\mathbf{k}} = \epsilon_{\mathbf{k}} \pm \Lambda_{\mathbf{k}}$. Thus it is important to observe that to enter the BEC regime the system's chemical potential must be below both bands (in the single-band case it corresponds simply to a negative chemical potential), but here the crossover is expected to take place around $\mu \lesssim E_0$. Thus in our next approximations we shall consider $|\mu| \gg T_c$ so that we can neglect the exponentially small contributions from Fermi distributions in Eq. 4.14. Keeping that in mind and performing a gradient expansion for $(\omega_m, \mathbf{q}) \ll k_{\mathrm{F}}$, as described in App. C, we get

$$\Gamma_q^{-1} = \Gamma_0^{-1} - \delta^2 \Gamma_{\mathbf{q}^2}^{-1} + J(\alpha)\left(i\omega_m + \frac{\mathbf{q}^2}{4m}\right), \tag{4.15}$$

where

$$\Gamma_0^{-1} = -\frac{m}{2\pi a_s} + \sum_{\mathbf{k}} \left(\frac{1}{\epsilon_{\mathbf{k}}} - \frac{1+\Theta_{\mathbf{k}}}{\xi_{\mathbf{k}}} \right), \tag{4.16}$$

$$\Gamma_{\mathbf{q}^2}^{-1} = \frac{\mathbf{q}^2}{4m} \sum_{\mathbf{k}} \frac{\epsilon_{\mathbf{k}}}{\xi_{\mathbf{k}}} \frac{\Theta_{\mathbf{k}}}{\xi_{\mathbf{k}}^2 - \Lambda_{\mathbf{k}}^2} + \sum_{\mathbf{k}} \frac{1}{\xi_{\mathbf{k}}^3} \left[\left(\frac{\mathbf{k}\cdot\mathbf{q}}{2m} \right) (1+\Theta_{\mathbf{k}}) + \frac{\epsilon_{\mathbf{k}}}{2} \frac{V_{\mathbf{k}} V_{\mathbf{q}}}{\xi_{\mathbf{k}}^2 - \Lambda_{\mathbf{k}}^2} \right]^2, \tag{4.17}$$

$$J(\alpha) = \sum_{\mathbf{k}} \left(\frac{1+\Theta_{\mathbf{k}}}{2\xi_{\mathbf{k}}^2} + \frac{\Theta_{\mathbf{k}}}{\xi_{\mathbf{k}}^2 - \Lambda_{\mathbf{k}}^2} \right) = \frac{\pi}{4} \frac{\nu_0}{\sqrt{\epsilon_F}} \frac{1}{\sqrt{-\mu}} + \sum_{\mathbf{k}} \Theta_{\mathbf{k}} \left(\frac{1}{2\xi_{\mathbf{k}}^2} + \frac{1}{\xi_{\mathbf{k}}^2 - \Lambda_{\mathbf{k}}^2} \right), \tag{4.18}$$

with ν_0 the density of states at the Fermi level.

From Eqs. 4.16-4.18 we can observe how hybridization modifies the pair susceptibility in comparison to Eq. 2.43. It is also important to note that the term $\Gamma_{\mathbf{q}^2}^{-1}$ comes accompanied by δ^2 implying that it is most relevant in high mass asymmetry problems.

To demonstrate that indeed the inclusion of the thermal fluctuations corrects the critical temperature in the strong coupling regime is to show the equivalence between the interband effective action and a bosonic one. To achieve that we need to identify the effective chemical potential to which the bosons are submitted and their dispersions. So, to get rid of the multiplicative factor $J(\alpha)$ accompanying the term $(i\omega_m + \mathbf{q}^2/4m)$ in Eq. 4.15, we reparametrize the bosonic fields as $\Delta_q \to J^{-1/2}\Delta_q$ and our action turns out to be

$$S^{(2)}[\Delta] = \sum_q \bar{\Delta}_q(-i\omega_m + \epsilon_{\mathbf{q}} + \mu_{\text{eff}})\Delta_q, \tag{4.19}$$

where the effective chemical potential is then identified as

$$\mu_{\text{eff}} = \frac{\Gamma_0^{-1}}{J(\alpha)}, \tag{4.20}$$

and the energy dispersion with

$$\epsilon_{\mathbf{q}} = \frac{\mathbf{q}^2}{4m} - \frac{\delta^2 \Gamma_{\mathbf{q}^2}^{-1}}{J(\alpha)}. \tag{4.21}$$

To understand how the second term in Eq. 4.21 modifies the usual $\mathbf{q}^2/4m$ dispersion we need to check every q_i component in $\Gamma_{\mathbf{q}^2}^{-1}$. Let us observe that integrals containing the product of an arbitrary scalar function $f(k_x^2, k_y^2, k_z^2)$ with $\mathbf{k}\cdot\mathbf{q}$ will be such that only even powers of k_i survive, so recalling that $V_k \propto k_z$, we may write

$$\sum_{\mathbf{k}} f(k_x^2, k_y^2, k_z^2)(\mathbf{k}\cdot\mathbf{q})^2 = \sum_{\mathbf{k}} f(k_x^2, k_y^2, k_z^2)(q_x^2 k_x^2 + q_y^2 k_y^2 + q_z^2 k_z^2), \tag{4.22}$$

$$\sum_{\mathbf{k}} f(k_x^2, k_y^2, k_z^2) V_{\mathbf{k}} V_{\mathbf{q}} (\mathbf{k}\cdot\mathbf{q}) = -q_z^2 \sum_{\mathbf{k}} f(k_x^2, k_y^2, k_z^2) |V_{\mathbf{k}}|^2 \tag{4.23}$$

and $\Gamma_{\mathbf{q}^2}^{-1}$ may be rewritten as

$$\Gamma_{\mathbf{q}^2}^{-1} = \sum_{i,j} \Lambda_{ij} \frac{q_i q_j}{4m}, \tag{4.24}$$

where $\mathbf{\Lambda}$ is a symmetric block-diagonal matrix reflecting tetragonal symmetry whose components are

$$\Lambda_{xx} = \sum_{\mathbf{k}} \left[\frac{\epsilon_{\mathbf{k}}}{\xi_{\mathbf{k}}} \frac{\Theta_{\mathbf{k}}}{\xi_{\mathbf{k}}^2 - \Lambda_{\mathbf{k}}^2} + \frac{k_x^2}{2m} \frac{(1+\Theta_{\mathbf{k}})^2}{\xi_{\mathbf{k}}^3} \right], \tag{4.25}$$

$$\Lambda_{yy} = \sum_{\mathbf{k}} \left[\frac{\epsilon_{\mathbf{k}}}{\xi_{\mathbf{k}}} \frac{\Theta_{\mathbf{k}}}{\xi_{\mathbf{k}}^2 - \Lambda_{\mathbf{k}}^2} + \frac{k_y^2}{2m} \frac{(1+\Theta_{\mathbf{k}})^2}{\xi_{\mathbf{k}}^3} \right], \tag{4.26}$$

$$\Lambda_{zz} = \sum_{\mathbf{k}} \left[\frac{\epsilon_{\mathbf{k}}}{\xi_{\mathbf{k}}} \frac{\Theta_{\mathbf{k}}}{\xi_{\mathbf{k}}^2 - \Lambda_{\mathbf{k}}^2} + \frac{k_z^2}{2m} \frac{(1+\Theta_{\mathbf{k}})^2}{\xi_{\mathbf{k}}^3} - \frac{2\epsilon_{\mathbf{k}}\Theta_{\mathbf{k}}(1+\Theta_{\mathbf{k}})}{\xi_{\mathbf{k}}^3} + \frac{\alpha^2(2+\gamma^2)\epsilon_F}{2} \frac{\epsilon_{\mathbf{k}}^2}{\xi_{\mathbf{k}}^3} \frac{\Theta_{\mathbf{k}}}{\xi_{\mathbf{k}}^2 - \Lambda_{\mathbf{k}}^2} \right], \tag{4.27}$$

with $\Lambda_{xx} = \Lambda_{yy}$, while the remaining off-diagonal components are zero. The anisotropic parameter is explicit here solely for the sake of completeness, in the numerical results we are still assuming $\gamma = 0$.

Thus the anisotropic boson dispersion becomes

$$\boxed{\epsilon_{\mathbf{q}} = \sum_{i,j} \left[\delta_{ij} - \frac{\delta^2 \Lambda_{ij}(\alpha)}{J(\alpha)} \right] \frac{q_i q_j}{4m},} \tag{4.28}$$

with the components q_x and q_y contributing equally to the energy while the q_z component retains most of the influence from the hybridization.

4.2.1 Binding Energy

The binding energy E_B, or equivalently the critical chemical potential $\mu_c = -E_B/2$, is defined through the zeroth order vertex function that, following App. C.1, reads[1]

$$\frac{\Gamma_0^{-1}}{\pi \nu_0} = -\frac{1}{k_F a_s} + \sqrt{-\mu} \left[1 - \sum_{n=1}^{\infty} C_n(\delta) \left(\frac{2\alpha^2}{-\mu} \right)^n \right], \tag{4.29}$$

where the coefficients C_n are given by

$$C_n(\delta) \equiv \frac{2}{\pi} \int_0^\infty \int_0^\infty \frac{x\,\mathrm{d}x\,\mathrm{d}y}{x^2+y^2+1} \frac{y^{2n}}{[(x^2+y^2+1)^2 - \delta^2(x^2+y^2)^2]^n}, \tag{4.30}$$

with $n \geq 1$ and the convergence of the series in Eq. 4.29 is guaranteed in the BEC limit. (See Fig. C.1 for comparison between the coefficients.)

Thus the critical chemical potential μ_c is obtained solving the equation

$$-\frac{1}{k_F a_s} + \sqrt{-\mu_c} \left[1 - \sum_{n=1}^{\infty} C_n \left(\frac{2\alpha^2}{-\mu_c} \right)^n \right] = 0, \tag{4.31}$$

an interesting point is that turning-off the hybridization we obtain the usual $\mu_c = (k_F a_s)^{-2}$. However, unlike the single-band case, this equation is still solvable for some negative values of

[1] The chemical potential is normalized by the Fermi energy.

$(k_F a_s)^{-1}$ indicating the possibility of a BEC pairing even in a weak coupling regime. At first order approximation, $n = 1$, the hybridization contribution to μ_c is

$$\mu_c^{(1)} = -\frac{1}{4}\left[(k_F a_s)^{-1} + \sqrt{(k_F a_s)^{-2} + 8\alpha^2 C_1(\delta)}\right]^2, \tag{4.32}$$

for instance at the unitary point, $(k_F a_s)^{-1} = 0$, we still have a finite binding energy of $E_B^{(1)} = \sqrt{2}\alpha^2 C_1(\delta)\epsilon_F$. As mentioned, in the weak coupling regime, $(k_F a_s)^{-1} \gg -1$, we get $\mu_c^{(1)} \to -[2\alpha^2 C_1(\delta)]^2/(k_F a_s)^{-2}$.

Finally, Fig. 4.2 shows the complete numerical solution of Eq. 4.31 as function of the scattering length for different values of hybridization $\alpha = \{0.5, 1.0, 2.0\}$ and mass asymmetry $\delta = \{0.1, 0.3, 0.7, 0.9\}$. And, as expected, it is in agreement with the above analytical considerations, since all curves show a growth with both hybridization and mass asymmetry, and present a finite value in the BCS limit.

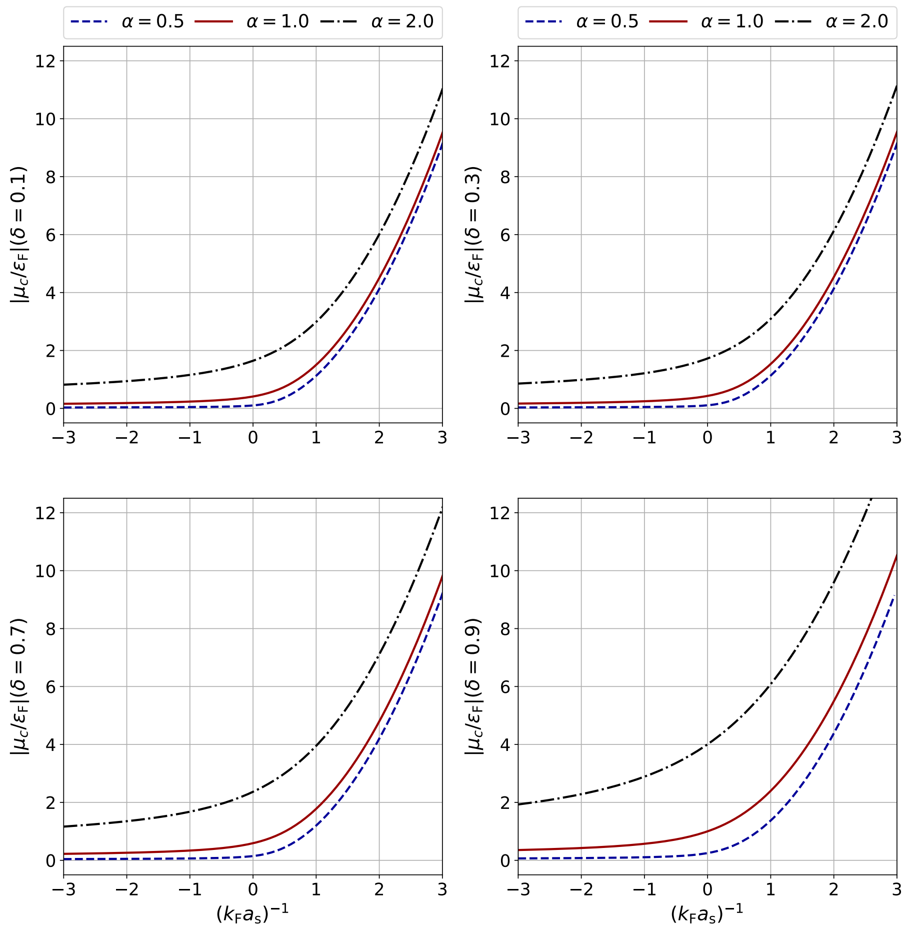

Figure 4.2: Critical chemical potential as function of the scattering length for different values of hybridization and mass asymmetry. Although the critical chemical potential fastly decreases for negative $(k_F a_s)^{-1}$ it is still non-zero. Higher values of hybridization or mass asymmetry increase μ_c.

4.2.2 Corrected Condensation Temperature

Aware of the proper bosonic dispersion given by Eq. 4.28 we can finally obtain the condensation temperature by taking the limit $\mu_{\text{eff}} \to 0$ in which the Bose-Einstein distribution becomes

$$n_B(\mu_{\text{eff}} \to 0) = n_0 + \int \frac{\mathrm{d}^3 q}{(2\pi)^3} \frac{1}{\exp\left[\frac{1}{T}\sum_{i,j}\left(\delta_{ij} - \delta^2\Lambda_{ij}J^{-1}\right)\frac{q_i q_j}{4m}\right] - 1}, \tag{4.33}$$

where, as in Eq. 2.5, n_0 is the number of condensate bosons. Then, redefining our variables of integration $q_i \to q_i\sqrt{1 - \delta^2\Lambda_{ii}J^{-1}}$, we get an integral which we already know how to evaluate

$$n_B(\mu_{\text{eff}} \to 0) = n_0 + \zeta(3/2)\left(\frac{2mT}{\pi}\right)^{3/2} \prod_i \left(1 - \frac{\delta^2\Lambda_{ii}}{J}\right)^{-1/2}, \tag{4.34}$$

resulting in a condensation temperature

$$\boxed{T_c = \frac{\pi}{\left(\prod_i m_i\right)^{1/3}} \left[\frac{n_B}{\zeta(3/2)}\right]^{2/3},} \tag{4.35}$$

generalized to the case of anisotropic masses

$$m_i \equiv \frac{m}{1 - \delta^2\Lambda_{ii}J^{-1}}, \tag{4.36}$$

with $i = x, y, z$. Fixing $(k_F a_s)^{-1} = -0.5$ and using the mean-field solution of $\mu(\alpha \gg 1)$ we estimate the anisotropic masses to yield, for $\delta = 0.7$, $m_x = m_y \simeq 1.55m$ and $m_z \simeq 1.68m$, while increasing the mass asymmetry to $\delta = 0.9$ results in $m_x = m_y \simeq 3.37m$ and $m_z \simeq 3.46m$. Conversely, in the usual BEC limit $(k_F a_s)^{-1} \to \infty$, for $\delta = 0.9$ and $\alpha = 0.5$, we have $m_x = m_y \simeq 5.06m$ and $m_z \simeq 4.94m$; increasing hybridization to $\alpha = 2.0$ we get $m_x = m_y \simeq 4.26m$ and $m_z \simeq 3.99m$.

Although we have indeed obtained an analytical expression for the condensation temperature our goal has not yet been completely achieved. If hybridization is to have an analogous role as the scattering length driving the system into the strong coupling regime, then we must show that $T_c(\alpha)$ is also finite in the limit $\alpha \to \infty$. To do that we must once more turn to the numerical analysis.

So to proceed further we need to specify n_B. We shall assume that in the strong coupling regime all fermions form pairs, i. e., the bosonic density is half of the total fermion density, $n_B = n/2$ [5]. This hypothesis is accurate while dealing with dilute gas systems. In condensed matter, since the interacting particles are only the ones around the Fermi surface, the density may be treated as a free parameter or be modeled after a specific material. Nevertheless it will provide us with some quantitative results. Using Eq. 3.59 the condensation temperature becomes

$$\frac{T_c}{\epsilon_F} = \frac{1}{2\pi}\left[\frac{F_\delta}{\zeta(3/2)}\right]^{2/3} \prod_i \left[1 - \frac{\delta^2\Lambda_{ii}(\alpha)}{J(\alpha)}\right]^{1/3}, \tag{4.37}$$

where, we recall, there is still a dependence of the chemical potential present in $\lambda_i(\alpha)$ and $J(\alpha)$. So to determine the condensation temperature as a function of the scattering length or the hybridization we must also establish the chemical potential evolution with the respective variable. At a first approximation we can use the mean-field results to this end.

As expected, while varying the scattering length, there is a saturated temperature as $(k_F a_s)^{-1} \to \infty$ and for the particular case of equal masses we recover the expression for a gas of identical bosons with mass $2m$ and density $n_B = k_F^3/(3\pi^2)$. The condensation temperature also becomes independent of hybridization $T_c(\delta = 0) \simeq 0.35\epsilon_F$, i. e., a factor $z^{2/3}$ larger than the single-band case, $T_c = 0.22\epsilon_F$, due to the $z = 2$ bands of our problem. On the other hand, for very distinct masses, $\delta = 0.9$, we have $T_c(\alpha = 0.5) \simeq 0.43\epsilon_F$ and $T_c(\alpha = 2.0) \simeq 0.53\epsilon_F$ indicating the rising of the temperature with δ as well as α.

In the case of a fixed negative scattering length we have showed that only high values of δ allow the system to effectively enter in the BEC regime via an odd-parity hybridization. Therefore we estimate that for $(k_F a_s)^{-1} = -0.5$ we have $T_c(\delta = 0.7) \simeq 0.48\epsilon_F$ and $T_c(\delta = 0.9) \simeq 0.65\epsilon_F$ whilst increasing the scattering length to $(k_F a_s)^{-1} = -0.1$ implies in $T_c(\delta = 0.7) \simeq 0.47\epsilon_F$ and $T_c(\delta = 0.9) \simeq 0.64\epsilon_F$. Thus there is an increasing in temperature with δ and a small decrease with $(k_F a_s)^{-1}$, but most important the *condensate temperature is always finite.*

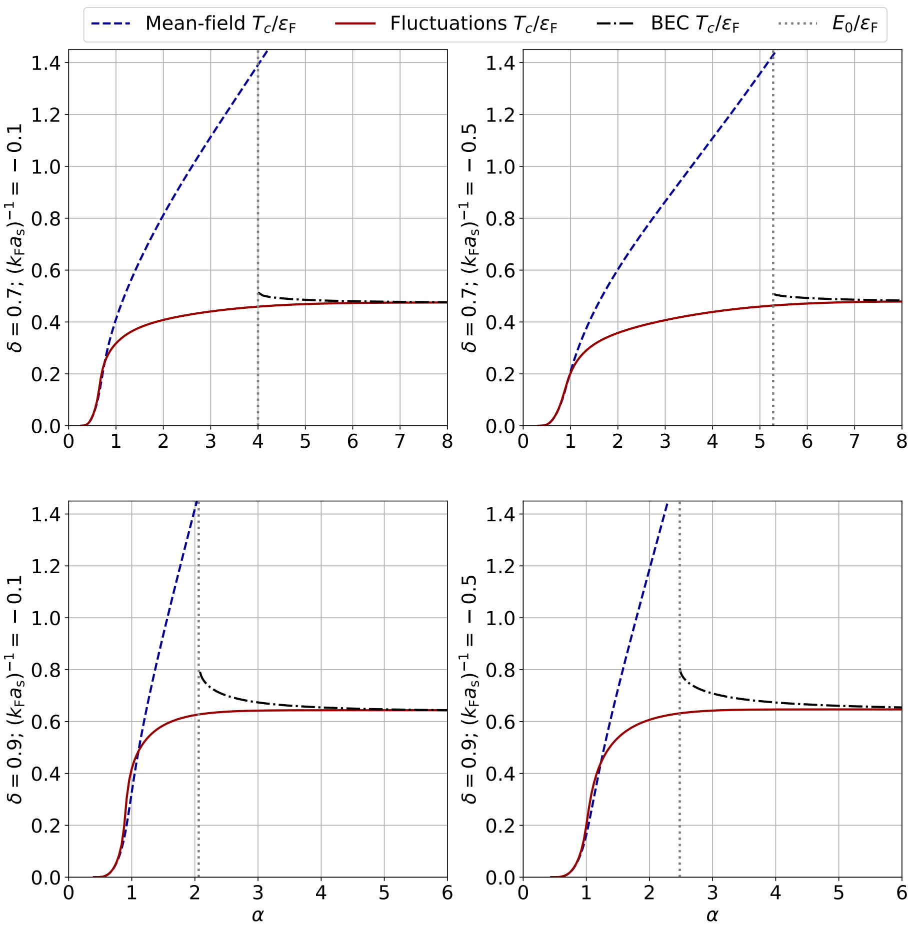

Figure 4.3: Comparison between critical temperatures obtained with different methods for $(k_F a_s)^{-1} = \{-0.5, -0.1\}$, characteristic of the BCS regime, and high mass asymmetries $\delta = \{0.7, 0.9\}$. The full red line, corresponding to the inclusion of fluctuations, correctly describes both limits and provides a good interpolation between them.

4.3 Interband BCS-BEC Crossover

As we have already stated, the complete profile of the BCS-BEC crossover is attained by including the effect of the pair susceptibility into the occupation number equation. More specifically, we should calculate $\delta n = T\partial_\mu \sum_q \ln \Gamma_q^{-1}$, add it in Eq. 3.44 and then, once again, solve the coupled equations. Although we have successfully obtained the interband vertex function and the calculation of δn is possible, the numerical computation of the corrected number equation is not.

However, an alternative approach [10,11] resides in the observation that, in the strong coupling regime, the role of δn is to describe the bosonic pair formation, i. e.

$$\delta n \simeq \sum_{\mathbf{q}} \frac{1}{e^{\sum_i q_i^2/(4m_i T_c)} - 1} = \zeta(3/2)\left(\frac{T_c}{\pi}\right)^{3/2} \prod_i \sqrt{m_i}, \tag{4.38}$$

where we used the dispersion calculated in Eq. 4.28 and the anisotropic masses expressed in Eq. 4.36.

Since the $\mathbf{q}$ sum in Eq. 4.38 could be analytically calculated it is now a feasible task to solve the (Fermi normalized) occupation number equation

$$F_\delta \simeq \frac{\zeta(3/2)}{2} \frac{(2\pi T_c)^{3/2}}{\prod_i \sqrt{1-\delta^2 \Lambda_{ii} J^{-1}}} + \int \mathrm{d}^3k \left[1 - \frac{1}{2}\tanh\left(\frac{\xi_{\mathbf{k}}^+}{2T_c}\right) - \frac{1}{2}\tanh\left(\frac{\xi_{\mathbf{k}}^-}{2T_c}\right)\right], \tag{4.39}$$

together with Eq. 3.85, which, for convenience, we write once again

$$\frac{\pi}{k_F a_s} = \int \frac{\mathrm{d}^3k}{2\pi}\left[\frac{1}{\epsilon_{\mathbf{k}}} - \frac{1}{2}\tanh\left(\frac{\xi_{\mathbf{k}}^+}{2T_c}\right)\left(\frac{1+\Theta_{\mathbf{k}}}{\xi_{\mathbf{k}}} - \frac{\Theta_{\mathbf{k}}}{\Lambda_{\mathbf{k}}}\right) - \frac{1}{2}\tanh\left(\frac{\xi_{\mathbf{k}}^-}{2T_c}\right)\left(\frac{1+\Theta_{\mathbf{k}}}{\xi_{\mathbf{k}}} + \frac{\Theta_{\mathbf{k}}}{\Lambda_{\mathbf{k}}}\right)\right].$$

Thus Fig. 4.3 shows the complete temperature evolution with the odd parity hybridization for $\delta = \{0.7, 0.9\}$ and $(k_F a_s)^{-1} = \{-0.5, -0.1\}$. As expected the condensation temperature no longer presents a diverging behavior, in matter of fact, it saturates (not surprisingly) to the temperature calculate in the previous section. The vertical dashed line indicates the region around which the smooth transition from the BCS to the BEC limit takes place.

Lastly, we demonstrate in Fig. 4.4, that the chemical potential is not substantially modified by the inclusion of gaussian fluctuations. Nevertheless its faster decrease, mainly in the weak coupling regime, implicates in a BCS-BEC transition reached at smaller values of hybridization (in comparison with the mean-field analysis). This result however should be considered with caution since the approximation given by Eq. 4.38 becomes less reliable as we approach the BCS limit.

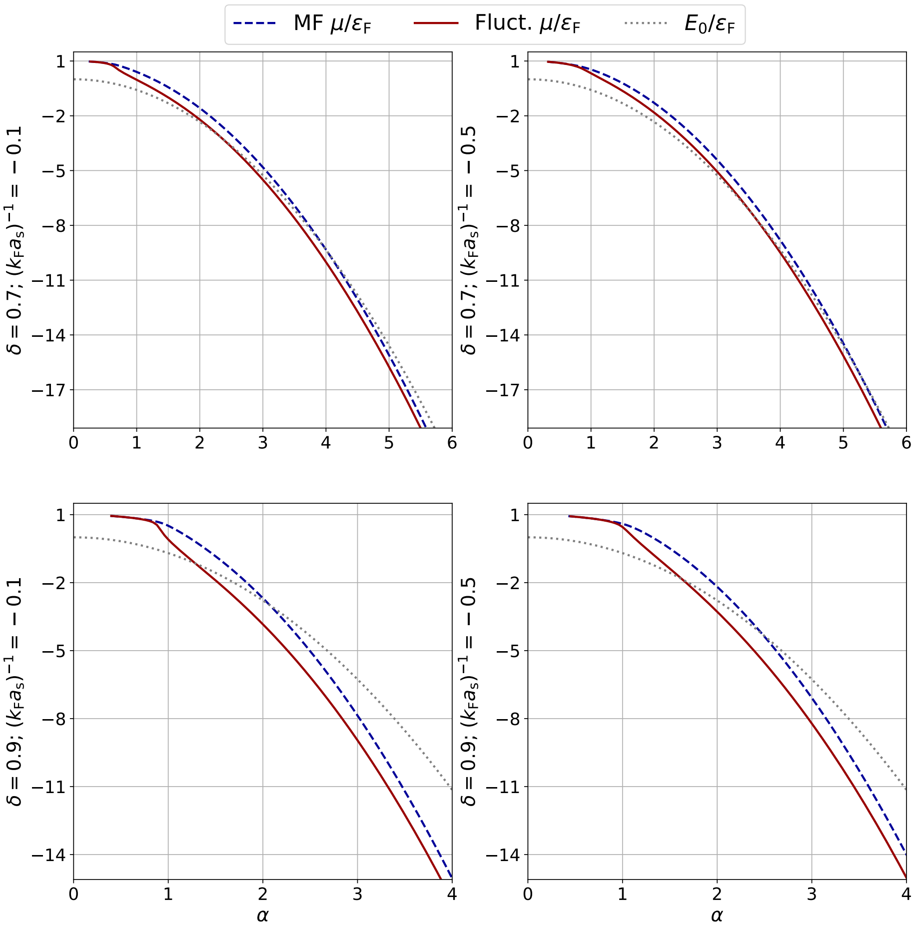

Figure 4.4: Chemical potential curves obtained via mean-field (dotted blue line) and fluctuations (full red line) approaches for $(k_F a_s)^{-1} = \{-0.5, -0.1\}$ and $\delta = \{0.7, 0.9\}$. The inclusion of the thermal fluctuations contributes to the BCS-BEC crossover as μ intercepts E_0 at smaller α values.

Chapter 5

Conclusions and Perspectives

In this thesis we develop a systematic way to understand the influence of an odd-parity hybridization in a two-band superconductor.

We started our analysis describing a single-band superconductor, which is solely characterized by the ratio of the scattering length to the average interparticle distance $(k_F a_s)^{-1}$. We detailed the weak (BCS) and strong (BEC) coupling regimes and demonstrated how, via variation of scattering length, it is possible to link them both. Next we presented studies that considered spin-orbit coupling interaction in ultracold fermionic gases and showed a BCS-BEC crossover driven through SOC variation.

Observing some mathematical similarities between SOC in fermionic gases and hybridization in multi-band systems, a spontaneous question raised is how exactly does hybridization operates in condensed matter and, more specifically, how does it affect the strong coupling regime of such systems. To address these issues, we specifically considered a model of two fermion species interacting attractively and that can be hybridized with each other. We pointed out that hybridization symmetry is linked to the difference of quantum numbers of the orbitals and it can be even- or odd-parity. However, previous studies showed that even-parity hybridization destroys the superconducting state, which narrowed our investigation to odd-parity hybridization. Additionally, in a two-band system the mass asymmetry of the interacting fermions, δ, although absent in SOC gases, must be carefully considered. As it was defined, a small δ corresponds to similar effective masses and as δ increases approaching the unit it indicates a scenario with very distinct masses, characteristic of heavy fermions systems. In matter of fact, the mass asymmetry term $\delta\epsilon_{\mathbf{k}}$ in the interband case is analogous to a Zeeman field in SOC systems abruptly diminishing superconductivity in the weak coupling regime.

Using both analytical and numerical methods we obtained the solutions for the intra ($g_1 = 0$) and interband ($g_2 = 0$) scenarios. At a mean-field level, we solved the coupled equations and showed how the order parameters, chemical potential and critical temperature varied with the free parameters of the model, namely $(k_F a_s)^{-1}$, α and δ. We also calculated the minimum energy of the bands E_0 which determines the region around the system enters in the BEC phase. From the numerical results, we see that the intraband case exhibited the suppression of the superconducting properties for increased hybridization strength. On the other hand, in the interband case, hybridization favors the pair formation and induces a BCS-BEC crossover with a similar signature as the one presented via scattering length variation. However, the BEC transition is favored solely for high values of the mass asymmetry, $\delta \gtrsim 0.7$, where the criterion $\mu \simeq E_0$ is met. Another feature of the interband model is the divergence of the critical temperature in the strong-coupling regime with increasing α. This divergence however is merely a pathology of the mean-field approximation which does not properly describe the tight bosonic pair in the BEC limit.

We also demonstrated that the odd-parity hybridization can induce a p-wave intraband order parameter in the (initially) pure interband Hamiltonian. Then, by including the thermal fluctuations at one-loop level, we calculated the interband vertex function and showed that, in the strong coupling regime, our effective action is equivalent to another one describing non-interacting bosons with an anisotropic energy dispersion. It allowed us to obtain the system's binding energy, which increases with δ and α, and a *finite* condensation temperature as function of α that also increases with δ. Another important remark is that the α-saturated temperature is usually higher than the scattering length one what increases its experimental appeal.

Although the complete solution of the crossover could not been attained due to the complexity of the numerical calculations, an adequate ansatz for the occupation number fluctuation allowed us to overcome this issue and smoothly link the weak and the strong regimes via hybridization. Therefore we were able to demonstrate theoretically that an odd-parity hybridization can indeed play a similar role as the scattering length or the SOC interaction in the interband sector of a two-band superconductor and successfully promote an α-driven BCS-BEC crossover.

As future lines of work it may be interesting to further analyze both the intra and interband sectors altogether. Besides under the new light of the relevance of the mass asymmetry parameter a revision of the even-parity hybridization results would be greatly appreciated. Another point for consideration would be the study of a model with bands possessing different Fermi surfaces or under the influence of a magnetic field. It also be interesting to explore a possible topological transition in multi-band systems which is hint in our work by the steep profiles of the order parameter and critical temperature for high δ. Besides, while analyzing the evolution of the interband critical temperature with hybridization, there is an indication of some scaling between the several $T_c(\delta)$ since these curves intersect around $\alpha \simeq 1.08$. Furthermore, it would also be ideal to include the exact pair susceptibility in these studies. This last task could be made (numerically) simpler in 2D systems. Naturally due to the richness of the multi-band model these are some but not all of the possibilities for future explorations and we hope that we have been able to contribute in this endeavor.

Appendix A

Mean-Field Equations

As stated in the main text, we need to compute the inverse of the matrix $\mathbf{G}^{-1}$. Although it is a bothersome task to calculate the complete matrix we shall not need all of its elements to obtain the dynamical equations.

We start from the follow identity involving square matrices

$$\mathbf{G} \equiv \begin{pmatrix} \mathbf{A} & \mathbf{B} \\ \mathbf{C} & \mathbf{D} \end{pmatrix}^{-1} = \begin{bmatrix} \left(\mathbf{A} - \mathbf{B}\mathbf{D}^{-1}\mathbf{C}\right)^{-1} & -\mathbf{A}^{-1}\mathbf{B}\left(\mathbf{D} - \mathbf{C}\mathbf{A}^{-1}\mathbf{B}\right)^{-1} \\ -\mathbf{D}^{-1}\mathbf{C}\left(\mathbf{A} - \mathbf{B}\mathbf{D}^{-1}\mathbf{C}\right)^{-1} & \left(\mathbf{D} - \mathbf{C}\mathbf{A}^{-1}\mathbf{B}\right)^{-1} \end{bmatrix}. \tag{A.1}$$

In our case we can identify the block matrices as

$$\mathbf{A} \equiv \begin{pmatrix} i\omega_n - \xi^A_{\mathbf{k}} & -\bar{V}_{\mathbf{k}} \\ -V_{\mathbf{k}} & i\omega_n - \xi^B_{\mathbf{k}} \end{pmatrix} \Longrightarrow \mathbf{A}^{-1} = \frac{1}{\det\mathbf{A}} \begin{pmatrix} i\omega_n - \xi^B_{\mathbf{k}} & \bar{V}_{\mathbf{k}} \\ V_{\mathbf{k}} & i\omega_n - \xi^A_{\mathbf{k}} \end{pmatrix} \tag{A.2}$$

with $\det\mathbf{A} = (i\omega_n - \xi^B_{\mathbf{k}})(i\omega_n - \xi^A_{\mathbf{k}}) - |V_{\mathbf{k}}|^2$;

$$\mathbf{B} \equiv \begin{pmatrix} \Omega & -\Delta \\ \Delta & 0 \end{pmatrix} \Longrightarrow \mathbf{B}^{-1} = \frac{1}{\Delta^2} \begin{pmatrix} 0 & \Delta \\ -\Delta & \Omega \end{pmatrix}; \tag{A.3}$$

$$\mathbf{C} \equiv \begin{pmatrix} \Omega & \Delta \\ -\Delta & 0 \end{pmatrix} \Longrightarrow \mathbf{C}^{-1} = \frac{1}{\Delta^2} \begin{pmatrix} 0 & -\Delta \\ \Delta & \Omega \end{pmatrix}; \tag{A.4}$$

$$\mathbf{D} \equiv \begin{pmatrix} i\omega_n + \xi^A_{\mathbf{k}} & -V_{\mathbf{k}} \\ -\bar{V}_{\mathbf{k}} & i\omega_n + \xi^B_{\mathbf{k}} \end{pmatrix} \Longrightarrow \mathbf{D}^{-1} = \frac{1}{\det\mathbf{D}} \begin{pmatrix} i\omega_n + \xi^B_{\mathbf{k}} & V_{\mathbf{k}} \\ \bar{V}_{\mathbf{k}} & i\omega_n + \xi^A_{\mathbf{k}} \end{pmatrix} \tag{A.5}$$

with $\det\mathbf{D} = (i\omega_n + \xi^B_{\mathbf{k}})(i\omega_n + \xi^A_{\mathbf{k}}) - |V_{\mathbf{k}}|^2$.

We also assume the antisymmetric character of the hybridization $V_{-\mathbf{k}} = -V_{\mathbf{k}}$ and, with no loss of generalization, the s-wave symmetry of the mean-field order parameters $\bar{\Delta} = \Delta$, $\bar{\Omega} = \Omega$ (for notational convenience we suppress the subscript '0').

Fortunately the whole information for the mean-field analysis is contained within the block $-\mathbf{D}^{-1}\mathbf{C}(\mathbf{A}-\mathbf{B}\mathbf{D}^{-1}\mathbf{C})^{-1}$ so the first product to be calculated is

$$\mathbf{D}^{-1}\mathbf{C} = \frac{1}{\det\mathbf{D}}\begin{bmatrix} (i\omega_n+\xi^B_\mathbf{k})\Omega - V_\mathbf{k}\Delta & (i\omega_n+\xi^B_\mathbf{k})\Delta \\ \bar{V}_\mathbf{k}\Omega - (i\omega_n+\xi^A_\mathbf{k})\Delta & \bar{V}_\mathbf{k}\Delta \end{bmatrix} \tag{A.6}$$

and $\mathbf{B}\mathbf{D}^{-1}\mathbf{C}$ reads

$$\mathbf{B}\mathbf{D}^{-1}\mathbf{C} = \frac{1}{\det\mathbf{D}}\begin{bmatrix} \Omega[(i\omega_n+\xi^B_\mathbf{k})\Omega - V_\mathbf{k}\Delta] - \Delta[\bar{V}_\mathbf{k}\Omega - (i\omega_n+\xi^A_\mathbf{k})\Delta] & (i\omega_n+\xi^B_\mathbf{k})\Delta\Omega - \bar{V}_\mathbf{k}\Delta^2 \\ (i\omega_n+\xi^B_\mathbf{k})\Omega\Delta - V_\mathbf{k}\Delta^2 & (i\omega_n+\xi^B_\mathbf{k})\Delta^2 \end{bmatrix}, \tag{A.7}$$

thus

$$\begin{aligned}\left(\mathbf{A}-\mathbf{B}\mathbf{D}^{-1}\mathbf{C}\right)^{-1} &= \frac{1}{\det\left(\mathbf{A}-\mathbf{B}\mathbf{D}^{-1}\mathbf{C}\right)}\frac{1}{\det\mathbf{D}} \\ &\times\begin{bmatrix} (i\omega_n-\xi^B_\mathbf{k})\det\mathbf{D} - (i\omega_n+\xi^B_\mathbf{k})\Delta^2 & \bar{V}_\mathbf{k}\det\mathbf{D} + (i\omega_n+\xi^B_\mathbf{k})\Delta\Omega - \bar{V}_\mathbf{k}\Delta^2 \\ V_\mathbf{k}\det\mathbf{D} + (i\omega_n+\xi^B_\mathbf{k})\Omega\Delta - V_\mathbf{k}\Delta^2 & (i\omega_n-\xi^A_\mathbf{k})\det\mathbf{D} - (i\omega_n+\xi^B_\mathbf{k})\Omega^2 - (i\omega_n+\xi^A_\mathbf{k})\Delta^2 \end{bmatrix},\end{aligned} \tag{A.8}$$

with

$$\begin{aligned}
&\det\left(\mathbf{A}-\mathbf{B}\mathbf{D}^{-1}\mathbf{C}\right)(\det\mathbf{D})^2 = \\
&= [(i\omega_n-\xi^A_\mathbf{k})\det\mathbf{D} - (i\omega_n+\xi^B_\mathbf{k})\Omega^2 - (i\omega_n+\xi^A_\mathbf{k})\Delta^2][(i\omega_n-\xi^B_\mathbf{k})\det\mathbf{D} - (i\omega_n+\xi^B_\mathbf{k})\Delta^2] \\
&+ [\bar{V}_\mathbf{k}\det\mathbf{D} + (i\omega_n+\xi^B_\mathbf{k})\Delta\Omega - \bar{V}_\mathbf{k}\Delta^2][-V_\mathbf{k}\det\mathbf{D} - (i\omega_n+\xi^B_\mathbf{k})\Omega\Delta + V_\mathbf{k}\Delta^2] \\
&= (i\omega_n-\xi^A_\mathbf{k})(i\omega_n-\xi^B_\mathbf{k})\det\mathbf{D}^2 - (i\omega_n-\xi^A_\mathbf{k})(i\omega_n+\xi^B_\mathbf{k})\Delta^2\det\mathbf{D} \\
&- (i\omega_n+\xi^B_\mathbf{k})(i\omega_n-\xi^B_\mathbf{k})\Omega^2\det\mathbf{D} + (i\omega_n+\xi^B_\mathbf{k})^2\Omega^2\Delta^2 \\
&- (i\omega_n+\xi^A_\mathbf{k})(i\omega_n-\xi^B_\mathbf{k})\Delta^2\det\mathbf{D} + (i\omega_n+\xi^A_\mathbf{k})(i\omega_n+\xi^B_\mathbf{k})\Delta^4 \\
&- |V_\mathbf{k}|^2\det D^2 + 2|V_\mathbf{k}|^2\Delta^2\det\mathbf{D} - (i\omega_n+\xi^a_\mathbf{k})^2\Delta^2\Omega^2 - |V_\mathbf{k}|^2\Delta^4 \\
&= \det\mathbf{A}(\det\mathbf{D})^2 - [(i\omega_n-\xi^A_\mathbf{k})(i\omega_n+\xi^B_\mathbf{k}) + (i\omega_n+\xi^A_\mathbf{k})(i\omega_n-\xi^B_\mathbf{k}) - 2|V_\mathbf{k}|^2]\Delta^2\det\mathbf{D} \\
&+ (\omega_n^2+\xi^{B2}_\mathbf{k})\Omega^2\det\mathbf{D} + \Delta^4\det\mathbf{D} \\
&= [\det\mathbf{A}\det\mathbf{D} + 2(\omega_n^2+\xi^A_\mathbf{k}\xi^B_\mathbf{k}+|V_\mathbf{k}|^2)\Delta^2 + (\omega_n^2+\xi^{B2}_\mathbf{k})\Omega^2 + \Delta^4]\det\mathbf{D},
\end{aligned} \tag{A.9}$$

and

$$
\begin{aligned}
&\det\mathbf{A}\det\mathbf{D} = \\
&= [(i\omega_n - \xi^B_{\mathbf{k}})(i\omega_n - \xi^A_{\mathbf{k}}) - |V_{\mathbf{k}}|^2][(i\omega_n + \xi^B_{\mathbf{k}})(i\omega_n + \xi^A_{\mathbf{k}}) - |V_{\mathbf{k}}|^2] \\
&= [(i\omega_n)^2 - \xi^{B2}_{\mathbf{k}}][(i\omega_n)^2 - \xi^{A2}_{\mathbf{k}}] + |V_{\mathbf{k}}|^4 - |V_{\mathbf{k}}|^2[(i\omega_n - \xi^B_{\mathbf{k}})(i\omega_n - \xi^A_{\mathbf{k}}) + (i\omega_n + \xi^B_{\mathbf{k}})(i\omega_n + \xi^A_{\mathbf{k}})] \\
&= (\omega_n^2 + \xi^{a2}_{\mathbf{k}})(\omega_n^2 + \xi^{b2}_{\mathbf{k}}) + |V_{\mathbf{k}}|^4 - |V_{\mathbf{k}}|^2[-\omega_n^2 - i\omega_n(\xi^B_{\mathbf{k}} + \xi^A_{\mathbf{k}}) + \xi^B_{\mathbf{k}}\xi^A_{\mathbf{k}} - \omega_n^2 + i\omega_n(\xi^B_{\mathbf{k}} + \xi^A_{\mathbf{k}}) + \xi^B_{\mathbf{k}}\xi^A_{\mathbf{k}}] \\
&= \omega_n^4 + (\xi^{A2}_{\mathbf{k}} + \xi^{B2}_{\mathbf{k}})\omega_n^2 + \xi^{A2}_{\mathbf{k}}\xi^{B2}_{\mathbf{k}} + 2|V_{\mathbf{k}}|^2(\omega_n^2 - \xi^A_{\mathbf{k}}\xi^B_{\mathbf{k}}) + |V_{\mathbf{k}}|^4 \\
&= \omega_n^4 + (\xi^{A2}_{\mathbf{k}} + \xi^{B2}_{\mathbf{k}} + 2|V_{\mathbf{k}}|^2)\omega_n^2 + (\xi^A_{\mathbf{k}}\xi^B_{\mathbf{k}} - |V_{\mathbf{k}}|^2)^2,
\end{aligned}
\tag{A.10}
$$

so that

$$
\begin{aligned}
&\det\left(\mathbf{A} - \mathbf{B}\mathbf{D}^{-1}\mathbf{C}\right)\det\mathbf{D} = \\
&= \omega_n^4 + (\xi^{A2}_{\mathbf{k}} + \xi^{B2}_{\mathbf{k}} + 2|V_{\mathbf{k}}|^2 + \Omega^2 + 2\Delta^2)\omega_n^2 + (\xi^A_{\mathbf{k}}\xi^B_{\mathbf{k}} - |V_{\mathbf{k}}|^2)^2 + 2(\xi^A_{\mathbf{k}}\xi^B_{\mathbf{k}} + |V_{\mathbf{k}}|^2)\Delta^2 + \xi^{B2}_{\mathbf{k}}\Omega^2 + \Delta^4 \\
&= \omega_n^4 + (\xi^{A2}_{\mathbf{k}} + \xi^{B2}_{\mathbf{k}} + 2|V_{\mathbf{k}}|^2 + \Omega^2 + 2\Delta^2)\omega_n^2 + (\xi^A_{\mathbf{k}}\xi^B_{\mathbf{k}} - |V_{\mathbf{k}}|^2 + \Delta^2)^2 + 4|V_{\mathbf{k}}|^2\Delta^2 + \xi^{B2}_{\mathbf{k}}\Omega^2 \\
&= \omega_n^4 + 2A_{\mathbf{k}}\,\omega_n^2 + B_{\mathbf{k}} \\
&= \det\mathbf{G}^{-1},
\end{aligned}
\tag{A.11}
$$

where we recalled the definitions presented in Eqs. 3.23.

Finally the last product is

$$
\begin{aligned}
\mathbf{D}^{-1}\mathbf{C}\left(\mathbf{A} - \mathbf{B}\mathbf{D}^{-1}\mathbf{C}\right)^{-1} &= \frac{1}{\det\mathbf{G}^{-1}}\frac{1}{\det\mathbf{D}}\begin{bmatrix} (i\omega_n + \xi^B_{\mathbf{k}})\Omega - V_{\mathbf{k}}\Delta & (i\omega_n + \xi^B_{\mathbf{k}})\Delta \\ \bar{V}_{\mathbf{k}}\Omega - (i\omega_n + \xi^A_{\mathbf{k}})\Delta & \bar{V}_{\mathbf{k}}\Delta \end{bmatrix} \\
&\times \begin{bmatrix} (i\omega_n - \xi^B_{\mathbf{k}})\det\mathbf{D} - (i\omega_n + \xi^B_{\mathbf{k}})\Delta^2 & \bar{V}_{\mathbf{k}}\det\mathbf{D} + (i\omega_n + \xi^B_{\mathbf{k}})\Delta\Omega - \bar{V}_{\mathbf{k}}\Delta^2 \\ V_{\mathbf{k}}\det\mathbf{D} + (i\omega_n + \xi^B_{\mathbf{k}})\Omega\Delta - V_{\mathbf{k}}\Delta^2 & (i\omega_n - \xi^A_{\mathbf{k}})\det\mathbf{D} - (i\omega_n + \xi^B_{\mathbf{k}})\Omega^2 - (i\omega_n + \xi^A_{\mathbf{k}})\Delta^2 \end{bmatrix}.
\end{aligned}
\tag{A.12}
$$

A.1 Interband G Components

The relevant components for the interband case are

$$
\begin{aligned}
-(\det\mathbf{G}^{-1}\det\mathbf{D})\mathbf{G}_{32} &= \left[(i\omega_n+\xi^B_{\mathbf{k}})\Omega - V_{\mathbf{k}}\Delta\right]\left[\bar{V}_{\mathbf{k}}\det\mathbf{D} + (i\omega_n+\xi^B_{\mathbf{k}})\Delta\Omega - \bar{V}_{\mathbf{k}}\Delta^2\right] \\
&+ (i\omega_n+\xi^B_{\mathbf{k}})\Delta\left[(i\omega_n-\xi^A_{\mathbf{k}})\det\mathbf{D} - (i\omega_n+\xi^B_{\mathbf{k}})\Omega^2 - (i\omega_n+\xi^A_{\mathbf{k}})\Delta^2\right] \\
&= \bar{V}_{\mathbf{k}}\Omega(i\omega_n+\xi^B_{\mathbf{k}})\det\mathbf{D} + (i\omega_n+\xi^B_{\mathbf{k}})^2\Omega^2\Delta - \bar{V}_{\mathbf{k}}(i\omega_n+\xi^B_{\mathbf{k}})\Omega\Delta^2 \\
&- |V_{\mathbf{k}}|^2\Delta\det\mathbf{D} - V_{\mathbf{k}}(i\omega_n+\xi^B_{\mathbf{k}})\Omega\Delta^2 + |V_{\mathbf{k}}|^2\Delta^3 \\
&+ (i\omega_n+\xi^B_{\mathbf{k}})(i\omega_n-\xi^A_{\mathbf{k}})\Delta\det\mathbf{D} - (i\omega_n+\xi^B_{\mathbf{k}})^2\Omega^2\Delta \\
&- (i\omega_n+\xi^B_{\mathbf{k}})(i\omega_n+\xi^A_{\mathbf{k}})\Delta^3 \\
&= \left[\bar{V}_{\mathbf{k}}\Omega(i\omega_n+\xi^B_{\mathbf{k}}) - |V_{\mathbf{k}}|^2\Delta + \Delta(i\omega_n+\xi^B_{\mathbf{k}})(i\omega_n-\xi^A_{\mathbf{k}})\right]\det\mathbf{D} \\
&+ \Delta^3\left[|V_{\mathbf{k}}|^2 - (i\omega_n+\xi^B_{\mathbf{k}})(i\omega_n+\xi^A_{\mathbf{k}})\right] \\
&= \left[-\omega_n^2 + (\xi^B_{\mathbf{k}}-\xi^A_{\mathbf{k}})i\omega_n - \xi^A_{\mathbf{k}}\xi^B_{\mathbf{k}} - |V_{\mathbf{k}}|^2\right]\Delta\det\mathbf{D} - \Delta^3\det\mathbf{D} \\
&= \left[-\omega_n^2 + (\xi^B_{\mathbf{k}}-\xi^A_{\mathbf{k}})i\omega_n - \xi^A_{\mathbf{k}}\xi^B_{\mathbf{k}} - |V_{\mathbf{k}}|^2 - \Delta^2\right]\Delta\det\mathbf{D}
\end{aligned}
\tag{A.13}
$$

and

$$
\begin{aligned}
-(\det\mathbf{G}^{-1}\det\mathbf{D})\mathbf{G}_{41} &= \left[\bar{V}_{\mathbf{k}}\Omega - (i\omega_n+\xi^A_{\mathbf{k}})\Delta\right]\left[(i\omega_n-\xi^B_{\mathbf{k}})\det\mathbf{D} - (i\omega_n+\xi^B_{\mathbf{k}})\Delta^2\right] \\
&\bar{V}_{\mathbf{k}}\Delta\left[V_{\mathbf{k}}\det\mathbf{D} + (i\omega_n+\xi^B_{\mathbf{k}})\Omega\Delta - V_{\mathbf{k}}\Delta^2\right] \\
&= \bar{V}_{\mathbf{k}}\Omega(i\omega_n-\xi^B_{\mathbf{k}})\det\mathbf{D} - \bar{V}_{\mathbf{k}}(i\omega_n+\xi^B_{\mathbf{k}})\Omega\Delta^2 - (i\omega_n+\xi^A_{\mathbf{k}})(i\omega_n-\xi^B_{\mathbf{k}})\Delta\det\mathbf{D} \\
&+ (i\omega_n+\xi^A_{\mathbf{k}})(i\omega_n+\xi^B_{\mathbf{k}})\Delta^3 + |V_{\mathbf{k}}|^2\Delta\det\mathbf{D} + \bar{V}_{\mathbf{k}}(i\omega_n+\xi^B_{\mathbf{k}})\Omega\Delta^2 - |V_{\mathbf{k}}|^2\Delta^3 \\
&= \left[\bar{V}_{\mathbf{k}}\Omega(i\omega_n-\xi^B_{\mathbf{k}}) - (i\omega_n+\xi^A_{\mathbf{k}})(i\omega_n-\xi^B_{\mathbf{k}})\Delta + |V_{\mathbf{k}}|^2\Delta\right]\det\mathbf{D} \\
&- \Delta^3\left[-(i\omega_n+\xi^A_{\mathbf{k}})(i\omega_n+\xi^B_{\mathbf{k}}) + |V_{\mathbf{k}}|^2\right] \\
&= -\left[-\omega_n^2 - (\xi^B_{\mathbf{k}}-\xi^A_{\mathbf{k}})i\omega_n - \xi^A_{\mathbf{k}}\xi^B_{\mathbf{k}} - |V_{\mathbf{k}}|^2 - \Delta^2\right]\Delta\det\mathbf{D},
\end{aligned}
\tag{A.14}
$$

where, in the last lines, we have already dismissed the antisymmetric terms (when summing over $\mathbf{k}$ they vanish).

Thus

$$
\mathbf{G}_{32} - \mathbf{G}_{41} = \frac{2\Delta(\omega_n^2 + \xi^A_{\mathbf{k}}\xi^B_{\mathbf{k}} + |V_{\mathbf{k}}|^2 + \Delta^2)}{\omega_n^4 + 2A_{\mathbf{k}}\omega_n^2 + B_{\mathbf{k}}},
\tag{A.15}
$$

which leads to Eq. 3.26.

A.2 Intraband G Components

In the intraband scenario we need only the component $\mathbf{G}_{31}$ that is obtained from the product

$$\begin{aligned}
-(\det\mathbf{G}^{-1}\det\mathbf{D})\mathbf{G}_{31} &= \left[(i\omega_n+\xi_{\mathbf{k}}^B)\Omega - V_{\mathbf{k}}\Delta\right]\left[(i\omega_n-\xi_{\mathbf{k}}^B)\det\mathbf{D}-(i\omega_n+\xi_{\mathbf{k}}^B)\Delta^2\right] \\
&+ (i\omega_n+\xi_{\mathbf{k}}^B)\Delta\left[V_{\mathbf{k}}\det\mathbf{D}+(i\omega_n+\xi_{\mathbf{k}}^B)\Omega\Delta - V_{\mathbf{k}}\Delta^2\right] \\
&= -(\omega_n^2+\xi_{\mathbf{k}}^{B2})\Omega\det\mathbf{D} - (i\omega_n+\xi_{\mathbf{k}}^B)^2\Omega\Delta^2 - V_{\mathbf{k}}(i\omega_n-\xi_{\mathbf{k}}^B)\Delta\det\mathbf{D} \\
&+ V_{\mathbf{k}}(i\omega_n+\xi_{\mathbf{k}}^B)\Delta^3 + V_{\mathbf{k}}(i\omega_n+\xi_{\mathbf{k}}^B)\Delta\det\mathbf{D} + (i\omega_n+\xi_{\mathbf{k}}^B)^2\Omega\Delta^2 \\
&- V_{\mathbf{k}}(i\omega_n+\xi_{\mathbf{k}}^B)\Delta^3 \\
&= -(\omega_n^2+\xi_{\mathbf{k}}^{B2})\Omega\det\mathbf{D},
\end{aligned} \tag{A.16}$$

where, once again, we have omitted the antisymmetric $\mathbf{k}$ terms. Thus

$$\mathbf{G}_{31} = \frac{\Omega(\omega_n^2+\xi_{\mathbf{k}}^{B2})}{\omega_n^4+2A_{\mathbf{k}}\omega_n^2+B_{\mathbf{k}}}, \tag{A.17}$$

and then follows Eq. 3.35.

A.3 Matsubara Summation

The summation over the fermionic frequencies, ω_n, can be done by noting that both intra and interband gap equations present the same simple poles structure, namely

$$S \equiv \sum_n h(\omega_n) = \frac{2}{\beta}\sum_n \frac{-(i\omega_n)^2+K}{(i\omega_n-\omega_1)(i\omega_n-\omega_2)(i\omega_n-\omega_3)(i\omega_n-\omega_4)}, \tag{A.18}$$

where $\omega_1=-\omega_2=\omega_{\mathbf{k}}^+$, $\omega_3=-\omega_4=\omega_{\mathbf{k}}^-$ and K is any constant.

This sum can be formally replaced by a closed contour complex integral of the product of $h(z)$ with a suitable convergent function $g(z)$. For fermions, it can be rewritten as

$$S = \frac{1}{2\pi i}\oint \mathrm{d}z g(z)h(-iz) = -\sum_{\text{Poles}} \operatorname{Res}\left[g(z)h(-iz)\right]\Big|_{z=\text{Pole}}, \tag{A.19}$$

with $g(z)=\frac{\beta}{2}\tanh\left(\frac{\beta}{2}z\right)$. So that our original sum becomes the evaluation of residues.

Particularly in our problem, the summation becomes

$$
\begin{aligned}
S &= -\sum_n \mathrm{Res}\left[\frac{-z^2+K}{(z-\omega_1)(z-\omega_2)(z-\omega_3)(z-\omega_4)}\tanh\left(\frac{\beta}{2}z\right)\right]\Bigg|_{z=\omega_n} \\
&= -\frac{-\omega_1^2+K}{(\omega_1-\omega_2)(\omega_1-\omega_3)(\omega_1-\omega_4)}\tanh\left(\frac{\beta}{2}\omega_1\right) - \frac{-\omega_2^2+K}{(\omega_2-\omega_1)(\omega_2-\omega_3)(\omega_2-\omega_4)}\tanh\left(\frac{\beta}{2}\omega_2\right) \\
&\quad - \frac{-\omega_3^2+K}{(\omega_3-\omega_1)(\omega_3-\omega_2)(\omega_3-\omega_4)}\tanh\left(\frac{\beta}{2}\omega_3\right) - \frac{-\omega_4^2+K}{(\omega_4-\omega_1)(\omega_4-\omega_2)(\omega_4-\omega_3)}\tanh\left(\frac{\beta}{2}\omega_4\right) \\
&= -\frac{-\omega_{\mathbf{k}}^{+2}+K}{2\omega_{\mathbf{k}}^{+}(\omega_{\mathbf{k}}^{+}-\omega_{\mathbf{k}}^{-})(\omega_{\mathbf{k}}^{+}+\omega_{\mathbf{k}}^{-})}\tanh\left(\frac{\beta}{2}\omega_{\mathbf{k}}^{+}\right) - \frac{-\omega_{\mathbf{k}}^{+2}+K}{-2\omega_{\mathbf{k}}^{+}(-\omega_{\mathbf{k}}^{+}-\omega_{\mathbf{k}}^{-})(-\omega_{\mathbf{k}}^{+}+\omega_{\mathbf{k}}^{-})}\tanh\left(-\frac{\beta}{2}\omega_{\mathbf{k}}^{+}\right) \\
&\quad - \frac{-\omega_{\mathbf{k}}^{-2}+K}{2\omega_{\mathbf{k}}^{-}(\omega_{\mathbf{k}}^{-}-\omega_{\mathbf{k}}^{+})(\omega_{\mathbf{k}}^{-}+\omega_{\mathbf{k}}^{+})}\tanh\left(\frac{\beta}{2}\omega_{\mathbf{k}}^{-}\right) - \frac{-\omega_{\mathbf{k}}^{-2}+K}{-2\omega_{\mathbf{k}}^{-}(-\omega_{\mathbf{k}}^{-}-\omega_{\mathbf{k}}^{+})(-\omega_{\mathbf{k}}^{-}+\omega_{\mathbf{k}}^{+})}\tanh\left(-\frac{\beta}{2}\omega_{\mathbf{k}}^{-}\right) \\
&= -\frac{-\omega_{\mathbf{k}}^{+2}+K}{\omega_{\mathbf{k}}^{+}(\omega_{\mathbf{k}}^{+}-\omega_{\mathbf{k}}^{-})(\omega_{\mathbf{k}}^{+}+\omega_{\mathbf{k}}^{-})}\tanh\left(\frac{\beta}{2}\omega_{\mathbf{k}}^{+}\right) - \frac{-\omega_{\mathbf{k}}^{-2}+K}{\omega_{\mathbf{k}}^{-}(\omega_{\mathbf{k}}^{-}-\omega_{\mathbf{k}}^{+})(\omega_{\mathbf{k}}^{-}+\omega_{\mathbf{k}}^{+})}\tanh\left(\frac{\beta}{2}\omega_{\mathbf{k}}^{-}\right) \\
&= -\frac{1}{\omega_{\mathbf{k}}^{+2}-\omega_{\mathbf{k}}^{-2}}\left[\frac{K-\omega_{\mathbf{k}}^{+2}}{\omega_{\mathbf{k}}^{+}}\tanh\left(\frac{\beta}{2}\omega_{\mathbf{k}}^{+}\right) - \frac{K-\omega_{\mathbf{k}}^{-2}}{\omega_{\mathbf{k}}^{-}}\tanh\left(\frac{\beta}{2}\omega_{\mathbf{k}}^{-}\right)\right] \\
&= \frac{1}{\omega_{\mathbf{k}}^{+2}-\omega_{\mathbf{k}}^{-2}}\left[\omega_{\mathbf{k}}^{+}\tanh\left(\frac{\beta}{2}\omega_{\mathbf{k}}^{+}\right) - \omega_{\mathbf{k}}^{-}\tanh\left(\frac{\beta}{2}\omega_{\mathbf{k}}^{-}\right) + K\left(\frac{\tanh\left(\beta\omega_{\mathbf{k}}^{-}/2\right)}{\omega_{\mathbf{k}}^{-}} - \frac{\tanh\left(\beta\omega_{\mathbf{k}}^{+}/2\right)}{\omega_{\mathbf{k}}^{+}}\right)\right],
\end{aligned}
\tag{A.20}
$$

which, with the proper identifications, leads to the intra and interband gap equations showed in the main text.

Appendix B

Interband Vertex Function

B.1 Free Propagator's Inverse

Turning explicit the imaginary factor in the hybridization $V_{\mathbf{k}} = i\tilde{V_{\mathbf{k}}} \to iV_{\mathbf{k}}$ we can write the inverse of the free propagator as

$$\mathbf{G}_0^{-1}(k) = \begin{bmatrix} \mathbb{1}(i\omega_n - \xi_{\mathbf{k}}) + \sigma_3\delta\epsilon_{\mathbf{k}} - \sigma_2 V_{\mathbf{k}} & 0 \\ 0 & \mathbb{1}(i\omega_n + \xi_{\mathbf{k}}) - \sigma_3\delta\epsilon_{\mathbf{k}} + \sigma_2 V_{\mathbf{k}} \end{bmatrix}, \tag{B.1}$$

with the Pauli matrices

$$\sigma_1 = \begin{bmatrix} 0 & 1 \\ 1 & 0 \end{bmatrix}, \quad \sigma_2 = \begin{bmatrix} 0 & -i \\ i & 0 \end{bmatrix}, \quad \sigma_3 = \begin{bmatrix} 1 & 0 \\ 0 & -1 \end{bmatrix}, \tag{B.2}$$

which satisfy $[\sigma_i, \sigma_j] = 2i\epsilon_{ijk}\sigma_k$.

Using a unitary transformation $\mathbf{U}_{\mathbf{k}}^{-1} = \mathbf{U}_{\mathbf{k}}^{\dagger}$ we can change the basis to $\Psi_k \to \mathbf{U}_{\mathbf{k}}\tilde{\Psi}_k$ and diagonalize $\mathbf{U}_{\mathbf{k}}\mathbf{G}_0^{-1}\mathbf{U}_{\mathbf{k}}^{\dagger} \to \tilde{\mathbf{G}}_0^{-1}$. Explicitly

$$\mathbf{U}_{\mathbf{k}} = \begin{bmatrix} \exp(i\sigma_1\phi_{\mathbf{k}}) & 0 \\ 0 & \exp(-i\sigma_1\phi_{-\mathbf{k}}) \end{bmatrix} = \begin{bmatrix} \exp(i\sigma_1\phi_{\mathbf{k}}) & 0 \\ 0 & \exp(i\sigma_1\phi_{\mathbf{k}}) \end{bmatrix}, \tag{B.3}$$

where, see Fig. 4.1, $\sin(2\phi_{\mathbf{k}}) = V_{\mathbf{k}}/\Lambda_{\mathbf{k}}$ and $\cos(2\phi_{\mathbf{k}}) = \delta\epsilon_{\mathbf{k}}/\Lambda_{\mathbf{k}}$ with $\Lambda_{\mathbf{k}} = \sqrt{(\delta\epsilon_{\mathbf{k}})^2 + V_{\mathbf{k}}^2}$.

Thus

$$\mathbf{U}_{\mathbf{k}}\mathbf{G}_0^{-1}(k)\mathbf{U}_{\mathbf{k}}^{\dagger} = \begin{bmatrix} \mathbb{1}(i\omega_n - \xi_{\mathbf{k}}) + W_{\mathbf{k}} & 0 \\ 0 & \mathbb{1}(i\omega_n + \xi_{\mathbf{k}}) - W_{\mathbf{k}} \end{bmatrix}, \tag{B.4}$$

where

$$
\begin{aligned}
W_{\mathbf{k}} &\equiv \exp(i\sigma_1\phi_{\mathbf{k}})(\sigma_3\delta\epsilon_{\mathbf{k}} - \sigma_2 V_{\mathbf{k}})\exp(-i\sigma_1\phi_{\mathbf{k}}) \\
&= (\mathbb{1}\cos\phi_{\mathbf{k}} + i\sigma_1\sin\phi_{\mathbf{k}})(\sigma_3\delta\epsilon_{\mathbf{k}} - \sigma_2 V_{\mathbf{k}})(\mathbb{1}\cos\phi_{\mathbf{k}} - i\sigma_1\sin\phi_{\mathbf{k}}) \\
&= \delta\epsilon_{\mathbf{k}}(\mathbb{1}\cos\phi_{\mathbf{k}} + i\sigma_1\sin\phi_{\mathbf{k}})\sigma_3(\mathbb{1}\cos\phi_{\mathbf{k}} - i\sigma_1\sin\phi_{\mathbf{k}}) \\
&- V_{\mathbf{k}}(\mathbb{1}\cos\phi_{\mathbf{k}} + i\sigma_1\sin\phi_{\mathbf{k}})\sigma_2(\mathbb{1}\cos\phi_{\mathbf{k}} - i\sigma_1\sin\phi_{\mathbf{k}}) \\
&= \delta\epsilon_{\mathbf{k}}(\sigma_3\cos^2\phi_{\mathbf{k}} - i\sigma_3\sigma_1\cos\phi_{\mathbf{k}}\sin\phi_{\mathbf{k}} + i\sigma_1\sigma_3\cos\phi_{\mathbf{k}}\sin\phi_{\mathbf{k}} + \overbrace{\sigma_1\sigma_3\sigma_1}^{-\sigma_3}\sin^2\phi_{\mathbf{k}}) \\
&- V_{\mathbf{k}}(\sigma_2\cos^2\phi_{\mathbf{k}} - i\sigma_2\sigma_1\cos\phi_{\mathbf{k}}\sin\phi_{\mathbf{k}} + i\sigma_1\sigma_2\cos\phi_{\mathbf{k}}\sin\phi_{\mathbf{k}} + \overbrace{\sigma_1\sigma_2\sigma_1}^{-\sigma_2}\sin^2\phi_{\mathbf{k}}) \\
&= \delta\epsilon_{\mathbf{k}}[\sigma_3\overbrace{(\cos^2\phi_{\mathbf{k}} - \sin^2\phi_{\mathbf{k}})}^{\cos(2\phi_{\mathbf{k}})} - i\overbrace{(\sigma_3\sigma_1 - \sigma_1\sigma_3)}^{2i\sigma_2}\overbrace{\cos\phi_{\mathbf{k}}\sin\phi_{\mathbf{k}}}^{\sin(2\phi_{\mathbf{k}})/2}] \\
&- V_{\mathbf{k}}[\sigma_2(\cos^2\phi_{\mathbf{k}} - \sin^2\phi_{\mathbf{k}}) - i\overbrace{(\sigma_2\sigma_1 - \sigma_1\sigma_2)}^{-2i\sigma_3}\cos\phi_{\mathbf{k}}\sin\phi_{\mathbf{k}}] \\
&= \delta\epsilon_{\mathbf{k}}[\sigma_3\cos(2\phi_{\mathbf{k}}) + \sigma_2\sin(2\phi_{\mathbf{k}})] - V_{\mathbf{k}}[\sigma_2\cos(2\phi_{\mathbf{k}}) - \sigma_3\sin(2\phi_{\mathbf{k}})] \\
&= \sigma_3[\delta\epsilon_{\mathbf{k}}\cos(2\phi_{\mathbf{k}}) + V_{\mathbf{k}}\sin(2\phi_{\mathbf{k}})] + \sigma_2[\delta\epsilon_{\mathbf{k}}\sin(2\phi_{\mathbf{k}}) - V_{\mathbf{k}}\cos(2\phi_{\mathbf{k}})] \\
&= \sigma_3\Lambda_{\mathbf{k}},
\end{aligned} \tag{B.5}
$$

which results in

$$
\tilde{\mathbf{G}}_0^{-1}(k) = \begin{bmatrix} i\omega_n - \xi_{\mathbf{k}}^- & 0 & 0 & 0 \\ 0 & i\omega_n - \xi_{\mathbf{k}}^+ & 0 & 0 \\ 0 & 0 & i\omega_n + \xi_{\mathbf{k}}^- & 0 \\ 0 & 0 & 0 & i\omega_n + \xi_{\mathbf{k}}^+ \end{bmatrix}, \tag{B.6}
$$

i.e., the inverse of Eq. 4.3.

B.2 Fluctuations Matrix

The original fluctuations matrix one is given by

$$
\mathbf{\Delta}(k', k) = \begin{bmatrix} 0 & -i\sigma_2\Delta(k'-k) \\ i\sigma_2\bar{\Delta}(k-k') & 0 \end{bmatrix} \tag{B.7}
$$

and in the rotated basis it reads

$$
\begin{aligned}
\tilde{\mathbf{\Delta}}(k', k) &\equiv \mathbf{U}_{\mathbf{k}'}^\dagger \mathbf{\Delta}(k', k)\mathbf{U}_{\mathbf{k}} \\
&= \begin{bmatrix} 0 & -i\Delta(k'-k)Y(\mathbf{k}, \mathbf{k}') \\ i\bar{\Delta}(k-k')Y(\mathbf{k}, \mathbf{k}') & 0 \end{bmatrix},
\end{aligned} \tag{B.8}
$$

where we defined

$$
\begin{aligned}
Y(\mathbf{k},\mathbf{k}') &\equiv \exp(-i\sigma_1\phi_{\mathbf{k}'})\sigma_2\exp(i\sigma_1\phi_{\mathbf{k}}) \\
&= (\mathbb{1}\cos\phi_{\mathbf{k}'} - i\sigma_1\sin\phi_{\mathbf{k}'})\sigma_2(\mathbb{1}\cos\phi_{\mathbf{k}} + i\sigma_1\sin\phi_{\mathbf{k}}) \\
&= \sigma_2\cos\phi_{\mathbf{k}'}\cos\phi_{\mathbf{k}} + i\sigma_2\sigma_1\cos\phi_{\mathbf{k}'}\sin\phi_{\mathbf{k}} - i\sigma_1\sigma_2\sin\phi_{\mathbf{k}'}\cos\phi_{\mathbf{k}} + \sigma_1\sigma_2\sigma_1\sin\phi_{\mathbf{k}'}\sin\phi_{\mathbf{k}} \\
&= \sigma_2(\cos\phi_{\mathbf{k}'}\cos\phi_{\mathbf{k}} - \sin\phi_{\mathbf{k}'}\sin\phi_{\mathbf{k}}) + \sigma_3(\cos\phi_{\mathbf{k}'}\sin\phi_{\mathbf{k}} + \sin\phi_{\mathbf{k}'}\cos\phi_{\mathbf{k}}) \\
&= \sigma_2\cos(\phi_{\mathbf{k}'} + \phi_{\mathbf{k}}) + \sigma_3\sin(\phi_{\mathbf{k}'} + \phi_{\mathbf{k}}) \\
&= Y(\mathbf{k}',\mathbf{k}).
\end{aligned}
\tag{B.9}
$$

Finally we can reparametrize the momenta indexes to $k' \to k + q/2$ and $k \to k - q/2$ to arrive in Eq. 4.5

B.3 Trace of $(\mathrm{G}_0\boldsymbol{\Delta})^2$

The gaussian correction in our effective action is determined by

$$
\mathrm{Tr}(\mathbf{G}_0\boldsymbol{\Delta})^2 = \mathrm{Tr}(\tilde{\mathbf{G}}_0\tilde{\boldsymbol{\Delta}})^2 = \mathrm{Tr}[\tilde{\mathbf{G}}_0(k-q)\tilde{\boldsymbol{\Delta}}(k,2q)\tilde{\mathbf{G}}_0(k+q)\tilde{\boldsymbol{\Delta}}(k,-2q)], \tag{B.10}
$$

with Tr indicating the sum over the 4D Nambu space and internal degrees of freedom. So we have to compute the follow product

$$
\begin{aligned}
&\tilde{\mathbf{G}}_0(k\mp q)\tilde{\boldsymbol{\Delta}}(k,\pm 2q) \\
&= \cos(\phi_{\mathbf{k+q}} + \phi_{\mathbf{k-q}})\begin{bmatrix} 0 & 0 & 0 & -G^-_{k\mp q}\Delta_{\pm 2q} \\ 0 & 0 & G^+_{k\mp q}\Delta_{\pm 2q} & 0 \\ 0 & -G^-_{-k\pm q}\bar{\Delta}_{\mp 2q} & 0 & 0 \\ G^+_{-k\pm q}\bar{\Delta}_{\mp 2q} & 0 & 0 & 0 \end{bmatrix} \\
&+ i\sin(\phi_{\mathbf{k+q}} + \phi_{\mathbf{k-q}})\begin{bmatrix} 0 & 0 & -G^-_{k\mp q}\Delta_{\pm 2q} & 0 \\ 0 & 0 & 0 & G^+_{k\mp q}\Delta_{\pm 2q} \\ -G^-_{-k\pm q}\bar{\Delta}_{\mp 2q} & 0 & 0 & 0 \\ 0 & G^+_{-k\pm q}\bar{\Delta}_{\mp 2q} & 0 & 0 \end{bmatrix}
\end{aligned}
\tag{B.11}
$$

and the diagonal components of (since these are the only relevant terms in the calculation of the trace)

$$
\begin{aligned}
&\tilde{\mathbf{G}}_0(k-q)\tilde{\boldsymbol{\Delta}}(k,2q)\tilde{\mathbf{G}}_0(k+q)\tilde{\boldsymbol{\Delta}}(k,-2q)\\
&\propto -\cos^2(\phi_{\mathbf{k+q}}+\phi_{\mathbf{k-q}})\times\\
&\begin{bmatrix}
G^-_{k-q}G^+_{-k-q}|\Delta_{2q}|^2 & 0 & 0 & 0\\
0 & G^+_{k-q}G^-_{-k-q}|\Delta_{2q}|^2 & 0 & 0\\
0 & 0 & G^-_{-k+q}G^+_{k+q}|\Delta_{-2q}|^2 & 0\\
0 & 0 & 0 & G^+_{-k+q}G^-_{k+q}|\Delta_{-2q}|^2
\end{bmatrix}\\
&-\sin^2(\phi_{\mathbf{k+q}}+\phi_{\mathbf{k-q}})\times\\
&\begin{bmatrix}
G^-_{k-q}G^-_{-k-q}|\Delta_{2q}|^2 & 0 & 0 & 0\\
0 & G^+_{k-q}G^+_{-k-q}|\Delta_{2q}|^2 & 0 & 0\\
0 & 0 & G^-_{-k+q}G^-_{k+q}|\Delta_{-2q}|^2 & 0\\
0 & 0 & 0 & G^+_{-k+q}G^+_{k+q}|\Delta_{-2q}|^2
\end{bmatrix},
\end{aligned}
\tag{B.12}
$$

switching, when necessary, $q \to -q$ and taking the trace we arrive at

$$
\begin{aligned}
\mathrm{Tr}(\tilde{\mathbf{G}}_0\tilde{\boldsymbol{\Delta}})^2 = &-\frac{2}{\beta}\sum_k \cos^2(\phi_{\mathbf{k-q}}+\phi_{\mathbf{k+q}})(G^+_{k-q}G^-_{-k-q}+G^-_{k-q}G^+_{-k-q})|\Delta_{2q}|^2\\
&-\frac{2}{\beta}\sum_k \sin^2(\phi_{\mathbf{k-q}}+\phi_{\mathbf{k+q}})(G^+_{k-q}G^+_{-k-q}+G^-_{k-q}G^-_{-k-q})|\Delta_{2q}|^2,
\end{aligned}
\tag{B.13}
$$

that is Eq. 4.11.

B.4 Interband Matsubara Summation

Next we need to perform the sum of the fermionic frequencies of the follow structures

$$
\begin{aligned}
\frac{1}{\beta}\sum_{\omega_n} G^{\pm}_{k-q}G^{\pm}_{-k-q} &= \frac{1}{\beta}\sum_{\omega_n}\frac{1}{i(\omega_n-\omega_m)-\xi^{\pm}_{\mathbf{k}-\mathbf{q}}}\frac{1}{i(-\omega_n-\omega_m)-\xi^{\pm}_{-\mathbf{k}-\mathbf{q}}} \\
&= -\frac{1}{\beta}\sum_{\omega_n}\frac{1}{i\omega_n-i\omega_m-\xi^{\pm}_{\mathbf{k}-\mathbf{q}}}\frac{1}{i\omega_n+i\omega_m+\xi^{\pm}_{\mathbf{k}+\mathbf{q}}} \\
&= -\sum_{\text{Poles}}\text{Res}\left[\frac{1}{z-i\omega_m-\xi^{\pm}_{\mathbf{k}-\mathbf{q}}}\frac{\eta_F(z)}{z+i\omega_m+\xi^{\pm}_{\mathbf{k}+\mathbf{q}}}\right]\Bigg|_{z=\text{Pole}} \\
&= -\frac{\eta_F(i\omega_m+\xi^{\pm}_{\mathbf{k}-\mathbf{q}})}{i\omega_m+\xi^{\pm}_{\mathbf{k}-\mathbf{q}}+i\omega_m+\xi^{\pm}_{\mathbf{k}+\mathbf{q}}} - \frac{\eta_F(-i\omega_m-\xi^{\pm}_{\mathbf{k}+\mathbf{q}})}{-i\omega_m-\xi^{\pm}_{\mathbf{k}+\mathbf{q}}-i\omega_m-\xi^{\pm}_{\mathbf{k}-\mathbf{q}}} \\
&= -\frac{\eta_F(\xi^{\pm}_{\mathbf{k}-\mathbf{q}})}{2i\omega_m+\xi^{\pm}_{\mathbf{k}-\mathbf{q}}+\xi^{\pm}_{\mathbf{k}+\mathbf{q}}} + \frac{1-\eta_F(\xi^{\pm}_{\mathbf{k}+\mathbf{q}})}{2i\omega_m+\xi^{\pm}_{\mathbf{k}+\mathbf{q}}+\xi^{\pm}_{\mathbf{k}-\mathbf{q}}} \\
&= \frac{1-\eta_F(\xi^{\pm}_{\mathbf{k}+\mathbf{q}})-\eta_F(\xi^{\pm}_{\mathbf{k}-\mathbf{q}})}{2i\omega_m+\xi^{\pm}_{\mathbf{k}+\mathbf{q}}+\xi^{\pm}_{\mathbf{k}-\mathbf{q}}}
\end{aligned}
\tag{B.14}
$$

and bringing these together we obtain Eq. 4.14.

Appendix C

Interband in the Strong Coupling Regime

In the strong coupling regime we consider the bosonic excitations as perturbations around the Fermi surface, $(\omega_m, \mathbf{q}) \ll k_{\mathrm{F}}$, so we can use a gradient expansion in Eq. 4.14. Let us start with the quasi-particles energies

$$\begin{aligned}\xi^{\pm}_{\mathbf{k}+\mathbf{q}} &= \xi_{\mathbf{k}+\mathbf{q}} \pm \Lambda_{\mathbf{k}+\mathbf{q}} \\ &= \xi_{\mathbf{k}} \pm \Lambda_{\mathbf{k}} + q_i \left(\partial_i \xi_{\mathbf{k}} \pm \partial_i \Lambda_{\mathbf{k}}\right) + \frac{1}{2} q_i q_j \left(\partial_i \partial_j \xi_{\mathbf{k}} \pm \partial_i \partial_j \Lambda_{\mathbf{k}}\right),\end{aligned} \tag{C.1}$$

so using that $\partial_i \partial_j \xi_{\mathbf{k}} = \delta_{ij}/m$ we get

$$\xi^{+}_{\mathbf{k}+\mathbf{q}} + \xi^{-}_{\mathbf{k}-\mathbf{q}} = 2\xi_{\mathbf{k}} + \frac{\mathbf{q}^2}{m} + 2 q_i \partial_i \Lambda_{\mathbf{k}}, \tag{C.2}$$

$$\xi^{\pm}_{\mathbf{k}+\mathbf{q}} + \xi^{\pm}_{\mathbf{k}-\mathbf{q}} = 2\xi^{\pm}_{\mathbf{k}} + \frac{\mathbf{q}^2}{m} \pm q_i q_j \partial_i \partial_j \Lambda_{\mathbf{k}}; \tag{C.3}$$

other structures appearing are

$$\begin{aligned}\cos^2\left(\phi_{\mathbf{k}-\mathbf{q}} + \phi_{\mathbf{k}+\mathbf{q}}\right) &= \cos^2\left(2\phi_{\mathbf{k}} + q_i q_j \partial_i \partial_j \phi_{\mathbf{k}}\right) \\ &= \cos^2(2\phi_{\mathbf{k}}) - 2\cos(2\phi_{\mathbf{k}}) \sin(2\phi_{\mathbf{k}}) q_i q_j \partial_i \partial_j \phi_{\mathbf{k}},\end{aligned} \tag{C.4}$$

$$\begin{aligned}\sin^2\left(\phi_{\mathbf{k}-\mathbf{q}} + \phi_{\mathbf{k}+\mathbf{q}}\right) &= \sin^2\left(2\phi_{\mathbf{k}} + q_i q_j \partial_i \partial_j \phi_{\mathbf{k}}\right) \\ &= \sin^2(2\phi_{\mathbf{k}}) + 2\sin(2\phi_{\mathbf{k}}) \cos(2\phi_{\mathbf{k}}) q_i q_j \partial_i \partial_j \phi_{\mathbf{k}}.\end{aligned} \tag{C.5}$$

Keeping the contributions up to order of ω_n and $\mathbf{q}^2$, a typical term of Γ_q^{-1} reads

$$\begin{aligned}&\frac{\cos^2\left(\phi_{\mathbf{k}-\mathbf{q}} + \phi_{\mathbf{k}+\mathbf{q}}\right)}{2i\omega_m + \xi^{+}_{\mathbf{k}+\mathbf{q}} + \xi^{-}_{\mathbf{k}-\mathbf{q}}} = \frac{\cos^2(2\phi_{\mathbf{k}}) - 2\cos(2\phi_{\mathbf{k}}) \sin(2\phi_{\mathbf{k}}) q_i q_j \partial_i \partial_j \phi_{\mathbf{k}}}{2i\omega_m + 2\xi_{\mathbf{k}} + \mathbf{q}^2/m + 2q_i \partial_i \Lambda_{\mathbf{k}}} \\ &= \frac{\cos^2(2\phi_{\mathbf{k}})}{2\xi_{\mathbf{k}}} \left[1 - 2\tan(2\phi_{\mathbf{k}}) q_i q_j \partial_i \partial_j \phi_{\mathbf{k}}\right] \left[1 - \left(i\omega_m + q_i \partial_i \Lambda_{\mathbf{k}} + \frac{\mathbf{q}^2}{2m}\right) \frac{1}{\xi_{\mathbf{k}}} + \left(\frac{q_i \partial_i \Lambda_{\mathbf{k}}}{\xi_{\mathbf{k}}}\right)^2\right] \\ &= \frac{\cos^2(2\phi_{\mathbf{k}})}{2\xi_{\mathbf{k}}} \left[1 - \left(i\omega_m + q_i \partial_i \Lambda_{\mathbf{k}} + \frac{\mathbf{q}^2}{2m}\right) \frac{1}{\xi_{\mathbf{k}}} + q_i q_j \left(\frac{\partial_j \Lambda_{\mathbf{k}} \partial_i \Lambda_{\mathbf{k}}}{\xi^2_{\mathbf{k}}} - 2\tan(2\phi_{\mathbf{k}}) \partial_i \partial_j \phi_{\mathbf{k}}\right)\right],\end{aligned} \tag{C.6}$$

when adding both cosines coefficients the linear terms in q_i cancel one another out

$$\frac{\cos^2(\phi_{\mathbf{k}-\mathbf{q}}+\phi_{\mathbf{k}+\mathbf{q}})}{2i\omega_m+\xi^+_{\mathbf{k}+\mathbf{q}}+\xi^-_{\mathbf{k}-\mathbf{q}}}+\frac{\cos^2(\phi_{\mathbf{k}-\mathbf{q}}+\phi_{\mathbf{k}+\mathbf{q}})}{2i\omega_m+\xi^+_{\mathbf{k}-\mathbf{q}}+\xi^-_{\mathbf{k}+\mathbf{q}}}$$
$$=\frac{\cos^2(2\phi_{\mathbf{k}})}{\xi_{\mathbf{k}}}\left[1-\left(i\omega_m+\frac{\mathbf{q}^2}{2m}\right)\frac{1}{\xi_{\mathbf{k}}}+q_iq_j\left(\frac{\partial_j\Lambda_{\mathbf{k}}\partial_i\Lambda_{\mathbf{k}}}{\xi^2_{\mathbf{k}}}-2\tan(2\phi_{\mathbf{k}})\partial_i\partial_j\phi_{\mathbf{k}}\right)\right], \tag{C.7}$$

and the sines coefficients are

$$\frac{\sin^2(\phi_{\mathbf{k}-\mathbf{q}}+\phi_{\mathbf{k}+\mathbf{q}})}{2i\omega_m+\xi^\pm_{\mathbf{k}+\mathbf{q}}+\xi^\pm_{\mathbf{k}-\mathbf{q}}}=\frac{\sin^2(2\phi_{\mathbf{k}})+2\sin(2\phi_{\mathbf{k}})\cos(2\phi_{\mathbf{k}})q_iq_j\partial_i\partial_j\phi_{\mathbf{k}}}{2i\omega_m+2\xi^\pm_{\mathbf{k}}+\mathbf{q}^2/m\pm q_iq_j\partial_i\partial_j\Lambda_{\mathbf{k}}}$$
$$=\frac{\sin^2(2\phi_{\mathbf{k}})}{2\xi^\pm_{\mathbf{k}}}\left[1+2\cot(2\phi_{\mathbf{k}})q_iq_j\partial_i\partial_j\phi_{\mathbf{k}}\right]\left[1-\left(2i\omega_m\pm q_iq_j\partial_i\partial_j\Lambda_{\mathbf{k}}+\frac{\mathbf{q}^2}{m}\right)\frac{1}{2\xi^\pm_{\mathbf{k}}}\right]$$
$$=\frac{\sin^2(2\phi_{\mathbf{k}})}{2\xi^\pm_{\mathbf{k}}}\left[1-\left(i\omega_m+\frac{\mathbf{q}^2}{2m}\right)\frac{1}{\xi^\pm_{\mathbf{k}}}+q_iq_j\left(2\cot(2\phi_{\mathbf{k}})\partial_i\partial_j\phi_{\mathbf{k}}\mp\frac{\partial_i\partial_j\Lambda_{\mathbf{k}}}{2\xi^\pm_{\mathbf{k}}}\right)\right]. \tag{C.8}$$

Gathering all terms together the vertex function reads (for convenience we labeled $q\to 2q$)

$$\Gamma^{-1}_{2q}=\frac{2}{g_1}-\sum_{\mathbf{k}}I_{\mathbf{k}}+\left(i\omega_m+\frac{\mathbf{q}^2}{2m}\right)\sum_{\mathbf{k}}J_{\mathbf{k}}$$
$$-q_iq_j\sum_{\mathbf{k}}\sin(2\phi_{\mathbf{k}})\cos(2\phi_{\mathbf{k}})\left(\frac{1}{\xi^+_{\mathbf{k}}}+\frac{1}{\xi^-_{\mathbf{k}}}-\frac{2}{\xi_{\mathbf{k}}}\right)\partial_i\partial_j\phi_{\mathbf{k}}$$
$$-q_iq_j\sum_{\mathbf{k}}\left[\frac{\cos^2(2\phi_{\mathbf{k}})}{\xi^3_{\mathbf{k}}}\partial_j\Lambda_{\mathbf{k}}\partial_i\Lambda_{\mathbf{k}}+\frac{\sin^2(2\phi_{\mathbf{k}})}{4}\left(\frac{1}{\xi^{-2}_{\mathbf{k}}}-\frac{1}{\xi^{+2}_{\mathbf{k}}}\right)\partial_i\partial_j\Lambda_{\mathbf{k}}\right], \tag{C.9}$$

where we defined

$$I_{\mathbf{k}}\equiv\frac{\cos^2(2\phi_{\mathbf{k}})}{\xi_{\mathbf{k}}}+\frac{\sin^2(2\phi_{\mathbf{k}})}{2}\left(\frac{1}{\xi^+_{\mathbf{k}}}+\frac{1}{\xi^-_{\mathbf{k}}}\right), \tag{C.10}$$

$$J_{\mathbf{k}}\equiv\frac{\cos^2(2\phi_{\mathbf{k}})}{\xi^2_{\mathbf{k}}}+\frac{\sin^2(2\phi_{\mathbf{k}})}{2}\left(\frac{1}{\xi^{+2}_{\mathbf{k}}}+\frac{1}{\xi^{-2}_{\mathbf{k}}}\right). \tag{C.11}$$

Next we calculate the expressions

$$\frac{1}{\xi^+_{\mathbf{k}}}+\frac{1}{\xi^-_{\mathbf{k}}}=\frac{1}{\xi_{\mathbf{k}}+\Lambda_{\mathbf{k}}}+\frac{1}{\xi_{\mathbf{k}}-\Lambda_{\mathbf{k}}}=\frac{2\xi_{\mathbf{k}}}{\xi^2_{\mathbf{k}}-\Lambda^2_{\mathbf{k}}}, \tag{C.12}$$

$$\frac{1}{\xi^+_{\mathbf{k}}}+\frac{1}{\xi^-_{\mathbf{k}}}-\frac{2}{\xi_{\mathbf{k}}}=\frac{2\xi_{\mathbf{k}}}{\xi^2_{\mathbf{k}}-\Lambda^2_{\mathbf{k}}}-\frac{2}{\xi_{\mathbf{k}}}=\frac{2\Lambda^2_{\mathbf{k}}}{\xi_{\mathbf{k}}(\xi^2_{\mathbf{k}}-\Lambda^2_{\mathbf{k}})}, \tag{C.13}$$

$$\frac{1}{\xi^{+2}_{\mathbf{k}}}+\frac{1}{\xi^{-2}_{\mathbf{k}}}=\frac{1}{(\xi_{\mathbf{k}}+\Lambda_{\mathbf{k}})^2}+\frac{1}{(\xi_{\mathbf{k}}-\Lambda_{\mathbf{k}})^2}=2\frac{\xi^2_{\mathbf{k}}+\Lambda^2_{\mathbf{k}}}{(\xi^2_{\mathbf{k}}-\Lambda^2_{\mathbf{k}})^2}, \tag{C.14}$$

$$\frac{1}{\xi^{-2}_{\mathbf{k}}}-\frac{1}{\xi^{+2}_{\mathbf{k}}}=\frac{1}{(\xi_{\mathbf{k}}-\Lambda_{\mathbf{k}})^2}-\frac{1}{(\xi_{\mathbf{k}}+\Lambda_{\mathbf{k}})^2}=\frac{4\xi_{\mathbf{k}}\Lambda_{\mathbf{k}}}{(\xi^2_{\mathbf{k}}-\Lambda^2_{\mathbf{k}})^2}, \tag{C.15}$$

so that

$$
\begin{aligned}
I_{\mathbf{k}} &= \frac{\cos^2(2\phi_{\mathbf{k}})}{\xi_{\mathbf{k}}} + \frac{\xi_{\mathbf{k}} \sin^2(2\phi_{\mathbf{k}})}{\xi_{\mathbf{k}}^2 - \Lambda_{\mathbf{k}}^2} \\
&= \frac{(\xi_{\mathbf{k}}^2 - \Lambda_{\mathbf{k}}^2)\cos^2(2\phi_{\mathbf{k}}) + \xi_{\mathbf{k}}^2 \sin^2(2\phi_{\mathbf{k}})}{\xi_{\mathbf{k}}(\xi_{\mathbf{k}}^2 - \Lambda_{\mathbf{k}}^2)} \\
&= \frac{\xi_{\mathbf{k}}^2 - \Lambda_{\mathbf{k}}^2 + V_{\mathbf{k}}^2}{\xi_{\mathbf{k}}(\xi_{\mathbf{k}}^2 - \Lambda_{\mathbf{k}}^2)} \\
&= \frac{1}{\xi_{\mathbf{k}}}\left(1 + \frac{V_{\mathbf{k}}^2}{\xi_{\mathbf{k}}^2 - \Lambda_{\mathbf{k}}^2}\right)
\end{aligned}
\tag{C.16}
$$

and

$$
\begin{aligned}
J_{\mathbf{k}} &= \frac{\cos^2(2\phi_{\mathbf{k}})}{\xi_{\mathbf{k}}^2} + \sin^2(2\phi_{\mathbf{k}})\frac{\xi_{\mathbf{k}}^2 + \Lambda_{\mathbf{k}}^2}{(\xi_{\mathbf{k}}^2 - \Lambda_{\mathbf{k}}^2)^2} \\
&= \frac{(\xi_{\mathbf{k}}^2 - \Lambda_{\mathbf{k}}^2)^2\cos^2(2\phi_{\mathbf{k}}) + \xi_{\mathbf{k}}^2(\xi_{\mathbf{k}}^2 + \Lambda_{\mathbf{k}}^2)\sin^2(2\phi_{\mathbf{k}})}{\xi_{\mathbf{k}}^2(\xi_{\mathbf{k}}^2 - \Lambda_{\mathbf{k}}^2)^2} \\
&= \frac{\xi_{\mathbf{k}}^4 + \xi_{\mathbf{k}}^2\Lambda_{\mathbf{k}}^2\left[\sin^2(2\phi_{\mathbf{k}}) - 2\cos^2(2\phi_{\mathbf{k}})\right] + \Lambda_{\mathbf{k}}^4\cos^2(2\phi_{\mathbf{k}})}{\xi_{\mathbf{k}}^2(\xi_{\mathbf{k}}^2 - \Lambda_{\mathbf{k}}^2)^2} \\
&= \frac{\xi_{\mathbf{k}}^4 + \xi_{\mathbf{k}}^2(3V_{\mathbf{k}}^2 - 2\Lambda_{\mathbf{k}}^2) + \Lambda_{\mathbf{k}}^4 - \Lambda_{\mathbf{k}}^2 V_{\mathbf{k}}^2}{\xi_{\mathbf{k}}^2(\xi_{\mathbf{k}}^2 - \Lambda_{\mathbf{k}}^2)^2} \\
&= \frac{\xi_{\mathbf{k}}^2(\xi_{\mathbf{k}}^2 - \Lambda_{\mathbf{k}}^2) + V_{\mathbf{k}}^2(\xi_{\mathbf{k}}^2 - \Lambda_{\mathbf{k}}^2) + \Lambda_{\mathbf{k}}^2(\Lambda_{\mathbf{k}}^2 - \xi_{\mathbf{k}}^2)}{\xi_{\mathbf{k}}^2(\xi_{\mathbf{k}}^2 - \Lambda_{\mathbf{k}}^2)^2} + \frac{2V_{\mathbf{k}}^2}{(\xi_{\mathbf{k}}^2 - \Lambda_{\mathbf{k}}^2)^2} \\
&= \frac{1}{\xi_{\mathbf{k}}^2} + \frac{1}{\xi_{\mathbf{k}}^2}\frac{V_{\mathbf{k}}^2}{\xi_{\mathbf{k}}^2 - \Lambda_{\mathbf{k}}^2} + \frac{2V_{\mathbf{k}}^2}{(\xi_{\mathbf{k}}^2 - \Lambda_{\mathbf{k}}^2)^2},
\end{aligned}
\tag{C.17}
$$

thus, making the substitution given by Eq. 3.31, we can write

$$
\begin{aligned}
\Gamma_{2q}^{-1} =& -\frac{m}{2\pi a_s} + \sum_{\mathbf{k}}\left[\frac{1}{\epsilon_{\mathbf{k}}} - \frac{1}{\xi_{\mathbf{k}}}\left(1 + \frac{V_{\mathbf{k}}^2}{\xi_{\mathbf{k}}^2 - \Lambda_{\mathbf{k}}^2}\right)\right] \\
&+ \left(i\omega_m + \frac{\mathbf{q}^2}{2m}\right)\sum_{\mathbf{k}}\left[\frac{1}{\xi_{\mathbf{k}}^2}\left(1 + \frac{V_{\mathbf{k}}^2}{\xi_{\mathbf{k}}^2 - \Lambda_{\mathbf{k}}^2}\right) + \frac{2V_{\mathbf{k}}^2}{(\xi_{\mathbf{k}}^2 - \Lambda_{\mathbf{k}}^2)^2}\right] \\
&\underbrace{- q_i q_j \sum_{\mathbf{k}}\left[\frac{\delta\epsilon_{\mathbf{k}}}{\xi_{\mathbf{k}}}\frac{V_{\mathbf{k}}}{\xi_{\mathbf{k}}^2 - \Lambda_{\mathbf{k}}^2}\partial_i\partial_j(2\phi_{\mathbf{k}}) + \frac{1}{\xi_{\mathbf{k}}^3}\frac{(\delta\epsilon_{\mathbf{k}})^2}{\Lambda_{\mathbf{k}}^2}\partial_j\Lambda_{\mathbf{k}}\partial_i\Lambda_{\mathbf{k}} + \frac{\xi_{\mathbf{k}}}{\Lambda_{\mathbf{k}}}\frac{V_{\mathbf{k}}^2}{(\xi_{\mathbf{k}}^2 - \Lambda_{\mathbf{k}}^2)^2}\partial_i\partial_j\Lambda_{\mathbf{k}}\right]}_{K(\mathbf{q})}.
\end{aligned}
\tag{C.18}
$$

In the first two lines of Eq. C.18 we already have the expressions for Γ_0^{-1} and $J(\alpha)$ presented in the main text. To calculate $K(\mathbf{q})$ we must compute the derivatives it contains. Let us stat with

$$
\partial_i\Lambda_{\mathbf{k}} = \frac{\delta\epsilon_{\mathbf{k}}\partial_i\delta\epsilon_{\mathbf{k}} + V_{\mathbf{k}}\partial_i V_{\mathbf{k}}}{\Lambda_{\mathbf{k}}},
\tag{C.19}
$$

so

$$\partial_i \Lambda_{\mathbf{k}} \partial_j \Lambda_{\mathbf{k}} = \frac{(\delta\epsilon_{\mathbf{k}})^2 \partial_i \delta\epsilon_{\mathbf{k}} \partial_j \delta\epsilon_{\mathbf{k}} + \delta\epsilon_{\mathbf{k}} V_{\mathbf{k}} \left(\partial_i \delta\epsilon_{\mathbf{k}} \partial_j V_{\mathbf{k}} + \partial_j \delta\epsilon_{\mathbf{k}} \partial_i V_{\mathbf{k}}\right) + V_{\mathbf{k}}^2 \partial_i V_{\mathbf{k}} \partial_j V_{\mathbf{k}}}{\Lambda_{\mathbf{k}}^2}, \tag{C.20}$$

the second derivative of $\Lambda_{\mathbf{k}}$ is

$$\partial_i \partial_j \Lambda_{\mathbf{k}} = \frac{\partial_i \delta\epsilon_{\mathbf{k}} \partial_j \delta\epsilon_{\mathbf{k}} + \delta\epsilon_{\mathbf{k}} \partial_i \partial_j \delta\epsilon_{\mathbf{k}} + \partial_i V_{\mathbf{k}} \partial_j V_{\mathbf{k}} + V_{\mathbf{k}} \partial_i \partial_j V_{\mathbf{k}} - \partial_i \Lambda_{\mathbf{k}} \partial_j \Lambda_{\mathbf{k}}}{\Lambda_{\mathbf{k}}}; \tag{C.21}$$

the derivatives of $\phi_{\mathbf{k}}$ can be calculated by observing that $2\phi_{\mathbf{k}} = \arctan(V_{\mathbf{k}}/\delta\epsilon_{\mathbf{k}})$ then

$$\partial_i (2\phi_{\mathbf{k}}) = \frac{\delta\epsilon_{\mathbf{k}} \partial_i V_{\mathbf{k}} - V_{\mathbf{k}} \partial_i \delta\epsilon_{\mathbf{k}}}{\Lambda_{\mathbf{k}}^2} \tag{C.22}$$

and

$$\begin{aligned}
\partial_j \partial_i (2\phi_{\mathbf{k}}) = &\frac{\partial_j \delta\epsilon_{\mathbf{k}} \partial_i V_{\mathbf{k}} + \delta\epsilon_{\mathbf{k}} \partial_j \partial_i V_{\mathbf{k}} - \partial_j V_{\mathbf{k}} \partial_i \delta\epsilon_{\mathbf{k}} - V_{\mathbf{k}} \partial_j \partial_i \delta\epsilon_{\mathbf{k}}}{\Lambda_{\mathbf{k}}^2} \\
&- 2\frac{(\delta\epsilon_{\mathbf{k}} \partial_j \delta\epsilon_{\mathbf{k}} + V_{\mathbf{k}} \partial_j V_{\mathbf{k}})(\delta\epsilon_{\mathbf{k}} \partial_i V_{\mathbf{k}} - V_{\mathbf{k}} \partial_i \delta\epsilon_{\mathbf{k}})}{\Lambda_{\mathbf{k}}^4} \\
= &\frac{\partial_j \delta\epsilon_{\mathbf{k}} \partial_i V_{\mathbf{k}} + \delta\epsilon_{\mathbf{k}} \partial_j \partial_i V_{\mathbf{k}} - \partial_j V_{\mathbf{k}} \partial_i \delta\epsilon_{\mathbf{k}} - V_{\mathbf{k}} \partial_j \partial_i \delta\epsilon_{\mathbf{k}}}{\Lambda_{\mathbf{k}}^2} \\
&- 2\frac{(\delta\epsilon_{\mathbf{k}})^2 \partial_j \delta\epsilon_{\mathbf{k}} \partial_i V_{\mathbf{k}} + \delta\epsilon_{\mathbf{k}} V_{\mathbf{k}} (\partial_j V_{\mathbf{k}} \partial_i V_{\mathbf{k}} - \partial_j \delta\epsilon_{\mathbf{k}} \partial_i \delta\epsilon_{\mathbf{k}}) - V_{\mathbf{k}}^2 \partial_j V_{\mathbf{k}} \partial_i \delta\epsilon_{\mathbf{k}}}{\Lambda_{\mathbf{k}}^4}.
\end{aligned} \tag{C.23}$$

Multiplying the above expressions by $q_j q_i$, summing over i and j and using $\partial_i \epsilon_{\mathbf{k}} = k_i/m$, $\partial_j \partial_i \epsilon_{\mathbf{k}} = \delta_{ij}/m$ together with the linearity of the hybridization, $\partial_i V_{\mathbf{k}} = v_i$ and $\partial_j \partial_i V_{\mathbf{k}} = 0$, we arrive at

$$\sum_{i,j} q_i q_j \partial_i \Lambda_{\mathbf{k}} \partial_j \Lambda_{\mathbf{k}} = \frac{(\delta\epsilon_{\mathbf{k}})^2 (\delta\mathbf{k}\cdot\mathbf{q}/m)^2 + 2\delta\epsilon_{\mathbf{k}} V_{\mathbf{k}} (\delta\mathbf{k}\cdot\mathbf{q}/m) V_{\mathbf{q}} + V_{\mathbf{k}}^2 V_{\mathbf{q}}^2}{\Lambda_{\mathbf{k}}^2}, \tag{C.24}$$

$$\begin{aligned}
\sum_{i,j} q_i q_j \partial_i \partial_j \Lambda_{\mathbf{k}} &= \frac{(\delta\mathbf{k}\cdot\mathbf{q}/m)^2 + 2\delta\epsilon_{\mathbf{k}} \delta\epsilon_{\mathbf{q}} + V_{\mathbf{q}}^2}{\Lambda_{\mathbf{k}}} - \frac{[\delta\epsilon_{\mathbf{k}} (\delta\mathbf{k}\cdot\mathbf{q}/m) + V_{\mathbf{k}} V_{\mathbf{q}}]^2}{\Lambda_{\mathbf{k}}^3} \\
&= \frac{2\delta\epsilon_{\mathbf{k}} \delta\epsilon_{\mathbf{q}}}{\Lambda_{\mathbf{k}}} + \frac{V_{\mathbf{k}}^2 (\delta\mathbf{k}\cdot\mathbf{q}/m)^2 - 2\delta\epsilon_{\mathbf{k}} V_{\mathbf{k}} (\delta\mathbf{k}\cdot\mathbf{q}/m) V_{\mathbf{q}} + (\delta\epsilon_{\mathbf{k}})^2 V_{\mathbf{q}}^2}{\Lambda_{\mathbf{k}}^3},
\end{aligned} \tag{C.25}$$

$$\sum_{i,j} q_i q_j \partial_i \partial_j (2\phi_{\mathbf{k}}) = -\frac{2V_{\mathbf{k}} \delta\epsilon_{\mathbf{q}}}{\Lambda_{\mathbf{k}}^2} - 2\frac{[(\delta\epsilon_{\mathbf{k}})^2 - V_{\mathbf{k}}^2](\delta\mathbf{k}\cdot\mathbf{q}/m) V_{\mathbf{q}} + \delta\epsilon_{\mathbf{k}} V_{\mathbf{k}} [V_{\mathbf{q}}^2 - (\delta\mathbf{k}\cdot\mathbf{q}/m)^2]}{\Lambda_{\mathbf{k}}^4}. \tag{C.26}$$

From these equations is easy to see that the power series expansion in $q_i q_j$ appears in four structures, namely $\mathbf{q}^2$, $(\mathbf{k}\cdot\mathbf{q})^2$, $V_{\mathbf{q}}^2$ and $V_{\mathbf{q}}(\mathbf{k}\cdot\mathbf{q})$.

So evidencing each of the $\mathbf{q}$ functions $K(\mathbf{q})$ becomes

$$
\begin{aligned}
K(\mathbf{q}) = &-2\sum_{\mathbf{k}} \frac{\delta\epsilon_{\mathbf{k}}}{\xi_{\mathbf{k}}} \frac{V_{\mathbf{k}}}{\xi_{\mathbf{k}}^2 - \Lambda_{\mathbf{k}}^2} \left[\frac{V_{\mathbf{k}}\delta\epsilon_{\mathbf{q}}}{\Lambda_{\mathbf{k}}^2} + \frac{[(\delta\epsilon_{\mathbf{k}})^2 - V_{\mathbf{k}}^2](\delta\mathbf{k}\cdot\mathbf{q}/m)V_{\mathbf{q}} + \delta\epsilon_{\mathbf{k}} V_{\mathbf{k}}[V_{\mathbf{q}}^2 - (\delta\mathbf{k}\cdot\mathbf{q}/m)^2]}{\Lambda_{\mathbf{k}}^4} \right] \\
&+ \sum_{\mathbf{k}} \frac{1}{\xi_{\mathbf{k}}^3} \frac{(\delta\epsilon_{\mathbf{k}})^2}{\Lambda_{\mathbf{k}}^2} \frac{(\delta\epsilon_{\mathbf{k}})^2(\delta\mathbf{k}\cdot\mathbf{q}/m)^2 + 2\delta\epsilon_{\mathbf{k}} V_{\mathbf{k}}(\delta\mathbf{k}\cdot\mathbf{q}/m)V_{\mathbf{q}} + V_{\mathbf{k}}^2 V_{\mathbf{q}}^2}{\Lambda_{\mathbf{k}}^2} \\
&+ \sum_{\mathbf{k}} \frac{\xi_{\mathbf{k}}}{\Lambda_{\mathbf{k}}} \frac{V_{\mathbf{k}}^2}{(\xi_{\mathbf{k}}^2 - \Lambda_{\mathbf{k}}^2)^2} \left[\frac{2\delta\epsilon_{\mathbf{k}}\delta\epsilon_{\mathbf{q}}}{\Lambda_{\mathbf{k}}} + \frac{V_{\mathbf{k}}^2(\delta\mathbf{k}\cdot\mathbf{q}/m)^2 - 2\delta\epsilon_{\mathbf{k}} V_{\mathbf{k}}(\delta\mathbf{k}\cdot\mathbf{q}/m)V_{\mathbf{q}} + (\delta\epsilon_{\mathbf{k}})^2 V_{\mathbf{q}}^2}{\Lambda_{\mathbf{k}}^3} \right] \\
= &\frac{\delta\mathbf{q}^2}{m} \sum_{\mathbf{k}} \left[-\frac{\delta\epsilon_{\mathbf{k}}}{\xi_{\mathbf{k}}\Lambda_{\mathbf{k}}^2} \frac{V_{\mathbf{k}}^2}{\xi_{\mathbf{k}}^2 - \Lambda_{\mathbf{k}}^2} + \frac{\delta\epsilon_{\mathbf{k}}\xi_{\mathbf{k}}}{\Lambda_{\mathbf{k}}^2} \frac{V_{\mathbf{k}}^2}{(\xi_{\mathbf{k}}^2 - \Lambda_{\mathbf{k}}^2)^2} \right] \\
&+ \sum_{\mathbf{k}} \left(\frac{\delta\mathbf{k}\cdot\mathbf{q}}{m} \right)^2 \left[2\frac{\delta\epsilon_{\mathbf{k}}}{\xi_{\mathbf{k}}} \frac{V_{\mathbf{k}}}{\xi_{\mathbf{k}}^2 - \Lambda_{\mathbf{k}}^2} \frac{\delta\epsilon_{\mathbf{k}} V_{\mathbf{k}}}{\Lambda^4} + \frac{1}{\xi_{\mathbf{k}}^3} \frac{(\delta\epsilon_{\mathbf{k}})^2}{\Lambda_{\mathbf{k}}^2} \frac{(\delta\epsilon_{\mathbf{k}})^2}{\Lambda_{\mathbf{k}}^2} + \frac{\xi_{\mathbf{k}}}{\Lambda_{\mathbf{k}}} \frac{V_{\mathbf{k}}^2}{(\xi_{\mathbf{k}}^2 - \Lambda_{\mathbf{k}}^2)^2} \frac{V_{\mathbf{k}}^2}{\Lambda_{\mathbf{k}}^3} \right] \\
&+ 2V_{\mathbf{q}} \sum_{\mathbf{k}} \frac{\delta\mathbf{k}\cdot\mathbf{q}}{m} \left[-\frac{\delta\epsilon_{\mathbf{k}}}{\xi_{\mathbf{k}}} \frac{V_{\mathbf{k}}}{\xi_{\mathbf{k}}^2 - \Lambda_{\mathbf{k}}^2} \frac{(\delta\epsilon_{\mathbf{k}})^2 - V_{\mathbf{k}}^2}{\Lambda_{\mathbf{k}}^4} + \frac{1}{\xi_{\mathbf{k}}^3} \frac{(\delta\epsilon_{\mathbf{k}})^2}{\Lambda_{\mathbf{k}}^2} \frac{\delta\epsilon_{\mathbf{k}} V_{\mathbf{k}}}{\Lambda_{\mathbf{k}}^2} - \frac{\xi_{\mathbf{k}}}{\Lambda_{\mathbf{k}}} \frac{V_{\mathbf{k}}^2}{(\xi_{\mathbf{k}}^2 - \Lambda_{\mathbf{k}}^2)^2} \frac{\delta\epsilon_{\mathbf{k}} V_{\mathbf{k}}}{\Lambda_{\mathbf{k}}^3} \right] \\
&+ V_{\mathbf{q}}^2 \sum_{\mathbf{k}} \left[-2\frac{\delta\epsilon_{\mathbf{k}}}{\xi_{\mathbf{k}}} \frac{V_{\mathbf{k}}}{\xi_{\mathbf{k}}^2 - \Lambda_{\mathbf{k}}^2} \frac{\delta\epsilon_{\mathbf{k}} V_{\mathbf{k}}}{\Lambda^4} + \frac{1}{\xi_{\mathbf{k}}^3} \frac{(\delta\epsilon_{\mathbf{k}})^2}{\Lambda_{\mathbf{k}}^2} \frac{V_{\mathbf{k}}^2}{\Lambda_{\mathbf{k}}^2} + \frac{\xi_{\mathbf{k}}}{\Lambda_{\mathbf{k}}} \frac{V_{\mathbf{k}}^2}{(\xi_{\mathbf{k}}^2 - \Lambda_{\mathbf{k}}^2)^2} \frac{(\delta\epsilon_{\mathbf{k}})^2}{\Lambda_{\mathbf{k}}^3} \right] \\
= &\frac{\delta\mathbf{q}^2}{m} \sum_{\mathbf{k}} \frac{V_{\mathbf{k}}^2}{\Lambda_{\mathbf{k}}^2} \frac{\delta\epsilon_{\mathbf{k}}}{\xi_{\mathbf{k}}} \frac{-\xi_{\mathbf{k}}^2 + \Lambda_{\mathbf{k}}^2 + \xi_{\mathbf{k}}^2}{(\xi_{\mathbf{k}}^2 - \Lambda_{\mathbf{k}}^2)^2} \\
&+ \sum_{\mathbf{k}} \left(\frac{\delta\mathbf{k}\cdot\mathbf{q}}{m} \right)^2 \frac{1}{\xi_{\mathbf{k}}^3} \frac{1}{\Lambda_{\mathbf{k}}^4} \frac{2(\delta\epsilon_{\mathbf{k}})^2 V_{\mathbf{k}}^2 \xi_{\mathbf{k}}^2(\xi_{\mathbf{k}}^2 - \Lambda_{\mathbf{k}}^2) + (\delta\epsilon_{\mathbf{k}})^4(\xi_{\mathbf{k}}^2 - \Lambda_{\mathbf{k}}^2)^2 + V_{\mathbf{k}}^4 \xi_{\mathbf{k}}^4}{(\xi_{\mathbf{k}}^2 - \Lambda_{\mathbf{k}}^2)^2} \\
&+ 2V_{\mathbf{q}} \sum_{\mathbf{k}} \frac{\delta\mathbf{k}\cdot\mathbf{q}}{m} \frac{\delta\epsilon_{\mathbf{k}}}{\xi_{\mathbf{k}}^3} \frac{V_{\mathbf{k}}}{\Lambda_{\mathbf{k}}^4} \frac{(\xi_{\mathbf{k}}^2 - \Lambda_{\mathbf{k}}^2)[V_{\mathbf{k}}^2 - (\delta\epsilon_{\mathbf{k}})^2]\xi_{\mathbf{k}}^2 + (\delta\epsilon_{\mathbf{k}})^2(\xi_{\mathbf{k}}^2 - \Lambda_{\mathbf{k}}^2)^2 - V_{\mathbf{k}}^2 \xi_{\mathbf{k}}^4}{(\xi_{\mathbf{k}}^2 - \Lambda_{\mathbf{k}}^2)^2} \\
&+ V_{\mathbf{q}}^2 \sum_{\mathbf{k}} \frac{V_{\mathbf{k}}^2}{\Lambda_{\mathbf{k}}^4} \frac{(\delta\epsilon_{\mathbf{k}})^2}{\xi_{\mathbf{k}}^3} \frac{(\xi_{\mathbf{k}}^2 - \Lambda_{\mathbf{k}}^2)^2 - 2\xi_{\mathbf{k}}^2(\xi_{\mathbf{k}}^2 - \Lambda_{\mathbf{k}}^2) + \xi_{\mathbf{k}}^4}{(\xi_{\mathbf{k}}^2 - \Lambda_{\mathbf{k}}^2)^2} \\
= &\frac{\delta\mathbf{q}^2}{m} \sum_{\mathbf{k}} \frac{\delta\epsilon_{\mathbf{k}}}{\xi_{\mathbf{k}}} \frac{V_{\mathbf{k}}^2}{(\xi_{\mathbf{k}}^2 - \Lambda_{\mathbf{k}}^2)^2} + \sum_{\mathbf{k}} \left(\frac{\delta\mathbf{k}\cdot\mathbf{q}}{m} \right)^2 \frac{1}{\xi_{\mathbf{k}}^3} \left(1 + \frac{V_{\mathbf{k}}^2}{\xi_{\mathbf{k}}^2 - \Lambda_{\mathbf{k}}^2} \right)^2 \\
&- V_{\mathbf{q}} \sum_{\mathbf{k}} \frac{2\delta\mathbf{k}\cdot\mathbf{q}}{m} \frac{\delta\epsilon_{\mathbf{k}}}{\xi_{\mathbf{k}}^3} \frac{V_{\mathbf{k}}}{\xi_{\mathbf{k}}^2 - \Lambda_{\mathbf{k}}^2} \left(1 + \frac{V_{\mathbf{k}}^2}{\xi_{\mathbf{k}}^2 - \Lambda_{\mathbf{k}}^2} \right) + V_{\mathbf{q}}^2 \sum_{\mathbf{k}} \frac{(\delta\epsilon_{\mathbf{k}})^2}{\xi_{\mathbf{k}}^3} \frac{V_{\mathbf{k}}^2}{(\xi_{\mathbf{k}}^2 - \Lambda_{\mathbf{k}}^2)^2} \\
= &\frac{\delta\mathbf{q}^2}{m} \sum_{\mathbf{k}} \frac{\delta\epsilon_{\mathbf{k}}}{\xi_{\mathbf{k}}} \frac{V_{\mathbf{k}}^2}{(\xi_{\mathbf{k}}^2 - \Lambda_{\mathbf{k}}^2)^2} + \sum_{\mathbf{k}} \frac{1}{\xi_{\mathbf{k}}^3} \left[\left(\frac{\delta\mathbf{k}\cdot\mathbf{q}}{m} \right) \left(1 + \frac{V_{\mathbf{k}}^2}{\xi_{\mathbf{k}}^2 - \Lambda_{\mathbf{k}}^2} \right) - \frac{\delta\epsilon_{\mathbf{k}} V_{\mathbf{k}} V_{\mathbf{q}}}{\xi_{\mathbf{k}}^2 - \Lambda_{\mathbf{k}}^2} \right]^2 .
\end{aligned} \tag{C.27}
$$

Finally regrouping all the terms and returning with the original definition of imaginary $V_{\mathbf{k}}$ we arrive at the vertex function given by Eq. 4.15.

C.1 Evaluation of Γ_0^{-1}

The binding energy E_B or equivalently the critical chemical potential $\mu_c = E_B/2$ are defined through the zeroth order vertex function, namely (here we assume $\mu = |\mu|/\epsilon_F$ and $\mathbf{k}^2 = k^2 + k_z^2$)

$$\Gamma_0^{-1} = -\frac{m}{2\pi a_s} + \sum_{\mathbf{k}} \left(\frac{1}{\epsilon_{\mathbf{k}}} - \frac{1}{\xi_{\mathbf{k}}}\right) - \sum_{\mathbf{k}} \frac{\Theta_{\mathbf{k}}}{\xi_{\mathbf{k}}}$$

$$= \underbrace{\frac{1}{\epsilon_F}\left(\frac{k_F}{2\pi}\right)^3}_{\frac{\nu_0}{2\pi}} \left[-\frac{2\pi^2}{k_F a_s} + 4\pi \underbrace{\int_0^\infty \mathrm{d}\mathbf{k} \left(1 - \frac{\mathbf{k}^2}{\mathbf{k}^2 + \mu}\right)}_{\frac{\pi\sqrt{\mu}}{2}} - \int \frac{\mathrm{d}^3 k}{\mathbf{k}^2 + \mu} \frac{2\alpha^2 k_z^2}{(\mathbf{k}^2 + \mu)^2 - \delta^2 \mathbf{k}^4 - 2\alpha^2 k_z^2} \right]$$

$$= \pi\nu_0 \left[-\frac{1}{k_F a_s} + \sqrt{\mu} - \frac{2}{\pi} \int_0^\infty \int_0^\infty \frac{k\,\mathrm{d}k\,\mathrm{d}k_z}{\mathbf{k}^2 + \mu} \frac{2\alpha^2 k_z^2}{(\mathbf{k}^2 + \mu)^2 - \delta^2 \mathbf{k}^4 - 2\alpha^2 k_z^2} \right], \tag{C.28}$$

defining $x \equiv k/\sqrt{\mu}$ and $y \equiv k_z/\sqrt{\mu}$

$$\Gamma_0^{-1} = \pi\nu_0 \left[-\frac{1}{k_F a_s} + \sqrt{\mu} - \frac{2}{\pi}\sqrt{\mu} \int_0^\infty \int_0^\infty \frac{x\,\mathrm{d}x\,\mathrm{d}y}{x^2 + y^2 + 1} \frac{(2\alpha^2/\mu) y^2}{(x^2 + y^2 + 1)^2 - \delta^2 (x^2 + y^2)^2 - (2\alpha^2/\mu) y^2} \right]. \tag{C.29}$$

In the BEC limit the condition $\xi_{\mathbf{k}}^- > 0$ is always valid so we may use a power series expansion

$$\frac{(2\alpha^2/\mu) y^2}{(x^2 + y^2 + 1)^2 - \delta^2 (x^2 + y^2)^2 - (2\alpha^2/\mu) y^2} = \sum_{n=1}^{\infty} \left[\frac{(2\alpha^2/\mu) y^2}{(x^2 + y^2 + 1)^2 - \delta^2 (x^2 + y^2)^2} \right]^n \tag{C.30}$$

thus

$$\Gamma_0^{-1} = \pi\nu_0 \left[-\frac{1}{k_F a_s} + \sqrt{\mu} - \sqrt{\mu} \sum_{n=1}^{\infty} C_n(\delta) \left(\frac{2\alpha^2}{\mu}\right)^n \right], \tag{C.31}$$

with

$$C_n(\delta) \equiv \frac{2}{\pi} \int_0^\infty \int_0^\infty \frac{x\,\mathrm{d}x\,\mathrm{d}y}{x^2 + y^2 + 1} \frac{y^{2n}}{[(x^2 + y^2 + 1)^2 - \delta^2 (x^2 + y^2)^2]^n}. \tag{C.32}$$

arriving at Eq. 4.29. A comparison between the first four orders of C_n is presented in Fig. C.1.

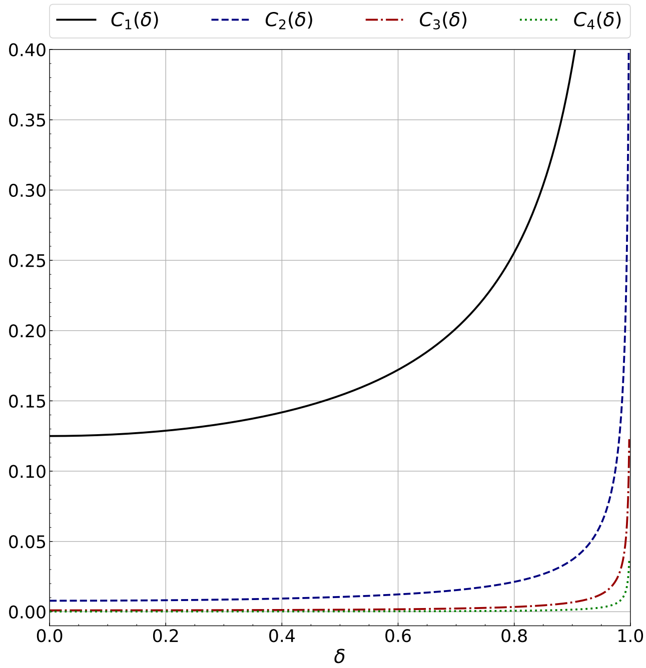

Figure C.1: Coefficients values (defined in Eq. 4.30) for the first four orders. To compare $C_1(0.9) \simeq 0.39$, $C_2(0.9) \simeq 0.037$, $C_3(0.9) \simeq 0.0067$ and $C_4(0.9) \simeq 0.0016$.

Appendix D

Intraband Fluctuations

The calculation of the intraband fluctuations follow the same lines as the interband case. We can identify the interaction term as

$$\mathbf{\Delta}(q) = \begin{bmatrix} 0 & 0 & \Delta_q & 0 \\ 0 & 0 & 0 & 0 \\ \bar{\Delta}_{-q} & 0 & 0 & 0 \\ 0 & 0 & 0 & 0 \end{bmatrix} = \frac{1}{2}\begin{bmatrix} 0 & (\mathbb{1}_2+\sigma_3)\Delta_q \\ (\mathbb{1}_2+\sigma_3)\bar{\Delta}_{-q} & 0 \end{bmatrix} \tag{D.1}$$

with the unitary transformation

$$\mathbf{U}_{\mathbf{k}} = \begin{bmatrix} \exp(i\sigma_1\phi_{\mathbf{k}}) & 0 \\ 0 & \exp(i\sigma_1\phi_{\mathbf{k}}) \end{bmatrix} \tag{D.2}$$

so that

$$\tilde{\mathbf{\Delta}}(k,2q) \equiv \mathbf{U}^{\dagger}_{\mathbf{k+q}}\mathbf{\Delta}(2q)\mathbf{U}_{\mathbf{k-q}} = \frac{1}{2}\begin{bmatrix} 0 & \Delta_q W_{2\mathbf{q}} \\ \bar{\Delta}_{-q}W_{2\mathbf{q}} & 0 \end{bmatrix} \tag{D.3}$$

where we defined

$$W_{2\mathbf{q}} \equiv \exp(-i\sigma_1\phi_{\mathbf{k+q}})(\mathbb{1}_2+\sigma_3)\exp(i\sigma_1\phi_{\mathbf{k-q}}); \tag{D.4}$$

knowing that (from the interband section)

$$\exp(-i\sigma_1\phi_{\mathbf{k+q}})\sigma_3\exp(i\sigma_1\phi_{\mathbf{k-q}}) = \sigma_3\cos(\phi_{\mathbf{k+q}}+\phi_{\mathbf{k-q}}) - \sigma_2\sin(\phi_{\mathbf{k+q}}+\phi_{\mathbf{k-q}}) \tag{D.5}$$

and

$$\exp(-i\sigma_1\phi_{\mathbf{k+q}})\mathbb{1}_2\exp(i\sigma_1\phi_{\mathbf{k-q}}) = \mathbb{1}_2\cos(\phi_{\mathbf{k+q}}-\phi_{\mathbf{k-q}}) - i\sigma_1\sin(\phi_{\mathbf{k+q}}-\phi_{\mathbf{k-q}}) \tag{D.6}$$

we get

$$W_{2\mathbf{q}} = \begin{bmatrix} C^{+}_{\mathbf{q}} & -iS^{-}_{\mathbf{q}} \\ -iS^{+}_{\mathbf{q}} & C^{-}_{\mathbf{q}} \end{bmatrix}, \tag{D.7}$$

where

$$S^{\pm}_{\mathbf{q}} \equiv \sin(\phi_{\mathbf{k+q}} - \phi_{\mathbf{k-q}}) \pm \sin(\phi_{\mathbf{k+q}} + \phi_{\mathbf{k-q}}), \tag{D.8}$$

$$C^{\pm}_{\mathbf{q}} \equiv \cos(\phi_{\mathbf{k+q}} - \phi_{\mathbf{k-q}}) \pm \cos(\phi_{\mathbf{k+q}} + \phi_{\mathbf{k-q}}) \tag{D.9}$$

Recalling the rotated free propagator

$$\tilde{\mathbf{G}}_0(k) = \begin{bmatrix} G^-_k & 0 & 0 & 0 \\ 0 & G^+_k & 0 & 0 \\ 0 & 0 & -G^-_{-k} & 0 \\ 0 & 0 & 0 & -G^+_{-k} \end{bmatrix}, \tag{D.10}$$

the product then holds

$$\tilde{\mathbf{G}}_0(k-q)\tilde{\mathbf{\Delta}}(k,2q) = \frac{1}{2}\begin{bmatrix} 0 & \Delta_q Y_{k-q} \\ -\bar{\Delta}_{-q} Y_{-k+q} & 0 \end{bmatrix} \tag{D.11}$$

with

$$Y_{\pm(k-q)} = \begin{bmatrix} G^-_{\pm(k-q)} C^+_{\mathbf{q}} & -iG^-_{\pm(k-q)} S^-_{\mathbf{q}} \\ -iG^+_{\pm(k-q)} S^+_{\mathbf{q}} & G^+_{\pm(k-q)} C^-_{\mathbf{q}} \end{bmatrix}, \tag{D.12}$$

so that $\mathrm{tr}(\mathbf{G}_0\mathbf{\Delta})^2 = \mathrm{tr}[\tilde{\mathbf{G}}_0(k-q)\tilde{\mathbf{\Delta}}(k,2q)\tilde{\mathbf{G}}_0(k+q)\tilde{\mathbf{\Delta}}(k,-2q)]$ becomes

$$\mathrm{tr}(\mathbf{G}_0\mathbf{\Delta})^2 = \frac{1}{4}\mathrm{tr}\begin{bmatrix} -|\Delta_q|^2 \mathrm{tr}(Y_{k-q}Y_{-k-q}) & 0 \\ 0 & -|\Delta_{-q}|^2 \mathrm{tr}(Y_{-k+q}Y_{k+q}) \end{bmatrix} \tag{D.13}$$

with

$$\begin{aligned} \mathrm{tr}[Y_{\pm(k-q)}Y_{\mp(k+q)}] = {} & G^-_{\pm(k-q)}G^-_{\mp(k+q)}(C^+_{\mathbf{q}})^2 + G^+_{\pm(k-q)}G^+_{\mp(k+q)}(C^-_{\mathbf{q}})^2 \\ & + G^-_{\pm(k-q)}G^+_{\mp(k+q)}(S^-_{\mathbf{q}})^2 + G^+_{\pm(k-q)}G^-_{\mp(k+q)}(S^+_{\mathbf{q}})^2 \end{aligned} \tag{D.14}$$

thus we may write

$$\begin{aligned} \sum_{k,q} \mathrm{tr}(\mathbf{G}_0\mathbf{\Delta})^2 = {} & -\frac{1}{2\beta}\sum_{k,q}\left[G^-_{k-q}G^-_{-k-q}(C^+_{\mathbf{q}})^2 + G^+_{k-q}G^+_{-k-q}(C^-_{\mathbf{q}})^2\right]|\Delta_{2q}|^2 \\ & -\frac{1}{2\beta}\sum_{k,q}\left[G^-_{k-q}G^+_{-k-q}(S^-_{\mathbf{q}})^2 + G^+_{k-q}G^-_{-k-q}(S^+_{\mathbf{q}})^2\right]|\Delta_{2q}|^2. \end{aligned} \tag{D.15}$$

Recalling the odd frequencies sum

$$\frac{1}{\beta}\sum_{\omega_n} G^{\pm}_{k-q}G^{\pm}_{-k-q} = \frac{1 - \eta_F(\xi^{\pm}_{\mathbf{k-q}}) - \eta_F(\xi^{\pm}_{\mathbf{k+q}})}{2i\omega_m + \xi^{\pm}_{\mathbf{k-q}} + \xi^{\pm}_{\mathbf{k+q}}}, \tag{D.16}$$

we can write the second order action as

$$S^{(2)}[\Delta] = \sum_q \left[\frac{|\Delta_q|^2}{g_2} + \frac{1}{2}\mathrm{tr}(\mathbf{G}_0\mathbf{\Delta})^2\right] \equiv \sum_q \Gamma^{-1}_q |\Delta_q|^2, \tag{D.17}$$

where the intraband vertex function is given by

$$\begin{aligned} \Gamma^{-1}_{2q} = {} & \frac{1}{g_2} - \frac{1}{4}\sum_{\mathbf{k}}\left[\frac{1 - \eta_F(\xi^-_{\mathbf{k-q}}) - \eta_F(\xi^-_{\mathbf{k+q}})}{2i\omega_m + \xi^-_{\mathbf{k-q}} + \xi^-_{\mathbf{k+q}}}(C^+_{\mathbf{q}})^2 + \frac{1 - \eta_F(\xi^+_{\mathbf{k-q}}) - \eta_F(\xi^+_{\mathbf{k+q}})}{2i\omega_m + \xi^+_{\mathbf{k-q}} + \xi^+_{\mathbf{k+q}}}(C^-_{\mathbf{q}})^2\right] \\ & - \frac{1}{4}\sum_{\mathbf{k}}\left[\frac{1 - \eta_F(\xi^-_{\mathbf{k-q}}) - \eta_F(\xi^+_{\mathbf{k+q}})}{2i\omega_m + \xi^-_{\mathbf{k-q}} + \xi^+_{\mathbf{k+q}}}(S^-_{\mathbf{q}})^2 + \frac{1 - \eta_F(\xi^+_{\mathbf{k-q}}) - \eta_F(\xi^-_{\mathbf{k+q}})}{2i\omega_m + \xi^+_{\mathbf{k-q}} + \xi^-_{\mathbf{k+q}}}(S^+_{\mathbf{q}})^2\right]. \end{aligned} \tag{D.18}$$

D.1 Strong Coupling Limit Expansions

Performing a power series expansion for $(\omega_m, \mathbf{q}) \ll k_F$ up to quadratic order results in

$$\cos(\phi_{\mathbf{k+q}} - \phi_{\mathbf{k-q}}) = \cos(2q_i\partial_i\phi_{\mathbf{k}}) = 1 - 2q_iq_j\partial_i\phi_{\mathbf{k}}\partial_j\phi_{\mathbf{k}}, \tag{D.19}$$

$$\cos(\phi_{\mathbf{k+q}} + \phi_{\mathbf{k-q}}) = \cos(2\phi_{\mathbf{k}} + q_iq_j\partial_i\partial_j\phi_{\mathbf{k}}) = \cos(2\phi_{\mathbf{k}}) - \sin(2\phi_{\mathbf{k}})q_iq_j\partial_i\partial_j\phi_{\mathbf{k}}, \tag{D.20}$$

so that

$$\begin{aligned}(C_{\mathbf{q}}^{+})^2 &= [1 + \cos(2\phi_{\mathbf{k}}) - q_iq_j(2\partial_i\phi_{\mathbf{k}}\partial_j\phi_{\mathbf{k}} + \sin(2\phi_{\mathbf{k}})\partial_i\partial_j\phi_{\mathbf{k}})]^2 \\ &= [1 + \cos(2\phi_{\mathbf{k}})]^2 - 2q_iq_j[1 + \cos(2\phi_{\mathbf{k}})](2\partial_i\phi_{\mathbf{k}}\partial_j\phi_{\mathbf{k}} + \sin(2\phi_{\mathbf{k}})\partial_i\partial_j\phi_{\mathbf{k}})\end{aligned} \tag{D.21}$$

and

$$\begin{aligned}(C_{\mathbf{q}}^{-})^2 &= [1 - \cos(2\phi_{\mathbf{k}}) - q_iq_j(2\partial_i\phi_{\mathbf{k}}\partial_j\phi_{\mathbf{k}} - \sin(2\phi_{\mathbf{k}})\partial_i\partial_j\phi_{\mathbf{k}})]^2 \\ &= [1 - \cos(2\phi_{\mathbf{k}})]^2 - 2q_iq_j[1 - \cos(2\phi_{\mathbf{k}})](2\partial_i\phi_{\mathbf{k}}\partial_j\phi_{\mathbf{k}} - \sin(2\phi_{\mathbf{k}})\partial_i\partial_j\phi_{\mathbf{k}}).\end{aligned} \tag{D.22}$$

The other terms are

$$\sin(\phi_{\mathbf{k+q}} - \phi_{\mathbf{k-q}}) = \sin(2q_i\partial_i\phi_{\mathbf{k}}) = 2q_i\partial_i\phi_{\mathbf{k}}, \tag{D.23}$$

$$\sin(\phi_{\mathbf{k+q}} + \phi_{\mathbf{k-q}}) = \sin(2\phi_{\mathbf{k}} + q_iq_j\partial_i\partial_j\phi_{\mathbf{k}}) = \sin(2\phi_{\mathbf{k}}) + \cos(2\phi_{\mathbf{k}})q_iq_j\partial_i\partial_j\phi_{\mathbf{k}}, \tag{D.24}$$

so

$$\begin{aligned}(S_{\mathbf{q}}^{+})^2 &= [2q_i\partial_i\phi_{\mathbf{k}} + \sin(2\phi_{\mathbf{k}}) + \cos(2\phi_{\mathbf{k}})q_iq_j\partial_i\partial_j\phi_{\mathbf{k}}]^2 \\ &= [2q_i\partial_i\phi_{\mathbf{k}} + \sin(2\phi_{\mathbf{k}})]^2 + 2q_iq_j\sin(2\phi_{\mathbf{k}})\cos(2\phi_{\mathbf{k}})\partial_i\partial_j\phi_{\mathbf{k}} \\ &= \sin^2(2\phi_{\mathbf{k}}) + 4q_i\partial_i\phi_{\mathbf{k}}\sin(2\phi_{\mathbf{k}}) + 2q_iq_j\left[2\partial_i\phi_{\mathbf{k}}\partial_j\phi_{\mathbf{k}} + \sin(2\phi_{\mathbf{k}})\cos(2\phi_{\mathbf{k}})\partial_i\partial_j\phi_{\mathbf{k}}\right]\end{aligned} \tag{D.25}$$

and

$$\begin{aligned}(S_{\mathbf{q}}^{-})^2 &= [2q_i\partial_i\phi_{\mathbf{k}} - \sin(2\phi_{\mathbf{k}}) - \cos(2\phi_{\mathbf{k}})q_iq_j\partial_i\partial_j\phi_{\mathbf{k}}]^2 \\ &= [2q_i\partial_i\phi_{\mathbf{k}} - \sin(2\phi_{\mathbf{k}})]^2 + 2q_iq_j\sin(2\phi_{\mathbf{k}})\cos(2\phi_{\mathbf{k}})\partial_i\partial_j\phi_{\mathbf{k}} \\ &= \sin^2(2\phi_{\mathbf{k}}) - 4q_i\partial_i\phi_{\mathbf{k}}\sin(2\phi_{\mathbf{k}}) + 2q_iq_j\left[2\partial_i\phi_{\mathbf{k}}\partial_j\phi_{\mathbf{k}} + \sin(2\phi_{\mathbf{k}})\cos(2\phi_{\mathbf{k}})\partial_i\partial_j\phi_{\mathbf{k}}\right].\end{aligned} \tag{D.26}$$

Expanding the denominators

$$\begin{aligned}\frac{1}{2i\omega_m + \xi_{\mathbf{k+q}}^{\pm} + \xi_{\mathbf{k-q}}^{\pm}} &= \frac{1}{2\xi_{\mathbf{k}}^{\pm}}\left(1 - \frac{2i\omega_m + \frac{\mathbf{q}^2}{m} \pm q_iq_j\partial_i\partial_j\Lambda_{\mathbf{k}}}{2\xi_{\mathbf{k}}^{\pm}}\right), \\ \frac{1}{2i\omega_m + \xi_{\mathbf{k+q}}^{+} + \xi_{\mathbf{k-q}}^{-}} &= \frac{1}{2\xi_{\mathbf{k}}}\left(1 - \frac{i\omega_m + \frac{\mathbf{q}^2}{2m} + q_i\partial_i\Lambda_{\mathbf{k}}}{\xi_{\mathbf{k}}} + \frac{q_iq_j\partial_i\Lambda_{\mathbf{k}}\partial_j\Lambda_{\mathbf{k}}}{\xi_{\mathbf{k}}^2}\right), \\ \frac{1}{2i\omega_m + \xi_{\mathbf{k+q}}^{-} + \xi_{\mathbf{k-q}}^{+}} &= \frac{1}{2\xi_{\mathbf{k}}}\left(1 - \frac{i\omega_m + \frac{\mathbf{q}^2}{2m} - q_i\partial_i\Lambda_{\mathbf{k}}}{\xi_{\mathbf{k}}} + \frac{q_iq_j\partial_i\Lambda_{\mathbf{k}}\partial_j\Lambda_{\mathbf{k}}}{\xi_{\mathbf{k}}^2}\right).\end{aligned} \tag{D.27}$$

Dismissing the Fermi distributions we have

$$\begin{aligned}\frac{(C^+_{\mathbf{q}})^2}{2i\omega_m+\xi^-_{\mathbf{k}-\mathbf{q}}+\xi^-_{\mathbf{k}+\mathbf{q}}} &= -[1+\cos(2\phi_{\mathbf{k}})]^2\frac{2i\omega_m+\frac{\mathbf{q}^2}{m}-q_iq_j\partial_i\partial_j\Lambda_{\mathbf{k}}}{(2\xi^-_{\mathbf{k}})^2}\\&+\frac{[1+\cos(2\phi_{\mathbf{k}})]^2-2q_iq_j[1+\cos(2\phi_{\mathbf{k}})](2\partial_i\phi_{\mathbf{k}}\partial_j\phi_{\mathbf{k}}+\sin(2\phi_{\mathbf{k}})\partial_i\partial_j\phi_{\mathbf{k}})}{2\xi^-_{\mathbf{k}}},\end{aligned} \tag{D.28}$$

$$\begin{aligned}\frac{(C^-_{\mathbf{q}})^2}{2i\omega_m+\xi^+_{\mathbf{k}-\mathbf{q}}+\xi^+_{\mathbf{k}+\mathbf{q}}} &= -[1-\cos(2\phi_{\mathbf{k}})]^2\frac{2i\omega_m+\frac{\mathbf{q}^2}{m}+q_iq_j\partial_i\partial_j\Lambda_{\mathbf{k}}}{(2\xi^+_{\mathbf{k}})^2}\\&+\frac{[1-\cos(2\phi_{\mathbf{k}})]^2-2q_iq_j[1-\cos(2\phi_{\mathbf{k}})](2\partial_i\phi_{\mathbf{k}}\partial_j\phi_{\mathbf{k}}-\sin(2\phi_{\mathbf{k}})\partial_i\partial_j\phi_{\mathbf{k}})}{2\xi^+_{\mathbf{k}}},\end{aligned} \tag{D.29}$$

$$\begin{aligned}\frac{(S^-_{\mathbf{q}})^2}{2i\omega_m+\xi^-_{\mathbf{k}-\mathbf{q}}+\xi^+_{\mathbf{k}+\mathbf{q}}} &= -\frac{\sin^2(2\phi_{\mathbf{k}})}{2\xi_{\mathbf{k}}}\left(\frac{i\omega_m+\frac{\mathbf{q}^2}{2m}-q_i\partial_i\Lambda_{\mathbf{k}}}{\xi_{\mathbf{k}}}-\frac{q_iq_j\partial_i\Lambda_{\mathbf{k}}\partial_j\Lambda_{\mathbf{k}}}{\xi^2_{\mathbf{k}}}\right)\\&+\frac{\sin^2(2\phi_{\mathbf{k}})-4q_i\partial_i\phi_{\mathbf{k}}\sin(2\phi_{\mathbf{k}})+2q_iq_j\left[2\partial_i\phi_{\mathbf{k}}\partial_j\phi_{\mathbf{k}}+\sin(2\phi_{\mathbf{k}})\cos(2\phi_{\mathbf{k}})\partial_i\partial_j\phi_{\mathbf{k}}\right]}{2\xi_{\mathbf{k}}}\\&-\frac{2\sin(2\phi_{\mathbf{k}})}{\xi^2_{\mathbf{k}}}q_iq_j\partial_i\phi_{\mathbf{k}}\partial_j\Lambda_{\mathbf{k}},\end{aligned} \tag{D.30}$$

$$\begin{aligned}\frac{(S^+_{\mathbf{q}})^2}{2i\omega_m+\xi^+_{\mathbf{k}-\mathbf{q}}+\xi^-_{\mathbf{k}+\mathbf{q}}} &= -\frac{\sin^2(2\phi_{\mathbf{k}})}{2\xi_{\mathbf{k}}}\left(\frac{i\omega_m+\frac{\mathbf{q}^2}{2m}+q_i\partial_i\Lambda_{\mathbf{k}}}{\xi_{\mathbf{k}}}-\frac{q_iq_j\partial_i\Lambda_{\mathbf{k}}\partial_j\Lambda_{\mathbf{k}}}{\xi^2_{\mathbf{k}}}\right)\\&+\frac{\sin^2(2\phi_{\mathbf{k}})+4q_i\partial_i\phi_{\mathbf{k}}\sin(2\phi_{\mathbf{k}})+2q_iq_j\left[2\partial_i\phi_{\mathbf{k}}\partial_j\phi_{\mathbf{k}}+\sin(2\phi_{\mathbf{k}})\cos(2\phi_{\mathbf{k}})\partial_i\partial_j\phi_{\mathbf{k}}\right]}{2\xi_{\mathbf{k}}}\\&-\frac{2\sin(2\phi_{\mathbf{k}})}{\xi^2_{\mathbf{k}}}q_iq_j\partial_i\phi_{\mathbf{k}}\partial_j\Lambda_{\mathbf{k}},\end{aligned} \tag{D.31}$$

and the linear term vanishes in the sum

$$\begin{aligned}\frac{(S^-_{\mathbf{q}})^2}{2i\omega_m+\xi^-_{\mathbf{k}-\mathbf{q}}+\xi^+_{\mathbf{k}+\mathbf{q}}}+\frac{(S^+_{\mathbf{q}})^2}{2i\omega_m+\xi^+_{\mathbf{k}-\mathbf{q}}+\xi^-_{\mathbf{k}+\mathbf{q}}} &= \frac{\sin^2(2\phi_{\mathbf{k}})}{\xi_{\mathbf{k}}}\left(1-\frac{i\omega_m+\frac{\mathbf{q}^2}{2m}}{\xi_{\mathbf{k}}}\right)\\&+\frac{2q_iq_j\sin(2\phi_{\mathbf{k}})\cos(2\phi_{\mathbf{k}})\partial_i\partial_j\phi_{\mathbf{k}}}{\xi_{\mathbf{k}}}+\frac{1}{\xi_{\mathbf{k}}}\left[2q_i\partial_i\phi_{\mathbf{k}}-\frac{q_i\sin(2\phi_{\mathbf{k}})\partial_i\Lambda_{\mathbf{k}}}{\xi_{\mathbf{k}}}\right]^2\end{aligned} \tag{D.32}$$

D.1.1 Intraband Vertex Function

Thus the order zero term of the vertex function is

$$
\begin{aligned}
\Gamma_0^{-1} &= \frac{1}{g_2} - \frac{1}{4}\sum_{\mathbf{k}}\left[\frac{[1+\cos(2\phi_{\mathbf{k}})]^2}{2\xi_{\mathbf{k}}^-} + \frac{[1-\cos(2\phi_{\mathbf{k}})]^2}{2\xi_{\mathbf{k}}^+} + \frac{\sin^2(2\phi_{\mathbf{k}})}{\xi_{\mathbf{k}}}\right] \\
&= \frac{1}{g_2} - \frac{1}{4}\sum_{\mathbf{k}}\left[\frac{1}{2}\frac{\xi_{\mathbf{k}}^+[1+2\cos(2\phi_{\mathbf{k}})+\cos^2(2\phi_{\mathbf{k}})] + \xi_{\mathbf{k}}^-[1-2\cos(2\phi_{\mathbf{k}})+\cos^2(2\phi_{\mathbf{k}})]}{\xi_{\mathbf{k}}^-\xi_{\mathbf{k}}^+} + \frac{\sin^2(2\phi_{\mathbf{k}})}{\xi_{\mathbf{k}}}\right] \\
&= \frac{1}{g_2} - \frac{1}{4}\sum_{\mathbf{k}}\left[\frac{1}{2}\frac{2\xi_{\mathbf{k}}[1+\cos^2(2\phi_{\mathbf{k}})] + 4\Lambda_{\mathbf{k}}\cos(2\phi_{\mathbf{k}})}{\xi_{\mathbf{k}}^2-\Lambda_{\mathbf{k}}^2} + \frac{\sin^2(2\phi_{\mathbf{k}})}{\xi_{\mathbf{k}}}\right] \\
&= \frac{1}{g_2} - \frac{1}{4}\sum_{\mathbf{k}}\left[\frac{2\delta\epsilon_{\mathbf{k}}}{\xi_{\mathbf{k}}^2-\Lambda_{\mathbf{k}}^2} + \frac{\xi_{\mathbf{k}}^2[1+\cos^2(2\phi_{\mathbf{k}})] + (\xi_{\mathbf{k}}^2-\Lambda_{\mathbf{k}}^2)\sin^2(2\phi_{\mathbf{k}})}{\xi_{\mathbf{k}}(\xi_{\mathbf{k}}^2-\Lambda_{\mathbf{k}}^2)}\right] \\
&= \frac{1}{g_2} - \frac{1}{4}\sum_{\mathbf{k}}\left[\frac{\xi_{\mathbf{k}}+2\delta\epsilon_{\mathbf{k}}}{\xi_{\mathbf{k}}^2-\Lambda_{\mathbf{k}}^2} + \frac{1}{\xi_{\mathbf{k}}}\frac{\xi_{\mathbf{k}}^2-V_{\mathbf{k}}^2}{\xi_{\mathbf{k}}^2-\Lambda_{\mathbf{k}}^2}\right] \\
&= \frac{1}{g_2} - \frac{1}{4}\sum_{\mathbf{k}}\frac{1}{\xi_{\mathbf{k}}}\left[1 + \frac{(\xi_{\mathbf{k}}+\delta\epsilon_{\mathbf{k}})^2}{\xi_{\mathbf{k}}^2-\Lambda_{\mathbf{k}}^2}\right],
\end{aligned}
\tag{D.33}
$$

with $g_2^{-1} = -m_A/(4\pi a_s) + \sum_{\mathbf{k}}[2(1-\delta)\epsilon_{\mathbf{k}}]^{-1}$.

The propagator term is $\Gamma^{-1}_{(2\mathbf{q})^2} = (\mathbf{q}^2/m + 2i\omega_m)\sum_{\mathbf{k}} J_{\mathbf{k}}$, where

$$
\begin{aligned}
-J_{\mathbf{k}} &= -\frac{[1+\cos(2\phi_{\mathbf{k}})]^2}{(2\xi_{\mathbf{k}}^-)^2} - \frac{[1-\cos(2\phi_{\mathbf{k}})]^2}{(2\xi_{\mathbf{k}}^+)^2} - \frac{\sin^2(2\phi_{\mathbf{k}})}{2\xi_{\mathbf{k}}^2} \\
&= -\frac{1}{4}\frac{\xi_{\mathbf{k}}^{+2}[1+2\cos(2\phi_{\mathbf{k}})+\cos^2(2\phi_{\mathbf{k}})] + \xi_{\mathbf{k}}^{-2}[1-2\cos(2\phi_{\mathbf{k}})+\cos^2(2\phi_{\mathbf{k}})]}{(\xi_{\mathbf{k}}^-\xi_{\mathbf{k}}^+)^2} - \frac{\sin^2(2\phi_{\mathbf{k}})}{2\xi_{\mathbf{k}}^2} \\
&= -\frac{1}{4}\frac{(\xi_{\mathbf{k}}^{+2}+\xi_{\mathbf{k}}^{-2})[1+\cos^2(2\phi_{\mathbf{k}})] + 2(\xi_{\mathbf{k}}^{+2}-\xi_{\mathbf{k}}^{-2})\cos(2\phi_{\mathbf{k}})}{(\xi_{\mathbf{k}}^-\xi_{\mathbf{k}}^+)^2} - \frac{\sin^2(2\phi_{\mathbf{k}})}{2\xi_{\mathbf{k}}^2} \\
&= -\frac{1}{4}\frac{2(\xi_{\mathbf{k}}^2+\Lambda_{\mathbf{k}}^2)[1+\cos^2(2\phi_{\mathbf{k}})] + 8(\xi_{\mathbf{k}}\Lambda_{\mathbf{k}})\cos(2\phi_{\mathbf{k}})}{(\xi_{\mathbf{k}}^2-\Lambda_{\mathbf{k}}^2)^2} - \frac{\sin^2(2\phi_{\mathbf{k}})}{2\xi_{\mathbf{k}}^2} \\
&= -\frac{2\xi_{\mathbf{k}}\delta\epsilon_{\mathbf{k}}}{(\xi_{\mathbf{k}}^2-\Lambda_{\mathbf{k}}^2)^2} - \frac{1}{2}\frac{\xi_{\mathbf{k}}^2(\xi_{\mathbf{k}}^2+\Lambda_{\mathbf{k}}^2)[1+\cos^2(2\phi_{\mathbf{k}})] + (\xi_{\mathbf{k}}^4-2\xi_{\mathbf{k}}^2\Lambda_{\mathbf{k}}^2+\Lambda_{\mathbf{k}}^4)\sin^2(2\phi_{\mathbf{k}})}{\xi_{\mathbf{k}}^2(\xi_{\mathbf{k}}^2-\Lambda_{\mathbf{k}}^2)^2} \\
&= -\frac{2\xi_{\mathbf{k}}\delta\epsilon_{\mathbf{k}}}{(\xi_{\mathbf{k}}^2-\Lambda_{\mathbf{k}}^2)^2} - \frac{1}{2}\frac{\xi_{\mathbf{k}}^2}{(\xi_{\mathbf{k}}^2-\Lambda_{\mathbf{k}}^2)^2} - \frac{1}{2}\frac{\xi_{\mathbf{k}}^2(\xi_{\mathbf{k}}^2+\Lambda_{\mathbf{k}}^2) + \xi_{\mathbf{k}}^2\Lambda_{\mathbf{k}}^2\cos^2(2\phi_{\mathbf{k}}) + \Lambda_{\mathbf{k}}^2(-2\xi_{\mathbf{k}}^2+\Lambda_{\mathbf{k}}^2)\sin^2(2\phi_{\mathbf{k}})}{\xi_{\mathbf{k}}^2(\xi_{\mathbf{k}}^2-\Lambda_{\mathbf{k}}^2)^2} \\
&= -\frac{2\xi_{\mathbf{k}}\delta\epsilon_{\mathbf{k}}}{(\xi_{\mathbf{k}}^2-\Lambda_{\mathbf{k}}^2)^2} - \frac{1}{2}\frac{\xi_{\mathbf{k}}^2}{(\xi_{\mathbf{k}}^2-\Lambda_{\mathbf{k}}^2)^2} - \frac{1}{2}\frac{\xi_{\mathbf{k}}^2(\xi_{\mathbf{k}}^2+\Lambda_{\mathbf{k}}^2) + \xi_{\mathbf{k}}^2(\delta\epsilon_{\mathbf{k}})^2 + V_{\mathbf{k}}^2(-2\xi_{\mathbf{k}}^2+\Lambda_{\mathbf{k}}^2)}{\xi_{\mathbf{k}}^2(\xi_{\mathbf{k}}^2-\Lambda_{\mathbf{k}}^2)^2} \\
&= -\frac{2\xi_{\mathbf{k}}\delta\epsilon_{\mathbf{k}}}{(\xi_{\mathbf{k}}^2-\Lambda_{\mathbf{k}}^2)^2} - \frac{1}{2}\frac{\xi_{\mathbf{k}}^2}{(\xi_{\mathbf{k}}^2-\Lambda_{\mathbf{k}}^2)^2} - \frac{1}{2}\frac{\xi_{\mathbf{k}}^2 + 2(\delta\epsilon_{\mathbf{k}})^2 - V_{\mathbf{k}}^2}{(\xi_{\mathbf{k}}^2-\Lambda_{\mathbf{k}}^2)^2} - \frac{1}{2}\frac{V_{\mathbf{k}}^2\Lambda_{\mathbf{k}}^2}{\xi_{\mathbf{k}}^2(\xi_{\mathbf{k}}^2-\Lambda_{\mathbf{k}}^2)^2} \\
&= -\frac{(\xi_{\mathbf{k}}+\delta\epsilon_{\mathbf{k}})^2}{(\xi_{\mathbf{k}}^2-\Lambda_{\mathbf{k}}^2)^2} - \frac{1}{2}\frac{V_{\mathbf{k}}^2(\Lambda_{\mathbf{k}}^2-\xi_{\mathbf{k}}^2)}{\xi_{\mathbf{k}}^2(\xi_{\mathbf{k}}^2-\Lambda_{\mathbf{k}}^2)^2} \\
&= -\frac{(\xi_{\mathbf{k}}+\delta\epsilon_{\mathbf{k}})^2}{(\xi_{\mathbf{k}}^2-\Lambda_{\mathbf{k}}^2)^2} + \frac{1}{2}\frac{V_{\mathbf{k}}^2}{\xi_{\mathbf{k}}^2(\xi_{\mathbf{k}}^2-\Lambda_{\mathbf{k}}^2)}.
\end{aligned}
\tag{D.34}
$$

The crossed term is $\sum_{i,j} \Gamma^{-1}_{4q_iq_j} = \sum_{i,j} q_i q_j \sum_{\mathbf{k}} K_{\mathbf{k}}$, with

$$\begin{aligned}
-K_{\mathbf{k}} = &-\frac{2[1+\cos(2\phi_{\mathbf{k}})](2\partial_i\phi_{\mathbf{k}}\partial_j\phi_{\mathbf{k}} + \sin(2\phi_{\mathbf{k}})\partial_i\partial_j\phi_{\mathbf{k}})}{2\xi^-_{\mathbf{k}}} + [1+\cos(2\phi_{\mathbf{k}})]^2 \frac{\partial_i\partial_j\Lambda_{\mathbf{k}}}{(2\xi^-_{\mathbf{k}})^2} \\
&- \frac{2[1-\cos(2\phi_{\mathbf{k}})](2\partial_i\phi_{\mathbf{k}}\partial_j\phi_{\mathbf{k}} - \sin(2\phi_{\mathbf{k}})\partial_i\partial_j\phi_{\mathbf{k}})}{2\xi^+_{\mathbf{k}}} - [1-\cos(2\phi_{\mathbf{k}})]^2 \frac{\partial_i\partial_j\Lambda_{\mathbf{k}}}{(2\xi^+_{\mathbf{k}})^2} \\
&+ \frac{2\sin(2\phi_{\mathbf{k}})\cos(2\phi_{\mathbf{k}})\partial_i\partial_j\phi_{\mathbf{k}}}{\xi_{\mathbf{k}}} + \frac{1}{\xi_{\mathbf{k}}}\left[2\partial_i\phi_{\mathbf{k}} - \frac{\sin(2\phi_{\mathbf{k}})\partial_i\Lambda_{\mathbf{k}}}{\xi_{\mathbf{k}}}\right]^2 \\
&\equiv A_{\mathbf{k}}\partial_i\phi_{\mathbf{k}}\partial_j\phi_{\mathbf{k}} + B_{\mathbf{k}}\partial_i\partial_j\phi_{\mathbf{k}} + C_{\mathbf{k}}\partial_i\partial_j\Lambda_{\mathbf{k}} + \frac{1}{\xi^3_{\mathbf{k}}}\frac{V^2_{\mathbf{k}}}{\Lambda^2_{\mathbf{k}}}\partial_i\Lambda_{\mathbf{k}}\partial_j\Lambda_{\mathbf{k}} - \frac{4}{\xi^2_{\mathbf{k}}}\frac{V_{\mathbf{k}}}{\Lambda_{\mathbf{k}}}\partial_i\phi_{\mathbf{k}}\partial_j\Lambda_{\mathbf{k}},
\end{aligned} \tag{D.35}$$

where the coefficients are

$$\begin{aligned}
A_{\mathbf{k}} &= \frac{4}{\xi_{\mathbf{k}}} - \frac{2[1+\cos(2\phi_{\mathbf{k}})]}{\xi^-_{\mathbf{k}}} - \frac{2[1-\cos(2\phi_{\mathbf{k}})]}{\xi^+_{\mathbf{k}}} \\
&= \frac{4}{\xi_{\mathbf{k}}} - 2\frac{\xi^+_{\mathbf{k}}[1+\cos(2\phi_{\mathbf{k}})] + \xi^-_{\mathbf{k}}[1-\cos(2\phi_{\mathbf{k}})]}{\xi^-_{\mathbf{k}}\xi^+_{\mathbf{k}}} \\
&= \frac{4}{\xi_{\mathbf{k}}} - 2\frac{2\xi_{\mathbf{k}} + 2\Lambda_{\mathbf{k}}\cos(2\phi_{\mathbf{k}})}{\xi^2_{\mathbf{k}} - \Lambda^2_{\mathbf{k}}} \\
&= \frac{4}{\xi_{\mathbf{k}}} - 4\frac{\xi_{\mathbf{k}} + \delta\epsilon_{\mathbf{k}}}{\xi^2_{\mathbf{k}} - \Lambda^2_{\mathbf{k}}} \\
&= -\frac{4}{\xi_{\mathbf{k}}}\frac{\Lambda^2_{\mathbf{k}} + \xi_{\mathbf{k}}\delta\epsilon_{\mathbf{k}}}{\xi^2_{\mathbf{k}} - \Lambda^2_{\mathbf{k}}};
\end{aligned} \tag{D.36}$$

$$\begin{aligned}
B_{\mathbf{k}} &= -\frac{[1+\cos(2\phi_{\mathbf{k}})]\sin(2\phi_{\mathbf{k}})}{\xi^-_{\mathbf{k}}} + \frac{[1-\cos(2\phi_{\mathbf{k}})]\sin(2\phi_{\mathbf{k}})}{\xi^+_{\mathbf{k}}} + \frac{2\sin(2\phi_{\mathbf{k}})\cos(2\phi_{\mathbf{k}})}{\xi_{\mathbf{k}}} \\
&= \sin(2\phi_{\mathbf{k}})\frac{\xi^-_{\mathbf{k}}[1-\cos(2\phi_{\mathbf{k}})] - \xi^+_{\mathbf{k}}[1+\cos(2\phi_{\mathbf{k}})]}{\xi^-_{\mathbf{k}}\xi^+_{\mathbf{k}}} + \frac{2\sin(2\phi_{\mathbf{k}})\cos(2\phi_{\mathbf{k}})}{\xi_{\mathbf{k}}} \\
&= \sin(2\phi_{\mathbf{k}})\frac{-2\Lambda_{\mathbf{k}} - 2\xi_{\mathbf{k}}\cos(2\phi_{\mathbf{k}})}{\xi^2_{\mathbf{k}} - \Lambda^2_{\mathbf{k}}} + \frac{2\sin(2\phi_{\mathbf{k}})\cos(2\phi_{\mathbf{k}})}{\xi_{\mathbf{k}}} \\
&= -\frac{2V_{\mathbf{k}}}{\xi^2_{\mathbf{k}} - \Lambda^2_{\mathbf{k}}} - \frac{2\sin(2\phi_{\mathbf{k}})\cos(2\phi_{\mathbf{k}})}{\xi_{\mathbf{k}}(\xi^2_{\mathbf{k}} - \Lambda^2_{\mathbf{k}})}\left(\xi^2_{\mathbf{k}} - \xi^2_{\mathbf{k}} + \Lambda^2_{\mathbf{k}}\right) \\
&= -\frac{2V_{\mathbf{k}}}{\xi^2_{\mathbf{k}} - \Lambda^2_{\mathbf{k}}} - \frac{2\delta\epsilon_{\mathbf{k}}V_{\mathbf{k}}}{\xi_{\mathbf{k}}(\xi^2_{\mathbf{k}} - \Lambda^2_{\mathbf{k}})} \\
&= -\frac{2V_{\mathbf{k}}}{\xi^2_{\mathbf{k}} - \Lambda^2_{\mathbf{k}}}\left(1 + \frac{\delta\epsilon_{\mathbf{k}}}{\xi_{\mathbf{k}}}\right) \\
&= -\frac{2V_{\mathbf{k}}}{\xi^2_{\mathbf{k}} - \Lambda^2_{\mathbf{k}}}\frac{\xi_{\mathbf{k}} + \delta\epsilon_{\mathbf{k}}}{\xi_{\mathbf{k}}};
\end{aligned} \tag{D.37}$$

$$
\begin{aligned}
C_{\mathbf{k}} &= \frac{[1+\cos(2\phi_{\mathbf{k}})]^2}{(2\xi_{\mathbf{k}}^-)^2} - \frac{[1-\cos(2\phi_{\mathbf{k}})]^2}{(2\xi_{\mathbf{k}}^+)^2} \\
&= \frac{\xi_{\mathbf{k}}^{+2}[1+2\cos(2\phi_{\mathbf{k}})+\cos^2(2\phi_{\mathbf{k}})] - \xi_{\mathbf{k}}^{-2}[1-2\cos(2\phi_{\mathbf{k}})+\cos^2(2\phi_{\mathbf{k}})]}{4(\xi_{\mathbf{k}}^2-\Lambda_{\mathbf{k}}^2)^2} \\
&= \frac{(\xi_{\mathbf{k}}^{+2}-\xi_{\mathbf{k}}^{-2})[1+\cos^2(2\phi_{\mathbf{k}})] + 2(\xi_{\mathbf{k}}^{+2}+\xi_{\mathbf{k}}^{-2})\cos(2\phi_{\mathbf{k}})}{4(\xi_{\mathbf{k}}^2-\Lambda_{\mathbf{k}}^2)^2} \\
&= \frac{4\xi_{\mathbf{k}}\Lambda_{\mathbf{k}}[1+\cos^2(2\phi_{\mathbf{k}})] + 4(\xi_{\mathbf{k}}^2+\Lambda_{\mathbf{k}}^2)\cos(2\phi_{\mathbf{k}})}{4(\xi_{\mathbf{k}}^2-\Lambda_{\mathbf{k}}^2)^2} \\
&= \frac{\xi_{\mathbf{k}}[\Lambda_{\mathbf{k}}^2+(\delta\epsilon_{\mathbf{k}})^2] + (\xi_{\mathbf{k}}^2+\Lambda_{\mathbf{k}}^2)\delta\epsilon_{\mathbf{k}}}{\Lambda_{\mathbf{k}}(\xi_{\mathbf{k}}^2-\Lambda_{\mathbf{k}}^2)^2} \\
&= \frac{\Lambda_{\mathbf{k}}^2(\xi_{\mathbf{k}}+\delta\epsilon_{\mathbf{k}}) + \xi_{\mathbf{k}}\delta\epsilon_{\mathbf{k}}(\xi_{\mathbf{k}}+\delta\epsilon_{\mathbf{k}})}{\Lambda_{\mathbf{k}}(\xi_{\mathbf{k}}^2-\Lambda_{\mathbf{k}}^2)^2} \\
&= \frac{(\xi_{\mathbf{k}}+\delta\epsilon_{\mathbf{k}})(\Lambda_{\mathbf{k}}^2+\xi_{\mathbf{k}}\delta\epsilon_{\mathbf{k}})}{\Lambda_{\mathbf{k}}(\xi_{\mathbf{k}}^2-\Lambda_{\mathbf{k}}^2)^2}.
\end{aligned} \tag{D.38}
$$

Using that

$$
\sum_{i,j} q_i q_j \partial_i \Lambda_{\mathbf{k}} \partial_j \Lambda_{\mathbf{k}} = \frac{(\delta\epsilon_{\mathbf{k}})^2(\delta\mathbf{k}\cdot\mathbf{q}/m)^2 + 2\delta\epsilon_{\mathbf{k}} V_{\mathbf{k}}(\delta\mathbf{k}\cdot\mathbf{q}/m)V_{\mathbf{q}} + V_{\mathbf{k}}^2 V_{\mathbf{q}}^2}{\Lambda_{\mathbf{k}}^2}, \tag{D.39}
$$

$$
\sum_{i,j} q_i q_j \partial_i \partial_j \Lambda_{\mathbf{k}} = \frac{2\delta\epsilon_{\mathbf{k}}\delta\epsilon_{\mathbf{q}}}{\Lambda_{\mathbf{k}}} + \frac{V_{\mathbf{k}}^2(\delta\mathbf{k}\cdot\mathbf{q}/m)^2 - 2\delta\epsilon_{\mathbf{k}} V_{\mathbf{k}}(\delta\mathbf{k}\cdot\mathbf{q}/m)V_{\mathbf{q}} + (\delta\epsilon_{\mathbf{k}})^2 V_{\mathbf{q}}^2}{\Lambda_{\mathbf{k}}^3}, \tag{D.40}
$$

$$
\sum_{i,j} q_i q_j \partial_i(\phi_{\mathbf{k}}) \partial_j(\phi_{\mathbf{k}}) = \frac{1}{4}\frac{(\delta\epsilon_{\mathbf{k}})^2 V_{\mathbf{q}}^2 - 2\delta\epsilon_{\mathbf{k}} V_{\mathbf{q}} V_{\mathbf{k}}(\delta\mathbf{k}\cdot\mathbf{q}/m) + V_{\mathbf{k}}^2(\delta\mathbf{k}\cdot\mathbf{q}/m)^2}{\Lambda_{\mathbf{k}}^4}, \tag{D.41}
$$

$$
\sum_{i,j} q_i q_j \partial_i \partial_j(\phi_{\mathbf{k}}) = -\frac{V_{\mathbf{k}}\delta\epsilon_{\mathbf{q}}}{\Lambda_{\mathbf{k}}^2} - \frac{[(\delta\epsilon_{\mathbf{k}})^2 - V_{\mathbf{k}}^2](\delta\mathbf{k}\cdot\mathbf{q}/m)V_{\mathbf{q}} + \delta\epsilon_{\mathbf{k}} V_{\mathbf{k}}[V_{\mathbf{q}}^2 - (\delta\mathbf{k}\cdot\mathbf{q}/m)^2]}{\Lambda_{\mathbf{k}}^4}, \tag{D.42}
$$

$$
\sum_{i,j} q_i q_j \partial_i(\Lambda_{\mathbf{k}}) \partial_j(\phi_{\mathbf{k}}) = \frac{1}{2}\frac{[(\delta\epsilon_{\mathbf{k}})^2 - V_{\mathbf{k}}^2](\delta\mathbf{k}\cdot\mathbf{q}/m)V_{\mathbf{q}} + \delta\epsilon_{\mathbf{k}} V_{\mathbf{k}}[V_{\mathbf{q}}^2 - (\delta\mathbf{k}\cdot\mathbf{q}/m)^2]}{\Lambda_{\mathbf{k}}^3}, \tag{D.43}
$$

we get

$$
\begin{aligned}
&-\sum_{i,j}\Gamma^{-1}_{4q_iq_j} = -\sum_{\mathbf{k}}\frac{1}{\xi_{\mathbf{k}}}\frac{\Lambda_{\mathbf{k}}^2+\xi_{\mathbf{k}}\delta\epsilon_{\mathbf{k}}}{\xi_{\mathbf{k}}^2-\Lambda_{\mathbf{k}}^2}\frac{(\delta\epsilon_{\mathbf{k}})^2V_{\mathbf{q}}^2-2\delta\epsilon_{\mathbf{k}}V_{\mathbf{q}}V_{\mathbf{k}}(\delta\mathbf{k}\cdot\mathbf{q}/m)+V_{\mathbf{k}}^2(\delta\mathbf{k}\cdot\mathbf{q}/m)^2}{\Lambda_{\mathbf{k}}^4}\\
&+\sum_{\mathbf{k}}\frac{2V_{\mathbf{k}}}{\xi_{\mathbf{k}}^2-\Lambda_{\mathbf{k}}^2}\frac{\xi_{\mathbf{k}}+\delta\epsilon_{\mathbf{k}}}{\xi_{\mathbf{k}}}\left[\frac{V_{\mathbf{k}}\delta\epsilon_{\mathbf{q}}}{\Lambda_{\mathbf{k}}^2}+\frac{[(\delta\epsilon_{\mathbf{k}})^2-V_{\mathbf{k}}^2](\delta\mathbf{k}\cdot\mathbf{q}/m)V_{\mathbf{q}}+\delta\epsilon_{\mathbf{k}}V_{\mathbf{k}}[V_{\mathbf{q}}^2-(\delta\mathbf{k}\cdot\mathbf{q}/m)^2]}{\Lambda_{\mathbf{k}}^4}\right]\\
&+\sum_{\mathbf{k}}\frac{V_{\mathbf{k}}^2}{\Lambda_{\mathbf{k}}^2\xi_{\mathbf{k}}^3}\frac{(\delta\epsilon_{\mathbf{k}})^2(\delta\mathbf{k}\cdot\mathbf{q}/m)^2+2\delta\epsilon_{\mathbf{k}}V_{\mathbf{k}}(\delta\mathbf{k}\cdot\mathbf{q}/m)V_{\mathbf{q}}+V_{\mathbf{k}}^2V_{\mathbf{q}}^2}{\Lambda_{\mathbf{k}}^2}\\
&+\sum_{\mathbf{k}}\frac{(\xi_{\mathbf{k}}+\delta\epsilon_{\mathbf{k}})(\Lambda_{\mathbf{k}}^2+\xi_{\mathbf{k}}\delta\epsilon_{\mathbf{k}})}{\Lambda_{\mathbf{k}}(\xi_{\mathbf{k}}^2-\Lambda_{\mathbf{k}}^2)^2}\left[\frac{2\delta\epsilon_{\mathbf{k}}\delta\epsilon_{\mathbf{q}}}{\Lambda_{\mathbf{k}}}+\frac{V_{\mathbf{k}}^2(\delta\mathbf{k}\cdot\mathbf{q}/m)^2-2\delta\epsilon_{\mathbf{k}}V_{\mathbf{k}}(\delta\mathbf{k}\cdot\mathbf{q}/m)V_{\mathbf{q}}+(\delta\epsilon_{\mathbf{k}})^2V_{\mathbf{q}}^2}{\Lambda_{\mathbf{k}}^3}\right]\\
&-\sum_{\mathbf{k}}\frac{4V_{\mathbf{k}}}{\Lambda_{\mathbf{k}}\xi_{\mathbf{k}}^2}\frac{[(\delta\epsilon_{\mathbf{k}})^2-V_{\mathbf{k}}^2](\delta\mathbf{k}\cdot\mathbf{q}/m)V_{\mathbf{q}}+\delta\epsilon_{\mathbf{k}}V_{\mathbf{k}}[V_{\mathbf{q}}^2-(\delta\mathbf{k}\cdot\mathbf{q}/m)^2]}{2\Lambda_{\mathbf{k}}^3}\\
&\equiv\sum_{\mathbf{k}}\left[K_1(2\delta\epsilon_{\mathbf{q}})+K_2\left(\frac{\delta\mathbf{k}\cdot\mathbf{q}}{m}\right)^2+K_3\frac{2\delta\mathbf{k}\cdot\mathbf{q}}{m}V_{\mathbf{q}}+K_4V_{\mathbf{q}}^2\right],
\end{aligned}
\tag{D.44}
$$

where

$$
\begin{aligned}
K_1 &= \frac{V_{\mathbf{k}}}{\xi_{\mathbf{k}}^2-\Lambda_{\mathbf{k}}^2}\frac{\xi_{\mathbf{k}}+\delta\epsilon_{\mathbf{k}}}{\xi_{\mathbf{k}}}\frac{V_{\mathbf{k}}}{\Lambda_{\mathbf{k}}^2}+\frac{(\xi_{\mathbf{k}}+\delta\epsilon_{\mathbf{k}})(\Lambda_{\mathbf{k}}^2+\xi_{\mathbf{k}}\delta\epsilon_{\mathbf{k}})}{\Lambda_{\mathbf{k}}(\xi_{\mathbf{k}}^2-\Lambda_{\mathbf{k}}^2)^2}\frac{\delta\epsilon_{\mathbf{k}}}{\Lambda_{\mathbf{k}}}\\
&= \frac{1}{(\xi_{\mathbf{k}}^2-\Lambda_{\mathbf{k}}^2)^2}\frac{\xi_{\mathbf{k}}+\delta\epsilon_{\mathbf{k}}}{\xi_{\mathbf{k}}}\frac{V_{\mathbf{k}}^2(\xi_{\mathbf{k}}^2-\Lambda_{\mathbf{k}}^2)+\xi_{\mathbf{k}}\delta\epsilon_{\mathbf{k}}(\Lambda_{\mathbf{k}}^2+\xi_{\mathbf{k}}\delta\epsilon_{\mathbf{k}})}{\Lambda_{\mathbf{k}}^2}\\
&= \frac{1}{(\xi_{\mathbf{k}}^2-\Lambda_{\mathbf{k}}^2)^2}\frac{\xi_{\mathbf{k}}+\delta\epsilon_{\mathbf{k}}}{\xi_{\mathbf{k}}}(\xi_{\mathbf{k}}^2-V_{\mathbf{k}}^2+\xi_{\mathbf{k}}\delta\epsilon_{\mathbf{k}})\\
&= \frac{(\xi_{\mathbf{k}}+\delta\epsilon_{\mathbf{k}})^2}{(\xi_{\mathbf{k}}^2-\Lambda_{\mathbf{k}}^2)^2}-\frac{V_{\mathbf{k}}^2}{(\xi_{\mathbf{k}}^2-\Lambda_{\mathbf{k}}^2)^2}\frac{\xi_{\mathbf{k}}+\delta\epsilon_{\mathbf{k}}}{\xi_{\mathbf{k}}},
\end{aligned}
\tag{D.45}
$$

$$
\begin{aligned}
K_2 &= \frac{V_{\mathbf{k}}^2}{\Lambda_{\mathbf{k}}^4}\left[-\frac{1}{\xi_{\mathbf{k}}}\frac{\Lambda_{\mathbf{k}}^2+\xi_{\mathbf{k}}\delta\epsilon_{\mathbf{k}}+2\delta\epsilon_{\mathbf{k}}(\xi_{\mathbf{k}}+\delta\epsilon_{\mathbf{k}})}{\xi_{\mathbf{k}}^2-\Lambda_{\mathbf{k}}^2}+\frac{(\delta\epsilon_{\mathbf{k}})^2}{\xi_{\mathbf{k}}^3}+\frac{(\xi_{\mathbf{k}}+\delta\epsilon_{\mathbf{k}})(\Lambda_{\mathbf{k}}^2+\xi_{\mathbf{k}}\delta\epsilon_{\mathbf{k}})}{(\xi_{\mathbf{k}}^2-\Lambda_{\mathbf{k}}^2)^2}+\frac{2\delta\epsilon_{\mathbf{k}}}{\xi_{\mathbf{k}}^2}\right] \\
&= \frac{V_{\mathbf{k}}^2}{(\xi_{\mathbf{k}}^2-\Lambda_{\mathbf{k}}^2)^2}\frac{1}{\xi_{\mathbf{k}}^3}\left[\frac{-\xi_{\mathbf{k}}^2(\xi_{\mathbf{k}}^2-\Lambda_{\mathbf{k}}^2)[\Lambda_{\mathbf{k}}^2+\xi_{\mathbf{k}}\delta\epsilon_{\mathbf{k}}+2\delta\epsilon_{\mathbf{k}}(\xi_{\mathbf{k}}+\delta\epsilon_{\mathbf{k}})]+(\xi_{\mathbf{k}}^2-\Lambda_{\mathbf{k}}^2)^2\delta\epsilon_{\mathbf{k}}(2\xi_{\mathbf{k}}+\delta\epsilon_{\mathbf{k}})}{\Lambda_{\mathbf{k}}^4}\right. \\
&+ \left.\frac{\xi_{\mathbf{k}}^3(\xi_{\mathbf{k}}+\delta\epsilon_{\mathbf{k}})(\Lambda_{\mathbf{k}}^2+\xi_{\mathbf{k}}\delta\epsilon_{\mathbf{k}})}{\Lambda_{\mathbf{k}}^4}\right] \\
&= \frac{V_{\mathbf{k}}^2}{(\xi_{\mathbf{k}}^2-\Lambda_{\mathbf{k}}^2)^2}\frac{1}{\xi_{\mathbf{k}}^3}\left[\frac{-2\xi_{\mathbf{k}}^2(\xi_{\mathbf{k}}^2-\Lambda_{\mathbf{k}}^2)\delta\epsilon_{\mathbf{k}}(\xi_{\mathbf{k}}+\delta\epsilon_{\mathbf{k}})+(\xi_{\mathbf{k}}^2-\Lambda_{\mathbf{k}}^2)^2\delta\epsilon_{\mathbf{k}}(2\xi_{\mathbf{k}}+\delta\epsilon_{\mathbf{k}})}{\Lambda_{\mathbf{k}}^4}\right. \\
&+ \left.\frac{[\xi_{\mathbf{k}}^3(\xi_{\mathbf{k}}+\delta\epsilon_{\mathbf{k}})-\xi_{\mathbf{k}}^2(\xi_{\mathbf{k}}^2-\Lambda_{\mathbf{k}}^2)](\Lambda_{\mathbf{k}}^2+\xi_{\mathbf{k}}\delta\epsilon_{\mathbf{k}})}{\Lambda_{\mathbf{k}}^4}\right] \\
&= \frac{V_{\mathbf{k}}^2}{(\xi_{\mathbf{k}}^2-\Lambda_{\mathbf{k}}^2)^2}\frac{1}{\xi_{\mathbf{k}}^3}\frac{-2\xi_{\mathbf{k}}^2(\xi_{\mathbf{k}}^2-\Lambda_{\mathbf{k}}^2)\delta\epsilon_{\mathbf{k}}(\xi_{\mathbf{k}}+\delta\epsilon_{\mathbf{k}})+(\xi_{\mathbf{k}}^2-\Lambda_{\mathbf{k}}^2)^2\delta\epsilon_{\mathbf{k}}(2\xi_{\mathbf{k}}+\delta\epsilon_{\mathbf{k}})+\xi_{\mathbf{k}}^2(\Lambda_{\mathbf{k}}^2+\xi_{\mathbf{k}}\delta\epsilon_{\mathbf{k}})^2}{\Lambda_{\mathbf{k}}^4} \\
&= \frac{V_{\mathbf{k}}^2}{(\xi_{\mathbf{k}}^2-\Lambda_{\mathbf{k}}^2)^2}\frac{1}{\xi_{\mathbf{k}}^3}\left[\frac{\Lambda_{\mathbf{k}}^4[\delta\epsilon_{\mathbf{k}}(2\xi_{\mathbf{k}}+\delta\epsilon_{\mathbf{k}})+\xi_{\mathbf{k}}^2]+\Lambda_{\mathbf{k}}^2[2\xi_{\mathbf{k}}^2\delta\epsilon_{\mathbf{k}}(\xi_{\mathbf{k}}+\delta\epsilon_{\mathbf{k}})-2\xi_{\mathbf{k}}^2\delta\epsilon_{\mathbf{k}}(2\xi_{\mathbf{k}}+\delta\epsilon_{\mathbf{k}})+2\xi_{\mathbf{k}}^3\delta\epsilon_{\mathbf{k}}]}{\Lambda_{\mathbf{k}}^4}\right. \\
&+ \left.\frac{-2\xi_{\mathbf{k}}^4\delta\epsilon_{\mathbf{k}}(\xi_{\mathbf{k}}+\delta\epsilon_{\mathbf{k}})+\xi_{\mathbf{k}}^4\delta\epsilon_{\mathbf{k}}(2\xi_{\mathbf{k}}+\delta\epsilon_{\mathbf{k}})+\xi_{\mathbf{k}}^4(\delta\epsilon_{\mathbf{k}})^2}{\Lambda_{\mathbf{k}}^4}\right] \\
&= \frac{V_{\mathbf{k}}^2}{(\xi_{\mathbf{k}}^2-\Lambda_{\mathbf{k}}^2)^2}\frac{(\xi_{\mathbf{k}}+\delta\epsilon_{\mathbf{k}})^2}{\xi_{\mathbf{k}}^3},
\end{aligned} \tag{D.46}
$$

$$
\begin{aligned}
K_3 &= \frac{1}{\xi_{\mathbf{k}}} \frac{\Lambda_{\mathbf{k}}^2 + \xi_{\mathbf{k}}\delta\epsilon_{\mathbf{k}}}{\delta\epsilon_{\mathbf{k}}(\Lambda_{\mathbf{k}}^2 + \xi_{\mathbf{k}}\delta\epsilon_{\mathbf{k}})} \frac{V_{\mathbf{k}}}{\Lambda_{\mathbf{k}}^4} + \frac{V_{\mathbf{k}}}{\xi_{\mathbf{k}}^2 - \Lambda_{\mathbf{k}}^2} \frac{\xi_{\mathbf{k}} + \delta\epsilon_{\mathbf{k}}}{\xi_{\mathbf{k}}} \frac{(\delta\epsilon_{\mathbf{k}})^2 - V_{\mathbf{k}}^2}{\Lambda_{\mathbf{k}}^4} + \frac{\delta\epsilon_{\mathbf{k}}}{\xi_{\mathbf{k}}^3} \frac{V_{\mathbf{k}}^3}{\Lambda_{\mathbf{k}}^4} \\
&- \frac{\delta\epsilon_{\mathbf{k}}(\xi_{\mathbf{k}} + \delta\epsilon_{\mathbf{k}})(\Lambda_{\mathbf{k}}^2 + \xi_{\mathbf{k}}\delta\epsilon_{\mathbf{k}})}{(\xi_{\mathbf{k}}^2 - \Lambda_{\mathbf{k}}^2)^2} \frac{V_{\mathbf{k}}}{\Lambda_{\mathbf{k}}^4} - \frac{(\delta\epsilon_{\mathbf{k}})^2 - V_{\mathbf{k}}^2}{\xi_{\mathbf{k}}^2} \frac{V_{\mathbf{k}}}{\Lambda_{\mathbf{k}}^4} \\
&= \frac{V_{\mathbf{k}}}{(\xi_{\mathbf{k}}^2 - \Lambda_{\mathbf{k}}^2)^2} \frac{1}{\xi_{\mathbf{k}}^3} \Bigg[\frac{(\xi_{\mathbf{k}}^2 - \Lambda_{\mathbf{k}}^2)\xi_{\mathbf{k}}^2[\delta\epsilon_{\mathbf{k}}(\Lambda_{\mathbf{k}}^2 + \xi_{\mathbf{k}}\delta\epsilon_{\mathbf{k}}) + (\xi_{\mathbf{k}} + \delta\epsilon_{\mathbf{k}})((\delta\epsilon_{\mathbf{k}})^2 - V_{\mathbf{k}}^2)] + \delta\epsilon_{\mathbf{k}} V_{\mathbf{k}}^2 (\xi_{\mathbf{k}}^2 - \Lambda_{\mathbf{k}}^2)^2}{\Lambda_{\mathbf{k}}^4} \\
&- \frac{\xi_{\mathbf{k}}^3\delta\epsilon_{\mathbf{k}}(\xi_{\mathbf{k}} + \delta\epsilon_{\mathbf{k}})(\Lambda_{\mathbf{k}}^2 + \xi_{\mathbf{k}}\delta\epsilon_{\mathbf{k}}) + \xi_{\mathbf{k}}(\xi_{\mathbf{k}}^2 - \Lambda_{\mathbf{k}}^2)^2[(\delta\epsilon_{\mathbf{k}})^2 - V_{\mathbf{k}}^2]}{\Lambda_{\mathbf{k}}^4} \Bigg] \\
&= \frac{V_{\mathbf{k}}}{(\xi_{\mathbf{k}}^2 - \Lambda_{\mathbf{k}}^2)^2} \frac{1}{\xi_{\mathbf{k}}^3} \Bigg[\frac{\Lambda_{\mathbf{k}}^4[-\xi_{\mathbf{k}}^2\delta\epsilon_{\mathbf{k}} + \delta\epsilon_{\mathbf{k}} V_{\mathbf{k}}^2 - \xi_{\mathbf{k}}[(\delta\epsilon_{\mathbf{k}})^2 - V_{\mathbf{k}}^2]]}{\Lambda_{\mathbf{k}}^4} \\
&+ \frac{\Lambda_{\mathbf{k}}^2[\overbrace{\xi_{\mathbf{k}}^4\delta\epsilon_{\mathbf{k}} - \xi_{\mathbf{k}}^3(\delta\epsilon_{\mathbf{k}})^2 - \xi_{\mathbf{k}}^2(-\xi_{\mathbf{k}} + \delta\epsilon_{\mathbf{k}})[(\delta\epsilon_{\mathbf{k}})^2 - V_{\mathbf{k}}^2] - 2\delta\epsilon_{\mathbf{k}} V_{\mathbf{k}}^2 \xi_{\mathbf{k}}^2 - \xi_{\mathbf{k}}^3\delta\epsilon_{\mathbf{k}}(\xi_{\mathbf{k}} + \delta\epsilon_{\mathbf{k}})}^{-\xi_{\mathbf{k}}^2(\xi_{\mathbf{k}}+\delta\epsilon_{\mathbf{k}})\Lambda_{\mathbf{k}}^2}]}{\Lambda_{\mathbf{k}}^4} \\
&+ \frac{\xi_{\mathbf{k}}^5(\delta\epsilon_{\mathbf{k}})^2 + \xi_{\mathbf{k}}^4(\xi_{\mathbf{k}} + \delta\epsilon_{\mathbf{k}})[(\delta\epsilon_{\mathbf{k}})^2 - V_{\mathbf{k}}^2] + \delta\epsilon_{\mathbf{k}} V_{\mathbf{k}}^2 \xi_{\mathbf{k}}^4 - \xi_{\mathbf{k}}^4(\delta\epsilon_{\mathbf{k}})^2(\xi_{\mathbf{k}} + \delta\epsilon_{\mathbf{k}}) - \xi_{\mathbf{k}}^5[(\delta\epsilon_{\mathbf{k}})^2 - V_{\mathbf{k}}^2]}{\Lambda_{\mathbf{k}}^4} \Bigg] \\
&= \frac{V_{\mathbf{k}}}{(\xi_{\mathbf{k}}^2 - \Lambda_{\mathbf{k}}^2)^2} \frac{1}{\xi_{\mathbf{k}}^3} \frac{\Lambda_{\mathbf{k}}^4[(\xi_{\mathbf{k}} + \delta\epsilon_{\mathbf{k}})V_{\mathbf{k}}^2 - \xi_{\mathbf{k}}\delta\epsilon_{\mathbf{k}}(\xi_{\mathbf{k}} + \delta\epsilon_{\mathbf{k}}) - \xi_{\mathbf{k}}^2(\xi_{\mathbf{k}} + \delta\epsilon_{\mathbf{k}})]}{\Lambda_{\mathbf{k}}^4} \\
&= \frac{V_{\mathbf{k}}(\xi_{\mathbf{k}} + \delta\epsilon_{\mathbf{k}})}{(\xi_{\mathbf{k}}^2 - \Lambda_{\mathbf{k}}^2)^2} \frac{V_{\mathbf{k}}^2 - \xi_{\mathbf{k}}(\xi_{\mathbf{k}} + \delta\epsilon_{\mathbf{k}})}{\xi_{\mathbf{k}}^3},
\end{aligned}
\tag{D.47}
$$

$$
\begin{aligned}
K_4 &= -\frac{1}{\xi_{\mathbf{k}}}\frac{\Lambda_{\mathbf{k}}^2+\xi_{\mathbf{k}}\delta\epsilon_{\mathbf{k}}}{\xi_{\mathbf{k}}^2-\Lambda_{\mathbf{k}}^2}\frac{(\delta\epsilon_{\mathbf{k}})^2}{\Lambda_{\mathbf{k}}^4}+\frac{2V_{\mathbf{k}}^2}{\xi_{\mathbf{k}}^2-\Lambda_{\mathbf{k}}^2}\frac{\xi_{\mathbf{k}}+\delta\epsilon_{\mathbf{k}}}{\xi_{\mathbf{k}}}\frac{\delta\epsilon_{\mathbf{k}}}{\Lambda_{\mathbf{k}}^4}+\frac{1}{\xi_{\mathbf{k}}^3}\frac{V_{\mathbf{k}}^4}{\Lambda_{\mathbf{k}}^4}+\frac{(\xi_{\mathbf{k}}+\delta\epsilon_{\mathbf{k}})(\Lambda_{\mathbf{k}}^2+\xi_{\mathbf{k}}\delta\epsilon_{\mathbf{k}})}{(\xi_{\mathbf{k}}^2-\Lambda_{\mathbf{k}}^2)^2}\frac{(\delta\epsilon_{\mathbf{k}})^2}{\Lambda_{\mathbf{k}}^4}\\
&-\frac{2\delta\epsilon_{\mathbf{k}}}{\xi_{\mathbf{k}}^2}\frac{V_{\mathbf{k}}^2}{\Lambda_{\mathbf{k}}^4}\\
&=\frac{1}{(\xi_{\mathbf{k}}^2-\Lambda_{\mathbf{k}}^2)^2}\frac{1}{\xi_{\mathbf{k}}^3}\left[\frac{2V_{\mathbf{k}}^2\xi_{\mathbf{k}}^2(\xi_{\mathbf{k}}^2-\Lambda_{\mathbf{k}}^2)(\xi_{\mathbf{k}}+\delta\epsilon_{\mathbf{k}})\delta\epsilon_{\mathbf{k}}+(\xi_{\mathbf{k}}^2-\Lambda_{\mathbf{k}}^2)^2V_{\mathbf{k}}^2(V_{\mathbf{k}}^2-2\xi_{\mathbf{k}}\delta\epsilon_{\mathbf{k}})}{\Lambda_{\mathbf{k}}^4}\right.\\
&\left.+\frac{\xi_{\mathbf{k}}^2(\delta\epsilon_{\mathbf{k}})^2[\xi_{\mathbf{k}}(\xi_{\mathbf{k}}+\delta\epsilon_{\mathbf{k}})-(\xi_{\mathbf{k}}^2-\Lambda_{\mathbf{k}}^2)](\Lambda_{\mathbf{k}}^2+\xi_{\mathbf{k}}\delta\epsilon_{\mathbf{k}})}{\Lambda_{\mathbf{k}}^4}\right]\\
&=\frac{1}{(\xi_{\mathbf{k}}^2-\Lambda_{\mathbf{k}}^2)^2}\frac{1}{\xi_{\mathbf{k}}^3}\left[\frac{\Lambda_{\mathbf{k}}^4[V_{\mathbf{k}}^2(V_{\mathbf{k}}^2-2\xi_{\mathbf{k}}\delta\epsilon_{\mathbf{k}})+\xi_{\mathbf{k}}^2(\delta\epsilon_{\mathbf{k}})^2]}{\Lambda_{\mathbf{k}}^4}\right.\\
&+\frac{\Lambda_{\mathbf{k}}^2[\overbrace{-2V_{\mathbf{k}}^2\xi_{\mathbf{k}}^2(\xi_{\mathbf{k}}+\delta\epsilon_{\mathbf{k}})\delta\epsilon_{\mathbf{k}}-2\xi_{\mathbf{k}}^2V_{\mathbf{k}}^2(V_{\mathbf{k}}^2-2\xi_{\mathbf{k}}\delta\epsilon_{\mathbf{k}})+2\xi_{\mathbf{k}}^3(\delta\epsilon_{\mathbf{k}})^3}^{2\xi_{\mathbf{k}}^2\Lambda_{\mathbf{k}}^2(\xi_{\mathbf{k}}\delta\epsilon_{\mathbf{k}}-V_{\mathbf{k}}^2)}]}{\Lambda_{\mathbf{k}}^4}\\
&\left.+\frac{\overbrace{2V_{\mathbf{k}}^2\xi_{\mathbf{k}}^4(\xi_{\mathbf{k}}+\delta\epsilon_{\mathbf{k}})\delta\epsilon_{\mathbf{k}}+\xi_{\mathbf{k}}^4V_{\mathbf{k}}^2(V_{\mathbf{k}}^2-2\xi_{\mathbf{k}}\delta\epsilon_{\mathbf{k}})+\xi_{\mathbf{k}}^4(\delta\epsilon_{\mathbf{k}})^4}^{\xi_{\mathbf{k}}^4\Lambda_{\mathbf{k}}^4}}{\Lambda_{\mathbf{k}}^4}\right]\\
&=\frac{1}{(\xi_{\mathbf{k}}^2-\Lambda_{\mathbf{k}}^2)^2}\frac{V_{\mathbf{k}}^4-2V_{\mathbf{k}}^2\xi_{\mathbf{k}}\delta\epsilon_{\mathbf{k}}+\xi_{\mathbf{k}}^2(\delta\epsilon_{\mathbf{k}})^2+2\xi_{\mathbf{k}}^3\delta\epsilon_{\mathbf{k}}-2\xi_{\mathbf{k}}^2V_{\mathbf{k}}^2+\xi_{\mathbf{k}}^4}{\xi_{\mathbf{k}}^3}\\
&=\frac{1}{(\xi_{\mathbf{k}}^2-\Lambda_{\mathbf{k}}^2)^2}\frac{V_{\mathbf{k}}^4-2V_{\mathbf{k}}^2\xi_{\mathbf{k}}(\xi+\delta\epsilon_{\mathbf{k}})+\xi_{\mathbf{k}}^2(\xi_{\mathbf{k}}+\delta\epsilon_{\mathbf{k}})^2}{\xi_{\mathbf{k}}^3}\\
&=\frac{1}{(\xi_{\mathbf{k}}^2-\Lambda_{\mathbf{k}}^2)^2}\frac{[\xi_{\mathbf{k}}(\xi+\delta\epsilon_{\mathbf{k}})-V_{\mathbf{k}}^2]^2}{\xi_{\mathbf{k}}^3}.
\end{aligned}
\tag{D.48}
$$

Thus

$$
\begin{aligned}
\sum_{i,j}\Gamma^{-1}_{4q_iq_j}&=-\frac{\delta\mathbf{q}^2}{m}\sum_{\mathbf{k}}\frac{\xi_{\mathbf{k}}+\delta\epsilon_{\mathbf{k}}}{\xi_{\mathbf{k}}}\frac{\xi_{\mathbf{k}}(\xi_{\mathbf{k}}+\delta\epsilon_{\mathbf{k}})-V_{\mathbf{k}}^2}{(\xi_{\mathbf{k}}^2-\Lambda_{\mathbf{k}}^2)^2}\\
&-\sum_{\mathbf{k}}\frac{1}{\xi_{\mathbf{k}}^3}\frac{1}{(\xi_{\mathbf{k}}^2-\Lambda_{\mathbf{k}}^2)^2}\left[V_{\mathbf{k}}(\xi_{\mathbf{k}}+\delta\epsilon_{\mathbf{k}})\frac{\delta\mathbf{k}\cdot\mathbf{q}}{m}+\left[V_{\mathbf{k}}^2-\xi_{\mathbf{k}}(\xi_{\mathbf{k}}+\delta\epsilon_{\mathbf{k}})\right]V_{\mathbf{q}}\right]^2.
\end{aligned}
\tag{D.49}
$$

So up to order $\mathbf{q}^2$ and ω_m we can write the vertex function as $\Gamma^{-1}_{2q}=\Gamma^{-1}_0+\Gamma^{-1}_{(2\mathbf{q})^2}+\sum_{i,j}\Gamma^{-1}_{4q_iq_j}$.

Recalling that for any scalar function $f(k_x^2,k_y^2,k_z^2)$ it is valid to write

$$
V_{\mathbf{q}}^2=\alpha^2(2+\gamma^2)\epsilon_F\frac{q_z^2}{2m},
\tag{D.50}
$$

$$
\sum_{\mathbf{k}}f(k_x^2,k_y^2,k_z^2)(\mathbf{k}\cdot\mathbf{q})^2=\sum_{\mathbf{k}}f(k_x^2,k_y^2,k_z^2)(q_x^2k_x^2+q_y^2k_y^2+q_z^2k_z^2),
\tag{D.51}
$$

$$
\sum_{\mathbf{k}}f(k_x^2,k_y^2,k_z^2)V_{\mathbf{q}}V_{\mathbf{k}}(\mathbf{k}\cdot\mathbf{q})=q_z^2\sum_{\mathbf{k}}f(k_x^2,k_y^2,k_z^2)V_{\mathbf{k}}^2
\tag{D.52}
$$

and so we get

$$
\begin{aligned}
-\sum_{i,j}\Gamma_{4q_iq_j} &= \frac{\delta\mathbf{q}^2}{m}\sum_{\mathbf{k}}\frac{\xi_{\mathbf{k}}+\delta\epsilon_{\mathbf{k}}}{\xi_{\mathbf{k}}}\frac{\xi_{\mathbf{k}}(\xi_{\mathbf{k}}+\delta\epsilon_{\mathbf{k}})-V_{\mathbf{k}}^2}{(\xi_{\mathbf{k}}^2-\Lambda_{\mathbf{k}}^2)^2}+\sum_{\mathbf{k}}\left(\frac{\delta\mathbf{k}\cdot\mathbf{q}}{m}\right)^2\frac{(\xi_{\mathbf{k}}+\delta\epsilon_{\mathbf{k}})^2}{\xi_{\mathbf{k}}^3}\frac{V_{\mathbf{k}}^2}{(\xi_{\mathbf{k}}^2-\Lambda_{\mathbf{k}}^2)^2}\\
&+V_{\mathbf{q}}\sum_{\mathbf{k}}V_{\mathbf{k}}\frac{2\delta\mathbf{k}\cdot\mathbf{q}}{m}\frac{\xi_{\mathbf{k}}+\delta\epsilon_{\mathbf{k}}}{\xi_{\mathbf{k}}^3}\frac{V_{\mathbf{k}}^2-\xi_{\mathbf{k}}(\xi_{\mathbf{k}}+\delta\epsilon_{\mathbf{k}})}{(\xi_{\mathbf{k}}^2-\Lambda_{\mathbf{k}}^2)^2}+V_{\mathbf{q}}^2\sum_{\mathbf{k}}\frac{1}{\xi_{\mathbf{k}}^3}\frac{[V_{\mathbf{k}}^2-\xi_{\mathbf{k}}(\xi_{\mathbf{k}}+\delta\epsilon_{\mathbf{k}})]^2}{(\xi_{\mathbf{k}}^2-\Lambda_{\mathbf{k}}^2)^2}\\
&=\frac{\delta\mathbf{q}^2}{m}\sum_{\mathbf{k}}\frac{\xi_{\mathbf{k}}+\delta\epsilon_{\mathbf{k}}}{\xi_{\mathbf{k}}}\frac{\xi_{\mathbf{k}}(\xi_{\mathbf{k}}+\delta\epsilon_{\mathbf{k}})-V_{\mathbf{k}}^2}{(\xi_{\mathbf{k}}^2-\Lambda_{\mathbf{k}}^2)^2}+\delta^2\sum_{\mathbf{k}}\frac{q_x^2k_x^2+q_y^2k_y^2+q_z^2k_z^2}{2m^2}\frac{(\xi_{\mathbf{k}}+\delta\epsilon_{\mathbf{k}})^2}{\xi_{\mathbf{k}}^3}\frac{V_{\mathbf{k}}^2}{(\xi_{\mathbf{k}}^2-\Lambda_{\mathbf{k}}^2)^2}\\
&+\frac{2\delta q_z^2}{m}\sum_{\mathbf{k}}\frac{V_{\mathbf{k}}^2(\xi_{\mathbf{k}}+\delta\epsilon_{\mathbf{k}})}{\xi_{\mathbf{k}}^3}\frac{V_{\mathbf{k}}^2-\xi_{\mathbf{k}}(\xi_{\mathbf{k}}+\delta\epsilon_{\mathbf{k}})}{(\xi_{\mathbf{k}}^2-\Lambda_{\mathbf{k}}^2)^2}+\alpha^2(2+\gamma^2)\epsilon_F\frac{q_z^2}{2m}\sum_{\mathbf{k}}\frac{1}{\xi_{\mathbf{k}}^3}\frac{[V_{\mathbf{k}}^2-\xi_{\mathbf{k}}(\xi_{\mathbf{k}}+\delta\epsilon_{\mathbf{k}})]^2}{(\xi_{\mathbf{k}}^2-\Lambda_{\mathbf{k}}^2)^2}\\
&\equiv\sum_{i,j}Y_{ij}\frac{q_iq_j}{m},
\end{aligned}
\tag{D.53}
$$

where the symmetric tensor $\mathbf{Y}$ is

$$Y_{xx}=\delta\sum_{\mathbf{k}}\frac{\xi_{\mathbf{k}}+\delta\epsilon_{\mathbf{k}}}{\xi_{\mathbf{k}}}\frac{\xi_{\mathbf{k}}(\xi_{\mathbf{k}}+\delta\epsilon_{\mathbf{k}})-V_{\mathbf{k}}^2}{(\xi_{\mathbf{k}}^2-\Lambda_{\mathbf{k}}^2)^2}+\delta^2\sum_{\mathbf{k}}\frac{k_x^2}{m}\frac{V_{\mathbf{k}}^2}{(\xi_{\mathbf{k}}^2-\Lambda_{\mathbf{k}}^2)^2}\frac{(\xi_{\mathbf{k}}+\delta\epsilon_{\mathbf{k}})^2}{\xi_{\mathbf{k}}^3}, \tag{D.54}$$

$$Y_{yy}=\delta\sum_{\mathbf{k}}\frac{\xi_{\mathbf{k}}+\delta\epsilon_{\mathbf{k}}}{\xi_{\mathbf{k}}}\frac{\xi_{\mathbf{k}}(\xi_{\mathbf{k}}+\delta\epsilon_{\mathbf{k}})-V_{\mathbf{k}}^2}{(\xi_{\mathbf{k}}^2-\Lambda_{\mathbf{k}}^2)^2}+\delta^2\sum_{\mathbf{k}}\frac{k_y^2}{m}\frac{V_{\mathbf{k}}^2}{(\xi_{\mathbf{k}}^2-\Lambda_{\mathbf{k}}^2)^2}\frac{(\xi_{\mathbf{k}}+\delta\epsilon_{\mathbf{k}})^2}{\xi_{\mathbf{k}}^3}, \tag{D.55}$$

$$
\begin{aligned}
Y_{zz}&=\delta\sum_{\mathbf{k}}\frac{\xi_{\mathbf{k}}+\delta\epsilon_{\mathbf{k}}}{\xi_{\mathbf{k}}}\frac{\xi_{\mathbf{k}}(\xi_{\mathbf{k}}+\delta\epsilon_{\mathbf{k}})-V_{\mathbf{k}}^2}{(\xi_{\mathbf{k}}^2-\Lambda_{\mathbf{k}}^2)^2}+\delta^2\sum_{\mathbf{k}}\frac{k_z^2}{m}\frac{V_{\mathbf{k}}^2}{(\xi_{\mathbf{k}}^2-\Lambda_{\mathbf{k}}^2)^2}\frac{(\xi_{\mathbf{k}}+\delta\epsilon_{\mathbf{k}})^2}{\xi_{\mathbf{k}}^3}\\
&+2\delta\sum_{\mathbf{k}}\frac{V_{\mathbf{k}}^2(\xi_{\mathbf{k}}+\delta\epsilon_{\mathbf{k}})}{\xi_{\mathbf{k}}^3}\frac{V_{\mathbf{k}}^2-\xi_{\mathbf{k}}(\xi_{\mathbf{k}}+\delta\epsilon_{\mathbf{k}})}{(\xi_{\mathbf{k}}^2-\Lambda_{\mathbf{k}}^2)^2}+\frac{\alpha^2(2+\gamma^2)\epsilon_F}{2}\sum_{\mathbf{k}}\frac{1}{\xi_{\mathbf{k}}^3}\frac{[V_{\mathbf{k}}^2-\xi_{\mathbf{k}}(\xi_{\mathbf{k}}+\delta\epsilon_{\mathbf{k}})]^2}{(\xi_{\mathbf{k}}^2-\Lambda_{\mathbf{k}}^2)^2},
\end{aligned}
\tag{D.56}
$$

with $Y_{xx}=Y_{yy}$ and the off-diagonal terms zero.

Thus, using $q_i\to\frac{q_i}{2}$, the action takes the form

$$S[\Delta]=\sum_q\bar{\Delta}_q\left[\Gamma_0^{-1}+\sum_{\mathbf{k}}J_{\mathbf{k}}\left(\frac{\mathbf{q}^2}{4m}+i\omega_m\right)-\sum_i Y_{ii}\frac{q_i^2}{4m}\right]\Delta_q, \tag{D.57}$$

that also represents a non-interacting bosonic system with effective chemical potential

$$\mu_{\text{eff}}=\frac{\Gamma_0^{-1}}{\sum_{\mathbf{k}}J_{\mathbf{k}}} \tag{D.58}$$

and energy dispersion

$$\epsilon_{\mathbf{q}}=\sum_{ij}\left(\delta_{ij}-\frac{Y_{ij}}{\sum_{\mathbf{k}}J_{\mathbf{k}}}\right)\frac{q_iq_j}{4m}, \tag{D.59}$$

with $J_{\mathbf{k}}$ given by Eq. D.34.

Bibliography

[1] J. M. Blatt, *Theory of Superconductivity.* Academic, 1964.

[2] J. Bardeen, L. N. Cooper, and J. R. Schrieffer, “Theory of superconductivity,” *Phys. Rev.*, vol. 108, pp. 1175–1204, Dec 1957.

[3] A. J. Leggett, *Modern Trends in the Theory of Condensed Matter.* LNP0115, Springer-Verlag, 1980.

[4] P. Nozières and S. Schmitt-Rink, “Bose condensation in an attractive fermion gas: From weak to strong coupling superconductivity,” *Journal of Low Temperature Physics*, vol. 59, pp. 195–211, may 1985.

[5] C. A. R. S. de Melo, M. Randeria, and J. R. Engelbrecht, “Crossover from BCS to Bose Superconductivity: Transition Temperature and Time-dependent Ginzburg-Landau Theory,” *Physical Review Letters*, vol. 71, pp. 3202–3205, nov 1993.

[6] C. A. Regal, M. Greiner, and D. S. Jin, “Observation of resonance condensation of fermionic atom pairs,” *Physical Review Letters*, vol. 92, jan 2004.

[7] M. W. Zwierlein, C. A. Stan, C. H. Schunck, S. M. F. Raupach, A. J. Kerman, and W. Ketterle, “Condensation of pairs of fermionic atoms near a feshbach resonance,” *Physical Review Letters*, vol. 92, mar 2004.

[8] T. Bourdel, L. Khaykovich, J. Cubizolles, J. Zhang, F. Chevy, M. Teichmann, L. Tarruell, S. J. J. M. F. Kokkelmans, and C. Salomon, “Experimental study of the BEC-BCS crossover region in lithium 6,” *Physical Review Letters*, vol. 93, jul 2004.

[9] G. Chen, M. Gong, and C. Zhang, “BCS-BEC crossover in spin-orbit-coupled two-dimensional fermi gases,” *Physical Review A*, vol. 85, jan 2012.

[10] Z.-Q. Yu and H. Zhai, “Spin-orbit coupled fermi gases across a feshbach resonance,” *Physical Review Letters*, vol. 107, nov 2011.

[11] L. He, X.-G. Huang, H. Hu, and X.-J. Liu, “BCS-BEC crossover at finite temperature in spin-orbit-coupled fermi gases,” *Physical Review A*, vol. 87, may 2013.

[12] J. Lee and D.-H. Kim, "Induced interactions in the BCS-BEC crossover of two-dimensional fermi gases with rashba spin-orbit coupling," *Physical Review A*, vol. 95, mar 2017.

[13] F. Deus, M. A. Continentino, and H. Caldas, "Induced p-wave superconductivity without spin-orbit interactions," *Annals of Physics*, vol. 362, pp. 208–222, nov 2015.

[14] H. Caldas, F. S. Batista, M. A. Continentino, F. Deus, and D. Nozadze, "A Two-band Model for p-wave Superconductivity," *Annals Phys.*, vol. 384, pp. 211–224, 2017.

[15] D. Reyes, M. A. Continentino, F. Deus, and C. Thomas, "Pressure induced BEC-BCS crossover in multi-band superconductors," *ArXiv e-prints*, Jan. 2018.

[16] S. N. Bose, "Plancks gesetz und lichtquantenhypothese," *Z. Physik*, vol. 26, p. 178–181, 1924.

[17] A. Einstein, "Quantentheorie des einatomigen idealen gases," *Sitzungsber. Kgl. Preuss. Akad. Wiss*, vol. 261, pp. 3–14, 1924.

[18] M. H. Anderson, J. R. Ensher, M. R. Matthews, C. E. Wieman, and E. A. Cornell, "Observation of bose-einstein condensation in a dilute atomic vapor," *Science*, vol. 269, pp. 198–201, jul 1995.

[19] H. K. Onnes, "The resistance of pure mercury at helium temperatures," *Commun. Phys. Lab.*, vol. 12, p. 120, 1911.

[20] W. M. R. Ochsenfeld, "Ein neuer effekt bei eintritt der supraleitfähigkeit," *Naturwissenschaften*, vol. 21, no. 44, pp. 787–789, 1933.

[21] J. N. R. L. W. Shubnikow, "Magnetic properties and critical currents of supra-conducting alloys," *Nature*, vol. 135, no. 3415, p. 581, 1935.

[22] F. L. H. London, "The electromagnetic equations of the supraconductor," *Proceedings of the Royal Society of London. Series A - Mathematical and Physical Sciences*, vol. 149, no. 866, pp. 71–88, 1935.

[23] V. L. Ginzburg and L. D. Landau, "On the theory of superconductivity," *Zhurnal Eksperimental'noi i Teoreticheskoi Fiziki*, vol. 20, pp. 1064–1082, 1950.

[24] A. B. Pippard, "Trapped flux in superconductors," *Philosophical Transactions of the Royal Society A: Mathematical, Physical and Engineering Sciences*, vol. 248, no. 941, pp. 97–129, 1955.

[25] L. N. Cooper, "Bound electron pairs in a degenerate fermi gas," *Physical Review*, vol. 104, pp. 1189–1190, nov 1956.

[26] E. Maxwell, "Isotope effect in the superconductivity of mercury," *Physical Review*, vol. 78, pp. 477–477, may 1950.

[27] J. G. Bednorz and K. A. Müller, "Possible high tc superconductivity in the ba-la-cu-o system," *Zeitschrift für Physik B Condensed Matter*, vol. 64, pp. 189–193, jun 1986.

[28] A. B. Vorontsov, M. G. Vavilov, and A. V. Chubukov, "Superconductivity and spin-density waves in multiband metals," *Physical Review B*, vol. 81, may 2010.

[29] A. C. Hewson, *The Kondo Problem to Heavy Fermions.* Cambridge University Press, 1997.

[30] M. Greiner, C. A. Regal, and D. S. Jin, "Emergence of a molecular bose–einstein condensate from a fermi gas," *Nature*, vol. 426, pp. 537–540, nov 2003.

[31] A. A. B. D. Simons, *Condensed Matter Field Theory.* Cambridge University Press, 2010.

[32] N. N. Bogoliubov, "On the theory of superfluidity," *J. Phys. (USSR)*, vol. 11, p. 23, 1947.

[33] L. Salasnich, *Quantum Physics of Light and Matter : Photons, Atoms, and Strongly Correlated Systems.* UNITEXT for Physics, Springer International Publishing, 2 ed., 2017.

[34] Y. Castin and F. Werner, "The unitary gas and its symmetry properties," in *The BCS-BEC Crossover and the Unitary Fermi Gas*, pp. 127–191, Springer Berlin Heidelberg, oct 2011.

[35] Q. Chen, J. Stajic, S. Tan, and K. Levin, "BCS–BEC crossover: From high temperature superconductors to ultracold superfluids," *Physics Reports*, vol. 412, pp. 1–88, jun 2005.

[36] M. Marini, F. Pistolesi, and G. Strinati, "Evolution from BCS superconductivity to bose condensation: analytic results for the crossover in three dimensions," *The European Physical Journal B*, vol. 1, pp. 151–159, feb 1998.

[37] E. Burovski, E. Kozik, N. Prokof'ev, B. Svistunov, and M. Troyer, "Critical temperature curve in BEC-BCS crossover," *Physical Review Letters*, vol. 101, aug 2008.

[38] O. Goulko and M. Wingate, "Thermodynamics of balanced and slightly spin-imbalanced fermi gases at unitarity," *Physical Review A*, vol. 82, nov 2010.

[39] W. Zwerger, ed., *The BCS-BEC Crossover and the Unitary Fermi Gas.* Springer Berlin Heidelberg, 2012.

[40] C.-Y. Wang and Y. He, "BCS–BEC crossover of spin imbalanced fermi gases with rashba spin–orbit coupling," *Physics Letters A*, vol. 379, pp. 3089–3096, dec 2015.

[41] K. H. Bennemann and J. B. Ketterson, eds., *The Physics of Superconductors.* Springer-Verlag, 2004.

[42] Y. Kamihara, T. Watanabe, M. Hirano, and H. Hosono, "Iron-based layered superconductor la[o1-xFx]FeAs (x= 0.05-0.12) with Tc= 26 k," *Journal of the American Chemical Society*, vol. 130, pp. 3296–3297, mar 2008.

[43] G. G. Lonzarich, N. D. Mathur, F. M. Grosche, S. R. Julian, I. R. Walker, D. M. Freye, and R. K. W. Haselwimmer *Nature*, vol. 394, pp. 39–43, jul 1998.

[44] D. C. Johnston, "The puzzle of high temperature superconductivity in layered iron pnictides and chalcogenides," *Advances in Physics*, vol. 59, pp. 803–1061, oct 2010.

[45] G. R. Stewart, "Superconductivity in iron compounds," *Reviews of Modern Physics*, vol. 83, pp. 1589–1652, dec 2011.

[46] P. Dai, J. Hu, and E. Dagotto, "Magnetism and its microscopic origin in iron-based high-temperature superconductors," *Nature Physics*, vol. 8, pp. 709–718, oct 2012.

[47] J. Paglione and R. L. Greene, "High-temperature superconductivity in iron-based materials," *Nature Physics*, vol. 6, pp. 645–658, aug 2010.

[48] P. J. Hirschfeld, M. M. Korshunov, and I. I. Mazin, "Gap symmetry and structure of fe-based superconductors," *Reports on Progress in Physics*, vol. 74, p. 124508, oct 2011.

[49] S. Raghu, X.-L. Qi, C.-X. Liu, D. J. Scalapino, and S.-C. Zhang, "Minimal two-band model of the superconducting iron oxypnictides," *Physical Review B*, vol. 77, jun 2008.

[50] A. Moreo, M. Daghofer, A. Nicholson, and E. Dagotto, "Interband pairing in multiorbital systems," *Physical Review B*, vol. 80, sep 2009.

[51] A. Moreo, M. Daghofer, J. A. Riera, and E. Dagotto, "Properties of a two-orbital model for oxypnictide superconductors: Magnetic order, B2g spin-singlet pairing channel, and its nodal structure," *Physical Review B*, vol. 79, apr 2009.

[52] A. Moreo and E. Dagotto, "Minimal-size real-space d -wave pairing operator in CuO2 planes," *Physical Review B*, vol. 100, dec 2019.

[53] H. Suhl, B. T. Matthias, and L. R. Walker, "Bardeen-cooper-schrieffer theory of superconductivity in the case of overlapping bands," *Physical Review Letters*, vol. 3, pp. 552–554, dec 1959.

[54] J. Nagamatsu, N. Nakagawa, T. Muranaka, Y. Zenitani, and J. Akimitsu, "Superconductivity at 39 K in magnesium diboride," *Nature*, vol. 410, pp. 63–64, mar 2001.

[55] T. Dahm, "Superconductivity of magnesium diboride: Theoretical aspects," in *Frontiers in Superconducting Materials*, pp. 983–1009, Springer-Verlag, 2004.

[56] J. Tahir-Kheli, "Interband pairing theory of superconductivity," *Physical Review B*, vol. 58, pp. 12307–12322, nov 1998.

[57] W. V. Liu and F. Wilczek, "Interior gap superfluidity," *Physical Review Letters*, vol. 90, jan 2003.

[58] E. Gubankova, W. V. Liu, and F. Wilczek, "Breached pairing superfluidity: Possible realization in QCD," *Physical Review Letters*, vol. 91, jul 2003.

[59] O. V. Dolgov, E. P. Fetisov, D. I. Khomskiî, and K. Svozil, "Model of interband pairing in mixed valence and heavy fermion systems," *Zeitschrift für Physik B Condensed Matter*, vol. 67, pp. 63–68, mar 1987.

[60] O. Dolgov, E. Fetisov, and D. Khomskii, "Superconductivity of heavy fermions in a two-band model," *Physics Letters A*, vol. 125, pp. 267–270, nov 1987.

[61] W. S. Chow, "Theory of superconductors with overlapping bands in the presence of nonmagnetic impurities," *Physical Review*, vol. 172, pp. 467–475, aug 1968.

[62] P. F. Bedaque, H. Caldas, and G. Rupak, "Phase separation in asymmetrical fermion superfluids," *Physical Review Letters*, vol. 91, p. 247002, dec 2003.

[63] H. Caldas, "Cold asymmetrical fermion superfluids," *Physical Review A*, vol. 69, p. 063602, jun 2004.

[64] J. Kondo, "Superconductivity in transition metals," *Progress of Theoretical Physics*, vol. 29, pp. 1–9, jan 1963.

[65] M. Dzero, J. Xia, V. Galitski, and P. Coleman, "Topological kondo insulators," *Annual Review of Condensed Matter Physics*, vol. 7, pp. 249–280, mar 2016.

[66] R. Kishore and S. K. Joshi, "Electron correlation in ferromagnetism. II. hybridization of s and d bands," *Physical Review B*, vol. 2, pp. 1411–1422, sep 1970.

[67] R. Jullien and B. Coqblin, "Study of the d-f hybridization in actinide metals and alloys," *Physical Review B*, vol. 8, pp. 5263–5271, dec 1973.

[68] M. G. A. Armen Sedrakian, John W. Clark, ed., *Pairing in fermionic systems : basic concepts and modern applications.* Singapore Hackensack, NJ: World Scientific, 2006.

[69] M. G. Alford, "Color superconductivity in ultra-dense quark matter,"

[70] W. V. Liu, F. Wilczek, and P. Zoller, "Spin-dependent hubbard model and a quantum phase transition in cold atoms," *Physical Review A*, vol. 70, sep 2004.

[71] L. M. Ferreira, T. Park, V. Sidorov, M. Nicklas, E. M. Bittar, R. Lora-Serrano, E. N. Hering, S. M. Ramos, M. B. Fontes, E. Baggio-Saitovich, H. Lee, J. L. Sarrao, J. D. Thompson, and P. G. Pagliuso, "Tuning the pressure-induced superconducting phase in doped CeRhIn5," *Physical Review Letters*, vol. 101, jul 2008.

[72] F. Deus, *Contributions to the Transport Properties of Many-Body Systems.* PhD thesis, Centro Brasileiro de Pesquisas Físicas, 2005.

[73] I. T. Padilha and M. A. Continentino, "Pressure induced superconductor quantum critical point in multi-band systems," *Journal of Magnetism and Magnetic Materials*, vol. 321, pp. 3466–3471, oct 2009.

[74] A. Ramires and M. A. Continentino, "Fluctuations in a superconducting quantum critical point of multi-band metals," *Journal of Physics: Condensed Matter*, vol. 23, p. 125701, mar 2011.

[75] M. A. Continentino, I. T. Padilha, and H. Caldas, "Mechanism for enhancement of superconductivity in multi-band systems with odd parity hybridization," *Journal of Statistical Mechanics: Theory and Experiment*, vol. 2014, p. P07015, jul 2014.

[76] S. M. Ramos, M. B. Fontes, E. N. Hering, M. A. Continentino, E. Baggio-Saitovich, F. D. Neto, E. M. Bittar, P. G. Pagliuso, E. D. Bauer, J. L. Sarrao, and J. D. Thompson, "Superconducting quantum critical point in CeCoIn(5-x)Sn(x)," *Physical Review Letters*, vol. 105, sep 2010.

[77] F. D. Neto, *Supercondutividade em Modelos Multi-bandas: Crossover BCS-BEC, Potencial Repulsivo e Aplicações.* PhD thesis, Universidade Federal Fluminense, 2011.

[78] M. Randeria, J.-M. Duan, and L.-Y. Shieh, "Superconductivity in a two-dimensional fermi gas: Evolution from cooper pairing to bose condensation," *Physical Review B*, vol. 41, pp. 327–343, jan 1990.

[79] M. Gong, S. Tewari, and C. Zhang, "BCS-BEC crossover and topological phase transition in 3d spin-orbit coupled degenerate fermi gases," *Physical Review Letters*, vol. 107, nov 2011.

[80] H. Caldas, C. W. Morais, and A. L. Mota, "Phase transition in asymmetrical superfluids: Equal fermi surfaces," *Physical Review D*, vol. 72, p. 045008, aug 2005.